Studies of histone modifications in yeast and humans

Kuo-Feng Hsu

Chemistry Research Laboratory
Hertford College, University of Oxford

Trinity Term 2016

A thesis submitted to the board of the Faculty of Physical Sciences of the University of Oxford in partial fulfilment of the requirements for the degree of Doctor of Philosophy

Studies of histone modifications in yeast and humans

Abstract

Kuo-Feng Hsu, Hertford College
DPhil Thesis, Trinity 2016

Epigenetic regulation is a complex biological process that has influence on the structure of chromatin and impacts on the regulation of DNA-associated events, including transcription, DNA replication, and DNA damage repair. Post-translational modifications (PTMs) to the tails of the core histone proteins are critically involved in epigenetic regulation.

The JmjC domain-containing histone demethylases play important roles in the regulation of chromatin structure and consequently gene regulation and biological events. The first aspect of my work was to explore the application of fission yeast to investigating human JmjC histone demethylase (KDM) function. The work focused on the human KDM4A and FBXL11 demethylases and investigation on the role of H3K36 modifications in the survival of *wee1* mutant *S. pombe*. The roles of the JmjC domain function of KDM4A and FBXL11 were also investigated. The results reveal KDM4A mediated demethylation of histone H3K36me3/me2 has synthetic lethality with respect to *wee1* mutant *S. pombe*, whereas FBXL11 mediated demethylation of histone H3K36me2 has more subtle effects.

Work on epigenetics is often limited by antibody properties. In the second and third parts of the work described in this thesis, mass spectrometric methods that are capable of histone profiling are described, with the aim of developing methods complementary to immunoblotting. An LC-MS-based method for profiling histones was developed and used for analysis of histone modification under different conditions. Using the high resolution of LC and MS instruments, this method provides robust analysis of modifications to intact histones. Histone profiles for human normal and cancer cell lines were investigated. Subsequently, the method was applied to analyse global changes in histone modification patterns under various conditions, focusing on hypoxia/ hypoxia related stresses. Hypoxia has effects on the activity of JmjC KDMs and the hypoxia-inducible factor (HIF) isoforms levels, so enabling regulation of expression. The effects of 2OG/Fe(II) oxygenase inhibitors of enzymes involved in hypoxic regulation on histone PTM patterns were also investigated. The results reveal that the extent to which hypoxia and hypoxia-mimetics (including inhibition that upregulate HIF-α levels) cause changes to histone profiles vary differently. The LC-MS-based method hence has potential application in drug discovery and in investigations on the role of histone modifications in healthy development and disease.

Acknowledgements

I would like to thank sincerely to my supervisor, Professor Chris Schofield for providing me with a great opportunity to investigate the scientific field of chemistry and biology. Over three years in Chemistry Research Laboratory, I have received his constant support, unparalleled enthusiasm and guidance. I would also like to express my great thanks to Dr. Sarah Wilkins for teaching me all I need in the experiments and helping me through my tough period in Oxford. Without her endless patience, encouragement and advice, much work done in the thesis would not have been possible.

Thanks to Dr. Tim Humphrey for collaborative project and enthusiastic guidance. I am also obliged to members of the Humphrey laboratory who helped me, especially Dr. Chen-Chun Pai and Sovan Sarkar for experimental advice and assistance.

Thanks to CRL Mass Spectrometry staff- Dr. James McCullagh, Lingzhi Gong, and James Wickens for experimental help.

I am grateful for the experimental assistance and advice provided by past and present members of the Schofield group, especially Dr. Louise Walport. Thanks to my colleagues who have encouraged and helped me in the lab, especially Shifali Shishodia**.**

Finally, my heartfelt thanks go to my wife for her endless love and support all the way since she has appeared in my life.

Contents

Abbreviations

Δ	gene disruption
°C	degrees Celsius
2OG	2-oxoglutarate
2TY	2 × Tryptone/yeast extract
5mC	5-methylcytosine
Amp	ampicillin
APS	ammonium persulfate
bp	base pair
BSA	bovine serum albumin
CDK	cyclin-dependent kinase
ChIP	chromatin immunoprecipitation
CP20	deferiprone
CpG	C-phosphate-G
C-terminus	carboxyl terminal
CV	column volume
Da	Dalton
DDR	DNA damage response
DFO	deferoxamine
DMEM	Dulbecco's Modified Eagle's Medium
DMOG	dimethyloxaloylglycine
DMSO	dimethyl sulphoxide
DNA	deoxyribosenucleic acid
DNMT	DNA methyltransferase
dNTP	deoxyribonucleotide triphosphate (A, C, G or T)
DSB	double-strand break
DSBH	double-stranded β-helix
DTT	dithiothreoitol
E. coli	*Escherichia coli*
EDTA	ethylenediaminetetraacetic acid
EMM	Edinburgh minimal medium
ESI	electrospray ionization
Exjade	deferasirox
FAD	flavin adenine dinucleotide
FBS	fetal bovine serum
FBXL	fbox, leucine-rich repeat protein
FDH	formaldehyde dehydrogenase
FIH	factor inhibiting HIF
FL	full length
FLAG	DYKDDDDK epitope
FPLC	fast protein liquid chromatography
H1	histone H1
H2A	histone H2A
H2B	histone H2B
H3	histone H3
H4	histone H4
HAT	histone acetyltransferase
HDAC	histone deacetylase
HDM	histone demethylases

HEK	human embryonic kidney
HEPES	4-(2-hydroxylethyl)-1-piperazineethanesulfonic acid
HIF	hypoxia inducible factor
HMT	histone methyltransferase
HPLC	high performance liquid chromatography
HR	homologous recombination
HRP	horseradish peroxidase
IOX2	(1-benzyl-4-hydroxy-2-oxo-1,2-dihydroquinoline-3-carbonyl) glycine
IPTG	isopropyl β-*D*-thiogalactopyranoside
JARID	Jumonji, AT rich interactive domain
JmjC	Jumonji C
JMJD	Jumonji C domain-containing proteins
K-Ac	N^{ε}-acetyllysine
KDM	lysine demethylase
me	methylation
me2	dimethylation
me3	trimethylation
KMT	lysine methyltransferase
LB	lysogeny broth
LCMS	liquid chromatography mass spectrometry
LSD	lysine specific demethylase
M	molar
m/z	mass to charge ratio
MALDI	matrix-assisted laser desorption / ionization
me	methyl
MS	mass spectrometry
MS/MS	tandem mass spectrometry
MW	molecular weight
NaCl	sodium chloride
NAD+	nicotinamide adenine dinucleotide
NaOH	sodium hydroxide
nmt	no message in thiamine
NOG	*N*-oxalylglycine
N-terminus	amino terminal
OD	optical density
PBS	phosphate-buffered saline
PCR	polymerase chain reaction
PDB	protein data bank
PEG	polyethylene glycol
PEI	polyethylenimine
PHD	plant homeodomain
PHD 1-3	prolyl hydroxylase 1-3
PMSF	phenylmethylsulfonyl fluoride
PTMs	post-translational modifications
RCF(g)	relative centrifugal force
RNA	ribonucleic acid
RPLC	reversed-phase liquid chromatography
RPM	revolutions per minute
S. cerevisiae	*Saccharomyces cerevisiae*

S. pombe	*Schizosaccharomyces pombe*
SAM	*S*-(5'-adenosyl)-l-methionine
SDM	site-directed mutagenesis
SDS-PAGE	sodium dodecylsulfate polyacrylamide gel electrophoresis
TAE	tris-acetate-EDTA
TCA	trichloroacetic acid
TEMED	tetramethylethylenediamine
TFA	trifluoroacetic acid
TIC	total ion count
TOF	time-of-flight
Tris	*tris*-(hydroxylmethyl)aminomethane
Tween-20	polyoxyethylene (20) sorbitan monolaurate
UPLC	ultra- performance liquid chromatography
v/v	volume for volume
w/v	weight for volume
wt	wild-type
X-gal	5-bromo-4-chloro-3-indolyl-β-d-galactopyranoside
YE6S	yeast extract 6 supplements

Chapter 1
Introduction

1.1 Epigenetics - an overview

In the classical view of molecular genetics, the "central dogma" is that deoxyribonucleic acid (DNA) transfers information to ribonucleic acid (RNA), which then makes proteins, but that the information cannot be transferred back to DNA.[1] However, it has become clear that the situation is much more complicated than this. Waddington first used the word "epigenotype" to explain phenotypic variations arising from the same genes in 1942; Nanny subsequently reported that the same genotype might have different phenotypes that persist over many generations.[2,3] Since then, the concept of epigenetics has emerged and been discussed over many decades. The field of epigenetics is now well-established and involves the study of gene regulation at the transcriptional level, which is crucially involved in many biological processes such as cell differentiation.[4] The disruption of normal epigenetic mechanisms is linked to a variety of pathologies, most notably cancers.[5]

Patterns of epigenetic gene expression and associated phenotypes can persist through either mitosis or meiosis without changes of the primary (i.e. ATGC) DNA sequence. Hence, epigenetic regulation is generally considered as a way to control gene expression in a heritable manner without changing the human genome (e.g. DNA sequence). For example, monozygotic twins in humans have the same (a very similar 'ATCG') DNA sequences, but do not present with identical phenotypes. Epigenetic regulation can be achieved by different patterns of DNA methylation and histone modifications.

In general, the current evidence is that epigenetic regulation is predominantly mediated

by changes in DNA methylation, histone variants, histone modifications, chromatin remodeling, non-coding RNAs, and transcriptional factors. These variables are also linked to numerous biochemical mechanisms in cells. The importance of epigenetics with respect to cell fate, identity and phenotype as well as aging and tissue regeneration is of major interest but is not fully understood.[6-8] The scale of research in the epigenetic field has grown rapidly in recent years.

1.2 Structure of chromatin

Chromosomes are composed of chromatin, a macromolecular complex consisting of DNA and associated proteins, principally histones.[9] The interaction of negatively charged DNA with the oppositely charged arginine- and lysine-rich histone proteins contributes to the efficiency of DNA packaging into chromosomes.[10] The nucleosome is the basic unit of chromatin, and comprises two copies of the four core histone proteins (H2A, H2B, H3 and H4), around which wrap approximately 147 base pairs of DNA (Figure 1.1). The nucleosomes are interconnected by a short section of linker DNA, which is stablised by interaction with histone H1.[11,12] The varying degree of nucleosome packaging leads to the different types of chromatin, including relatively open euchromatin and condense heterochromatin.[13] The mitotic/meiotic chromosome is identified as the most obvious higher-order structure of chromatin in which DNA is condensed 10,000-20,000 fold.[14]

Structurally, core histone proteins contain a conserved histone fold domain, which is a globular core domain consisting of three α-helices separated by two loops, and a flexible N-terminal tail that extends from the histone octamer structure beyond the DNA (Figure 1.1).

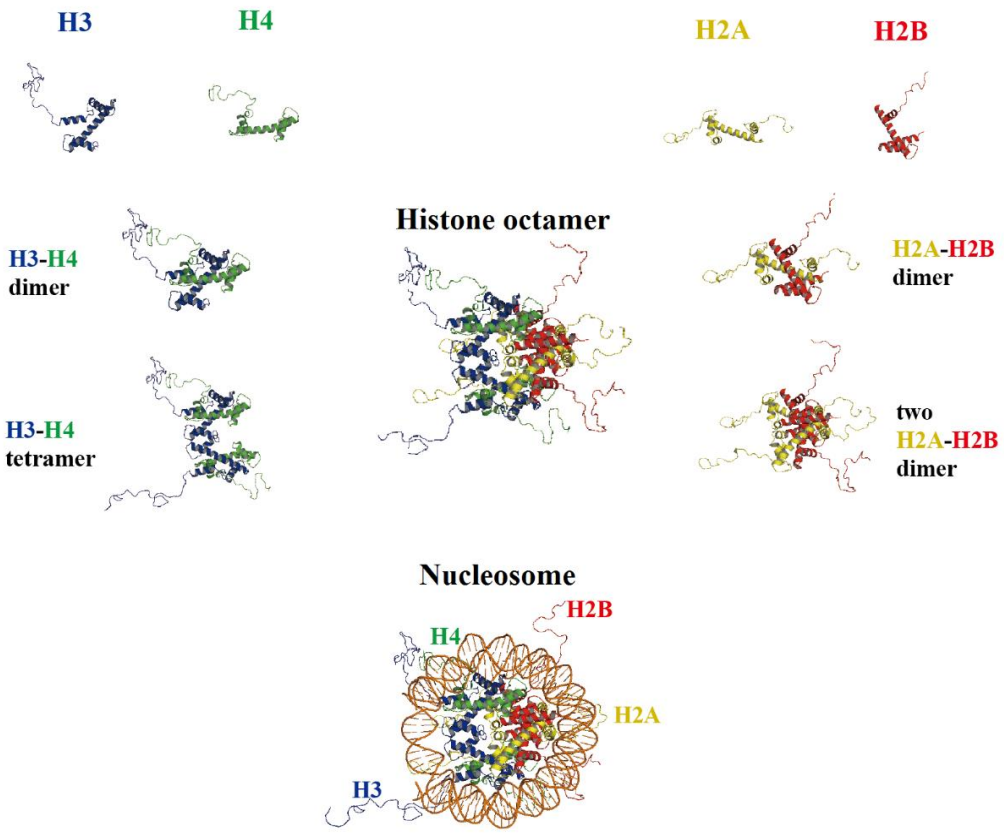

Figure 1.1 Scheme of nucleosome assembly and crystal structure of a nucleosome (PDB ID: 1KX5).[15] H2A (yellow), H2B (red), H3 (blue) and H4 (green) proteins. Note that the N-terminal tails of histones extend beyond the core of the histone octamer.

The N-terminal tails of H2B and H3 are reported to be necessary for the structure and stability of nucleosome.[16] The tails of histones have been demonstrated to be disordered and highly dynamic even in a condensed chromatin by magic angle spinning NMR spectroscopy and ion mobility mass spectrometry.[17,18] However, the histone tails are involved in intra- and inter-nucleosome contacts; secondary structure predictions have indicated that the core histone tails have some structured regions.[19] Further, NMR and circular dichroism analysis revealed that the α-helical content in H3 and H4 tails can be enhanced by acetylation of the histone tails.[19] These studies imply that the histone tails, particularly for H3 and H4, can exhibit (at least partially) structured regions that are influenced by histone post-translational modifications (PTMs) and have a role in regulating chromatin structure.

1.3 Histone variants

Animal nucleosomes typically have four canonical core histones (H2A, H2B, H3 and H4). The canonical histones are expressed in a replication-coupled manner in order to be ready to package biosynthesized DNA. Histone variants are expressed in a replication-independent fashion throughout the cell cycle to replace the canonical histones in specific situations.[20] Only one H4 species (the canonical H4 histone) has been identified, whilst multiple histone variants have been identified for H2A, H2B and H3.[21] In general, H2A variants are the most diverse group of the core histones displaying substantial variation in both the N- and C- terminal regions.[22] The number of identified H3 variants is fewer than the H2A and H2B variants.

Human histone variants have the conserved histone fold domain, but have variations in amino acid sequences and size that can change the physical properties of the nucleosome; these changes affect gene expression.[22] The roles of histone variants have been reported to include the regulation of dynamic interplay between nucleosomes and regulatory DNA-binding proteins.[22]

H2A.X, H2A.Z, macroH2A and H2ABbd are referred to as non-canonical H2A variants and have their own specific functions.[21] For H3, replication-dependent H3.1 and H3.2 are classed as canonical H3 variants, whereas replication-independent H3.3 and other variants (CenH3, H3.1t and H3.3C) are considered as non-canonical H3.[21] Dysregulation or mutation of histone variants has been linked to human cancers.[23] For example, dysregulation of H2A.Z is found in breast and colon cancer, whilst reduced levels of macroH2A are associated with lung cancer.[24-26] The known human core histone variants, their location and biological functions are summarised in Table 1.1.[21]

Table 1.1 Human core histone variants.[21]

Histone	Category	Histone variant	No. of gene copies	Location	Function
H2A	Canonical H2A	Multiple H2A variants	15	Throughout the genome	Core histone
	H2A.X	H2A.X	1	Throughout the genome	DNA repair
	H2A.Z	H2A.Z1 H2A.Z2	1 1	Throughout the genome	Gene expression, chromosome segregation
	MacroH2A	mH2A1 mH2A2	1 1	Inactive X chromosome	Gene silencing
	H2A.Bbd	H2A.Bbd	3	Active X chromosome	Active transcription
H2B	Canonical H2B	Multiple H2B variants	17	Throughout the genome	Core histone
	H2BE	H2BE	1	The genome of olfactory neurons	Not determined
	TSH2B	TSH2B	1	Sperm; telomeres	Chromatin-to-nucleoprotamine transition
	H2BFWT	H2BFWT	1	Sperm	Not determined
H3	Canonical H3	H3.1 H3.2	10 3	Throughout the genome	Core histone
	Replacement H3	H3.3	2	Throughout the genome	Gene expression, chromosome segregation
	CenH3	CENP-A	1	Centromeres	Chromosome segregation, kinetochore assembly
	Testis - specific H3	H3.4 (H3.1t) H3.5 (H3.3C)	1 1	Sperm; Seminiferous tubules	Not determined
H4	Canonical H4	H4	14	Throughout the genome	Core histone

1.4 Epigenetic modifications

The dynamics of chromatin structure mediated by post-translational modifications (PTMs) of DNA and histone proteins plays an important role in controlling gene transcription.[4] Epigenetic modifications are believed to contribute to the determination of phenotypes in organisms. Epigenetic marks are generally considered to have the potential to be cleared and then re-established over each generation. However, incomplete clearance of epigenetic marks has been reported in some model organisms, supporting the possibility of transgenerational epigenetic inheritance.[27] In general, epigenetic modifications can be divided into several main categories, including DNA methylation, histone modifications and nucleosome positioning. Of note, there is powerful evidence that epigenetic factors can interact and regulate gene expression.

1.4.1 DNA methylation

The first discovered epigenetic modification identified was probably cytosine methylation. DNA methylation occurs principally within the context of CpG dinucleotides.[28] The CpG islands (CGIs) are defined by the National Center for Biotechnology Information (NCBI) as regions containing at least 200 bases with a percentage of G/C content greater than 50% and with an observed-to-expected CpG ratio of at least 60%.[29] In general, CGIs are approximately 1,000 bp in length and overlap 60-70% of human gene promoters. CGIs are often unmethylated in normal cells, whilst methylated CGIs occur in the differentiated tissue or at an early development stage.[30] DNA methylation has an impact on genome imprinting by marking CGIs of silenced gene. For instance, hypermethylated CGIs are observed along the inactive X chromosome.[31] Methylated DNA can recruit methyl-CpG-binding domain (MBD) proteins, which in turn can recruit histone modifying complexes, to inactivate transcription.[32] In contrast, DNA methylation across the gene body has a different role, which is correlated with gene expression.[32] A number of possible effects, including elongation efficiency and preventing spurious transcription, have been proposed.[33,34] In a recent study, a direct relationship between DNA methylation and histone methylation has been reported; it was suggested that histone lysine methylation, such as H3K9 methylation can mediate the targeting of DNA methylation.[35] Consistent with its important biological roles, aberrant DNA methylation is related to a growing number of human disease.[36]

DNA methylation is mediated by the DNA methyltransferase (DNMT) enzyme family, which transfer a methyl group from *S*-adenosyl methionine to the C5 position of cytosine to form 5-methylcytosine (5mC). In humans, three members of the DNMT

family have been shown to possess enzymatic activity on cytosine bases; these are known as DNMT1, DNMT3a and DNMT3b. The ubiquitin-like plant homeodomain and RING finger domain-containing protein 1 (UHRF1) has been reported to recruit DNMT1 to a hemi-methylated DNA substrate. DNMT1 carries out replication-dependent methylation and is referred to as the maintenance DNMT.[37] DNMT3a and DNMT3b are *de novo* methyltransferases which methylate cytosine bases in unmethylated CpG dinucleotides.[38]

DNA demethylation takes place globally during the post-fertilisation period and primordial germ cell development to reset the epigenome for totipotency.[39] DNA demethylation can be either an active or passive process. The passive process occurs in the absence of methylation of newly synthesised strands during replication. It is proposed that active DNA demethylation is mediated by Ten-Eleven-Translocation (TET) enzymes, the activation-induced deaminase (AID), or catalytic polypeptide-like 1 (Apobec1), in addition to thymine-DNA glycosylase (TDG) and base excision repair (BER) mediated processes.[40] The TET enzymes can catalyse the conversion of 5mC to form 5-hydroxymethylcytosine (5hmC), 5-formylcytosine (5fC), and finally, to produce 5-carboxycytosine (5caC).[41] Subsequently, 5caC can be converted back to cytosine via the action of TDG followed by BER.[41]

1.4.2 Histone modifications

The term post-translational modification (PTM) refers to the covalent and enzymatic modification of a protein after translation. The 20 standard amino acid residues of proteins are encoded by DNA and are transcribed into proteins via the steps of transcription and ribosomal translation.[42] In the process of protein biosynthesis, polypeptide chains may be modified to form the mature protein. After synthesis,

proteins can be modified in different ways, including by addition of functional groups such as phosphate, acetyl or methyl groups, proteolytic processing, or folding processes.[42] Amino acid residues possessing chemically reactive functional groups tend to be the main sites for PTM; for instance, the amine of lysine, the guanidinium group of arginine and the hydroxyl groups of serine, threonine and tyrosine.[42] Known histone PTMs are described below.

The core histones contain globular structured parts and flexible N-terminal tails (see Section 1.2). These histone tails present some of the most highly post-translationally modified regions within the human proteome, with well-known modifications occurring on lysine, arginine, serine, threonine, and tyrosine residues. These modifications constitute the epigenetic phenomena and function by changing chromatin structure and/or affecting the recruitment of associated proteins to chromatin to influence fundamental biological events.[43] Common and well-characterised modifications include acetylation of lysine residues, methylation of both lysine and arginine residues, phosphorylation of serine, threonine and tyrosine residues and ubiquitylation of lysine residue; these and other histone PTMs are listed in Table1.2.[43,44] With new advanced progress in mass spectrometry and biotechnology, many new modifications have been discovered, such as crotonylation, propionylation, butyrylation and hydroxybutyrylation of lysine residues, methylation of glutamine residue. The database of epigenetic marks is expanding rapidly; however, further studies are needed to determine the biological roles for most of the recently identified modifications.[45-48]

PTMs to the tails of the core histone proteins influence the structure of chromatin and impact on the regulation of DNA-associated events, including transcription, DNA replication, and damage repair.[49,50] It is widely accepted that histone PTMs make major

contributions to gene regulation.[51] The term 'histone code' has been used to describe how the different histone modifications act sequentially or in combination to cause distinct outcomes. The patterns of histone modifications are altered by enzymes known as 'writers' and 'erasers'. Histone methyltransferases (HMTs) and acetyltransferases (HATs), which methylate and acetylate histones respectively, are examples of 'writers,' whereas the histone demethylases (HDMs) and deacetylases (HDACs) that remove these modifications are erasers (Figure 1.2). Most histone PTMs can recruit effector proteins containing specialised PTM-binding domains, so-called 'readers'.[52,53] Collectively, these three major epigenetic factors (writers, erasers and readers) modulate the chromatin to establish a favorable local environment for gene regulation.

The chromatin environment can be affected by alteration of the nucleosome structure or recruitment of transcription factors and their associated proteins. In addition, the interplay of histone modifications has been reported and referred to as histone crosstalk.[54] For example, phosphorylation of H3S10 is reported to guide Gcn5, a histone acetyltransferase, to acetylate H3K14 on the same histone tail.[55] Mono-ubiquitylation of H2BK120 in the C-terminal region of the histone can stimulate Set1/compass to methylate H3K4, suggesting that crosstalk among histone modifications can also occur between the different histones.[56] However, these interactions are very complex and can be regulated in many ways, for example the methylation of H3K4 by Set1 can also be inhibited by the nearby methylated H3R2.[54] The most common histone modifications are described in more detailed below.

Table 1.2 Common and well-characterised PTMs identified on core histones.[43,57]

PTM	Enzymes	Modified residues	Site	Function
Acetylation	HAT/HDAC	Kac	H2A (5, 9, 13, 15, 36), H2B (5, 12, 15, 20), H3 (4, 9, 14, 18, 23, 27, 36, 56), H4 (5, 8, 12, 16)	Active transcription, repair, replication, chromosome condensation
Methylation	HMT/HDM	Kme1, Kme2, Kme3	H3(4, 36, 79)	Active transcription
			H3(9, 27), H4 (20)	Repressive transcription, repair
	HPRMT	Rme2a, Rme2s	H3(2, 17, 26), H4 (3)	Active transcription
Phosphorylation	Protein kinase/ Protein phosphatase	Sph, Tph, Yph	H2A (1, 120), H2B (14), H3 (3, 10, 28, 41, 45), H4 (1)	Active transcription, repair, chromosome condensation
Ubiquitination	Ubiquitin ligases/ deubiquitinating enzymes	Kub	H2A (119)	Repressive transcription, repair
			H2B (120)	Active transcription, repair
Sumoylation	SUMO-activating enzyme (E1), SUMO-conjugating enzyme (E2), SUMO ligase (E3)/ SUMO protease (Ulp/SENP)	Ksu	H2B (6/7), H2A (126)	Repressive transcription
ADP ribosylation	PARP/ PARG	Ear, Kar	H2A (13), H3(37)	Active transcription
Deimination	PADI4	R → citrulline	H2A (3), H2B (30), H3(2, 17, 26), H4(3)	Active /repressive transcription
Proline isomerization	Proline isomerase	P-cis → P-trans	H3 (30-38)	Transcription

HAT: histone acetyltransferases; HDAC: histone deacetylases; HMT: histone methyltransferases; HDM: histone demethylases; HPRMT: histone protein arginine methyltransferases; Ulp: Ubl (ubiquitin-like protein)- specific proteases; SENP: SUMO specific protease; PADI4: Peptidyl Arginine Deiminase 4; PARP: Poly (ADP-ribose) polymerase; PARG: Poly (ADP-ribose) glycohydrolase

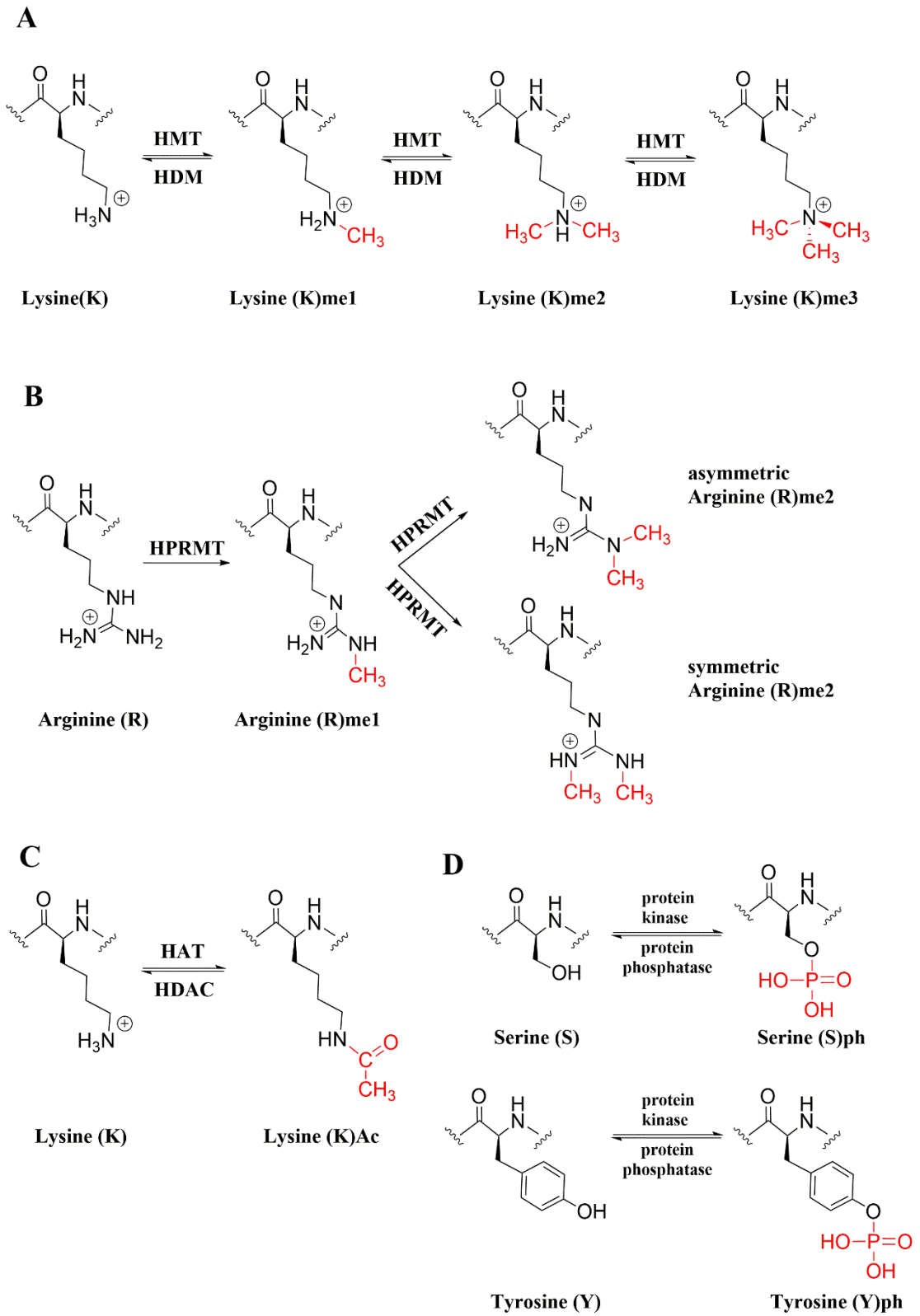

Figure 1.2 Overview of dynamic histone methylation, acetylation and phosphorylation. (A) Lysine methylation. (B) Arginine methylation. (C) Lysine acetylation. (D) Serine and Tyrosine phosphorylation. PTMs are shown in red. HMT: histone methyltransferases; HDM: histone demethylases; HPRMT: histone protein arginine methyltransferases; HAT: histone acetyltransferases; HDAC: histone deacetylases.

1.4.2.1 Phosphorylation

Phosphorylation has an important role in controlling protein function due to the addition of a negatively charged group, which can substantially change protein structure and properties.[42] Phosphorylation is one of most important PTMs of histones; it modulates chromatin structure and functions as a signal and platform to recruit chromatin-associated factors.[43] Serine, threonine and tyrosine residues in histones can be phosphorylated by protein kinases, including haploid germ cell–specific nuclear protein kinase (Haspin), mitogen- and stress-activated protein kinase 1 (MSK1) and MSK2. Dephosphorylation is catalysed by histone phosphatase (Figure 1.2D).

Perhaps the best characterised function of a phosphorylated histone mark is that of γ-H2A.X. When cells suffer from DNA damage, the histone variant H2A.X is phosphorylated to give γ-H2A.X, and marks the DNA break point[58]. γ-H2A.X plays a critical role for the recruitment of DNA repair proteins.[59] After the phosphorylation event, γ-H2A.X can be removed either via dephosphorylation or replacement by newly made H2A.X.[60] Phosphorylation of histones can also be involved in chromosome condensation and segregation during cell division or interplay with other histone modifications to modulate chromatin and thus mediate gene expression.[61,62]

1.4.2.2 Acetylation

Acetylation is a well-documented histone modification that occurs on lysine residues. Addition or removal of acetyl groups on lysine residues in histones is catalyzed by the histone modifying enzymes histone acetyl transferases (HATs) or histone deacetylases (HDACs), respectively (Figure 1.2C). Histone acetylation reduces the positive charge of lysine residues and thus may change the interaction between histones and negatively charged DNA, resulting in a more relaxed chromatin structure. The effects of histone

acetylation on chromatin structure provide a favorable and accessible local region for transcription factors and regulatory proteins to bind, inducing active transcription.[63,64]

As with other modifications, most acetylation sites have been found on histone N-terminal regions, which are likely more accessible for modification. However, acetylation of H3K56 within the core domain has been identified and recently reported as having a regulatory role in the recovery from UV-induced checkpoint arrest.[65] From a structural viewpoint, the K56 residue of H3 is located at the entry-exit point of the DNA and facing toward the DNA major groove, so acetylated H3K56 is in a particularly good position to affect the interaction of histone and DNA.[57] Overall, histone acetylation is believed to act as a central switch to enable transformation between active and repressive chromatin domains in gene transcription.[63]

1.4.2.3 Ubiquitylation

Ubiquitylation can occur on lysine residues with the most well-known sites being H2AK119 and H2BK120 in humans.[43] The human enzymes polycomb complex protein BMI-1/ E3 ubiquitin-protein ligase RING1A (Bmi1/Ring1A) and ring finger protein 20 /ring finger protein 40 (RNF20/RNF40) are responsible for ubiquitylation of H2AK119 and H2BK120, respectively.[66,67] Unlike acetylation, which predominantly causes activation of transcription, ubiquitylation has variable effects, depending on the context and the specific residue undergoing modification. Mono-ubiquitylation can signal to recruit associated 'reader' proteins or can itself directly change the chromatin structure due to its large size, thereby regulating gene transcription. Ubiquitylation of H2BK120 has been reported to function cooperatively with facilitates chromatin transcription (FACT, a histone chaperone) in transcriptional elongation, whereas H2AK119 correlates with transcriptional repression.[68] Deubiquitinating enzymes are responsible

for removal of ubiquitin from histones.[43]

1.4.2.4 Methylation

Unlike acetylation, methylation does not change the charge of the arginine or lysine residues and has no direct effect on chromatin structure. Instead, histone readers containing specific domains including Bromo, Chromo, plant homeodomain (PHD) or Tudor domains, can recognise histone methylation exclusively and distinguish between mono-, di- and trimethylated residues. Thus, the site of the modified residue and the different methylation states determine how histone methylation signals for transcription factors and regulatory complex recruitment and alters gene expression.[69]

In addition to methylation on the basic side chain of arginine and lysine residues, methylation can also occur on histidine residues. Histidine methylation appears to be rare and is not well-characterised, although monomethylated histidine has been reported.[70] Histone arginine and lysine methylation are further described below.

Arginine methylation

Arginine residues can be N^{ω}-monomethylated (me1), N^{ω}-asymmetrically dimethylated (me2a) or N^{ω}-symmetrically dimethylated (me2s) on their guainidino group (Figure 1.2B). There are nine identified human protein arginine methyltransferases (PRMT1-9), which catalyse methylation of specific arginine sites on the histone tails by transferring a methyl group from S-adenosylmethionine.[71] The tails of histone H2A, H3 and H4 are prime targets for this family of PRMTs. Additionally, a number of non-histone substrates have been identified for the PRMTs.[72] The nine PRMTs are categorised into three types (type I-III), according to their enzymatic function.[71] All PRMTs catalyse the formation of a mono-methylarginine intermediate. Type I PRMTs

(PRMT1, 2, 3, 4, 6 and 8) further catalyse the conversion of Rme1 into Rme2a, whereas type II (PRMT5, 7 and 9) catalyse the final product of Rme2s.[71] PRMT7 is also a Type III PRMT and can catalyse the monomethylation of certain substrates.[73]

The arginine residues of histone H3 are identified to be both or asymmetrically dimethylated, such as H3R8me2a (catalyzed by PRMT2)/H3R8me2s (catalyzed by PRMT5) and H3R26me2a (catalyzed by PRMT4). Other residues of histone H2A and H4 can have both methylated forms, such as H2AR3me2a/H4R3me2a (catalyzed by PRMT1 and 6), and H2AR3me2s/H4R3me2s (catalyzed by PRMT5 and 7).

In all cases the two different dimethylated arginine residues are related to distinct downstream effects.[71,74] In general, asymmetrically dimethylated arginine is considered as an activating mark for transcription, e.g. as for H3R26me2a, H2AR3me2a and H4R3me2a. In contrast, symmetrically dimethylated arginine is generally considered to be a repressive mark e.g. H3R8me2s, H2AR3me2s and H4R3me2s. This phenomenon can be explained by recruitment of different proteins to asymmetrically or symmetrically dimethylated arginines.[71] For example, H4R3me2a recruits the p300/CBP-associated factor to the nucleosome, increasing acetylation levels at H3K9 and H3K14 and thereby activating gene transcription.[71] Sometimes, H3R2me2a leads to gene repression and H3R2me2s keeps genes poised in euchromatin for transcriptional activation.[71,75,76]

JMJD6 was reported as the first N-methyl arginine demethylase, catalysing both symmetrical and asymmetrical H3R2me2 and H4R3me2.[77] However, the arginine demethylase activity of JMJD6 has been challenged and JMJD6 has since been reassigned as a lysyl hydroxylase, acting on the splicing regulatory protein U2AF65 and histones.[77,78]

Lysine methylation

Lysine methylation is a highly abundant modification of histones and can occur on all four core histones.[43] Most histone methylation sites are identified on histone tails, although there is also a well-known methylation site on the globular domain of H3, located at K79.[79]

Histone methylations contribute to the exquisite dynamics and interplay of chromatin architecture and gene expression.[80] In active chromatin, H3K4 methylation (me1, me2, and me3) and H3K9me1 are enriched at the enhancer, the promoter and the 5' end of the coding gene.[81] H3K27me1 and H4K20me1 are enriched over the coding gene region, whilst H3K36me3 is abundant over the body of the coding gene.[80-82]

In poised chromatin, the promoter and the coding gene are enriched in the repressive mark H3K27me3, whereas the region near the transcription start site is enriched in the activating mark H3K4me3.[83] The unique combination of active and repressive histone marks, H3K4me3 and H3K27me3, can poise the coding gene for activation and is proposed to form a "bivalent domain".[80,83]

In inactive chromatin, the promoter and the coding gene region are enriched in H3K9me2/me3 and H3K27me2/me3.[81] The 5' end of the coding gene and the promoter are enriched in H3K79me3.[80]

In general, lysine methylation on three histone sites, H3K4, H3K36 and H3K79, is classified as relating to the activation of transcription, whilst methylation on H3K9, H3K27 and H4K20 are involved in transcriptional repression.[80] However, the methylation of histone lysine residues has variable effects on gene.[80] It is important to consider the context and environment, which affect the action of histone marks toward to activation or repression of transcription, consistent with dynamics of chromatin in

gene expression.[44,54]

Lysine residues can be N^{ε}-mono-, N^{ε}-di- or N^{ε}-trimethylated, as catalysed by HMTs, making use of S-adenosyl methionine as the methyl donor.[79] The major class of histone lysine methyltransferases (KMTs) are SET (Su(var)3-9, Enhancer-of-zeste, trithorax)-domain containing proteins. An additional methyltransferase, the DOT1 (disruptor of telomeric silencing-1)-like protein has also been identified to methylate H3K79 to form mono, di, and trimethylated states.[43,79] Notably, there is no currently known demethylase acting on N^{ε}-methylation of H3K79. The KMTs have high selectivity for methylation-state and usually modify one single lysine residue on a single histone.[84] They have been shown not only to methylate histones but also non-histone substrates.[84]

Some covalent modifications such as acetylation and phosphorylation of histone tails have long been known to be enzymatically reversible by the action of the phosphatase and deacetylase. However, histone methylation was considered as an enzymatically irreversible reaction for many years, based on the comparable turnover rates of bulk histone and the methyl group on lysine and arginine residues.[85] Although some researchers reported observed enzymatic activity in the 1960s, there was no demethylase identified until 2004. [86,87] In 2004, Shi *et al* identified lysine-specific demethylase 1 (LSD1), a nuclear member of the amine oxidase family, as the first histone lysine demethylase, opening up the field of histone demethylases.[87] LSD1 contains a SWIRM domain, flavin adenine dinucleotide (FAD)-dependent amine oxidase domain and tower domain.[88] FAD-dependent amine oxidases use a cofactor FAD to catalyse oxidative cleavage of the carbon bond of the substrate to form an imine intermediate, which is later hydrolysed to produce an amine and an aldehyde.[88,89] In the reaction, FAD is reduced to $FADH_2$, which is reoxidised to FAD by O_2, concomitantly

producing H_2O_2.[89,90] This mechanism has been reported to be compatible for nuclear amine oxidase LSD1 (Figure 1.3A).[87]

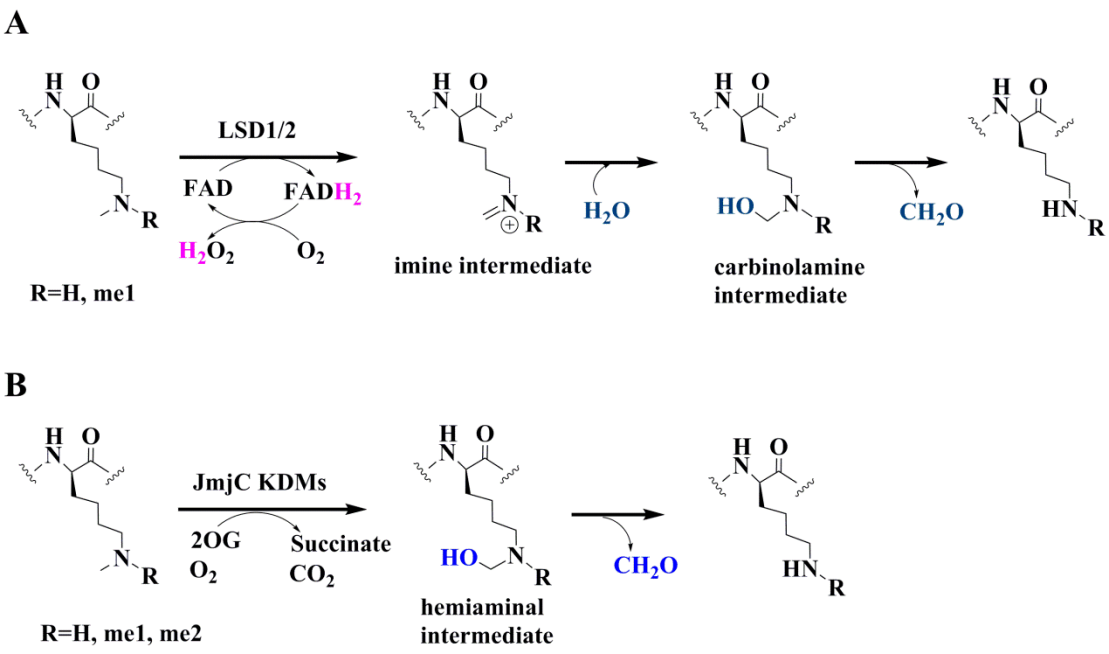

Figure 1.3 Scheme of proposed mechanism for histone lysine demethylation. Outline of the mechanisms of (A) LSD1/2 and (B) JmjC KDMs catalysed lysine demethylation.

In vitro, the products of the LSD1 catalysed demethylation reaction (histone peptides, formaldehyde and H_2O_2) can be detected in a number of ways, including by mass spectrometry, and formaldehyde dehydrogenase assays, supporting the proposed enzymatic mechanism.[91] In the LSD1-mediated lysine demethylation reaction, a protonated nitrogen on the lysine residue is required, limiting LSD1 to only reverse mono- and dimethylated lysine residue, but not trimethylated lysine.[87] LSD1 specifically demethylates H3K4me2/me1 and H3K9me2/me1 on the nucleosome in the presence of Co-REST, a corepressor for RE1 silencing transcription factor (REST), and the androgen receptor, respectively.[87,92] Another member of LSD family, LSD2 has been identified as a H3K4-specific demethylase.[93] LSD1 and LSD2 are also named as lysine demethylase 1A (KDM1A) and lysine demethylase 1B (KDM1B) reflecting histone demethylase function.

The Jumonji C family of histone demethylases (JmjC KDMs), make up the second identified KDM class, and contain about 20 identified enzymes in humans; they are a part of the large 2-oxoglutarate (2OG)/Fe (II) dependent oxygenase super-family.[94] The JmjC KDMs demethylate lysine residues via an Fe(II)-mediated oxidative process in which the N^{ε}-methyl group is oxidised to form a hemiaminal intermediate, fragmenting immediately into the demethylated product and formaldehyde (Figure 1.3 B).[91,95]

Unlike KDM1, JmjC KDMs catalyse the conversion of a methyl- lysine residue into a hemiaminal species instead of an imine species, and therefore they have the ability to demethylate all three methylated lysine states.[69] The JmjC domain features a double-stranded β-helix (DSBH) and is the catalytic domain for the enzymatic activity.[96,97] DSBH is highly conserved among different JmjC KDMs. A view from a crystal structure of a peptide containing H3K9me3 bound to the catalytic domain of KDM4A shows the general structured features of JmjC KMDs (Figure 1.4).[98]

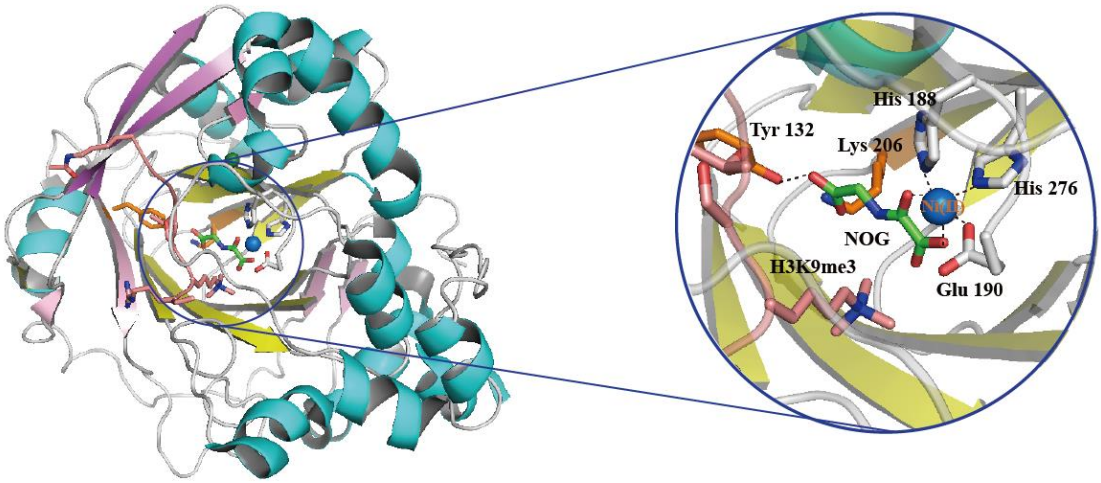

Figure 1.4 View from a crystal structure of a H3K9me3 peptide bound to the catalytic domain of KDM4A (PDB ID: 2OQ6)[98]. The ß-strands that make up the JmjC double-stranded ß-helix (DSBH) are shown in yellow. Ni(II) and *N*-oxalylglycine (NOG) are used to substitute Fe(II) and 2OG, respectively.

1.5 2OG/Fe(II)-dependent oxygenase

The 2OG/Fe(II)-dependent oxygenases are a superfamily of enzymes found in almost all living organisms. They catalyse a vast variety of oxidative reactions, introducing molecular oxygen from dioxygen into their substrates or byproducts such as hydroxylation, demethylation, epoxidation and ring opening.[97,99,100] In humans, there have been over 60 members of 2OG/Fe(II)-dependent oxygenases identified to date that catalyse either hydroxylation or demethylation on a wide variety of substrates including proteins and small molecules.[101]

Crystallographic studies of 2OG/Fe(II)-dependent oxygenases provide a detailed insight into structure features, such as the active site clefts and iron binding sites. The most prominent characteristic of all 2OG/Fe(II)-dependent oxygenases is the DSBH fold, also known as the 'jelly-roll' fold, consisting of eight strands.[96] The active sites of 2OG oxygenases contain a highly conserved iron- binding motif which usually consists of two histidyl and one aspartyl or glutamyl, referred to as the HXD/E…H motif.[96,102] The triad of residues from the HXD/E…H motif bind to iron to form one half of the octahedral metal binding geometry. Water molecules occupy the other iron binding sites, completing the octahedral geometry around the metal in the resting state of the enzyme, which has been observed in X-ray crystal structures.[103] During catalysis, 2OG uses its 1-carboxylate and 2-oxo groups to coordinate the iron in a bidentate manner, substituting two bound water molecules.[96] The octahedral iron binding model of 2OG/Fe(II)-dependent oxygenases is supported by crystallographic analyses using manganese and *N*-oxalylglycine (Figure 1.5).

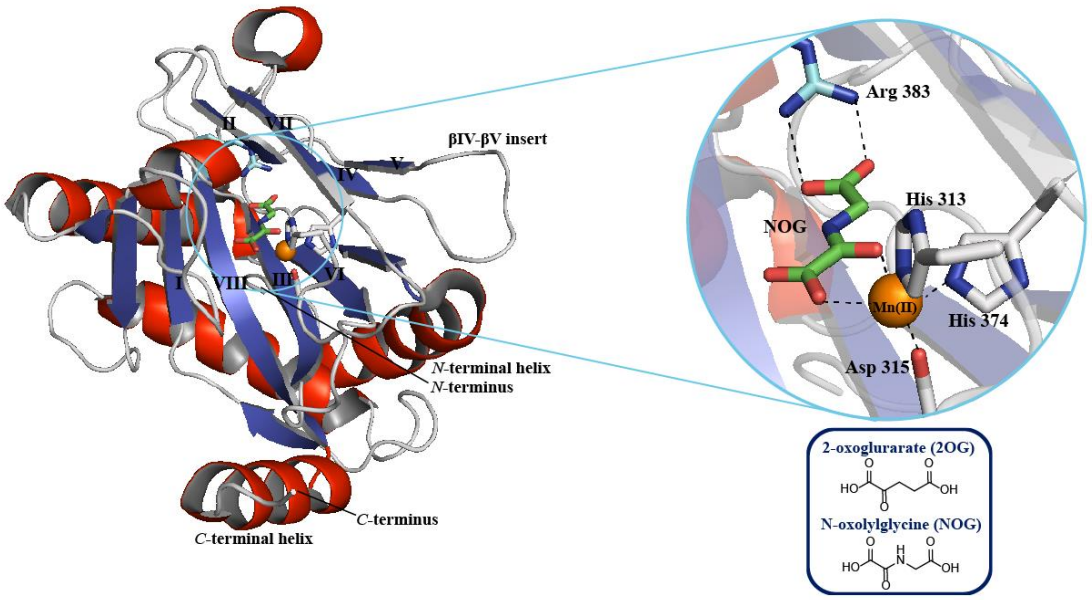

Figure 1.5 General structural features of 2OG/Fe(II)-dependent oxygenases. (A) View from a crystal structure of catalytic domain of Hypoxia-inducible factor (HIF) prolyl hydroxylase PHD2 (PDB ID: 3HQR)[104]. The conserved DSBH core fold consists of eight strands, labelled I to VIII. The inset shows the enzyme active site with residues binding to metal and 2OG. Mn(II) and *N*-oxalylglycine (NOG) substitute for Fe(II) and 2OG respectively. NOG is an analogue of 2OG and both chemical structures are shown.

Of note, iron binding is less tight in 2OG/Fe(II)-dependent oxygenases than in the haem oxygenases, and can be removed by treatment with iron chelators such as deferoxamine (DFO) or exchanged with excess transition metals.[105] The strength of iron binding has been shown to vary considerably amongst different 2OG/Fe(II)-dependent oxygenases and it may have some functional relevance.[105,106]

Spectroscopic studies for the detection of reaction intermediates and structure studies from some members of 2OG/Fe(II)-dependent oxygenases, including human prolyl hydroxylase domain-containing protein 2 (PHD2), JMJD2A (also known as KDM4A), bacteria deacetoxycephalosporin C synthase (DAOCS), Taurine α-ketoglutarate dioxygenase (TauD), led to the scheme of a consensus mechanism for general 2OG/Fe(II)-dependent oxygenase catalysis (Figure 1.6).[98,103,104,107]

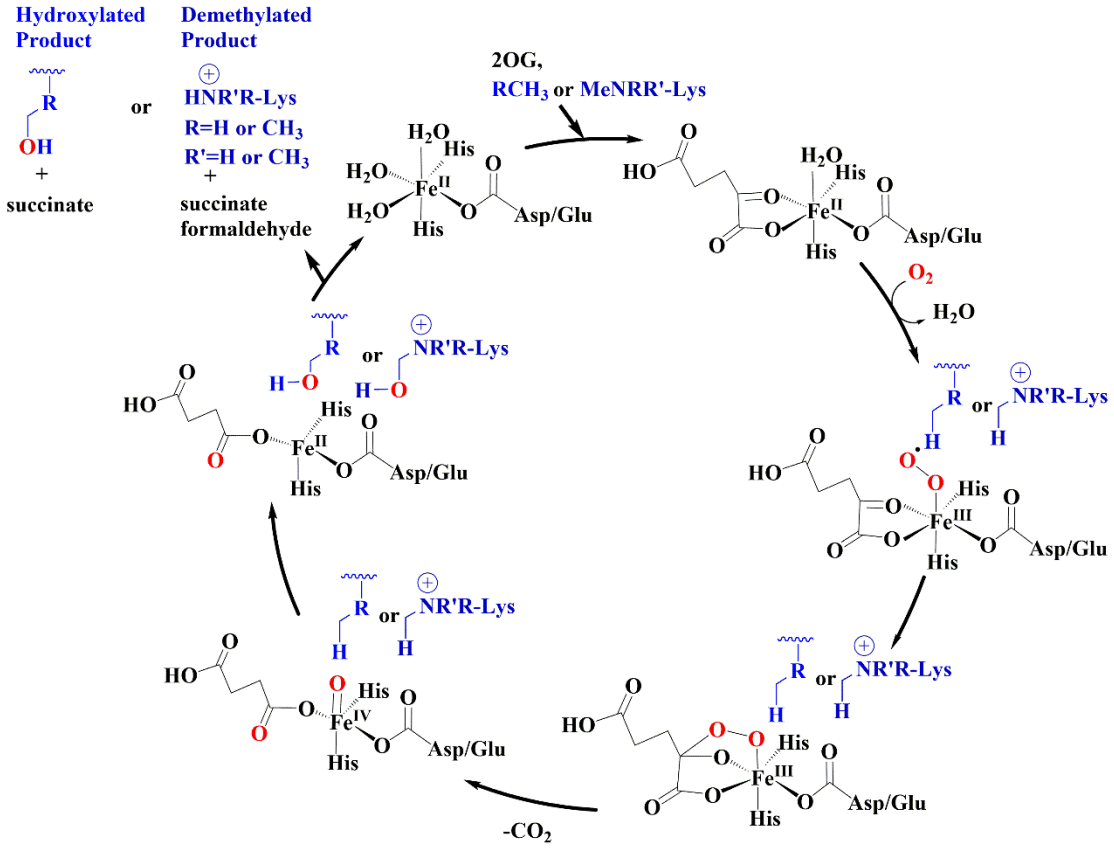

Figure 1.6 Consensus mechanism for 2OG/Fe(II)-dependent oxygenase. The hydroxylated product and demethylated product are generated from different substrates by hydroxylation and demethylation respectively.

The 2OG oxygenase reaction begins with the binding of 2OG to the active site Fe(II). Substrates (RH, and methylated lysine residue demonstrated in Figure 1.6) bind in the next step and lead to weakening of the bond between the remaining water molecule and Fe(II), thereby allowing molecular oxygen to bind.[108] An oxidative decarboxylation step, likely via a cyclic peroxide species as shown, generates an Fe^{IV}=O species, which then reacts with the substrate in a radical process to form the hydroxylated product with concomitant release of succinate and CO_2. In the case of the methylated lysine substrate, hydroxylation of the N^{ε}-methyl group occurs and a hemiaminal intermediate is formed, which then collapse to generate the demethylated product and formaldehyde. The metal-to-ligand charge transfer band induced by the binding of 2OG to Fe(II) and Fe^{IV}=O species can be characterised using spectroscopy and supports the consensus

mechanism.[109] In addition, some 2OG oxygenases have been found to be more active after addition of ascorbate, although the mechanism for this remains unclear.[110]

Oxygen sensing

Oxygen is an essential cosubstrate for the enzymatic reactions of all 2OG/Fe(II)-dependent oxygenases, previous studies have shown that some members of this family respond to low oxygen (hypoxia) and have been characterised as oxygen sensors.[111-113] The human enzyme, PHD2 is the best-known and possibly the most well-documented example of human oxygen sensor.[111] PHD2 has been demonstrated to react with oxygen at a slow rate and thereby under hypoxia, PHD2 becomes inactive, inducing the accumulation of HIF and downstream upregulation of hypoxia-associated genes, such as vascular endothelial growth factor (*VEGF*) and erythropoietin (*EPO*).[111,113] The relationship between oxygen and some JmjC KDMs has been investigated; a recent study revealed KDM4E (JMJD2E) also reacts slowly with oxygen and has a graded response to the physiological range of O_2 concentrations.[114] Another study showed that decreased enzymatic activity of Jumonji histone demethylases was observed under hypoxia in macrophages.[115] These studies have suggested there is a high correlation of hypoxia and epigenetic transformations.

1.6 JmjC KDMs

The JmjC KDM family is the largest family of histone demethylases and contains members that have been identified to remove the methyl group from almost all the known histone lysine methylation sites.[91,116] Among the known core histone lysine marks, PHF8 has been reported to demethylate H4K20me1, involved in cell cycle and PHF2 has recently been shown to demethylate H4K20me3, which is involved in the regulation of proinflammatory gene, although the activity of PHF2 remains

controversial.[117-119] However, there is no enzyme identified to date for the removal of H4K20me2 or any methylation state of H3K79. Like KMTs and PRMTs, some JmjC KDMs such as KDM2A (FBXL11), KDM3C (JMJD1C) and KDM4C (JMJD2C) have been recently proposed to catalyse demethylation of non-histone substrates, such as p65, mediator of DNA damage checkpoint 1 (MDC1) and chromodomain Y-like protein 1 (CDYL1) .[120-122] Crystal structures of JmjC KDMs including KDM4A, KDM2A and PHF have provided information on how this domain can contribute to selectivity.[96] The crystal structures reveal that methylation state selectivity is conferred by the size of the active site, the ability of methyl groups on lysine residues to fit into the active site and the position of the N^{ε}-methyl group. For example, in case of KDM4A, the tri-N^{ε}-methyl group fit snugly into the active site with one methyl group pointing directly toward the active site, whereas N^{ε}-methyl group from monomethylated lysine residue can be observed to occupy conformations not pointing toward to the active site. This supports the observed experimental data that the tri-methylated form of lysine is a much better substrate for KDM4A than the monomethylated form.[96,98]

The human JmjC family members can be classified into seven subfamilies based on phylogenetic analyses. The subfamilies of JmjC KDMs and their known histone substrates are summarised in Table 1.3.[79,116,123] In addition to the highly conserved catalytic JmjC domain common to all JmjC KDMs, most of the enzymes have other secondary domains, functioning in different ways such as to provide structural stability and/ or substrate recognition. For instance, the JmjN domain of KDM4 is required for enzymatic activity, though not directly involved in catalysis itself; the CxxC domain of FBXL11 recognises non-methylated CpG DNA; and PHD and Tudor domains in a number of JmjC KDMs function in binding to histone marks such as H3K4me3.[94,102,124]

Table 1.3 JmjC KDMs and their histone substrates.[79,116,123]

Subfamily	Enzyme (alternate name)	Core histone substrates
KDM2	KDM2A(FBXL11)	H3K36me2/1
	KDM2B (FBXL10)	H3K36me2/1, H3K4me3
KDM3	KDM3A (JMJD1A)	H3K9me2/1
	KDM3B (JMJD1B)	H3K9me2/1
	KDM3C (JMJD1C)	H3K9me2/1
KDM4	KDM4A (JMJD2A)	H3K9me3/2, H3K36me3/2
	KDM4B (JMJD2B)	H3K9me3/2, H3K36me3/2
	KDM4C (JMJD2C)	H3K9me3/2, H3K36me3/2
	KDM4D (JMJD2D)	H3K9me3/2
	KDM4E (JMJD2E)	H3K9me3/2
KDM5	KDM5A (JARID1A)	H3K4me3/2
	KDM5B (JARID1B)	H3K4me3/2
	KDM5C (JARID1C)	H3K4me3/2
	KDM5D (JARID1D)	H3K4me3/2
KDM6	KDM6A (UTX)	H3K27me3/2
	KDM6B (JMJD3)	H3K27me3/2
	KDM6C (UTY)	H3K27me3/2
KDM7	KDM7A (KIAA1718)	H3K9me2/1, H3K27me2/1
	KDM7B (PHF8)	H3K9me2/1, H3K27me2/1, H4K20me1
	PHF2	H3K9me2/1, H4K20me3
Others	MINA53	H3K9me3
	NO66	H3K4me3/2, H3K36me3/2
	KDM8 (JMJD5)	H3K36me3/2*

*Indicates that demethylase function of JMJD5 remains controversial.[125]

1.7 Nucleosome positioning

In addition to DNA methylation and histone modification, nucleosome positioning has been considered to be a factor that influences gene transcription.[126,127] Nucleosome positioning is related to the packaging of the genomic DNA, and appears to affect gene expression. Genome-wide nucleosome mapping has revealed a higher GC content and a higher degree of cytosine methylation in nucleosomal DNA than in nucleosome linker DNA[128]. The positions of nucleosomes at the transcription start sites (TSSs) impact on the initiation of transcription, for example, the blocking of TSSs by nucleosomes has been related to gene repression.[129] Histone variants are involved in nucleosome positioning and related to gene expression, as described in Section 1.3.[22] Together, different epigenetic processes coordinately establish the chromatin states that alter the gene expression.

1.8 Histone PTMs and cancer

Aberrant histone PTM profiles, as well as the dysregulated activity of histone-modifying enzymes and/or -binding proteins are linked to the development of cancer. [130,131] Investigations of the different presentation of histone PTMs in normal and cancer cells will be helpful in understanding the relationship between cancer and epigenetics, including the identification of novel histone modifications and biomarkers for the prediction of cancer and oncogenic pathways. Furthermore, any changes in histone PTMs associated with cancer are likely to be regulated by histone-modifying enzymes, which open up the field of epigenetic drugs as potential cancer therapeutics. HDAC inhibitors, including hydroxamates (Vorinostat), cyclic peptides (Romidepsin), benzamides (Entinostat) and fatty acids (Butyrates), are presently being applied in clinical trials for patients with cancer of the lung, breast, pancreas, renal and bladder,

melanoma, glioblastoma, leukemias, lymphomas, and multiple myeloma.[132]

1.9 Mass spectrometry-based analysis of histone PTMs

In line with the rapid development of the field of epigenetics in recent years, mass spectrometry (MS) is increasingly being utilised to investigate chromatin biology and epigenetic regulation as well as chromatin modifying enzymes, due to its ability to acquire detailed information of PTMs. MS becomes a useful tool for elucidating the highly divergent and dynamic transformations observed on proteins involved in epigenetic processes, particularly in histones.[133] The MS-based proteomics is making a growing contribution to recent studies of epigenetics.[46]

1.9.1 Basis of mass spectrometry

A mass spectrometer usually consists of three main parts: an ion source, a mass analyzer, and a detector.[134] In general, the mass spectrometer detects the moving ionized gas-phase ions in the electromagnetic field. Electrospray ionization (ESI) and matrix-assisted laser desorption/ionization (MALDI) are two commonly used methods to ionize peptides or proteins.[135,136] There are five major types of mass analyzers: time-of-flight (TOF), quadrupole, ion traps, orbitraps, and Fourier transform ion cyclotron resonance (FTICR) methods.[137] The frequency-domain signal can be transformed into the mass spectrum in which the *m/z* values of ions and their intensities are shown. Given the accuracy of mass, the value of *m/z* can be used to infer the composition of the measured ion. However, this value alone cannot determine the sequence of the measured ions (where these ions correspond to peptides). An additional complication arises from the fact that peptides with the same sequence containing the same modification but at different sites share the same *m/z* and cannot be distinguished by use of the mass of the parent ion alone. Further, of note, an isobaric issue can occur,

where different PTMs can cause the same change in mass, for example trimethylation and acetylation give the nominally same mass shift of 42 Da and thereby cannot be resolved in a low resolution MS instrument such as a linear ion trap.[138] As these two modification differ in mass by 0.036 Da, they can be differentiated by a high resolution MS instrument such as an Orbitrap or Fourier transform ion cyclotron resonance MS in the case of small peptides, but not for large molecules such as proteins.[139] For determining the amino acid sequence of the peptides, the desired peptide must be isolated and then further fragmented into its smaller ions. The signals of fragments are displayed in a tandem mass spectrometry (MS/MS).[140] The efficiency of fragmentation, signal-to-noise ratio, and other features subsequently influence the confidence of assigning a particular peptide sequence and modification state to a particular MS/MS and to the respective precursor ion in the MS.

1.9.2 MS for identifying histone PTMs

When a residue of a peptide or protein is modified through gaining or losing a chemical group, its elemental composition is changed, leading to an alteration of its molecular weight. A modified protein can be considered as a new species. The unmodified protein can be differentiated from its modified forms via MS based on the different molecular weights. Accordingly, MS is a potentially effective method for analysing histone PTMs, by providing more comprehensive information than antibody-based methods such as those using immunofluorescence, immunoblotting and chromatin immunoprecipitation.[141,142] MS based identification of PTMs on intact histones may provide insights into combinational modification patterns.[143] Furthermore, MS may be used in combination with different labelling strategies to enable quantitative analysis of modifications.[144]

Three main MS-based strategies can be envisaged for histone investigations (Figure 1.7).[133] The 'bottom-up' approach features the use of proteases such as trypsin and endopeptidase Arg-C to hydrolyse histones into peptides (< 25 residues), which can then be analysed by MS/MS.[143] However, the bottom-up approach is of limited use for analysis of multivalent, combinatorial PTMs and histone variants, because the digested peptides may not contain all modified residues and the same sequences of digested peptides coexist in some histone variants. As such, different approaches may be employed to characterise larger peptides or intact histones, known as 'middle-down' and 'top-down' strategies respectively. Similar to the top-down strategy looking at whole proteins, intact mass spectrometry also has potential for providing a comprehensive view of intact histones and their PTMs. It is also powerful for analysing histone variants at the intact level without the need to analysing individual digested peptides.

MS-based proteomics provide fundamental contribution to the study of epigenetics, particularly for histone biology research through the ways described below. MS can identify and validate known histone marks identified by other biochemical approaches. MS can also be applied to detect the alterations of histone modifications and quantify changes under various cellular physiological or pathological conditions. Furthermore, the intact histone mass profiles that can be acquired by MS provide an overview and may be able to characterise the interplay of histone PTMs.

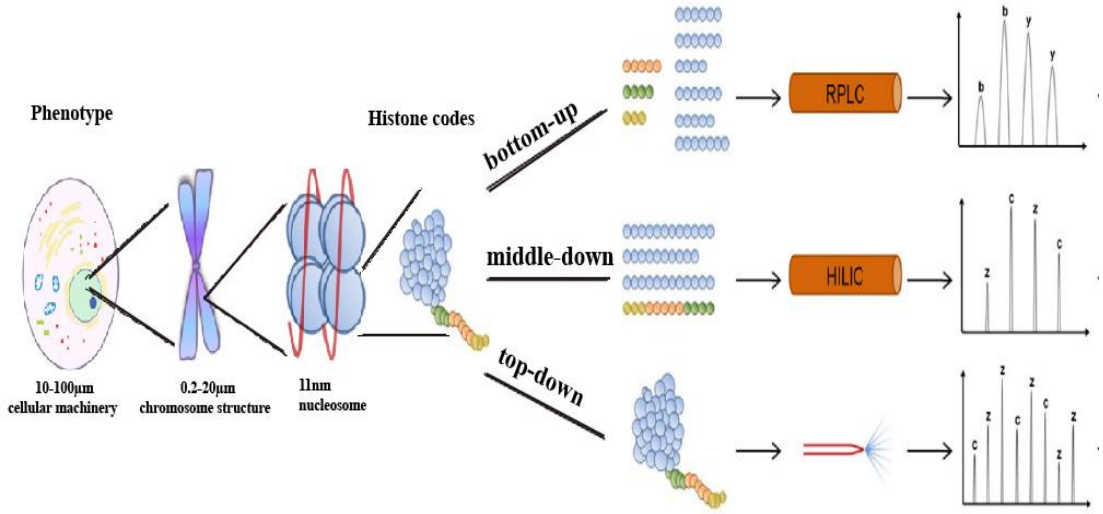

Figure 1.7 Mass spectrometry-based strategies for the analysis of histones. Left: The view from phenotype to histone codes: the cellular phenotype can be affected by epigenetic factors such as histone modifications. Right: The three major MS-based strategies applied to histone biology. The selection of the appropriate approach is mainly dependent on the aim of the project and available instrumentation: (1) The bottom-up approach employs a digestion procedure to cleave proteins into small peptides, which can be separated by using reversed-phase chromatography (RPLC). (2) The middle–down approach allows an overview of the histone tails. Hydrophilic interaction liquid chromatography (HILIC) provides the effective separation for histone tails. (3) The top–down approach allows a comprehensive view of intact histones. However, a high purity of sample is required and thus the separation and purification of the different histone types is mostly carried out offline. Data analysis requires more advanced bioinformatic software. The image is modified and adapted from Sidoli S *et al.,*2012[133].

1.10 Aims of this work

As the JmjC domain in proteins is highly conserved from yeast to humans, the function of JmjC KDMs in the fission yeast system is of interest as the simplicity of the yeast model may provide a useful system for the study of inhibitors of the human JmjC KDMs. Thus, investigating the role of JmjC KDMs in yeast was the first focus of this work. The other focus of this work was to develop an LC-MS-based method to investigate PTM patterns on intact histones from human cell lines and tissues. It was envisaged that the methodology could be applied to identify changes in the global histone PTMs profiles that occur upon treatment of cells with various pathophysiologically relevant stresses, including hypoxia, hypoxia-mimetics and inhibitors of epigenetic enzymes.

Chapter 2
Studies on JmjC KDMs in fission yeast

2.1 Introduction to fission yeast

2.1.1 Characteristics of fission yeast

Yeasts are rapidly growing, unicellular eukaryotes with a cellular organization similar to higher organisms. Yeasts have been used as a model system to investigate the molecular biology of eukaryotic cells for more than two decades.[145] The advantages of yeasts as model organisms include short doubling time, well-established cell cycle, small genome size, ease of genetic engineering and low costs of associated materials.[146,147]

Fission yeast usually exists in a haploid form, which is highly amenable to genetic manipulation. Specific genetic phenotypes can be easily produced in haploid fission yeast cells, such as leucine auxotrophy (i.e. inability to synthesise leucine).[148]

2.1.2 Fission yeast as a model for studying epigenetics

Fission yeast is potentially an excellent model organism for epigenetic research. The basic chromatin structure (i.e. nucleosomes) is conserved from yeasts through to more complex eukaryotic organisms, including humans.[146] Changes in the structure of chromatin (i.e. from heterochromatin to euchromatin) regulate fundamental processes in fission yeast, including transcription, replication, recombination and DNA repair.[149] Several mechanisms of chromatin regulation found in human cells are also present in fission yeast. In particular, many histone PTMs have been identified in fission yeast, along with several histone modifying enzymes.[149-152] Notably, no DNA methylation has been detected in fission yeast despite the existence of a homologue of cytosine 5-

methyltransferase.[153] In this respect, the use of fission yeast facilitates investigation of chromatin regulation by histone PTMs. Overall, fission yeast is a valuable model system for understanding the interplay of histone modifications and associated proteins involved in transcriptional regulation.

2.1.3 Histone lysine methyltransferases in fission yeast

Lysine methylation is reported to be one of the most abundant post-translational modifications (PTMs) of histones. It can involve the addition of up to three methyl groups to the ε-amine of a lysine residue.[43] Histone lysine-methylation plays important roles in regulating the structure of chromatin in fission yeast; for example, methylation of H3K9 leads to the recruitment of Swi6 to chromatin, in turn promoting the formation of heterochromatin.[154,155]

Fission yeast contains four reported histone lysine methyltransferases, each of which has specific functions associated with the regulation of chromatin and gene expression.[156] Set1 catalyses the mono, di-, and tri-methylation of H3K4 and these modifications enhance active chromatin states.[157] Methylation of H3K9 is catalysed by Clr4, and is reported to be important for heterochromatin assembly.[158] All three methylation states of H4K20 are produced by Set9 catalysis; H4K20 methylation is an important marker of DNA damage sites.[159] Methylation of H3K36 has been researched extensively in recent years since it has a variety of roles in cells, including in transcriptional activation, repression, alternative splicing, dosage compensation, as well as in DNA damage repair. [82,160-163] Although at least eight enzymes are reported to catalyse H3K36 methylation in humans, only one enzyme, Set2, is responsible for catalysing all three methylation states of H3K36 in fission and budding yeast.[164] Notably, there is no H3K27 or H3K79 methylation in fission yeast.[165-167]

2.1.4 The relationship between Set2 and Wee1-50 in fission yeast

Recent work from Dr. Tim Humphrey's group at the Oxford Institute for Radiation Oncology (Department of Oncology, University of Oxford) has identified a role for the histone methyltransferase Set2 in regulating DNA repair mechanisms in fission yeast. They found that Set2-mediated formation of H3K36me3 facilitates transcription of a gene encoding Cdc22, which is a subunit of ribonucleoside reductase (RNR) (Pai *et al.*, manuscript in preparation). RNR, a diphosphate reductase, catalyses the *de novo* synthesis of deoxyribonucleotides (dNTPs), the building blocks of DNA.[168] The reductase activity of RNR is essential for maintaining the dNTP 'pool' required for efficient DNA synthesis and repair.

The dNTP pool is also regulated indirectly via the activity of Wee1, a nuclear serine/threonine-specific protein kinase in fission yeast.[169] Wee1 is normally involved in controlling cell division through inhibition of Cyclin-dependent kinase 1 (Cdk1).[170] Inhibition of Wee1 is reported to activate Cdk1-dependent DNA replication, resulting in nucleotide shortage.[169] Additionally, a temperature-sensitive mutation in *wee1* (*wee1-50*) is found to degrade Cdc22 through Cdk1 activation. Notably, deletion of *set2* combined with the *wee1-50* mutation causes synthetic lethality in fission yeast; this is proposed to be due to critical dNTP depletion (Figure 2.1).

The role of Set2 in maintaining the nucleotide pool is thought to be mediated by its histone methyltransferase activity, specifically, the formation of H3K36me3 from H3K36me2.[171] Histone demethylases have, in effect, the opposite enzymatic activity to that of histone methyltransferases. It was hence hypothesized that overexpression of demethylases acting on H3K36 would have similar biological outcomes to *set2* deletion in fission yeast, and may result in synthetic lethality when combined with the *wee1-50* mutation.

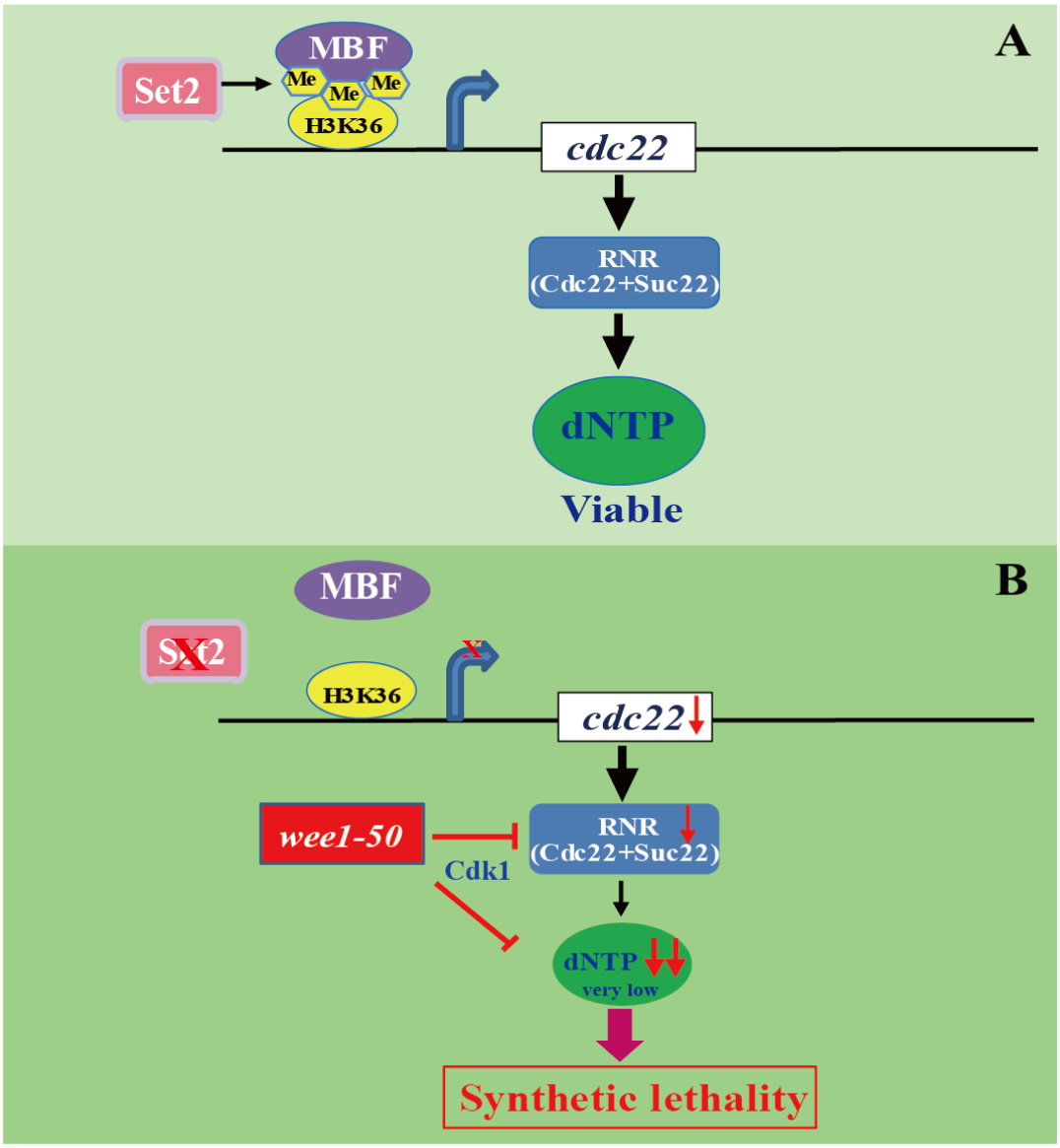

Figure 2.1 A model for synthetic lethality caused by the deletion of *set2* in *wee1-50* mutant fission yeast. (A) Set2-mediated H3K36me3 facilitates transcription of a gene encoding Cdc22 and maintains the dNTP pool for cell growth. (B) The deletion of *set2* causes downregulation of a gene encoding Cdc22 and subsequently results in a decrease in the dNTP pool. *wee1-50* causes the depletion of dNTP. Combination of *set2Δ* and *wee1-50* causes the critical dNTP depletion and then induces synthetic lethality.

2.1.5 Histone lysine demethylases in fission yeast

In humans, H3K36 demethylation is catalyzed by JmjC-domain containing KDMs belonging to the KDM2 and KDM4 subfamilies (see Section 1.6).[94,172,173] Two of the human enzymes, FBXL11 (KDM2A) and JMJD2A (KDM4A) have orthologues in fission yeast (Figure 2.2). Epe1 is a putative homologue of FBXL11 and is reported to modulate heterochromatin formation.[151] However, Epe1 has not directly been shown to function as a histone H3K36me2/me1 demethylase , which might be explained by the absence of two conserved iron-binding residues within its JmjC domain.[172] The fission yeast protein Jmj3 is most similar to JMJD2A and is predicted to demethylate H3K36me3/me2;[174] however, there are currently no reports of Jmj3-catalysed histone demethylation.

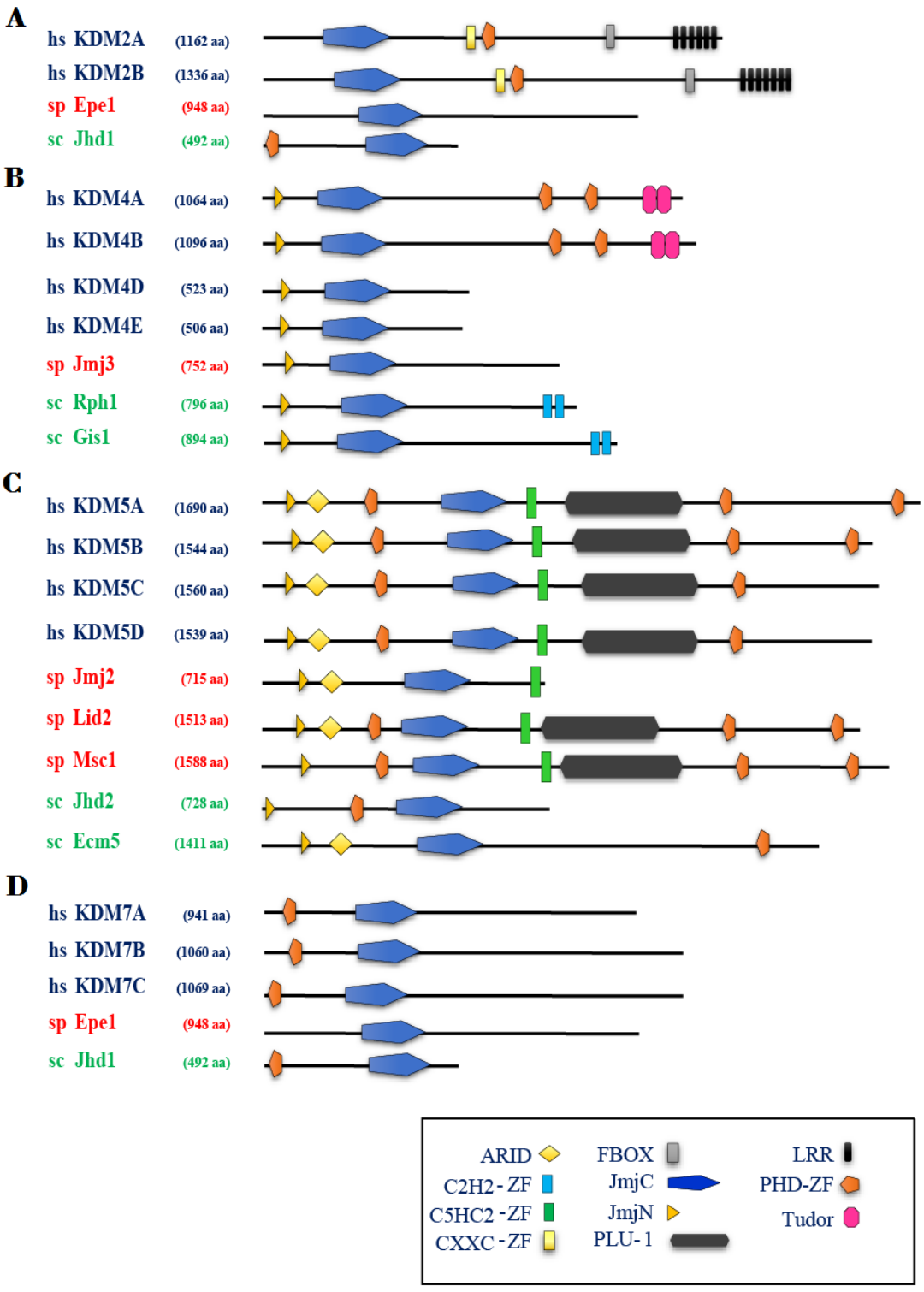

Figure 2.2 Schematic diagram of JmjC KDM orthologues in humans and yeast showing the domain architecture. Putative orthologues for (A) KDM2, (B) KDM4, (C) KDM5 and (D) KDM7 have been identified in yeast. hs: *Homo sapiens;* sp: *Schizosaccharomyces pombe;* sc*: Saccharomyces cerevisiae*. ARID: AT-rich interaction domain; JmjC: Jumonji C domain; JmjN: Jumonji N domain; PHD: plant homeobox domain; LRR: leucine rich repeats; zf: zinc finger.

2.2 Objectives

The aim of my work was to gain insights into the relationship between H3K36 methylation states and Set2-mediated DNA repair mechanisms in the fission yeast *Schizosaccharomyces pombe* (*S. pombe).*[171] It was of particular interest to determine whether JmjC KDMs might contribute to regulating the nucleotide pool via demethylation of H3K36. If this were the case, the biological consequences of KDM overexpression should be similar to the effects of *set2* deletion; specifically, KDM overexpression would be expected to cause synthetic lethality in fission yeast carrying the *wee1-50* mutation. Given that a H3K36me3 demethylase has yet to be identified in fission yeast, two human KDMs acting on H3K36, FBXL11 and JMJD2A, were chosen for investigation in this study.

With a better understanding of the interactions between H3K36 demethylases and the *wee1-50* mutant, the results of synthetically lethal interactions could possibly be exploited for the treatment of certain types of cancers exhibiting overexpression of H3K36 demethylases.[175-177] In addition, the development of a fission yeast model system for the screening of inhibitors for human KDMs was a desirable goal.

The work described in this chapter was carried out in collaboration with Dr. Tim Humphrey (CRUK/MRC Oxford Institute for Radiation Oncology, Department of Oncology, University of Oxford).

2.3 Synthetic lethality of *set2* deletion and *wee1-50* mutation

Preliminary experiments were carried out to validate previous results that deletion of *set2* (and loss of H3K36me3) leads to synthetic lethality in *S. pombe* carrying the *wee1-50* mutation (Pai *et al.*, manuscript in preparation). *wee1-50* is a temperature-sensitive mutation; at the restrictive temperature (35 °C) the *wee1-50* mutant cells divide at approximately half the size of normal cells, whereas at the permissive temperature (25 °C) they grow normally.[178] Thus, *wee1-50* cells grown at 25 °C were considered as a control group due to their wild-type phenotype, whereas *wee1-50* cells grown at 35 °C present the mutant phenotype (i.e. smaller size).

Serial dilution growth assays confirmed that deletion of *set2* has no effect on cell viability in wild-type *S. pombe,* but results in synthetic lethality in a *wee1-50 set2*Δ strain at 35 °C (Figure 2.3). In contrast, no synthetic lethality appeared in a *wee1-50 clr4*Δ strain, in which the H3K9 methyltransferase Clr4 had been deleted. This indicates that cells deficient in methylated H3K36 and not H3K9 were synthetically lethal with loss of Wee1 function.

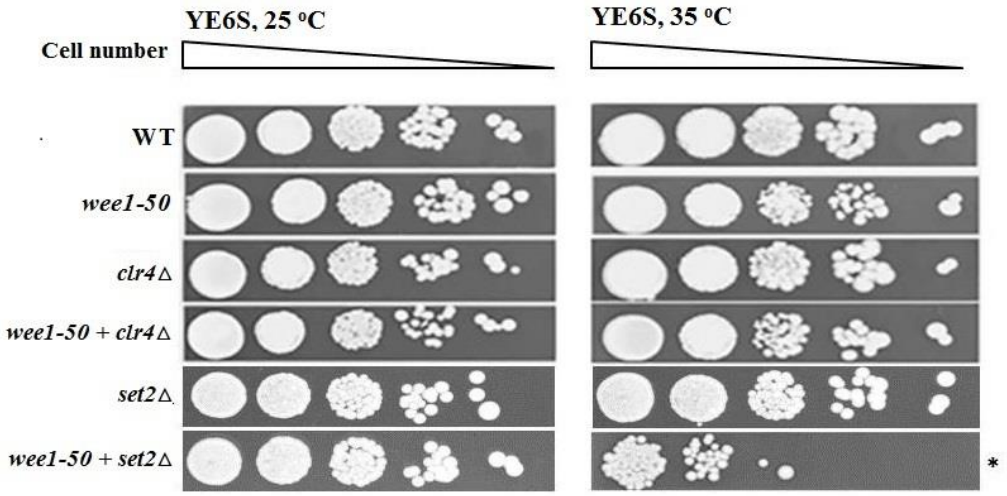

Figure 2.3 Deletion of histone methyltransferases in wild-type and *wee1-50 S. pombe*, 10-fold serial dilutions of wild-type (2094), *wee1-50* (358), *clr4*Δ (3273), *wee1-50*+ *clr4*Δ, *set2* (3271) and *wee1-50*+ *set2*Δ were spotted onto YE6S at 25 or 35 °C. * Indicates decreased cell viability compared to wild-type *S. pombe*.

2.4 Overexpression of human KDMs in *wee1-50* fission yeast

2.4.1 Optimisation of vectors for KDM overexpression

Over recent years, *S. pombe* (fission yeast) has become well-established as an alternative experimental cellular model to *S. cerevisiae* (budding yeast) for studying human genes, in part due to the development of regulatable promoters for controlled gene expression.[179] Of these, the thiamine-repressible *nmt1* (no message in thiamine) promoter is one of the most widely used for gene overexpression studies.[179] In the work described below, the thiamine-regulated pREP series of expression vectors (pREP3X, pREP41X and pREP81X) was used to overexpress human FBXL11 and JMJD2A in fission yeast. The pREP vectors each contain a *nmt1* promoter that has been modified to give increased levels of gene expression (300-fold, 25-fold and seven-fold for the 3X, 41X and 81X promoters, respectively).[180] Expression of a gene under the control of the modified *nmt1* promoter is activated upon removal of thiamine from the growth medium. [179]

It was desirable to produce KDMs in fission yeast with a tag so that the expression levels of each protein could be monitored easily by western blot analysis. Consequently, DNA fragments encoding for full-length JMJD2A and FBXL11 fused to a N-terminal FLAG tag (Asp-Tyr-Lys-Asp-Asp-Asp-Asp-Lys) were amplified by PCR from mammalian expression plasmids (pcDNA3-N-FLAG)[a] and cloned into the pREP3X, pREP41X and pREP81X vectors (Section 6.6.3). Expression vectors encoding catalytically inactive mutants of JMJD2A-H188A and FBXL11-H212A were prepared by site-directed mutagenesis, as were C-terminally truncated variants containing only the JmjC domain (Figure 2.4, Appendix 1). The impact of overexpressing these proteins

[a] pcDNA3-N-FLAG FBXL11 was a kind gift from Robert Klose, Department of Biochemistry, University of Oxford.

on *S. pombe* cell viability was determined by serial dilution growth assays, while the extent of overexpression was established by western blotting.

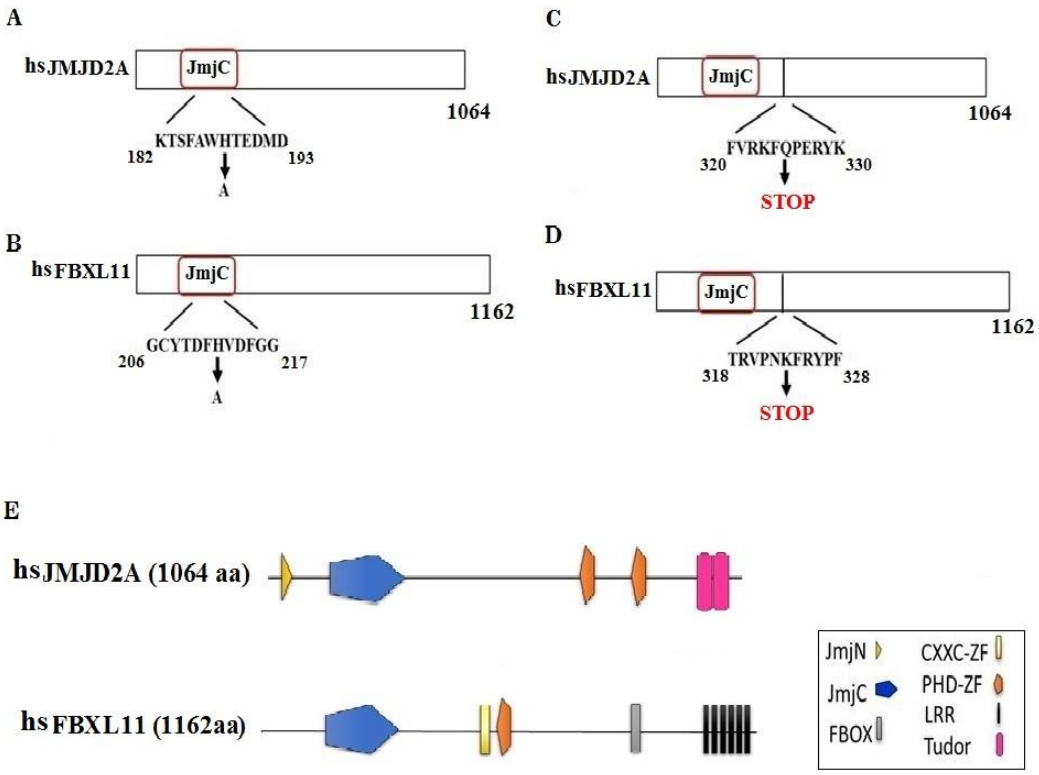

Figure 2.4 KDM constructs used in this work. Sites of mutagenesis for the generation of (A) the H188A variant of hsJMJD2A, (B) the H212A variant of hsFBXL11, (C) C-terminally truncated hsJMJD2A$_{1\text{-}324}$, and (D) C-terminally truncated hsFBXL11$_{1\text{-}322}$. (E) The domain architecture of JMJD2A and FBXL11 proteins. JmjC, Jumonji C domain; PHD, plant homeobox domain; LRR, leucine rich repeats; hs: *Homo sapiens*.

As expected, different levels of overexpression were achieved by use of the pPREP3X, pPREP41X and pPREP81X vectors for both JMJD2A and FBXL11 (Figure 2.5). The serial dilution assays show that overexpression of JMJD2A from the pREP41X or pREP81X vectors had no effect on cell growth. However, decreased cell viability was observed for yeast transformed with the pREP3X construct, correlating with the higher expression levels of JMJD2A observed on the western blot (Figure 2.5A). This observation suggests that high levels of human JMJD2A protein may be toxic to fission yeast. In contrast, the different levels of expression of FBXL11 enabled by the

pREP3X/41X/81X vectors had little influence on cell viability (Figure 2.5B). Consequently, pREP41X and pREP81X were chosen as the optimal vectors for expression of JMJD2A, while all three pREP vectors were deemed suitable for overexpression of FBXL11 in *S. pombe*.

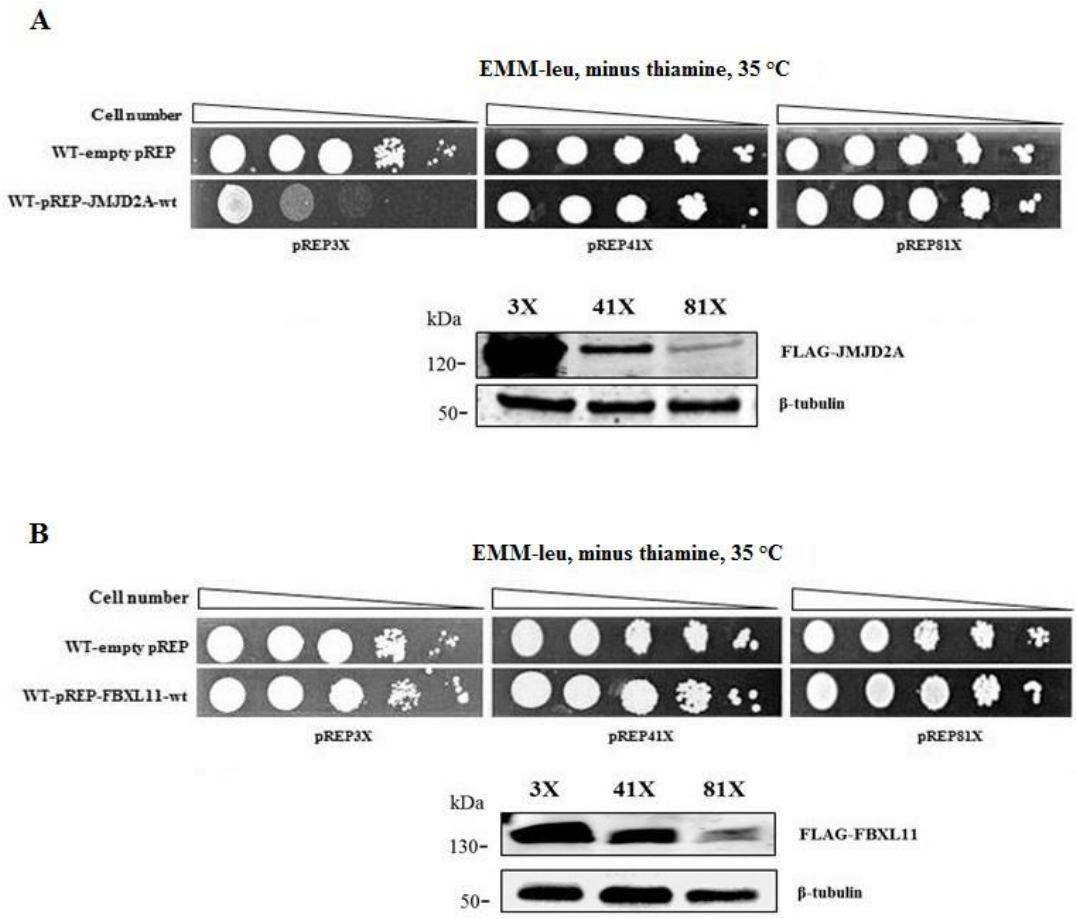

Figure 2.5 Impact of different expression levels for H3K36 demethylases on the cell viability of *S. pombe*. (A) Upper panel: 10-fold serial dilutions of wild-type (2094) transformed with an empty pREP vector or pREP-JMJD2A-wt were spotted onto EMM minus leucine without thiamine at 35 °C. Lower panel: western blot analysis using an anti-FLAG antibody to detect FLAG-JMJD2A in *S. pombe* transformants harboring different pREP3X-, pREP41X- and pREP81X-JMJD2A expression plasmids. (B) Upper panel: 10-fold serial dilutions of wild-type (2094) transformed with an empty pREP vector or pREP-FBXL11-wt were spotted onto EMM minus leucine without thiamine and grown at 35 °C. Lower panel: western blot analysis using an anti-FLAG antibody to detect FLAG-FBXL11 in *S. pombe* transformants harboring different pREP3X-, pREP41X- and pREP81X-FBXL11 expression plasmids Leucine is used as a selection marker and thiamine represses KDM expression. *wee1-50* cells grown at 35 °C presented the mutant phenotype. Antibodies are listed in Section 6.8. The results were reproduced in at least two independent experiments.

2.4.2 Overexpression of JMJD2A

To avoid toxicity associated with protein overexpression, the pREP41X and pREP81X constructs were used to overexpress FLAG-tagged JMJD2A in wild-type *S. pombe* or in the *wee1*-50 mutant strain. Expression of JMJD2A was modulated by the presence of thiamine in the growth medium. Using the pREP41X vector, overexpression of JMJD2A in wild-type cells at 25 or 35 °C was observed to have no impact on cell survival when compared to wild-type cells transformed with the corresponding empty vector (Figure 2.6). In the *wee1-50* strain, overexpression of wild-type JMJD2A led to decreased viability at 35 °C compared to growth in the absence of the *wee1-50* phenotype at 25 °C. This observation suggests that overexpression of JMJD2A is synthetically lethal when coupled with loss of Wee1 function. However, decreased cell viability was also observed at 35 °C in *wee1-50* cells overexpressing the H188A variant of JMJD2A, which is predicted to be catalytically inactive.[181] These findings could be explained if there was partial retention of activity by the H188A mutant or if overexpression of this inactive protein functioned as a dominant negative mutant. Alternatively, it is possible that the effects of JMJD2A on *wee1-50* yeast are mediated independently of its demethylase activity (i.e. by binding or via a domain other than the JmjC demethylase domain). Similar results were observed in the pREP81X experiments (Figure 2.7), except that less of an impact on cell viability was observed for the overexpression of JMJD2A (wt or H188A) when combined with the *wee1-50* mutation at 35 °C.

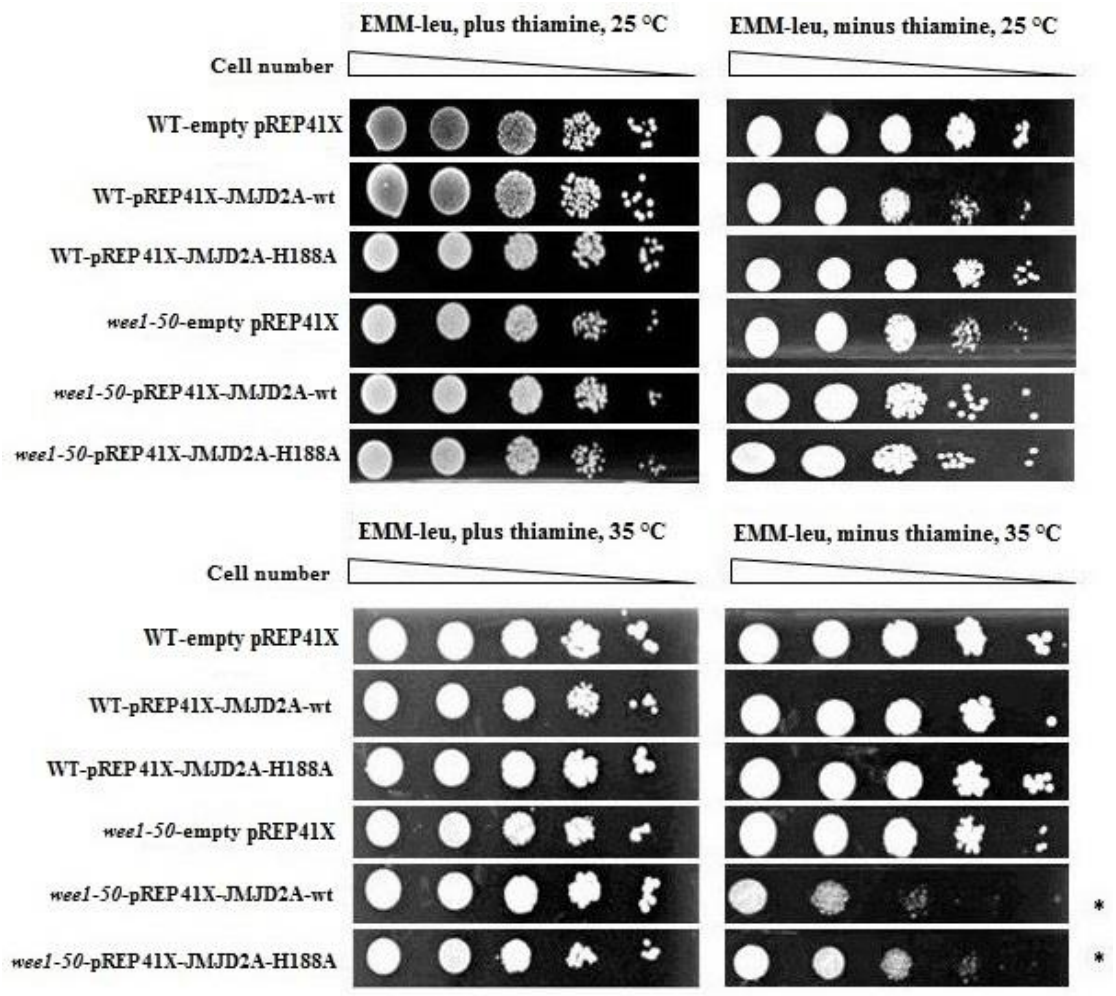

Figure 2.6 Impact of JMJD2A overexpression on wild-type and *wee1-50 S. pombe* viability. 10-fold serial dilutions of wild-type *S. pombe* (2094; transformed with an empty vector pREP41X, pREP41X-JMJD2A-wt, or pREP41X-JMJD2A-H188A) and *wee1-50 S. pombe* (358; transformed with an empty vector pREP41X, pREP41X-JMJD2A-wt, or pREP41X-JMJD2A-H188A) were spotted onto EMM minus leucine + 5 μg/mL thiamine as a loading control, and onto EMM minus leucine without thiamine at 25 °C or 35 °C. Leucine is used as a selection marker and thiamine represses KDM expression. *wee1-50* cells grown at 35 °C presented the mutant phenotype. * Indicates decreased cell viability when compared to wild-type or *wee1-50 S. pombe* transformed with an empty vector. The results were reproduced in at least two independent experiments.

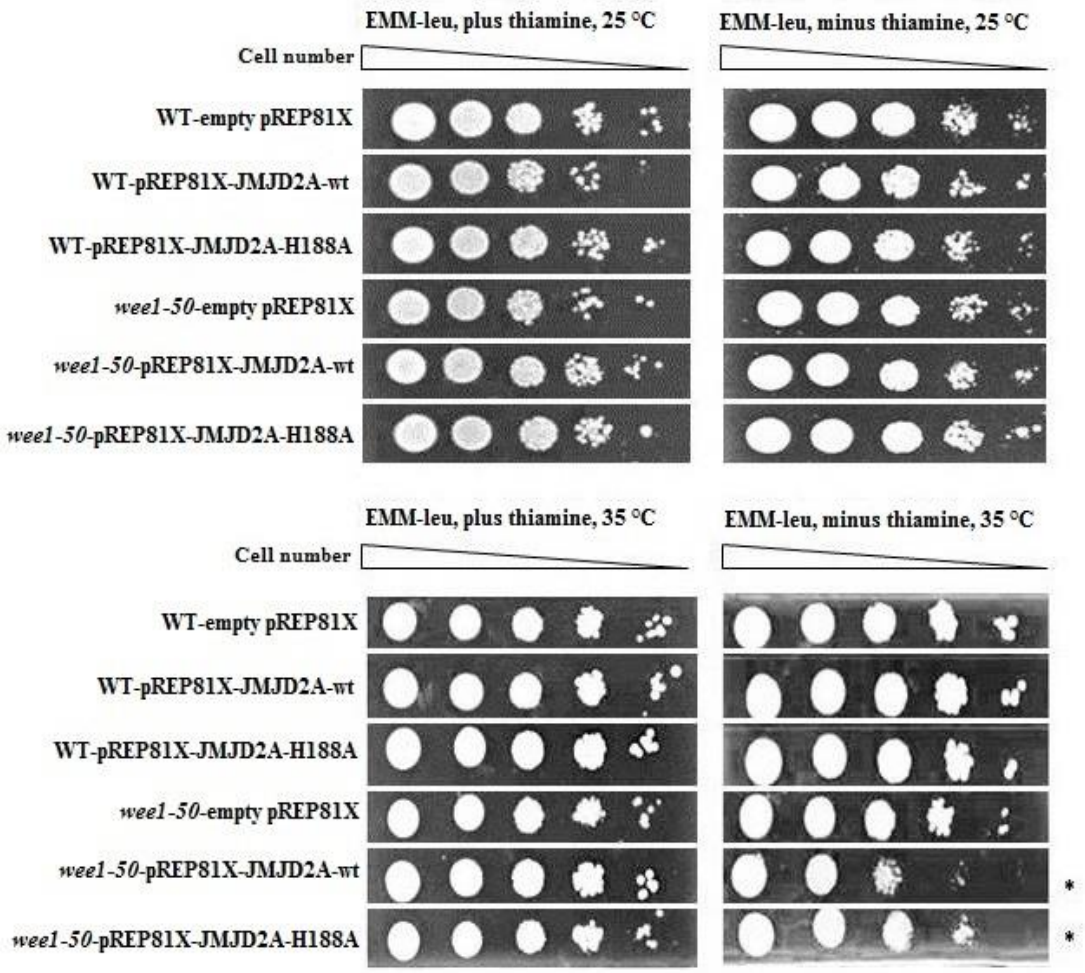

Figure 2.7 Impact of JMJD2A overexpression on wild-type and *wee1-50 S. pombe* viability. 10-fold serial dilutions of wild-type *S. pombe* (2094; transformed with an empty vector pREP81X, pREP81X-JMJD2A-wt, or pREP81X-JMJD2A-H188A) and *wee1-50 S. pombe* (358; transformed with an empty vector pREP81X, pREP81X-JMJD2A-wt, or pREP81X-JMJD2A-H188A) were spotted onto EMM minus leucine + 5 μg/mL thiamine as a loading control, and onto EMM minus leucine without thiamine at 25 °C or 35 °C. Leucine is used as a selection marker and thiamine represses KDM expression. *wee1-50* cells grown at 35 °C presented the mutant phenotype. * Indicates decreased cell viability when compared to wild-type or *wee1-50 S. pombe* transformed with an empty vector. The results were reproduced in at least two independent experiments.

To investigate the role of histone H3K36 modifications in the synthetic lethality observed for JMJD2A gene overexpression and *wee1-50* mutation, western blot analyses were performed on lysates from wild-type cells overexpressing FLAG-tagged JMJD2A (Figure 2.8). JMJD2A proteins were expressed in cells using the pREP41X construct; similar levels of expression were observed for the wild-type protein and the H188A variant, and no JMJD2A was detected in cells transformed with the empty vector.

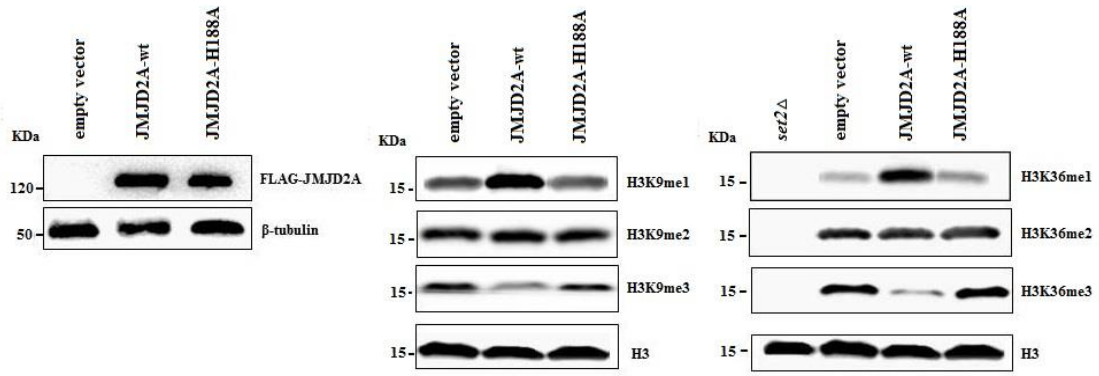

Figure 2.8 Western blot analyses. Expression levels of FLAG-JMJD2A, mono-, di-, and trimethylated H3K9 and H3K36 in wild-type (WT) cells containing pREP41X-empty vector, pREP41X-JMJD2A-wt, pREP41X-JMJD2A-H188A and *set2*Δcells. β-tubulin and H3 were shown as loading controls. Antibodies are listed in Section 6.8. The results were reproduced in at least two independent experiments.

No H3K36me3 was detected in *set2*Δ cells, suggesting a complete requirement of Set2 for H3K36 tri-methylation in fission yeast, consistent with literature reports.[182] Significantly reduced levels of H3K36me3 and H3K9me3 were observed in cells overexpressing wild-type JMJD2A, whereas overexpression of the H188A variant had no obvious impact on the levels of these marks compared to the empty vector control. These data suggest that mutation of the catalytic histidine residue within the JmjC domain (H188A) of JMJD2A does inactivate its demethylase activity, consistent with previous reports.[183] While overexpression of the H188A variant of JMJD2A did not alter the levels of H3K36me3, it did cause a decrease in the viability of *wee1-50* cells

as observed in the serial dilution assays (Figures 2.6 and 2.7). Thus, it might act as a dominant negative mutant that causes cell death above a threshold level. Although the H188A variant does not catalyse demethylation of H3K36me3, it might bind to the methylated H3K36 substrate and block the site from being demethylated by an endogenous H3K36me3 demethylase.

2.4.3 Overexpression of FBXL11

Consistent with previous experiments (Figure 2.5), overexpression of FLAG-tagged FBXL11 using the pREP3X vector had no effect on the viability of wild-type cells compared to the empty vector control (Figure 2.9). Decreased cell viability was observed in *wee1-50* cells overexpressing wildtype FBXL11 at 35 °C, compared to 25 °C. However, no change in cell viability was observed with overexpression of the catalytically inactive H212A variant of FBXL11 in the presence of the *wee1-50* phenotype.[172] Similar results were observed in experiments using pREP41X, although less of an impact on cell viability was observed in *wee1-50* cells overexpressing wild-type FBXL11 (Figure 2.10). There was no difference in growth between wild-type cells and *wee1-50* cells overexpressing FBXL11 from pREP81X (Figure 2.11). This is likely due to the expression levels of FBXL11 from the 81X promoter (Figure 2.5), which may be too low to have a detectable impact on cell viability in *wee1-50* cells.

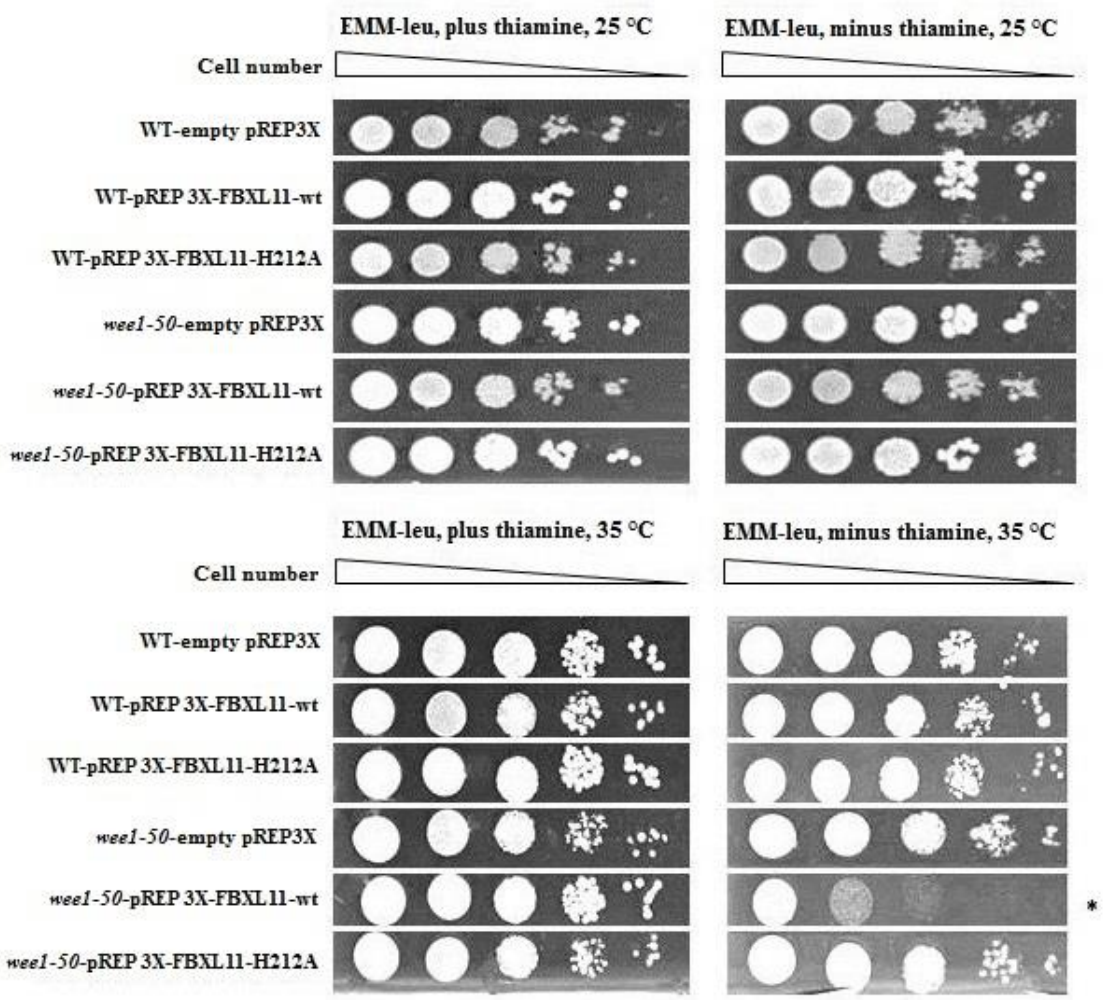

Figure 2.9 Impact of FBXL11 overexpression on wild-type and *wee1-50 S. pombe* viability. 10-fold serial dilutions of wild-type (2094; transformed with an empty vector pREP3X, pREP3X-FBXL11-wt, or pREP3X-FBXL11-H212A) and *wee1-50* (358; transformed with an empty vector pREP3X, pREP3X-FBXL11-wt, or pREP3X-FBXL11-H212A) *S. pombe* were spotted onto EMM minus leucine + 5 μg/mL thiamine as a loading control, and onto EMM minus leucine without thiamine at 25 °C or 35 °C. Leucine is used as a selection marker and thiamine represses KDM expression. *wee1-50* cells grown at 35 °C presented the mutant phenotype. * Indicates decreased cell viability when compared to wild-type or *wee1-50 S. pombe* transformed with an empty vector. The results were reproduced in at least two independent experiments.

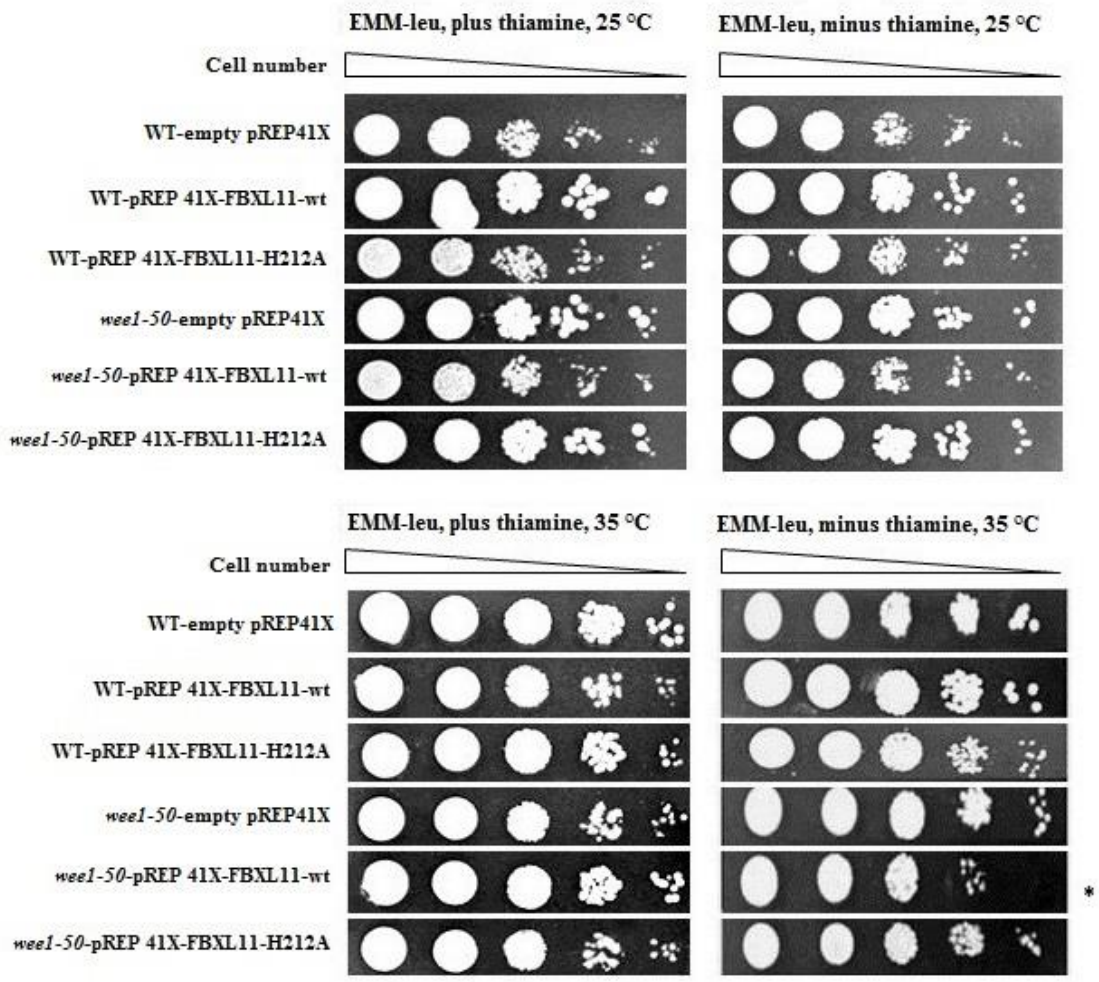

Figure 2.10 Impact of FBXL11 overexpression on wild-type and *wee1-50 S. pombe* viability. 10-fold serial dilutions of wild-type (2094; transformed with an empty vector pREP41X, pREP41X-FBXL11-wt, or pREP41X-FBXL11-H212A) and *wee1-50* (358; transformed with an empty vector pREP41X, pREP41X-FBXL11-wt, or pREP41X-FBXL11-H212A) *S. pombe* were spotted onto EMM minus leucine + 5 μg/mL thiamine as a loading control, and onto EMM minus leucine without thiamine at 25 °C or 35 °C. Leucine is used as a selection marker and thiamine represses KDM expression. *wee1-50* cells grown at 35 °C presented the mutant phenotype. * Indicates decreased cell viability when compared to wild-type or *wee1-50 S. pombe* transformed with an empty vector. The results were reproduced in at least two independent experiments.

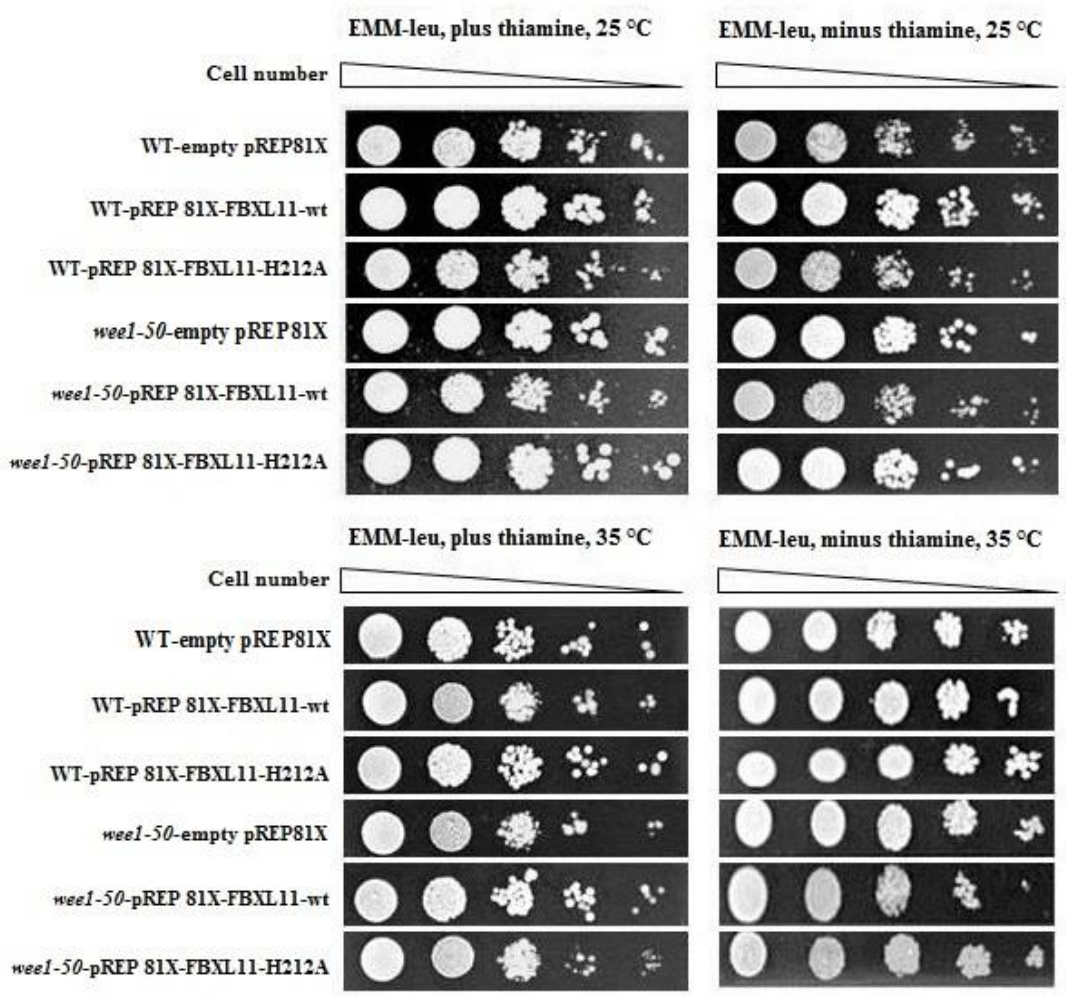

Figure 2.11 Impact of FBXL11 overexpression on wild-type and *wee1-50 S. pombe* viability. 10-fold serial dilutions of wild-type (2094; transformed with an empty vector pREP81X, pREP81X-FBXL11-wt, or pREP81X-FBXL11-H212A) and *wee1-50* (358; transformed with an empty vector pREP81X, pREP81X-FBXL11-wt, or pREP81X-FBXL11-H212A) *S. pombe* were spotted onto EMM minus leucine + 5 μg/mL thiamine as a loading control, and onto EMM minus leucine without thiamine at 25 °C or 35 °C. Leucine is used as a selection marker and thiamine represses KDM expression. *wee1-50* cells grown at 35 °C presented the mutant phenotype. The results were reproduced in at least two independent experiments.

To investigate the role of H3K36 methylation status on the synthetic lethality of FBXL11 overexpression when combined with *wee1-50*, western blot analyses were carried out on lysates from wild-type cells overexpressing FLAG-tagged FBXL11 (Figure 2.12). FBXL11 proteins were expressed in cells using the pREP3X construct; similar levels of expression were observed for the wild-type protein and H212A variant, and no FBXL11 was detected in cells transformed with the empty vector.

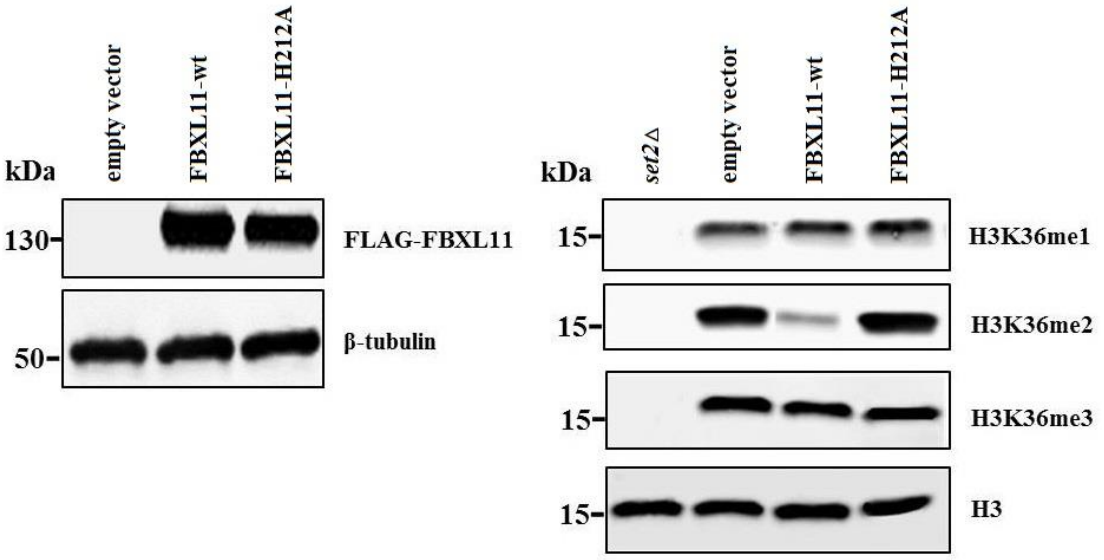

Figure 2.12 Western blot analyses. Expression levels of FLAG-FBXL11, H3K36me1, H3K36me2 and H3K36me3 in wild-type cells containing pREP3X-empty vector, pREP3X-FBXL11-wt, pREP3X-FBXL11-H212A and *set2*Δcells. β-tubulin and H3 were used as loading controls. Antibodies are listed in Section 6.8. The results were reproduced in at least two independent experiments.

Overexpression of wild-type FBLX11 had no impact on the levels of H3K36me3, but led to reduced levels of H3K36me2 (Figure 2.12), consistent with reports that FBXL11 catalyses demethylation of H3K36me2 to H3K36me1.[172] No changes in the levels of H3K36me3, H3K36me2 and H3K36me1 were observed in cells overexpressing the H212A mutant compared with wild-type cells, suggesting that this mutation has abolished demethylase activity.[172]

2.5 Importance of structural domains in JmjC KDMs

JMJD2A and FBXL11 belong to the JmjC family of histone KDMs.[94] As described in Section 1.5, the JmjC domain is structurally conserved in this family of KDMs and contains the essential residues for binding 2-OG and Fe(II), which are required to catalyse demethylation of methyllysine residues. JmjC KDMs contain other structural domains in addition to the catalytic JmjC domain. For JMJD2A these include a JmjN domain, two PHD fingers and two Tudor domains (Figure 2.4E). Similarly, FBXL11 contains a CxxC zinc finger, a PHD zinc finger, an F-box, and six leucine-rich repeat (LRR) domains (Figure 2.4E).

Truncated expression constructs for JMJD2A (residues 1-324) and FBXL11 (residues 1-322) were generated to investigate the importance of the JmjC domain in mediating the observed synthetic lethality with *wee1-50* in *S. pombe*. Since the JmjC domain is located near the N-terminus in both proteins, constructs containing the JmjC domain alone were generated using site-directed mutagenesis to insert a stop codon shortly after the end of the JmjC domain (Figure 2.4). The resultant constructs, containing the JmjN and JmjC domains but no other structural domains, were overexpressed in wild-type and *wee1-50* fission yeast to look for synthetic lethality. Overexpression of $JMJD2A_{1-324}$ and $FBXL11_{1-322}$ was carried out using the pREP41X and pREP3X vectors, respectively.

Neither of the truncated constructs, $JMJD2A_{1-324}$ or $FBXL11_{1-322}$, show synthetic lethality with loss of Wee1 function (Figures 2.13 and 2.14, respectively), whereas the full-length proteins were synthetically lethal. However, western blot analyses of wild-type cell lysates overexpressing FLAG-tagged $JMJD2A_{1-324}$ or $FBXL11_{1-322}$ proteins revealed a loss of demethylase activity for both proteins (Figure 2.15).

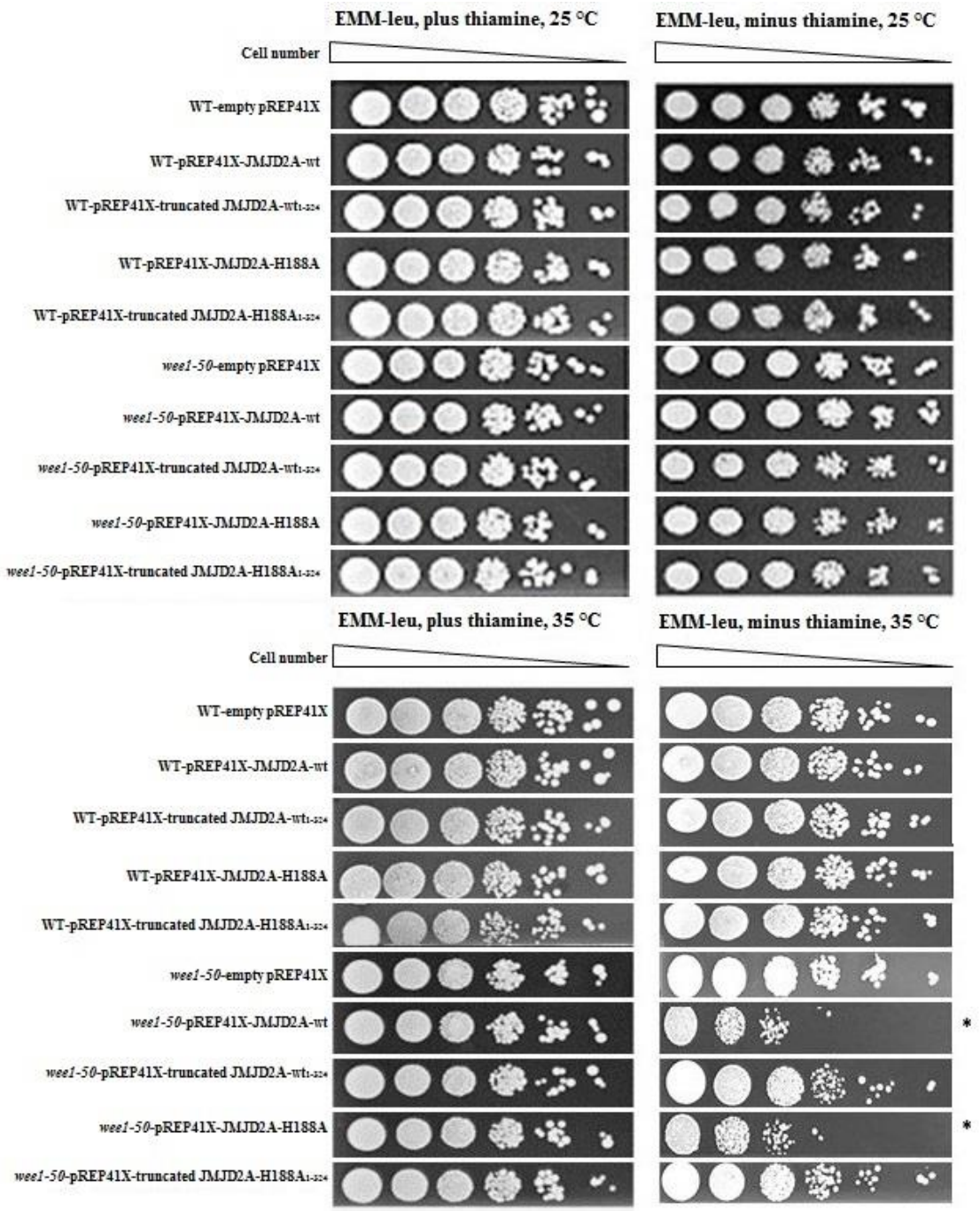

Figure 2.13 Impact of JMJD2A overexpression on wild-type and *wee1-50 S. pombe* viability. 10-fold serial dilutions of wild-type (2094; transformed with an expressing empty vector pREP41X, pREP41X-JMJD2A-wt, pREP41X-truncated JMJD2A-wt_{1-324}, pREP41X-JMJD2A-H188A or pREP41X-truncated JMJD2A-$H188A_{1-324}$) and *wee1-50* (358; transformed with an empty vector pREP41X, pREP41X-JMJD2A-wt, pREP41X-truncated JMJD2A-wt_{1-324}, pREP41X-JMJD2A-H188A or pREP41X-truncated JMJD2A-$H188A_{1-324}$) were spotted onto EMM minus leucine + 5 μg/mL thiamine as a loading control, and onto EMM minus leucine without thiamine at 25 °C or 35 °C. Leucine is used as a selection marker and thiamine represses KDM expression. *wee1-50* cells grown at 35 °C presented the mutant phenotype. * Indicates decreased cell viability compared to wild-type or *wee1-50 S. pombe* transformed with an empty vector. The results were reproduced in at least two independent experiments.

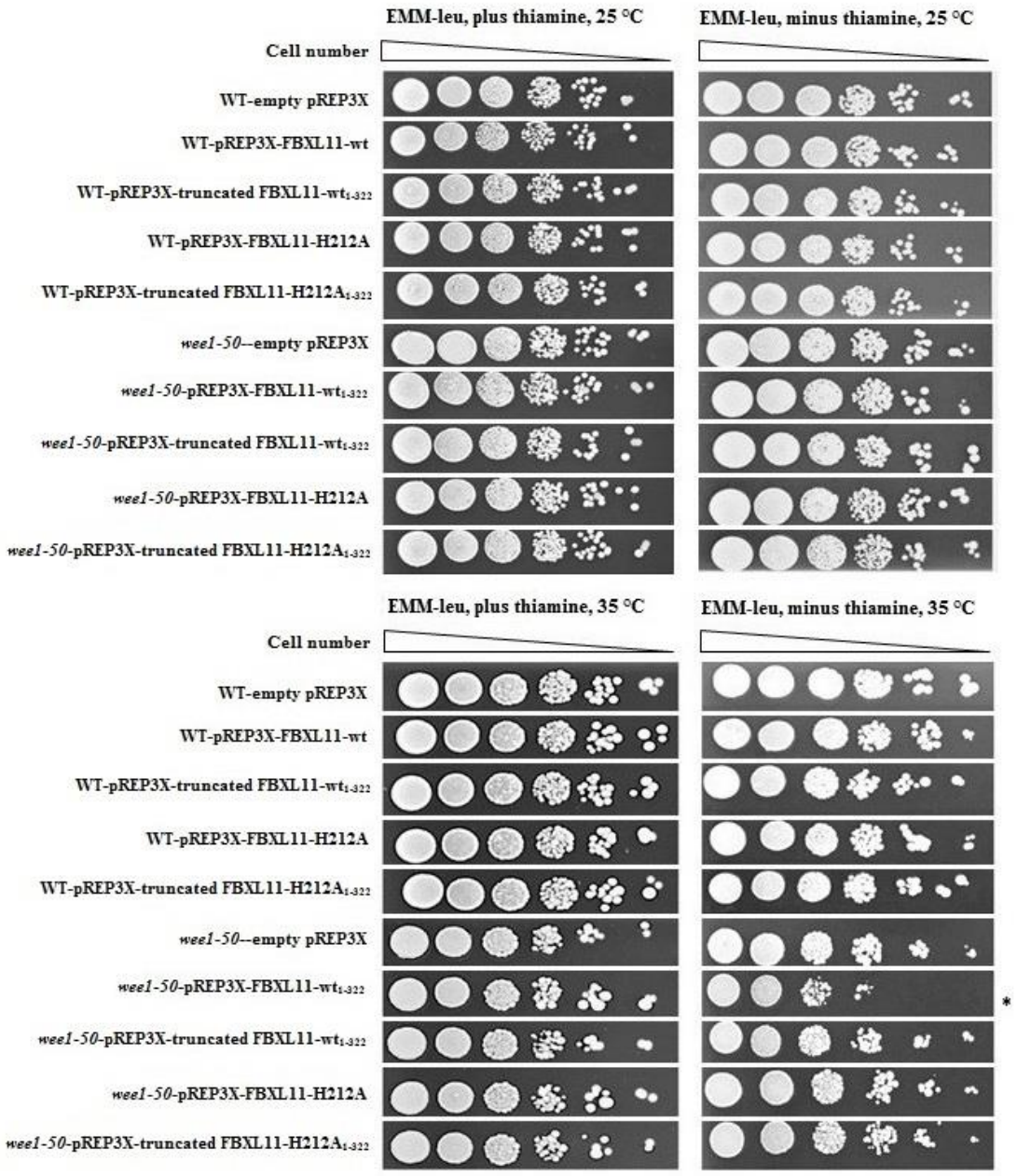

Figure 2.14 Impact of FBXL11 overexpression on wild-type and *wee1-50 S. pombe* viability. 10-fold serial dilutions of wild-type (2094; transformed with an expressing empty vector pREP3X, pREP3X- FBXL11-wt, pREP3X-truncated FBXL11-wt$_{1-322}$, pREP3X- FBXL11-H212A or pREP3X-truncated FBXL11-H212A$_{1-322}$) and *wee1-50* (358; transformed with an empty vector pREP3X, pREP3X- FBXL11-wt, pREP3X-truncated FBXL11-wt$_{1-322}$, pREP3X-FBXL11-H212A or pREP3X-truncated FBXL11-H212A$_{1-322}$) were spotted onto EMM minus leucine + 5 μg/mL thiamine as a loading control, and onto EMM minus leucine without thiamine at 25 °C or 35 °C. Leucine is used as a selection marker and thiamine represses KDM expression. *wee1-50* cells grown at 35 °C presented the mutant phenotype. * Indicates decreased cell viability compared to wild-type or *wee1-50 S. pombe* transformed with an empty vector. The results were reproduced in at least two independent experiments.

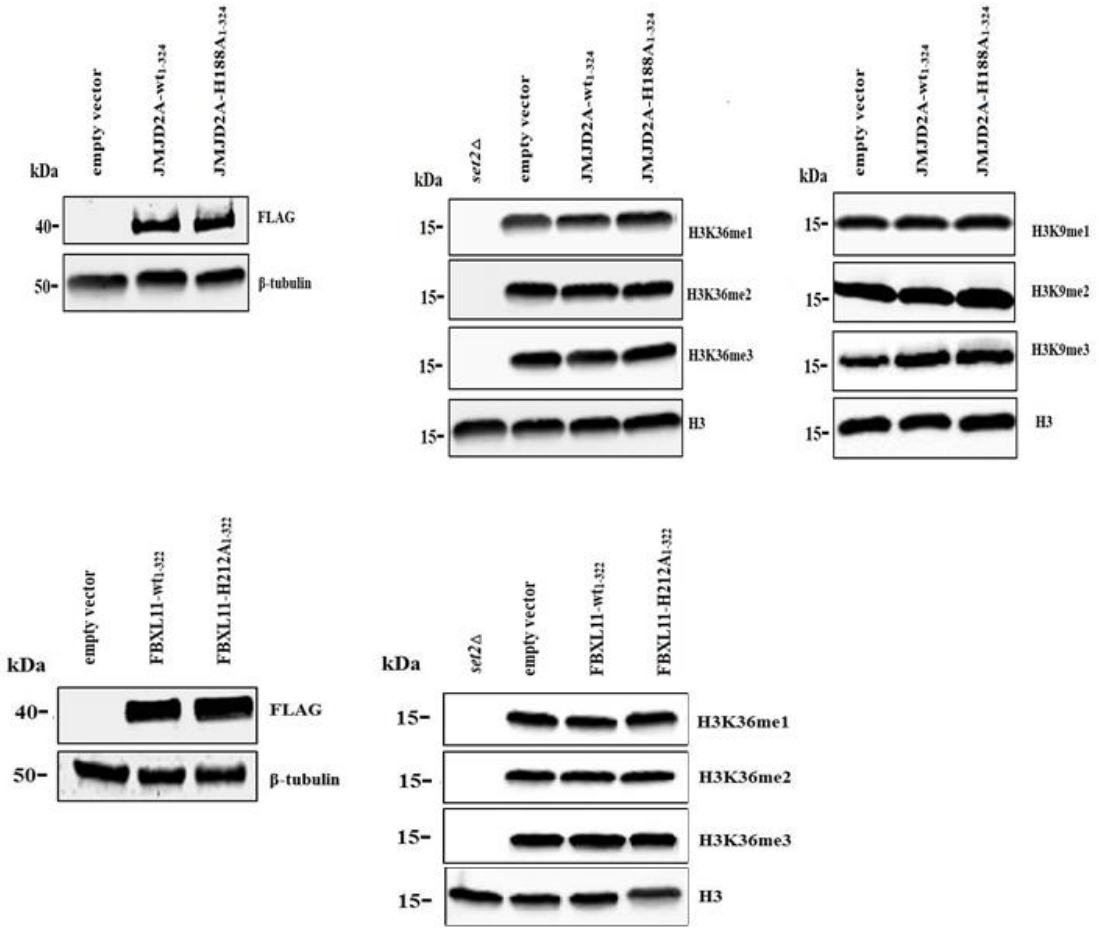

Figure 2.15 Western blot analyses of wild-type *S. pombe* cell lysates overexpressing the JmjC domains of JMJD2A or FBXL11. Upper panel: Expression levels of FLAG-JMJD2A$_{1-324}$, mono-, di-, and trimethylated H3K9 and H3K36 in wild-type cells containing pREP41X-empty vector, pREP41X-JMJD2A-wt$_{1-324}$, pREP41XJMJD2A-H188A$_{1-324}$ and *set2*Δcells. Lower panel: Expression levels of FLAG-FBXL11$_{1-322}$, and analysis of mono-, di-, and trimethylated H3K36 in wild-type cells containing pREP41X, pREP41X-FBXL11-wt$_{1-322}$, pREP41X-FBXL11-H212A$_{1-322}$ and *set2*Δ cells. β-tubulin and H3 were used as loading controls. Antibodies are listed in Section 6.8. The results were reproduced in at least two independent experiments.

While it is likely that histone demethylase activity is required for synthetic lethality of KDMs with *wee1-50*, it is also possible that the previously observed effects are mediated by domains other than the JmjC domain, which are not present in the truncated constructs.

2.6 A potential role for H3K36 demethylases in nucleotide depletion

2.6.1 Background

As described in Section 2.1.4, recent work by the Humphrey group has shown that the methyltransferase Set2 regulates the transcription of genes involved in nucleotide synthesis. Set2-catalysed trimethylation at H3K36 has been proposed to activate expression of *cdc22*, a subunit of ribonucleotide reductase (RNR), leading to increased dNTP synthesis. Thus, inhibition or deletion of Set2 (such as in *set2Δ* fission yeast) leads to a decrease in the nucleotide pool due to increase expression (and activity) of RNR. Nucleotide depletion resulting from set2 deletion alone is not sufficient to cause cell-lethality; however, when combined with other mutations that deplete the nucleotide pool (e.g. *wee1-50*), synthetic lethality is observed.

The fission yeast protein Spd1 functions as an endogenous inhibitor of RNR and regulates dNTP levels during the cell cycle.[184] Interestingly, deletion of Spd1 was found to rescue the synthetic lethality of the *set2*Δ and *wee1-50* mutation, providing further support to the hypothesis that the *set2*Δ/*wee1-50* synthetic lethality is caused by over-depletion of the nucleotide pool.

The following section describes studies on the role of H3K36 demethylases (JMJD2A and FBXL11) on the regulation of RNR. Overexpression of KDMs was carried out in *wee1-50* combined with *spd1* deletion strains to test whether spd1 deletion could rescue the cell death phenotype arising from the combined KDM overexpression and *wee1-50* mutation. This would suggest that the synthetic lethality with *wee1-50* caused by KDM overexpression, like *set2* deletion, resulted from reduced dNTP pools.

2.6.2 Results

Overexpression of JMJD2A was carried out using the pREP41X vector in *S. pombe* carrying the *wee1-50* mutation as well as the spd1 deletion (*wee1-50, spd1*Δ cells). As expected, overexpression of wild-type JMJD2A induced synthetic lethality in *wee1-50* cells, whereas increased cell viability was observed in *wee1-50*, *spd1*Δ cells overexpressing JMJD2A, indicating that *spd1* deletion rescues the lethality of JMJD2A overexpression in *wee1-50* mutant (Figure 2.16). Overexpression of the catalytically inactive H188A variant of JMJD2A caused synthetic lethality in *wee1-50,* but no rescue of this phenotype was observed in *wee1-50, spd1*Δ cells. This suggests that the cell death observed following overexpression of JMJD2A-H188A in a *wee1-50* background is independent of reduced dNTP levels, and is thus likely to have arisen through an independent mechanism. In this respect, the H188A variant could be behaving as a dominant negative mutant.

Overexpression of FBXL11 was also carried out in *wee1-50, spd1*Δ cells. The pREP3X vector was chosen for FBXL11 expression as it provided a significant and reliable result, as described earlier (Figure 2.5). As expected, overexpression of FBXL11 resulted in synthetic lethality with *wee1-50* mutant, whereas increased cell viability was observed in the *wee1-50*, *spd1*Δ double mutant overexpressing FBXL11 (Figure 2.17). Taken together, these findings support the proposal that deletion of *spd1* maintains RNR activity and offsets the low RNR expression caused by human H3K36 demethylase overexpression. It is therefore able to suppress synthetic lethality of H3K36 demethylase overexpression in a *wee1-50* mutant (Figure 2.18).

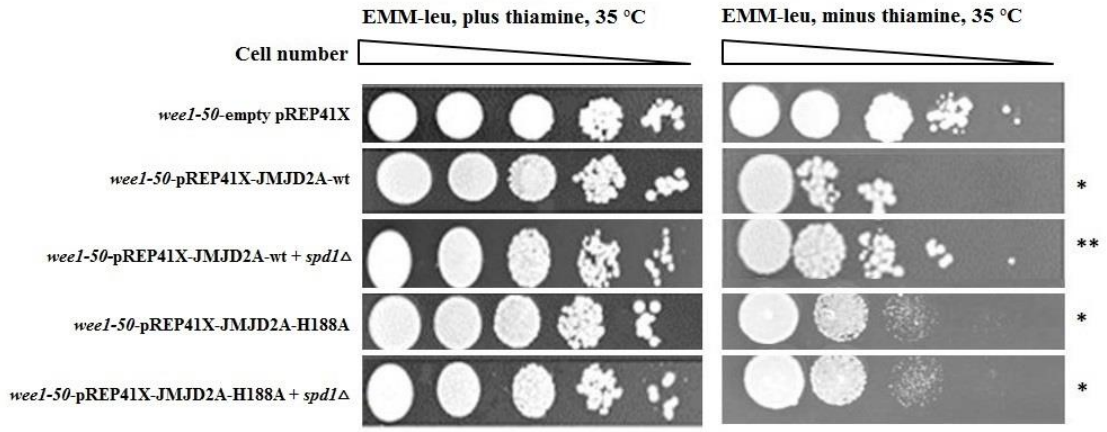

Figure 2.16 Impact of JMJD2A overexpression on the viability of *wee1-50 S. pombe* with/ without *spd1* deletion. 10-fold serial dilutions of *wee1-50* (358; transformed with an empty vector pREP41X, pREP41X-JMJD2A or pREP41X-JMJD2A-H188A) and *wee1-50* with *spd1* deletion (7972; transformed with an pREP41X-JMJD2A or pREP41X-JMJD2A-H188A) were spotted onto EMM minus leucine + 5 μg/mL thiamine and EMM minus leucine without thiamine at 35 ºC. Leucine is used as a selection marker and thiamine represses KDM expression. *wee1-50* cells grown at 35 °C presented the mutant phenotype. * Indicates decreased cell viability compared to *wee1-50* with an empty vector. ** Indicates *spd1* deletion rescues the lethality of JMJD2A-wt overexpression in *wee1-50* mutant.

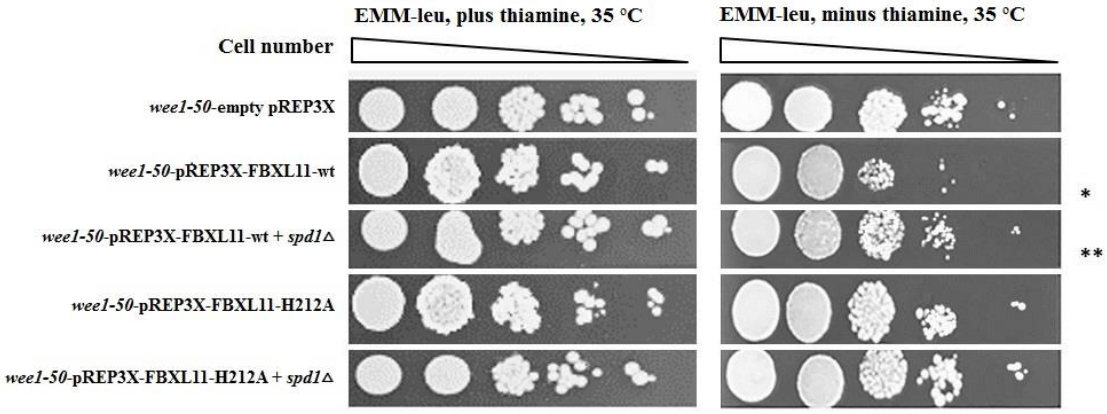

Figure 2.17 Impact of FBXL11 overexpression on the viability of *wee1-50 S. pombe* with/ without *spd1* deletion.10-fold serial dilutions of *wee1-50* (358; transformed with an empty vector pREP3X, pREP3X-FBXL11 or pREP3X-FBXL11-H212A) and *wee1-50* with *spd1* deletion (7972; transformed with an pREP3X-FBXL11 or pREP3X-FBXL11-H212A) were spotted onto EMM minus leucine + 5 μg/mL thiamine and EMM minus leucine without thiamine at 35 ºC. Leucine is used as a selection marker and thiamine represses KDM expression. *wee1-50* cells grown at 35 °C presented the mutant phenotype. * Indicates decreased cell viability compared to *wee1-50* with an empty vector. ** Indicates *spd1* deletion rescues the lethality of FBXL11-wt overexpression in *wee1-50* mutant.

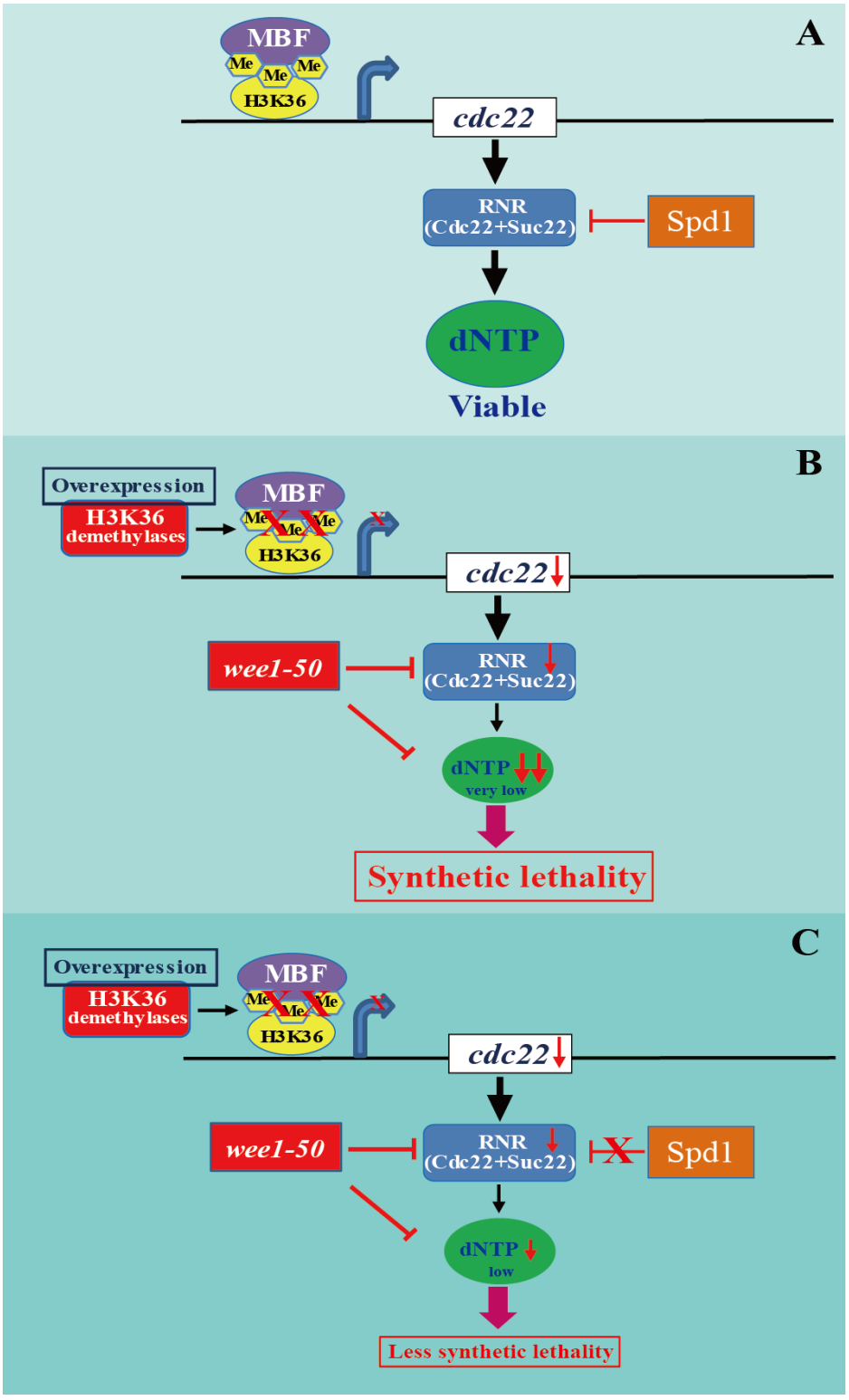

Figure 2.18 A model for synthetic lethality caused by human H3K36 demethylases (JMJD2A/FBXL11) overexpression and *wee1-50* mutant in fission yeast. (A) The role of H3K36me3/2 in RNR expression through MBF-induced gene regulation. RNR activity is inhibited by the Spd1 protein. The dynamic balance is maintained for cell growth during the cell cycle. (B) Overexpression of human H3K36 demethylases results in low levels of RNR and a decrease in the dNTP pool. *wee1-50* causes the depletion of dNTP. Both occurred and induced synthetic lethality. (C) Starvation of dNTP is alleviated by *spd1* deletion and the level of synthetic lethality is decreased.

2.7 Investigation of a putative KDM from fission yeast - Jmj3

The *S. pombe* protein Jmj3 has been assigned as a homologue of human JMJD2 (KDM4) and is proposed to have histone demethylase activity on H3K36 based on sequence orthology.[174] In this work, the putative demethylase activity of Jmj3 was investigated through overexpression in fission yeast using the pREP3X vector.

2.7.1 Sequence analysis and domain architecture of Jmj3

Bioinformatic and phylogenetic analyses imply that orthologues of the KMD4 family of JmjC demethylases exist in organisms ranging from yeast to humans.[94] In humans, JMJD2A/2B proteins contain JmjN, PHD-ZF, and Tudor domains besides the JmjC domain, whereas JMJD2D/2E proteins are shorter and lack the PHD-ZF and Tudor domains present in the C-terminal region of JMJD2A. In fission yeast, the Jmj3 protein contains only the JmjN and JmjC domains (Figure 2.19A). The budding yeast homologue, Rph1, contains the conserved iron and 2OG binding residues found in the human enzymes, and has been shown to have histone demethylase activity on tri- and dimethylated H3K36 *in vitro* and *in vivo*.[185] Another KDM4 homologue in budding yeast, Gis1, has a tyrosine residue (Tyr292) in place of the second conserved histidine in the iron-binding triad; accordingly, Gis1 does not have histone demethylase activity (Figure 2.19B). Comparison of the Jmj3 sequence with that of other KDM4 family members reveals that an arginine residue (Arg 213) substitutes for the first histidine of the iron-binding triad, and two leucine residues (Leu 210 and Leu 231) replace conserved residues in the 2-OG binding site. These changes in critical residues are likely to prevent demethylase activity of Jmj3 (at least via the normal mechanism for JmjC demethylase catalysis).

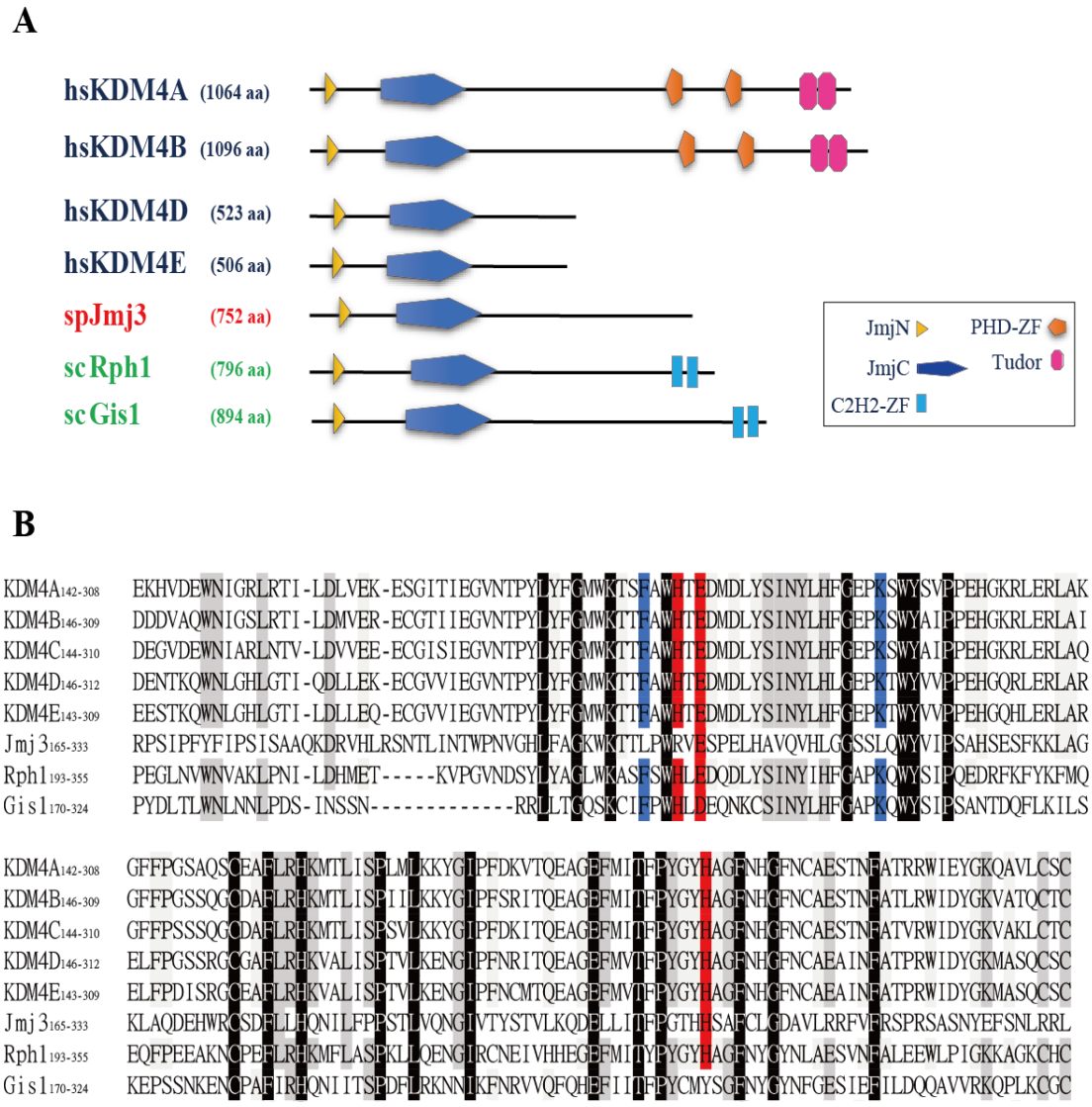

Figure 2.19 The KDM4 family proteins. (A) Diagrammatic representation of domains in KDM4 orthologues from humans and yeast. All family members contain a JmjC (Jumonji C) and JmjN (Jumonji N) domain. Members of this group contain additional C-terminal domains, including PHD-ZF, Tudor or C2H2-ZF domains. (B)The JmjC domains of KDM family members have conserved residues involved in Fe (II)-binding (red) and 2OG-binding site (blue). The fission yeast protein, Jmj3, has an arginine residue (Arg 213) in place of the first conserved histidine of the iron-binding triad and two leucine residues (Leu 210 and Leu 231) instead of the conserved residues of the 2-OG binding site. The budding yeast enzyme, Gis1, has a tyrosine residue (Tyr292) instead of the conserved histidine at the third position of the typical iron-binding triad. Residues that are highly conserved in organisms, are highlighted in black and grey. hs*: Homo sapiens,* sc*: Saccharomyces cerevisiae and* sp*: Schizosaccharomyces pombe*.

2.7.2 Analysis of Jmj3 activity in fission yeast

To investigate the putative H3K36 demethylase activity of Jmj3, the full-length protein was overexpressed in wild-type *S. pombe* cells using a pREP3X-Jmj3 plasmid (kindly provided by the Humphrey Laboratory). Serial dilution assays show overexpression of Jmj3 decreased cell viability in wild-type cells (Figure 2.20); similar effects were observed when the human Jmj3 homologue, JMJD2A, was overexpressed from the pREP3X plasmid (Figure 2.5). Next, western blotting was performed on cell-lysates to determine whether there is any change in the H3K36 methylation status when Jmj3 is overexpressed. As predicted from the sequence analysis described above, no demethylase activity was evident. There were no apparent changes in the levels of H3K36me3, H3K36me2 or H3K9me3 in Jmj3-overexpressing cells compared to the empty vector control (Figure 2.21). These findings indicate that Jmj3 is unlikely to be a functional orthologue of human KDM4, and may have an alternative function in *S. pombe.*

There was some concern regarding the validity of the western blotting results given the growth defects observed as a result of Jmj3 overexpression. The slow growth and inadequate levels of protein expression in cells expressing full-length Jmj3 made it difficult to reliably observe changes in the methylation status of H3K36. Attempts were made to produce recombinant Jmj3 protein in *E. coli* so that its demethylase activity could be investigated on histone peptides using an *in vitro* demethylase assay. However, despite extensive efforts to optimize expression conditions (e.g. use of different expression vectors, solubility tags, induction conditions etc.), no soluble Jmj3 protein was able to be produced.

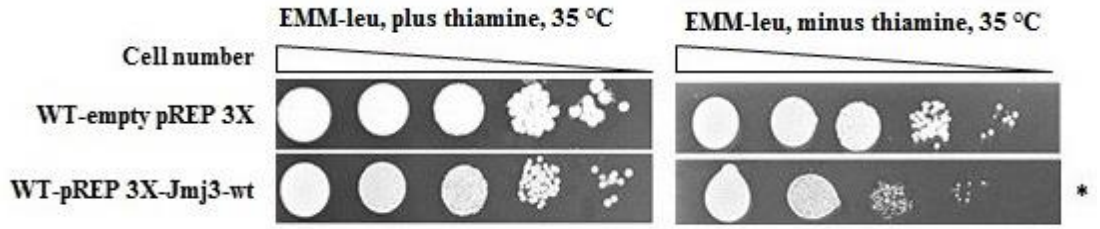

Figure 2.20 Effects of Jmj3 overexpression on wild-type. 10-fold serial dilutions of wild-type (2094) transformed with an empty vector pREP3X or pREP3X-Jmj3 were spotted onto EMM minus leucine + 5 μg/mL thiamine and EMM minus leucine without thiamine at 35 ºC. * Indicates decreased cell viability compared to wild-type or *wee1-50* with empty vector. The results were reproduced in at least two independent experiments.

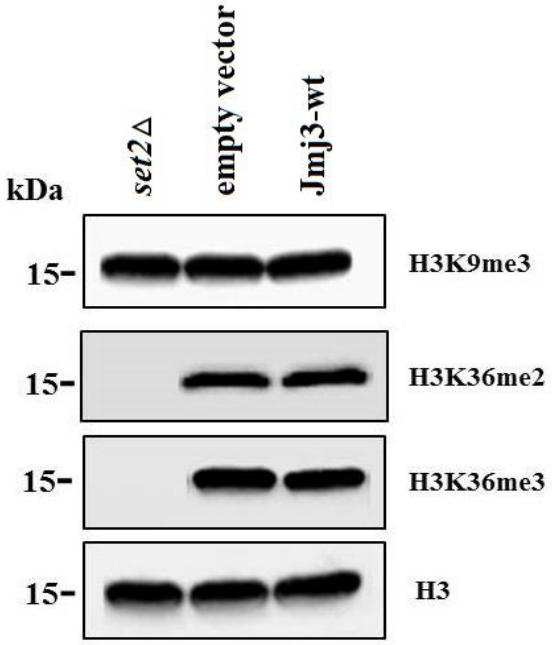

Figure 2.21 Western blot analyses of lysate from *S. pombe* cells overexpressing Jmj3. Expression levels of trimethylated H3K9, di-, and trimethylated H3K36 and trimethylated H3K9 in *set2*Δ cells, wild-type cells transformed with an empty vector or pREP3X-Jmj3. H3 was used as a loading control. The results were reproduced in at least two independent experiments.

Overall, a direct role for the fission yeast protein Jmj3 in H3K36 demethylation was not supported by this work. Western blotting showed no change in H3K36me3 and H3K36me2 marks when overexpression of Jmj3 was carried out in fission yeast. Therefore, further study for the enzymatic function and other possible biological functions of Jmj3 is needed.

2.8 Conclusions

Studies on the impact of two human JmjC domain- containing histone demethylases, JMJD2A and FBXL11 on cell viability of *S. pombe* reveal that these two human histone demethylases have H3K36demethylase activity in fission yeast. The demethylase activity was found to impact more strongly on cell survival in a *wee1-50* background compared to wild-type cells. The appropriate promoters for overexpression of hsJMJD2A and hsFBXL11 in *S. pombe* were pREP41X and pREP3X, respectively. The requirement for an intact catalytic structural domain in JMJD2A for its enzymatic function in fission yeast was confirmed. For hsFBXL11, the CxxC zinc finger and PHD domain appear to be as important for enzymatic activity as the catalytic JmjC domain in fission yeast. The results thus provide insights into the impact of two major human H3K36 demethylases in fission yeast.

Synthetic lethality of decreased H3K36me3 levels and *wee1* inhibition has been observed; the proposed mechanism involves the depletion of dNTPs and the regulation of RRM2 (ribonucleotide reductase subunit) as mediated by H3K36me3 and CDK activity.[171] Similar results were observed in this work using overexpression of hsJMJD2A/hsFBXL11 (H3K36 demethylase) in *S. pombe* with the *wee1-50* mutant. Importantly, deletion of *spd1* rescued the viability of overexpression of JMJD2A or FBXL11, in a *wee1-50* background in *S. pombe,* supporting the mechanism of synthetic lethality between the loss of methylation of H3K36 methylation and *wee1* inactivation to have arisen through dNTP depletion, which has been shown in mammalian cells.[171]

Theoretically, selective inhibitors of JMJD2A or FBXL11 should rescue the viability of overexpression of JMJD2A or FBXL11 in a *wee1-50* mutant in fission yeast. Based on this proposal, a yeast model for testing inhibitors of hsJMD2A or FBXL11 is possible

and might enable a practical, biological screening system with the potential to provide information about inhibitors for clinical use.

Chapter 3
Development of an LC-MS-based method for histone profiling

3.1 Introduction

3.1.1 Resources for human histone investigation

Investigations on histone modifications have recently been expanding, largely as a result of emerging evidence for the diverse functional roles of histone post-translational modification (PTMs).[186] The detailed characterization of histone modifications and connections to disease is complex, in part due to the existence of multiple histone variants. According to the Histone Infobase[187], a database dedicated to providing information about human histone variants and sites of post-translational modifications, there are reported to be 10 variants of histone H1, 19 of H2A and H2B, 6 of H3, but a single H4 protein. Further, six common types of histone modifications, ranging from low molecular weight modifications (methylation, acetylation, citrullination, phosphorylation) to 'heavy' modifications (ubiquitylation, poly-ADP ribosylation) are reported. The patterns of PTMs on core histones contain precise regulatory information and are in some cases inherited from previous generations.[188] While genes and proteins are often conserved across species, histone modification patterns appear to be organism-characteristic. For example, studies have identified different methylation states of H3K9 in regions of constitutive heterochromatin in plant species with larger genomes compared to those with smaller genomes.[189] Even within the same organism, there can be variations in patterns of histone PTMs in different cell types. Alterations in histone PTMs have been observed in many types of cancer cells and some may have important roles in tumorogenesis.[190]

3.1.2 Various approaches for studying histone PTMs

Of the four core histones, H3 has the largest number of known modification sites[187]. There are 21 modified H3 residues identified in human cells.[191] However, the accurate extent of modifications on specific residues is incompletely defined. Conventional immunoassay methods, including immunoprecipitation, western blotting, and immunofluorescence, have been dominant tools for biologists in addressing the characterisation of histones and their PTMs. However, these approaches have limitations that restrict their application. The reliability of immunoassays depends on highly specific commercially available antibodies for known modification sites. Sequence variants and PTMs can compromise the specificity of certain antibodies; some histone variants differ by only a few amino acids, which may not be included in the antigenic determinant. Therefore, the quantitative detection of specific PTMs and/or histone variants using antibodies is often challenging. The presence of multiple PTMs also presents an issue. For example, phosphorylation of H3S10 blocks the binding of antibodies that target modifications of H3K9.[192] To address this concern, antibodies could be developed that target both methylation of K9 and phosphorylation of S10, as well as the unmodified residues, a major undertaking. Hence, it is often difficult to obtain highly specific antibodies to fulfill experimental needs, especially in work involving multiple, sometimes linked, PTMs.

An alternative, direct approach for studying modifications of specific sites is sequencing by tandem mass spectrometry.[193] However, this MS technique involves complex sample preparation, is time-consuming and may be compromised by PTMs. To obtain small fragments (5-25 amino acids) of histone proteins for sequencing, enzymatic or chemical digestion of histone proteins is required. Moreover, such 'bottom-up' approaches cannot assess combinations of multiple PTMs unless they

locate on the same fragment of protein. MS analysis of intact histone proteins has the potential to provide a more comprehensive view of histone modifications.[194] Global modification patterns of intact H3 have been reported; however, the reported spectra were of relatively poor resolution and the analyses were not quantitative.[195] Several researchers have focused on developing LC–MS based methods for the analysis of core histones.[196,197] Top-down MS proteomics has also been applied to the analysis of histone PTMs.[198-201] However, these approaches require large amounts of the purified core histone (H2A, H2B, H3 and H4). In addition, top-down approaches have lower detection sensitivities compared to the bottom-up approaches and require a long time for data acquisition in order to generate a reliable MS/MS spectra.[46]

3.2 Aim of the work

The aim of the work described in this Chapter was to develop a rapid, reliable MS method to analyse intact histone proteins from experimental and clinical samples. An initial focus of this work was the optimization of histone extraction and LC–MS methods in order to profile histones. The robustness of the method was tested, and the optimised method was applied to investigate histone variants and their PTMs in normal and cancerous human cell lines. It is envisaged that the optimised method of profiling intact histones could be further developed as an assay to detect PTMs related to disease states, or to determine the effects of compounds on the epigenetic processes.

3.3 Choice of method for histone purification

Acid-extraction is widely used to isolate histones from cells and tissues. Here, an established acid extraction method[202] was employed to isolate histones from human embryonic kidney (HEK) 293T cells; three alternative purification steps following the acid-extraction step were assessed. In brief, nuclear extracts were prepared under acidic

conditions to selectively isolate histones, which were subsequently purified by dialysis tubing (approximately 3,000 molecular weight cut-of membrane) or by precipitation with either trichloroacetic acid (TCA) or acetone. Purified histones were later analysed by SDS-PAGE with Coomassie staining, and the yields quantified by Bradford assay (Figure 3.1). Acetone purification consistently produced the greatest yield of histones (68 ± 16 μg/ 10^6 cells) and was used in all further histone extractions.

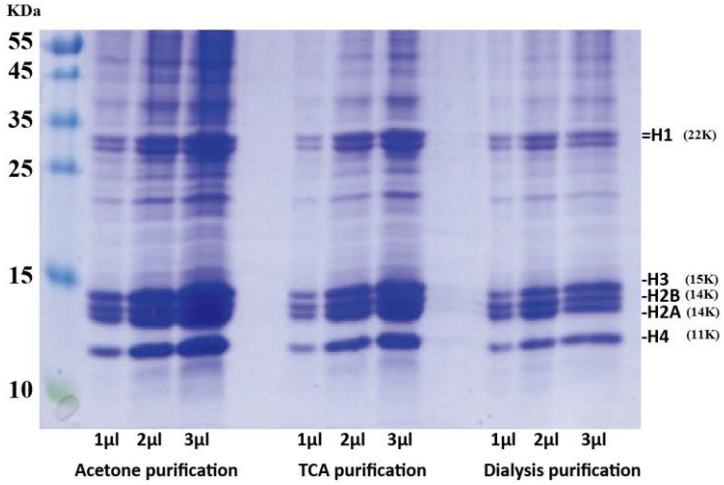

Purification approaches	Time	Yield (μg/ 10^6 cells)
Acetone	2.5 hours to overnight	68 ± 16
TCA	1.5 hours	44 ± 20
Dialysis	2 hours to overnight	24 ± 13

Figure 3.1 SDS-PAGE analysis of acid-extracted histones from HEK293T cells purified by acetone precipitation, TCA precipitation or dialysis. Bands corresponding to histones H1, H2A, H2B, H3 and H4 are indicated (upper panel). The left hand lane shows a molecular weight marker. Masses are given in kDa. The yield from each purification ± SD (as determined by Bradford assay) is shown (lower panel).

3.4 Optimization of liquid chromatography mass spectrometry

The quality of protein separation by liquid chromatography (LC) is attributed to factors including the ion-pairing agent, the components of the mobile phase, the characteristics of the column, the solvent gradient, and flow rate.[203] Optimal conditions for each with respect to histone separation were investigated as described below.

3.4.1 Choice of column for liquid chromatography

Although nanoscale (0.05-0.1 mm i.d.[b]) columns have better sensitivity, peak capacity and detection limit than capillary scale (0.3 mm i.d.), or microscale (1.0-2.1 mm i.d.) columns, they require more time-consuming methods.[204] It was found that for histone separation, an average of 70-90 minutes was required to achieve optimised separation using a nanoscale system. Given that a major focus of this work was to develop a rapid, efficient LC-MS method for histone separation, a microbore Ultra Performance (UP) LC column (2.1 mm i.d) was therefore employed.

3.4.2 Composition of the solvent phase

3.4.2.1 TFA-free as an ion-pairing agent

Ion-pair reagents are often used for effective separations of mixture of proteins when using reversed-phase high-performance liquid chromatography (RP-HPLC). These agents expose the hydrophobic core of protein analytes and can interact with the hydrophobic stationary phase, resulting in differential retention and analytes separation.[205] Trifluoroacetic acid (TFA) is the most frequently used ion-pairing agent, because it typically enables efficient and high resolution separations of proteins.[206] However, the formation of TFA adducts when combined with basic species occurs (even in very low amounts) complicating data analysis.[207,208] The effect of TFA adducts has been reported to likely be an issue in MS analysis of histones because histone proteins have a highly basic nature and contain multiple modifications that may react with TFA adducts.[204] To avoid this concern, the TFA-free mobile phase employing formic acid was used in LC-MS for histone analysis. The presence of formic acid in the mobile phase did not result in adducts (Figure 3.2).

[b] Internal diameter.

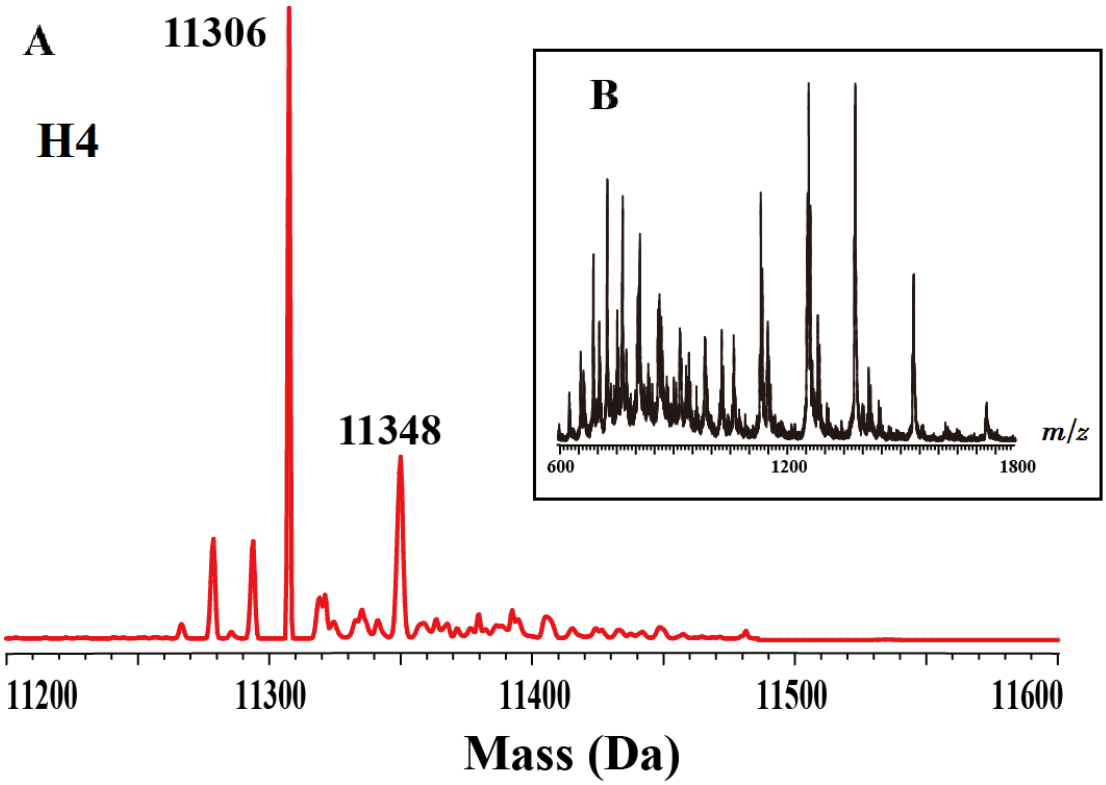

Figure 3.2 Using TFA-free mobile phase (0.1% (v/v) formic acid) for LC-MS separation of histones extracted from HEK293T cells. (A) Deconvoluted mass spectrum of H4: no adducts were observed. (B) The inset shows the raw data of mass spectrum (*m/z versus* ion intensities) of H4. Data were collected using an LCT ESI-TOF MS machine (Waters) and analysed using Mass Lynx software.

3.4.2.2 Gradient elution programme

Figure 3.3 shows the results of microscale LC-MS mediated separation of histones from human HEK293T cells, employing different gradient elution conditions using 0.5% (v/v) formic acid in water as 'solvent A' and 0.5 % (v/v) formic acid in acetonitrile as the mobile phase (solvent B) with a flow rate of 300 µL/min. Three different gradient programmes were tested (Figure 3.3); all show that separation of the core histone proteins can be achieved when using between 20 and 40% of solvent B.

Given the interest in histones rather than other nuclear proteins in this work, good separation of histones in the shortest time possible was desired. The 20-minute mobile phase programme was considered to give the optimal gradients for clear separation of histone proteins over the shortest time (Figure 3.3C).

A

90 min mobile phase gradient	
Time (min)	Solvent B (%)
0-5	5-25
5-15	25-35
15-60	35-65
60-75	65-95
75-80	95-5
80-90	5-5

B

60 min mobile phase gradient	
Time (min)	Solvent B (%)
0-2.5	5-5
2.5-5	5-20
5-7.5	20-20
7.5-45	20-60
45-50	60-95
50-52	95-95
52-55	95-5
55-60	5-5

C

20 min mobile phase gradient	
Time (min)	Solvent B (%)
0-1	5-24
1-4	24-30
4-5	30-30
5-11	30-36
11-13	36-36
13-14	36-85
14-15	85-85
15-16	85-5
16-20	5-5

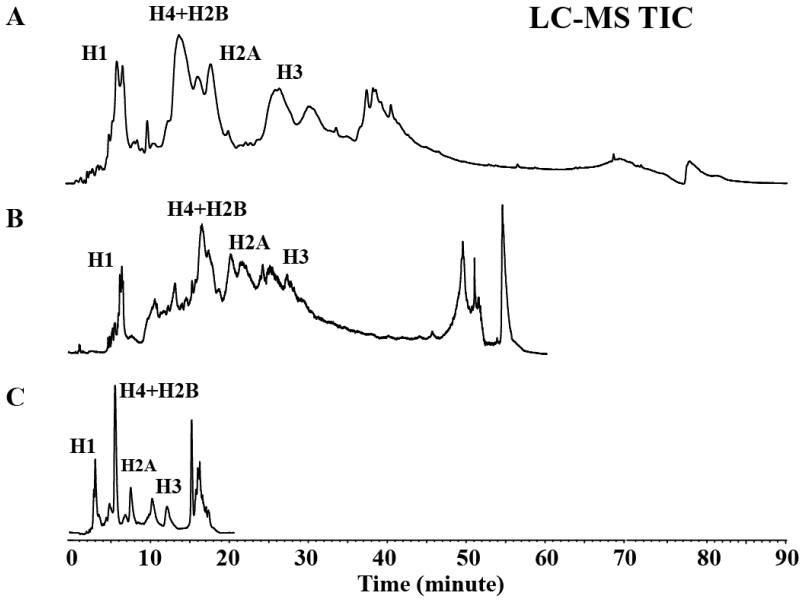

Figure 3.3 Various solvent gradient programmes for separation of human HEK293T histones. Solvent A (0.5% formic acid in Milli-Q water); solvent B (0.5% formic acid in acetonitrile). Tables A-C show 90, 60 and 20-minute gradient programmes, respectively. The lower panels (A-C) show total ion chromatograms corresponding to the solvent gradients shown in the Tables.

3.4.2.3 Concentration of formic acid

Varying the concentration of formic acid as the ion-pairing agent in the mobile phase was next evaluated, using the optimised gradient elution programme and a flow rate of 300 µL/min. Figure 3.3 shows the LC-MS separation profiles of human HEK293T histones with the optimised gradient over four different concentrations of formic acid in the mobile phase: 1, 0.5, 0.2, and 0.1% (v/v). In LC-MS chromatography, the peak shape was found to improve (with decreased peak widths at half height) when

increasing concentrations of formic acid in the mobile phase was used. An increased concentration of formic acid was found to enhance the separation resolution. No obvious difference in the resolution was observed between 0.5 and 1% (v/v) formic acid (Figure 3.4). The retention times of the histone proteins did not change substantially with different concentrations of formic acid in the mobile phase. The peak capacity increases as an increasing concentration of formic acid is used; however, 1% (v/v) formic acid in the mobile phase shows a higher noise level compared to 0.5% (v/v) formic acid. Overall, a concentration of 0.5% (v/v) formic acid is determined to be the optimal ion-pairing concentration in the mobile phase (Figure 3.4).

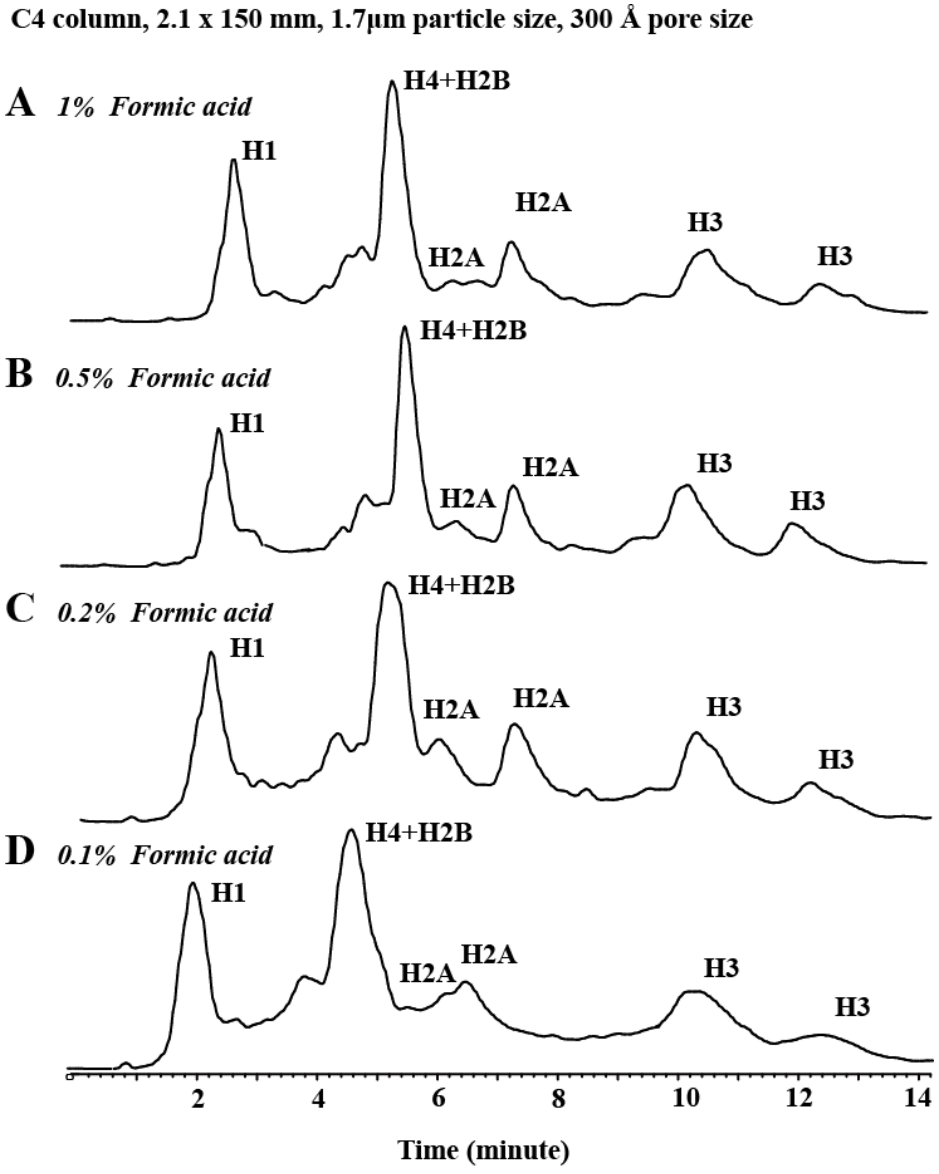

Figure 3.4 The effect of different concentrations of formic acid on histone separation. Panels A-D show chromatograms from LC separation of histones (from HEK293T cells) using a mobile phase containing 1.0, 0.5, 0.2, and 0.1% (v/v) formic acid. Data were collected using a LCT Premier ESI-TOF MS machine (Waters) equipped with a microbore C4 column (2.1 mm x 150 mm, 1.7 μm, 300 Å) at a flow rate of 300 μL/min. Data were analysed using Mass Lynx software.

Given the different calculated molecular masses of H4 (11236.2 Da) and H2B (i.e. 13760.9 Da for H2B type1-H), these two major nucleosome components can be identified unambiguously by MS, even if RPLC cannot separate them. In the context of histone profiling, the higher sensitivity of MS analysis and lack of interference from ion-pairing agent adducts were considered to be more important than complete separation of histone proteins; hence the formic acid procedure was used.

3.4.3 Optimised LC-MS method - Summary

A rapid, effective separation and analysis method for analysis of intact histones from human cells was desired. To achieve this goal, a microbore UPLC column coupled with LC-MS was selected for use. A TFA-free mobile phase employing formic acid was demonstrated to be suitable for histone separation whilst avoiding formation of TFA adducts. The concentration of formic acid, gradient programme and flow rate were optimized using a microbore column to achieve ideal sensitivity, peak capacity and resolution. The C4 column (2.1 mm x 150 mm, 1.7 μm, 300 Å) using 0.5% (v/v) formic acid mobile phase with a 20-minute gradient at a flow-rate of 300 μL/min was used for histone analysis of all the samples in this work (Figure 3.5).

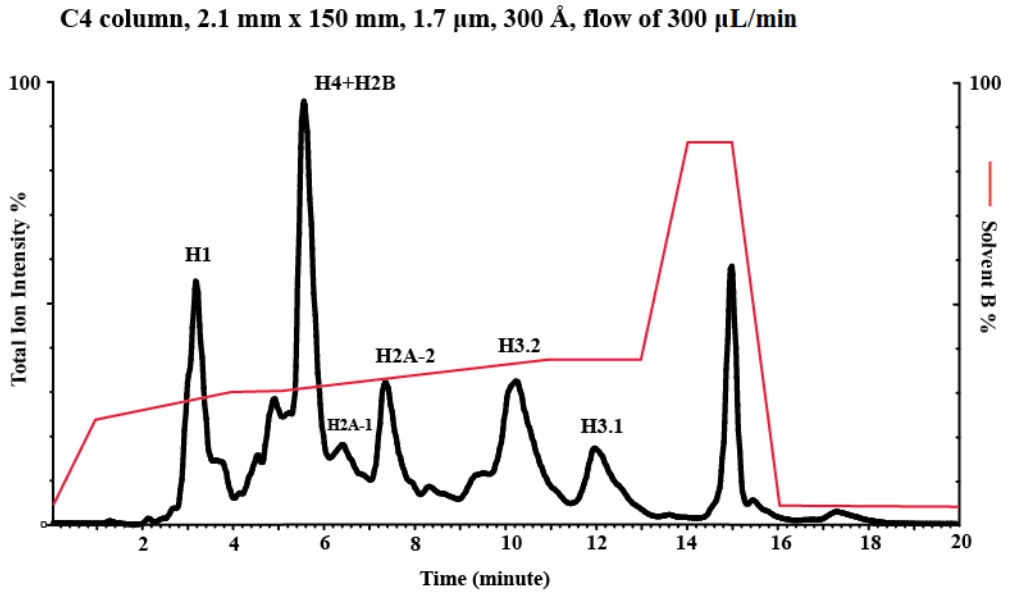

Figure 3.5 Optimised microbore LC-MS chromatogram (TIC) of human histones (left Y axis, black); the mobile phase gradient is superimposed (right Y axis, red).

Although co-elution of histones H4 and H2B was observed using the optimised method, the coupled LC-MS method enables identification of H4 and H2B due to substantial mass differences.

3.5 MS profiles for histones analysis under optimised LC conditions

Histones were prepared from HEK293T cells by acid-extraction following acetone purification[209] and analysed by LC-MS using the optimised protocols described in Section 3.4. In the following section, the results obtained from analysis of the different types of human histone studies using this LC-MS method are discussed. It should be noted that the interpretation of results is complicated by potential mass redundancies. Isobaric ions refer to the ions with the same mass and which share the same value of *m/z*. MS analysis of the intact histones is also complicated by their isotopic distribution patterns, in part because some histone variants differ in mass by just 1-2 Da. The isobaric concern exists with respect to modifications similar in mass, i.e. tri-methylation (+42Da) and acetylation (+42Da), as described in Section 1.9.1. It should also be noted that the intact histone analysis method does not inform on the residues modifications.

In cases where specific modifications are implied (e.g. N-terminal acetylation and certain phosphorylation), this is on the basis of previous literature.[187]

3.5.1 Histone H1

3.5.1.1 Background on histone H1

Histone H1 has been identified as a linker protein involved in the compaction of chromatin and related transcription repression.[210] Phosphorylation of H1 plays an important role in modulation of chromatin structure and subsequent regulation of gene transcription.[211] There are 10 variants of histone H1 identified in humans (Table 3.1).[187] The sequences of H1 variants analysed in this study are summarised in Appendix 2.

Table 3.1 Comparison of human histone H1 variants.[187]

variant	UniprotKB Accession number	number of amino acids	Calculated average mass (Da)	Observed mass (Da)* in this work	Δmass (Da)
H1.0	P07305	193	20731.74	n/a	n/a
H1.1	Q02539	214	21710.90	n/a	n/a
H1.2	P16403	212	21233.56	**21275.9±1.49**	**42±1.49**
H1.3	P16402	220	22218.71	**22260.7±1.56**	**42±1.56**
H1.4	P10412	218	21734.08	**21776.1±1.52**	**42±1.52**
H1.5	P16401	225	22448.98	n/a	n/a
H1oo	Q8IZA3	346	35813.49	n/a	n/a
H1t	P22492	206	21887.81	n/a	n/a
H1x	Q92522	212	22355.92	n/a	n/a
Testis-specific H1	Q75WM6	255	28115.95	n/a	n/a

* Observed masses were a 42 Da greater than the calculated masses and consistent with *N*-acetylation of histone H1.
n/a: not available.
H1 variants in bold denote those observed in this study (i.e. a mass consistent with this variant was observed).

3.5.1.2 Results

The H1 fraction of the LC-MS chromatogram was analysed (Figure 3.5). The spectrum shows ions with charge states ranging from 12+ to 34+, representing three species of

proteins with a *m/z* range of 500-2000 (Figure 3.6A). Multiple ions at the individual charge states were observed, indicating possible PTMs. The deconvoluted mass spectra (Figure 3.6B) indicate observation of three H1 variants corresponding to the H1 variants H1.2 (21276 Da), H1.4 (21776 Da) and H1.3 (22261 Da), although these observed mass are a 42 Da greater than the calculated masses (21234, 21734 and 22219, respectively, Table 3.1). The incremental shift of a +42Da is consistent with acetylation on N-termini of the H1 variants, as has been previously reported.[212] The results are also consistent with, and support, previous studies using tandem mass spectrometry to characterise H1 isoforms.[213]

H1.2 and H1.4 display some higher mass peaks with a +80 Da interval, consistent with phosphorylation (Figure 3.6B). This could correspond to phosphorylation of residues T30, T145, or S172 for H1.2 and T17, T145, T153, S171, or S186 for H1.4.[213] In contrast, no evidence for phosphorylation of H1.3 was observed.

The LC-MS method described here enables characterisation of phosphorylation on histones following acid-extraction without additional enrichment by ion affinity chromatography, as was used in previous reported studies.[214] The developed LC-MS method for resolution of the core histones is the primary focus and thus not all histone H1 variants are separated and identified. Su *et al.* have reported that use of capillary LC-MS enables separation of H1 variants and identified H1.1, H1.5, H1.0 and H1x which were extracted from HeLa cells using a hydroxyapaptite (HAP)-purification method.[215] The HAP-purified samples contained more types of H1 variants than my LC-MS method, in which only the most abundant H1 variants (H1.2, H1.3 and H1.4) were observed. The reason for that difference may be that HAP binds (more) native chromatin and fractionates the linker histones from the strongly bound core histones to enrich low abundance relating H1 variants, resulting in improved detection.[216] However,

similar patterns of histone H1 and modifications, particularly for phosphorylated H1 isoforms, were observed using the acid-extraction (my work) and the reported HAP-mediated separation method.[215]

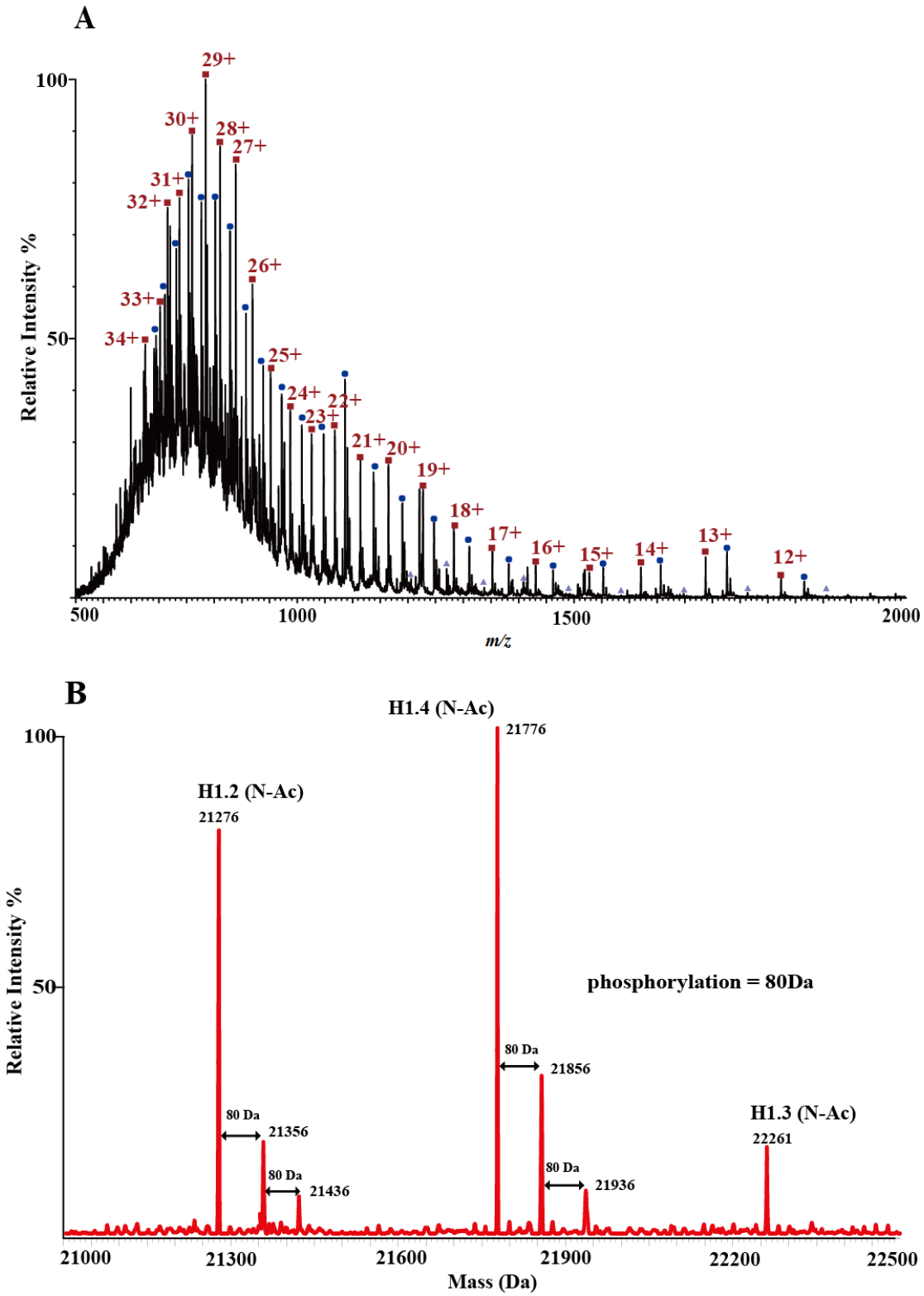

Figure 3.6 (A) Mass spectrum of H1 variants: H1.2 (■), H1.4 (●) and H1.3 (▲). (B) Deconvoluted mass spectrum shows H1 variants and their modifications. N-Ac: N-acetylation, corresponding to a +42Da shift. Each +80Da shift is consistent with a single phosphorylation.

3.5.2 Histone H2A

3.5.2.1 Background on histone H2A

According to UniprotKB[c], there are 19 identified variants of human histone H2A (Table 3.2). The majority of H2A variants consist of proteins with 128-130 amino acid residues whilst atypical variants such as macro-H2As, H2A-Bbd and H2A.X differ markedly in size.[187] Micro-H2As and H2A-Bbd are considered to have specific functions related to the X chromosome.[217,218] Many types of H2A PTMs have been characterised on specific lysine, arginine, serine and threonine residues.[187] Of these PTMs, acetylation is the most abundant modification on H2A and H2A phosphorylation has an important signaling function during DNA damage.[58] Two of H2A variants, H2A.X and H2A.Z are unique subtypes of H2A whose sequences vary significantly from the homologous H2A variants (Appendix 3) and are involved in DNA double strand break (DSB) or the heat shock response.[58] H2A.X is identified as being modified by phosphorylation on serine 139 (γH2AX) and tyrosine 142.[58] γH2AX is widely used as a marker of DSB, whereas Y142 phosphorylation has a critical role in apoptosis during DNA damage.[219] H2AZ is exchanged into nucleosomes during DSBs and alters chromatin to adopt an open status that is required for placement of other histone modifications.[220] Localization of DSB-associated proteins then facilitates DNA damage repair.[220] The sequences of the H2A variants analysed in this study are summarised in Appendix 3.

[c] UniprotKB (http://www.uniprot.org/).

Table 3.2 Comparison of human histone H2A variants.[187]

variant	UniprotKB Accession number	number of amino acids	Calculated average mass (Da)	Observed mass (Da)* in this work	Δmass (Da)
Core histone macro-H2A.1	O75367	372	39617.1	n/a	n/a
Core histone macro-H2A.2	Q9P0M6	372	40058.2	n/a	n/a
H2A type 1[b]	P0C0S8	129	13960.3	**14002.3±0.98**	**42±0.98**
H2A type 1-A[b]	Q96QV6	130	14102.3	n/a	n/a
H2A type 1-B/E[b]	P04908	129	14004.3	**14046.3±0.98**	**42±0.98**
H2A type 1-C[b]	Q93077	129	13974.3	**14016.3±0.98**	**42±0.98**
H2A type 1-D[b]	P20671	129	13976.3	**14018.3±0.98**	**42±0.98**
H2A type 1-H[b]	Q96KK5	127	13775.1	**13817.1±0.97**	**42±0.97**
H2A type 1-J	Q99878	127	13805.1	n/a	n/a
H2A type 2-A[a]	Q6FI13	129	13964.3	**14006.3±0.98**	**42±0.98**
H2A type 2-B	Q8IUE6	129	13864.1	n/a	n/a
H2A type 2-C[a]	Q16777	128	13857.2	**13899.2±0.97**	**42±0.97**
H2A type 3[b]	Q16777	129	13990.3	**14032.3±0.98**	**42±0.98**
H2A-Bbd type 1	Q7L7L0	115	12697.3	n/a	n/a
H2A-Bbd type 2/3	P0C5Z0	115	12713.4	n/a	n/a
H2A.J	Q9BTM1	128	13888.2	n/a	n/a
H2A.V	Q71UI9	128	13508.7	n/a	n/a
H2A.X[b]	P16104	142	15013.5	**15055.5±1.05**	**42±1.05**
H2A.Z[a]	P0C0S5	127	13421.6	**13421.6±0.94**	**0.94**

***** Observed masses were a 42 Da greater than the calculated masses indicating *N*-acetylation of histone H2A.
Histone H2A variants with N-terminal acetylation except core histonemacro-H2A.1, core histonemacro-H2A.2, H2A-Bbd type 1, H2A-Bbd type 2/3, H2A.V and H2A.Z.
n/a: not available.
H2A variants in bold denote those observed in this study.
[a] Indicates H2A variants eluted from fraction H2A-1 (Figure 3.5).
[b] Indicates H2A variants eluted from fraction H2A-2 (Figure 3.5).

3.5.2.2 Results

Using my optimised LC-MS method, the majority of H2A eluted in two peaks, corresponding to H2A-1 and H2A-2 (Figure 3.5). The ion spectra indicate charge states ranging from 9+ to 21+, representing several species in the *m/z* range of 600-1800. Some of the observed H2A-1 species correspond to H2A variants and/or their isoforms with PTMs (Figure 3.7). Notably, as with H1, all the observed H2A variants, except for

H2A.Z (13422 Da), were observed to have a mass shift of a +42 Da, corresponding to acetylation, likely of the N-terminus[197] (Figures 3.7B, Table 3.2). Three H2A variants, N-Ac H2A type 2-A, N-Ac type 2-C and H2A.Z were assigned as the three species observed at 14007 Da, 13900Da, and 13422Da, respectively (Figure 3.7B). The species at 14049 Da was provisionally assigned as N-Ac H2A type 2-C with an additional mono-acetylation (14007+42= 14049 Da).

The majority of the other H2A variants eluted in the fraction assigned as H2A-2. All the H2A variants in this fraction were shifted in mass, relative to the unmodified protein by 42Da, again likely due to N-terminal acetylation[197] (Figure 3.8, Table 3.2). The ion spectrum shows similar charge states to those observed in fraction H2A-1 (Figures 3.7A and 3.8A). The species observed in H2A fraction (Figure 3.8C) were assigned, on the basis of the observed masses, as H2A type1, type 1-B, type1-C, type 1-D, type 1-E, type 1-H, type 2-C, type 3 and H2A.X. The most abundant species were assigned as N-Ac H2A type 1 (14003 Da) followed by N-Ac H2A type 1-C/ 1-D (14017 Da) and N-Ac H2A type 1-B/E (14046 Da). Other species were assigned as minor H2A variants: N-Ac H2A type 1-H (13817 Da) and N-Ac H2A type 2-C (13900 Da). The H2A.X is also identified in this mass spectrum, with a mass of 15056 Da corresponding to N-Ac H2A.X[187] (Figure 3.8D). The phosphorylated form of this H2A variant (γH2AX) was not observed under these conditions (see Chapter 4, for further work on H2A.X)

Many PTMs have been identified on histone H2A with acetylation on K5, K9, K13, phosphorylation on S1, T120 and methylation on R3, K99 being reported.[221,222] Other PTMs such as methylation, ubiquitylation, ADP-ribosylation and citrullination are also documented.[223] Due to the small mass difference between many H2A variants, the additional complexity of multiple modifications on each H2A variant complicates the assignment of species in LC-MS profiles. Modifications such as mono-methylation,

acetylation, and even the larger mass shift of phosphorylation, interfere with the mass spectral interpretation when coupled with the differing masses of the H2A variants. For example, Figure 3.8 shows a species with a mass of 14046 Da which could be assigned, on the basis of the observed mass, as either N-Ac histone H2A type 1-B/E or N-Ac H2A type 1. Further note, mono-acetylation (+42 Da) the mass shift for a very similar to that for trimethylation (+43/42 Da); in particular provisional assignments of N-terminal acetylation are made on the basis of prior literature reports.[197]

In describing the mass shift the term 'methylation equivalent (m.e.)' is sometimes used. This corresponds to the number of 14 Da mass shifts. Note, however, that an increase by a certain number of methylation equivalents does not necessarily imply methylation. Thus, for example, +3 methylation equivalents could correspond to acetylation. Without additional information, the unambiguous determination of the species in these LC-MS profile alone is challenging, and all assignments should thus be regarded as provisional.

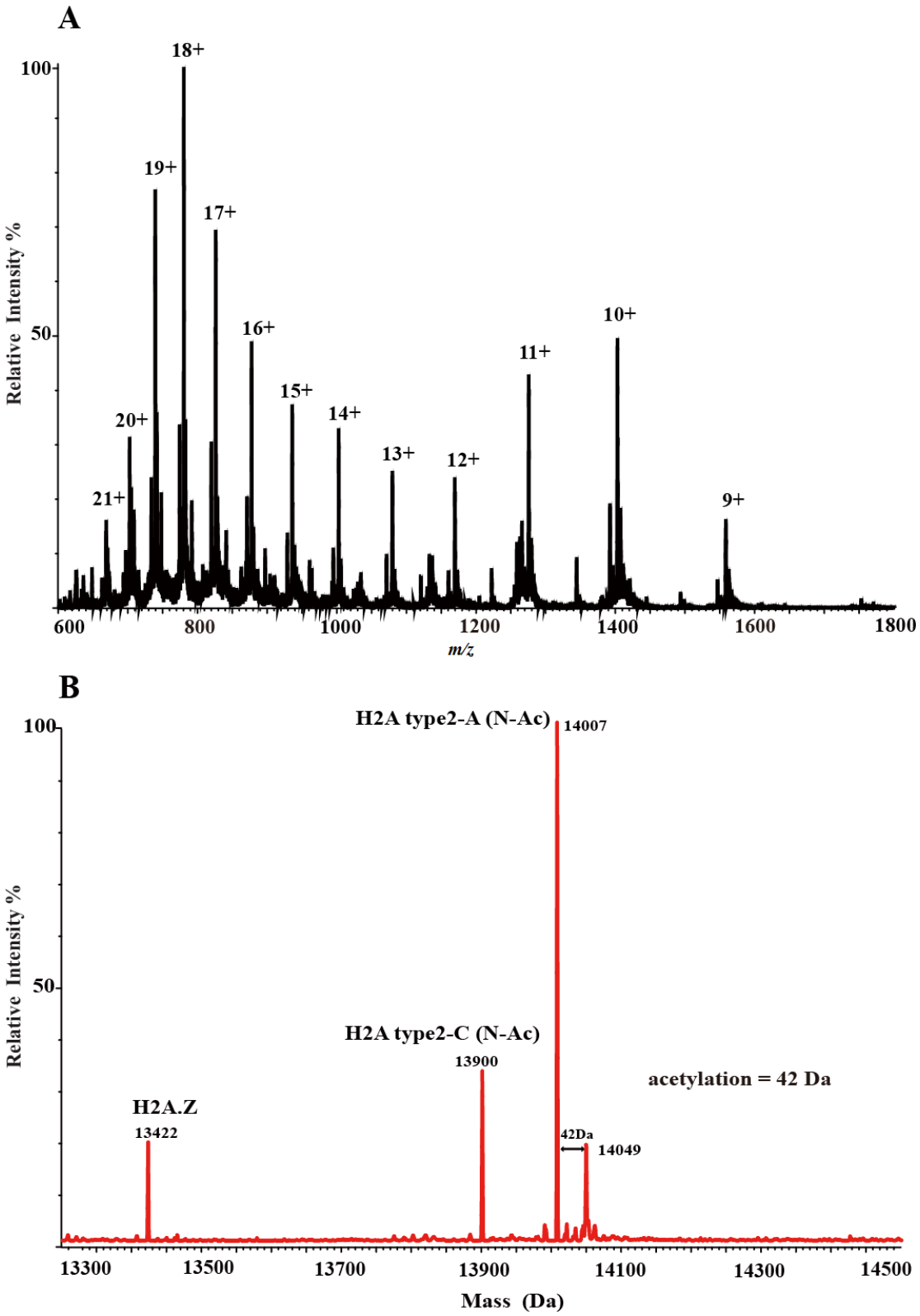

Figure 3.7 (A) Mass spectrum of H2A variants from fraction H2A-1 showing ions with charge states ranging from 9+ to 21+. (B) Deconvoluted mass spectrum shows H2A variants and their modifications from the fraction assigned as corresponding to H2A-1. N-Ac: N-acetylation, corresponding to a +42Da shift.

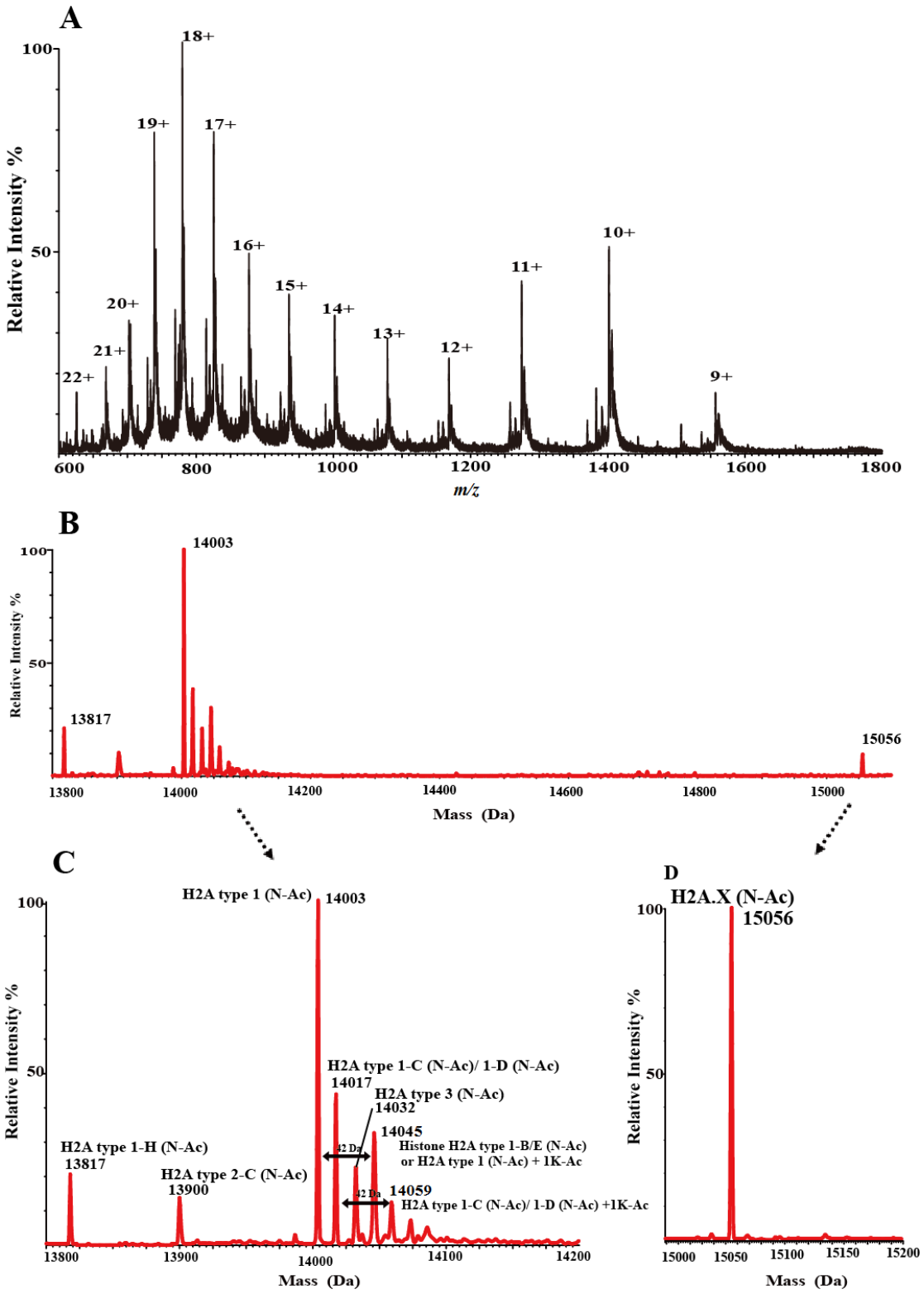

Figure 3.8 (A) Mass spectrum of H2A variants from fraction H2A-2 showing ions with charge states ranging from 9+ to 22+. (B) Deconvoluted mass spectrum for the fraction assigned as corresponding to H2A-2. (C) Magnification from (B) to show H2A variants and their modifications. (D) Magnification from (B) showing a species corresponding to the calculated mass of *N*-acetyl H2A.X (15056 Da). N-Ac: N-acetylation, corresponding to a +42Da shift.

3.5.3 Histone H2B

3.5.3.1 Background on histone H2B

Human histone H2B currently has 19 identified variants with most H2B variants consisting of 125 amino acid residues (Table 3.3)[187]. Acetylation and ubiquitylation are two common forms of H2B PTMs that have been well investigated. Acetylation of specific lysine residues alters the chromatin structure and helps DNA-binding proteins interact with nucleosome.[224] Ubiquitinated H2B is involved in chromatin remodeling and has an impact on transcription machinery.[225] The sequences of H2B variants analysed in this study are summarised in Appendix 4.

Table 3.3 Comparison of human histone H2B variants.[187]

variant	UniprotKB Accession number	number of amino acids	Calculated average mass (Da)	Observed mass (Da) in this work	Δ mass (Da)
H2B type 1-A	Q96A08	126	14063.3	n/a	n/a
H2B type 1-B	P33778	125	13819.0	**13819±0.97**	**±0.97**
H2B type 1-C/E/F/G/I	P62807	125	13774.9	**13775±0.96**	**±0.96**
H2B type 1-D	P58876	125	13804.9	**13805±0.97**	**±0.97**
H2B type 1-H	Q93079	125	13760.9	**13760±0.96**	**±0.96**
H2B type 1-J	P06899	125	13772.9	**13775±0.96**	**±0.96**
H2B type 1-K	O60814	125	13759.0	**13760±0.96**	**±0.96**
H2B type 1-L	Q99880	125	13821.0	n/a	n/a
H2B type 1-M	Q99879	125	13858.0	n/a	n/a
H2B type 1-N	Q99877	125	13790.9	**13789±0.97**	**±0.97**
H2B type 1-O	P23527	125	13775.0	**13775±0.96**	**±0.96**
H2B type 2-E	Q16778	125	13788.9	**13789±0.97**	**±0.97**
H2B type 2-F	Q5QNW6	125	13788.9	**13789±0.97**	**±0.97**
H2B type 3-B	Q8N257	125	13776.9	**13777±0.97**	**±0.97**
H2B type F-S	P0C1H6	125	17001.3	n/a	n/a
H2B type F-M	P57053	154	13813.0	n/a	n/a
H2B type W-T	Q7Z2G1	175	19618.5	n/a	n/a
Putative histone H2B type 2-C	Q6DN03	192	21340.9	n/a	n/a
Putative histone H2B type 2-D	Q6DRA6	163	17886.9	n/a	n/a

n/a: not available.
H2B variants in bold denote those observed in this study.

3.5.3.2 Results

Using the LC-MS method, histone H2B was found to elute along with H4 in fraction H2B+ H4 in LC-MS (Figure 3.5). The ion spectra manifest as two separate charge state envelops, one with charges states from 8+ to 21+ (corresponding to H2B) and the other with charge states ranging from 7+ to 18+ (corresponding to H4; Figure 3.9A). Through the coupled LC-MS method, H2B and H4 can be identified based on their distinct masses. Several species were observed in the deconvoluted mass spectra; these correspond to H2B type 1-H/1-K (calculated mass: 13760.9 Da/13759.0 Da; observed mass: 13760 Da, Table 3.3), H2B type 1-C, E, F, G, I/1-J/1-O (calculated mass: 13774.9 Da/ 13772.9 Da/ 13775.0 Da; observed mass: 13775 Da), H2B type 1-N/2-E/2-F (calculated mass: 13775.0 Da/ 13788.9 Da/ 13788.9 Da; observed mass: 13789 Da), H2B type 1-D (calculated mass: 13804.9 Da; observed mass: 13805 Da) and H2B type 1-B (calculated mass: 13819.0 Da; observed mass: 13819 Da) (Table 3.3).

Notably, no evidence for N-acetylated H2B variants was observed; this may be because the first amino acid of H2B is a proline residue, rather than the serine residue found in H2A (Appendix 3 and 4). As with other histones, mass shifts corresponding to many types of PTMs can be detected on H2B. H2B variants have been reported to carry acetylation at K5, K12, K15, K20, phosphorylation at S10 and methylation at K5, K43.[221,223]

As with H2A, the analysis of these histones is complicated by isobaric variants. Thus, the unambiguous assignment of H2B species cannot be made. The species observed at 13760 Da could not be conclusively assigned as either H2B1H or H2B1K, the calculated masses of which are 13760.9 and 13759.0 Da, respectively (Appendix 4). The same issue is encountered for the species observed at 13775 and 13789 Da (Appendix 4). H2B1C/E/F/G/I, H2B1J and H2B1O potentially contribute to the peak

at 13775 Da whilst H2B1N, H2B2E and H2B2F could contribute to the peak at 13789 Da. Likewise, the similar masses of H2B1B (13819 Da) and mono-acetylated H2BC1C (13817 Da) complicate assignment of the species at 13819 Da.

The species at 13831 Da, 13847 Da and 13861 Da correspond to the masses of mono-acetylated H2B1N/2E/2F, mono-acetylated H2B1D and mono-acetylated H2B1B, respectively (Figure 3.9B)

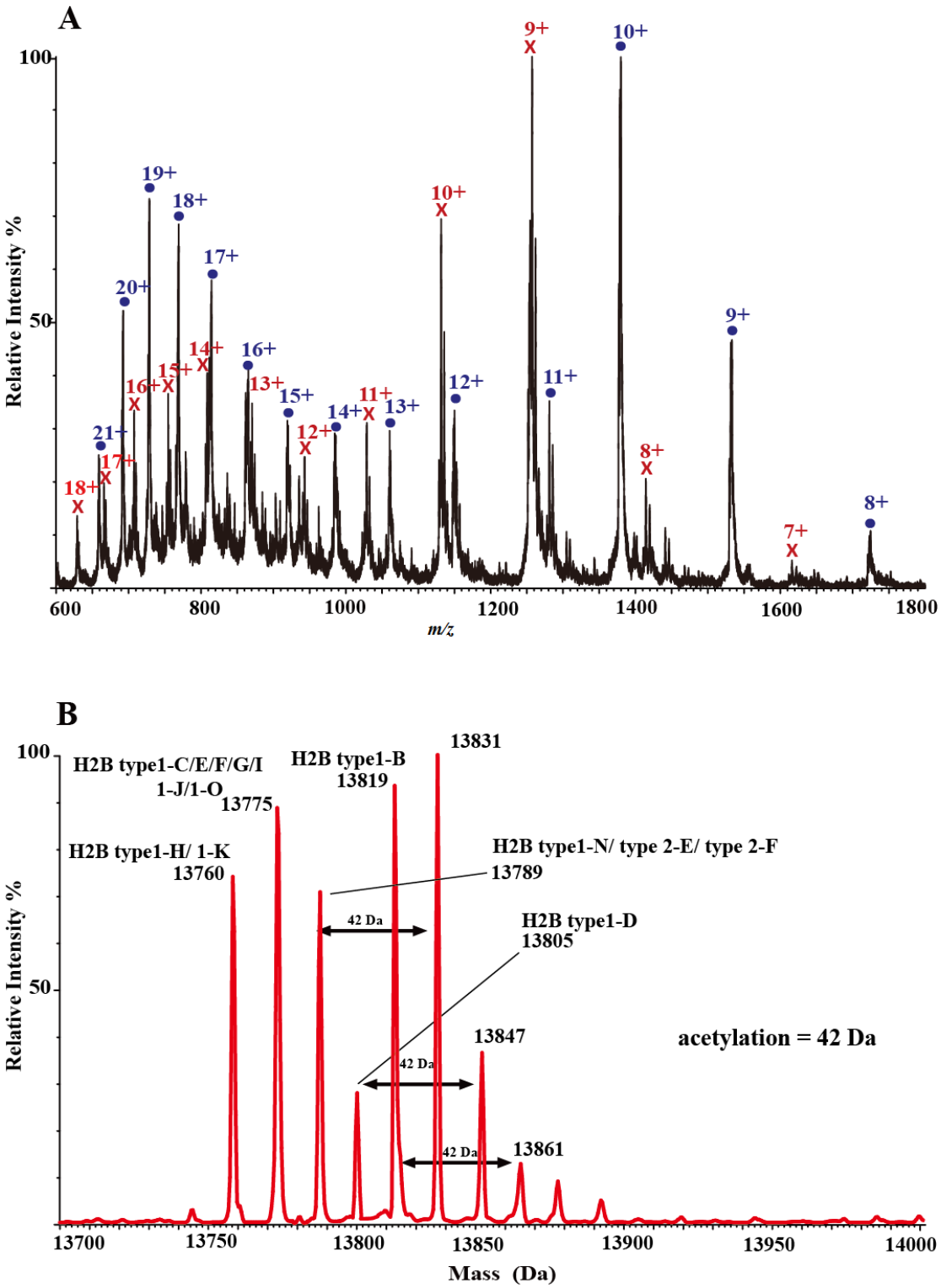

Figure 3.9 (A) The mass spectra of H2B (●) and H4 (X) show ions with charge states ranging from 8+ to 21+ and 7+ to 18+, respectively. (B) Deconvoluted mass spectrum from multiple ions (●) showing provisionally assigned H2B variants and their modifications.

3.5.4 Histone H3

3.5.4.1 Background on histone H3

Among all types of histones, histone H3 probably harbours the largest number of sites for PTMs. Methylation and acetylation are two major types of PTMs found on H3. Previous studies have shown many H3 arginine residues, including R3, R8, R17, R26 and lysine residues such as K4, K9, K23, K27, K36, K37, K56 and K79 have the capability for mono-, di- or tri-methylation.[223] Acetylation has been observed on K4, K9, K14, K18, K23 K27, K36 and K56.[187] In addition, functionally important phosphorylations at T3, S10, T11, S28, Y41 and T45 are reported. [223]

All human H3 variants consist of 134 or 135 amino acids, except for the atypical variant CENP-A which contains 140 residues (Table 3.4).[187] CENP-A is a centromeric histone, which exclusively substitutes conventional H3 in the centromeric region and plays an important role in interacting with kinetochore proteins and in mitotic progression.[226] Besides CENP-A, five other variants of H3 have been reported.[187] Of these, the major H3 variants are H3.1, H3.2 and H3.3. These are sub-classified as replication-dependent histone variants (H3.1 and H3.2) and a replication-independent histone variant (H3.3).[227,228] The incorporation of H3.1 into the nucleosome is mediated by the CAF-1 chaperone complex in a replication-dependent manner.[227] In contrast, expression of H3.3 is maintained throughout the cell cycle and H3.3 incorporated into nucleosomes independent of replication through the HIRA chaperone complex. [229,230] Appendix 5 gives a sequence alignment of the H3 variants. Only one residue is different between H3.1 and H3.2 (C96 in H3.1 and S96 in H3.2). Five different residues at positions of 31, 87, 89, 90 and 96 differ between H3.1 and H3.3 (A31, S87, V89, M90, C96 in H3.1 vs. S31, A87, I89, G90, S96 in H3.3). The replacement of a serine for a cysteine at residue position 96 results in a change of hydrophobicity of H3.2 compared to H3.1.[215]

Table 3.4 Comparison of human histone H3 variants.[187]

variant	UniprotKB Accession number	number of amino acids	Calculated average mass (Da)	Observed mass (Da)* in this work	Δmass (Da)
H3-like centromeric protein A	P49450	140	15990.6	n/a	n/a
H3.1	P68431	135	15272.9	**15273±1.07**	**±1.07**
H3.2	Q71DI3	135	15256.8	**15257±1.07**	**±1.07**
H3.3	P84243	135	12196.7	n/a	n/a
H3.1t	Q16695	135	15377.1	n/a	n/a
H3.3C	Q6NXT2	134	15082.5	n/a	n/a

n/a: not available.
H3 variants in bold denote those observed in this study.

3.5.4.2 Results

In reverse-phase LC, the retention time of proteins is dependent on their hydrophobicity; consistent with this, the species corresponding in mass to H3.2 eluted earlier than that of H3.1 (Figure 3.5). This observation supports the reported difference in hydrophobicity between H3.1 and H3.2.[215] Notably, H3.3 has previously been reported to co-elute with H3.2; however, in my work, H3.3 was not observed in the LC-MS profile.[215,231]

The ion-spectrum of the LC-MS profile shows charge states from 9+ to 23 +, and the deconvoluted mass spectrum demonstrated a complex pattern of native H3.1 and modified forms (Figure 3.10). H3.2 shows similar ion spectra with charge states from 9+ to 23+; likewise, the deconvoluted mass spectrum displays multiple species corresponding to the mass of H3.2 with multiple PTMs (Figure 3.11). In total, 17 apparent species for the H3.1 PTMs were clearly detected whilst 15 species were identified for the H3.2 isoforms (Figures 3.10 and 3.11). The species at 15273 Da and 15257 Da are consistent with the calculated masses of unmodified H3.1 and H3.2, respectively (Table 3.4).

In the H3.1 mass spectrum (Figure 3.10), the most abundant species was observed at 15343 Da followed by 15357 and 15371 Da. Highly modified states of H3.1 were noted at 15469, 15483 and 15497 Da, although the amounts of these species observed were relatively low. For the mass species corresponding to H3.2, the species at 15327 Da was the most abundant, followed by species at 15341 and 15313 Da. A species corresponding to a highly modified form of H3.2 was observed at 15453 Da (Figure 3.11B). Interestingly, comparing the H3.1 and H3.2 mass spectra, the most abundant species of both H3.1 and H3.2 is 70 Da (5x methylation equivalents) greater in mass than the unmodified species. Whilst the distribution pattern of species in H3.1 is similar to that in H3.2, they are not identical, which may be relevant to their different roles in biological processes.

For both the H3.1 and H3.2 mass spectra, a heterogeneous distribution of species with incremental shifts of 14 Da was observed. A +14 Da mass shift between adjacent species suggests a single methylation difference between them (Figures 3.10 and 3.11). Mass shifts of multiples of 14 Da could indicate multiple methylations, which could be due to multiple mono-methylations at different sites or combinations of mono-, di-, and tri-methylations. Additionally, the isobaric issue between acetylation and tri-methylation should be noted here; this isobaric concern might be solved by use of tandem mass spectrometry in a bottom-up approach. However, the current resolution and resolving power of LC-MS makes distinguishing these two isobaric species for intact histone isoforms challenging. Each peak could correspond to multiple variants with direct combinations of different methylations and acetylations as well as phosphorylation for the histone mass shift.

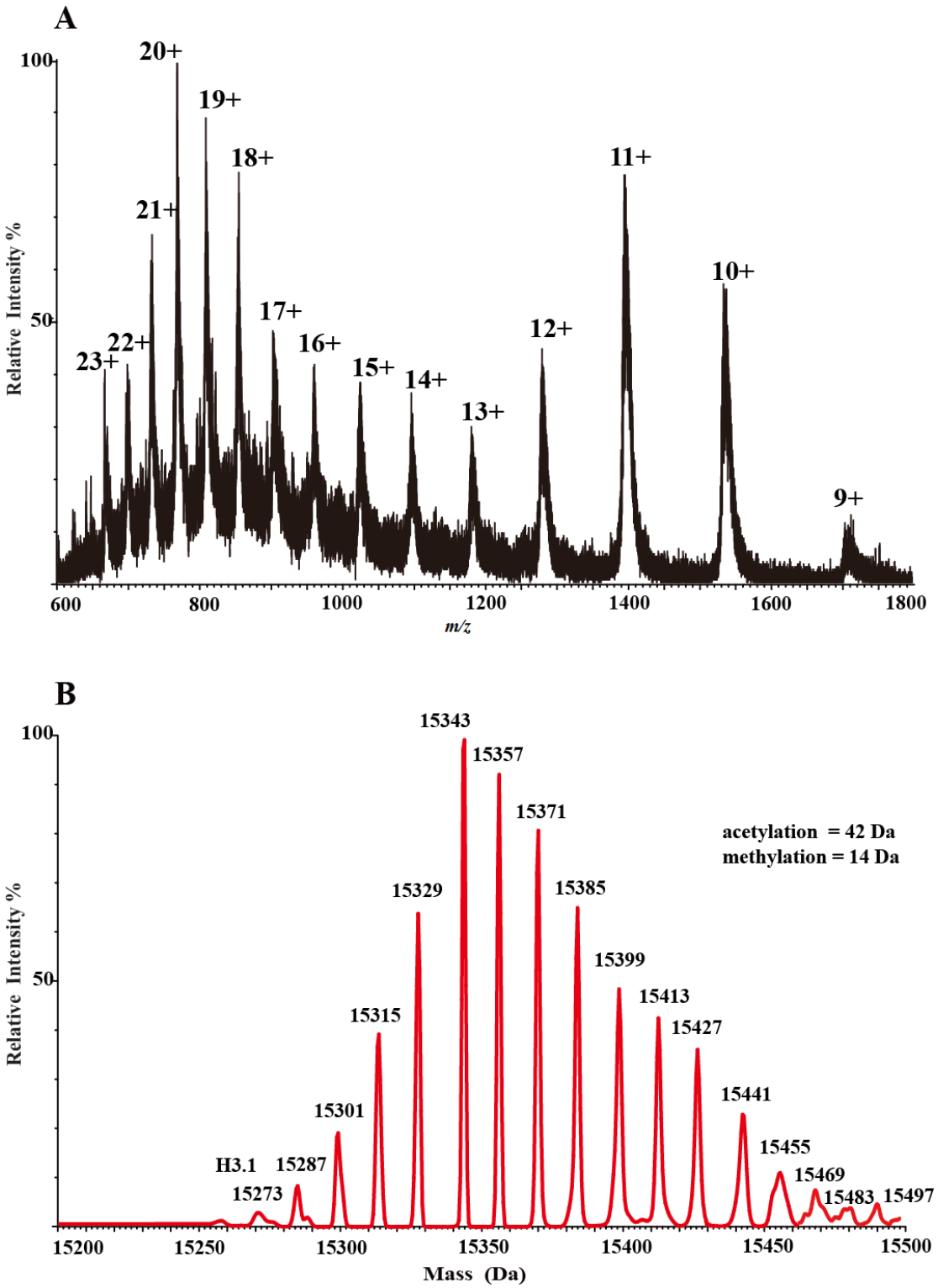

Figure 3.10 (A) Mass spectrum of H3.1 showing ions with charge states from 9+ to 23+. (B) Deconvoluted mass spectrum showing evidence for multiple PTMs on H3.1. The incremental +14 Da shifts likely indicate successive methylation, though other PTMs are possible.

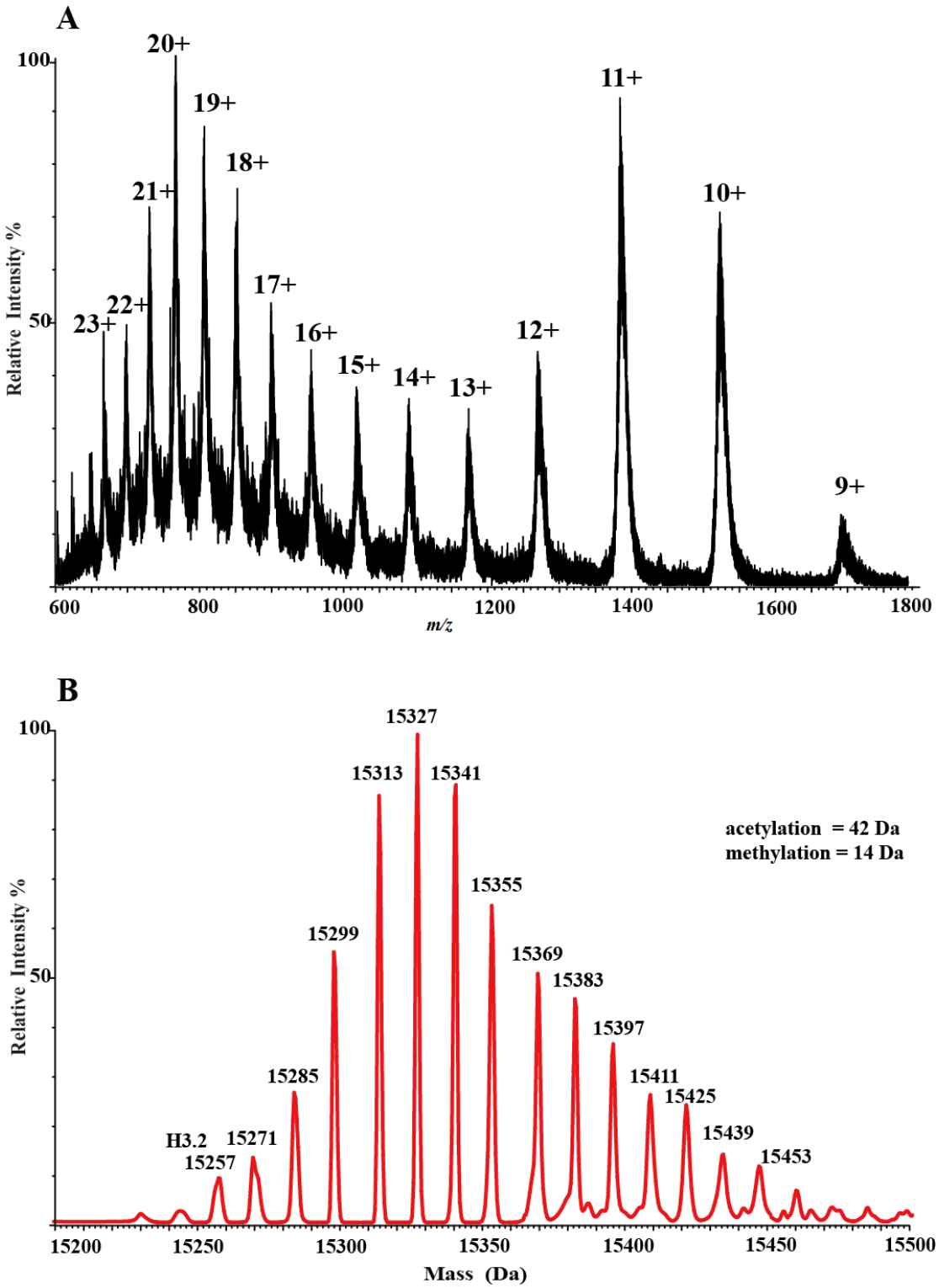

Figure 3.11 (A) Mass spectrum of H3.2 showing ions with charge states from 9+ to 23+. (B) Deconvoluted mass spectrum showing evidence for multiple PTMs on H3.2. The incremental +14 Da shifts likely indicate successive methylation, though other PTMs are possible.

3.5.5 Histone H4

3.5.5.1 Background on histone H4

To date, only one histone H4 has been identified in human cells (Table 3.5). H4 consists of 102 amino acid residues and is the most conserved histone.[21] Acetylation at K5, K8, K12, K16, methylations at R3, K20, and phosphorylation at S1, S47 of H4 have been reported.[223] H4 is involved in the structure of chromatin and participates in various biological events, e.g. transcriptional activation and DNA damage.[159]

Table 3.5 Comparison of human histone H4.[187]

variant	UniprotKB Accession number	number of amino acids	Calculated average mass (Da)	Observed mass (Da)* in this work	∆mass (Da)
H4	P62805	102	11236.2	**11278.2±0.79**	**42±0.79**

* Observed masses were a 42 Da greater than the calculated masses indicating *N*-acetylation of histone H4.

3.5.5.2 Results

The mass spectrum of histone H4 shows an envelope of charge states ranging from 7+ to 18+; the deconvoluted mass spectra displays several species (Figure 3.12A). Due to the absence of sequence variants of H4, the provisional assignment of species is likely simpler than for other core histones such as H2 and H3 variants. Again, the mass of the smallest species observed in the LC-MS profile is a 42 Da greater than the calculated H4 mass (11278 compared to 11236, Table 3.5), consistent with the presence of N-terminal acetylation. The most abundant species is at 11306 Da, which corresponds to N-Ac H4 with an additional di-methylation. The second most abundant species, observed at 11348 Da, corresponds to N-Ac H4 with di-methylation and a further mono-acetylation. The other observed species at 11278 Da, 11292 Da, 11320 Da and 11334 Da correspond to *N*-acetylated (N-Ac) H4+ N-Ac H4+ 1Me, N-Ac H4+ 1Ac, and N-Ac H4 + 1Ac+ 1Me, respectively (Figure 3.12B). However, given the isobaric nature of three methyl groups and one acetyl group, many combinations of methylations and

acetylations are possible, and so assignments should be considered provisional. For example, the species at 11320 Da is consistent with either N-Ac H4 +3Me or N-Ac H4+ 1Ac or a mixture of both species. Likewise, the species at 11334 Da could correspond to N-Ac H4+ 4Me or N-Ac H4+ 1Ac+ 1Me (or both). Di-methylation at K20 of H4 has been reported to be predominant PTM of H4.[232] Thus, the majority of the species at 11306 Da might be N-Ac H4 +K20me2. Further, K16 of H4 is commonly acetylated so the assignment of 11348 Da may correspond to N-Ac H4 +K20me2 +K16Ac.[232,233]

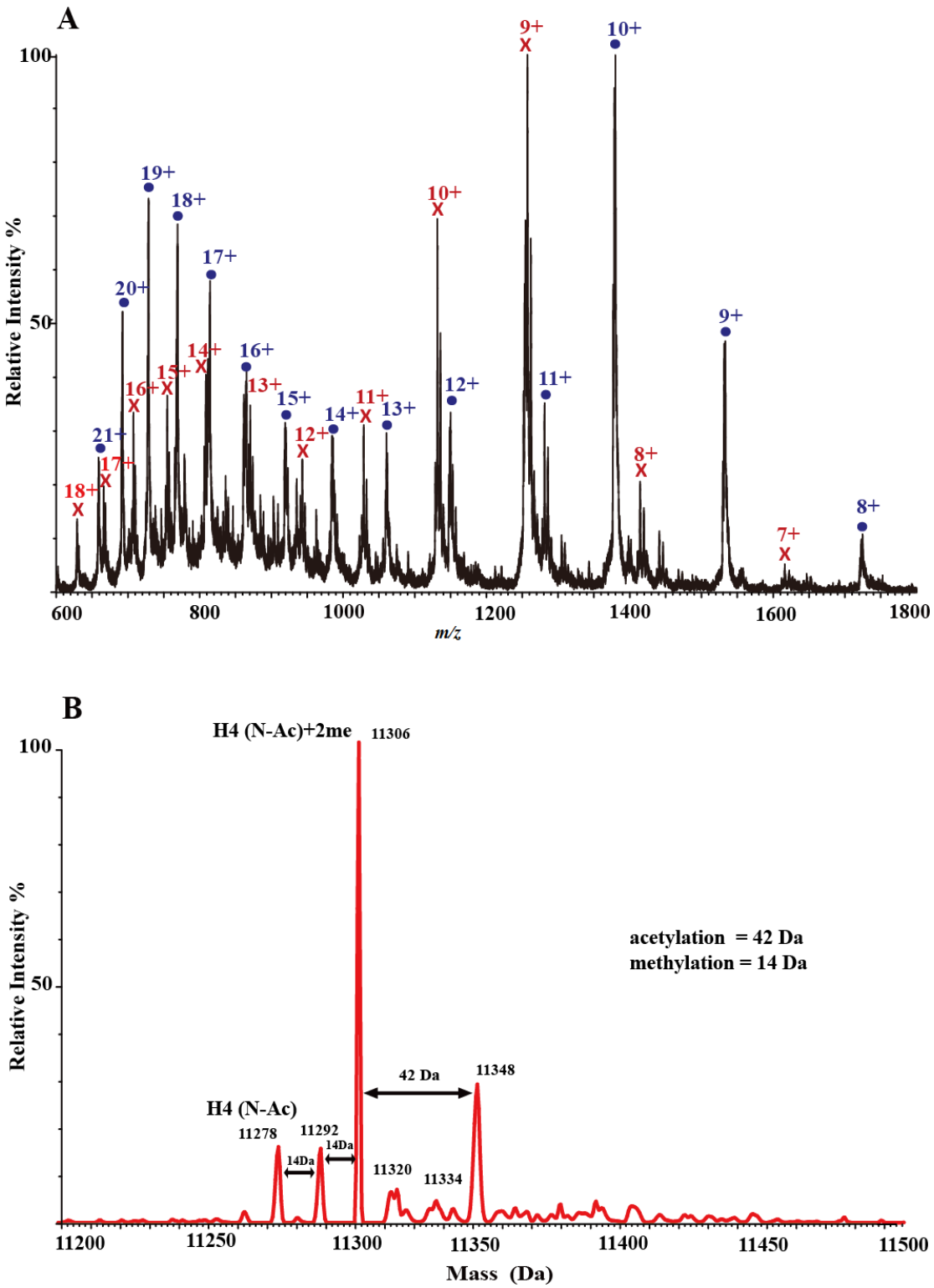

Figure 3.12 (A) Mass spectrum of H4 (X) and H2B (●) showing ions with charge states ranging from 8+ to 21+ and 7+ to 18+, respectively. (B) Deconvoluted mass spectrum from multiple ions (X) showing H4 and its PTMs.

3.5.6 Summary

Various types of PTMs on histones, including methylation (+14 Da), acetylation (+42 Da) and phosphorylation (+80Da), have only small effects on the chromatographic behaviour of the intact core histones and thus modified histone isoforms may be not separated into individual fractions. As a result, LC-MS-based methods are a powerful tool for separating different types of these core histones whilst still displaying individual histone variants and their PTMs simultaneously. Thus an overview of PTM patterns for intact histones can be obtained using the LC-MS approach.

3.5.7 Potential limitations of this method

3.5.7.1 Mass detection

The masses of intact core histones and their modified isoforms range from 11.2 to 16 kDa and the overlapping of their isotopic distribution leads to complication in data analysis. To address this issue, a higher resolution instrument, i.e. a LTQ-Orbitrap MS machine, was used. Here, the results of two examples of observed species in H4 and H3.2 are described (Figure 3.13).

As described above, for H3.2 (and H3.1, and to a lesser extent, for H4), a range of species differing by mass shift of +14 Da were observed. No overlap of isotopic distribution was observed between the observed species at 11278 Da and 11292 Da in the H4 intact mass profile (Figure 3.13, left panel) and no or subtle overlapping of isotopic distribution was observed between the species at 13527 Da and 15341 Da in H3.2 (Figure 3.13, right panel). Therefore, methylation (+14 Da) does not induce overlapping of isotopic distribution and therefore subsequently interfere with the interpretation of MS profile of intact histone. Potential overlapping of isotopic distribution becomes an issue when nearly isobaric histone variants or species carrying

tri-methylation (+42 Da) and acetylation (+42 Da) are considered.

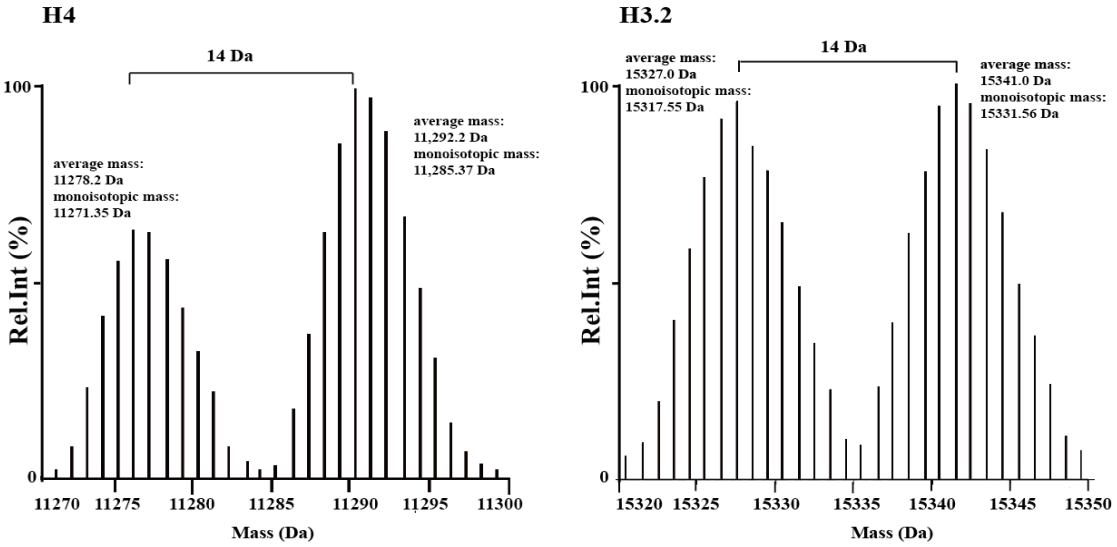

Figure 3.13 (Left) The isotopic distribution of N-Ac H4 (average mass: 11278.2 Da; monoisotopic mass: 11271.35 Da) and N-Ac H4 with mono-methylation (average mass: 11292.2 Da; monoisotopic mass:11285.37 Da). (Right) The isotopic distribution of H3.2 with five methylations (average mass: 15327.0 Da; monoisotopic mass: 15317.55 Da) and H3.2 with six methylations (average mass: 15341 Da; monoisotopic mass: 15331.56 Da).

In Section 3.5, the LC-MS profiles for H1, presented an unambiguous assignment for each species in mass spectra. The distinct masses for the H1 variants and the relatively limited number of coexisting modification patterns make for simplified interpretation of mass spectra for this intact histone. Likewise for histone H4, the lack of variants and the small number of PTMs observed render the identification of intact histone H4 with PTMs less complicated. However, the discrimination between histone variants and PTMs is a concern when interpreting H2A and H2B mass spectra due to their many variants with very similar masses (Tables 3.2; Figures 3.8 and 3.9). For histone H3, the LC-MS profiles show individual mass spectra for H3 variants (Figures 3.10 and 3.11), however, the interpretation of masses within these is more complicated due to their highly modified states.

The LTQ-Orbitrap hybrid mass spectrometer has been developed to provide high-resolution and accurate mass determination.[234] Xtract software is used to process the

LTQ-Orbitrap isotopically resolved spectra to achieve deconvolution.[46] This instrument was also used to resolve the issue of the ambiguous assignment of mass species of histones. The spectra collected using this machine demonstrate that the LTQ-Orbitrap has an advantage of higher accurate mass performance than LCT-TOF machine.

Using LCT-TOF, Figure 3.14A shows that the species at 14017 Da could be assigned as either the N-Ac H2A type 1-C (14016.3 Da) or the N-Ac H2A type 1-D (14018.3 Da). Monoisotopic analysis of the LTQ-Orbitrap spectrum (Figure 3.14B) reveals that the observed species at 14008.55 Da, which is closer to the calculated monoisotopic mass of the N-Ac H2A type 1-C (14007.9 Da) than the N-Ac H2A type 1-D (14009.9 Da). This result suggests that the major part of the species observed at 14017 Da in the LCT-TOF MS profile (Figure 3.13A) is due to H2A type 1-C rather than H2A type 1D.

In addition, the results shown in Figure 3.14 reveal that the high mass accuracy of LTQ-Orbitrap is within 10 ppm, whereas for the LCT-TOF MS method used for the majority of this work the mass accuracy is approximately 70 ppm (~1 Da error). However, the above mentioned isobaric issue between acetylation and methylation still exists for intact histone mass profiles.

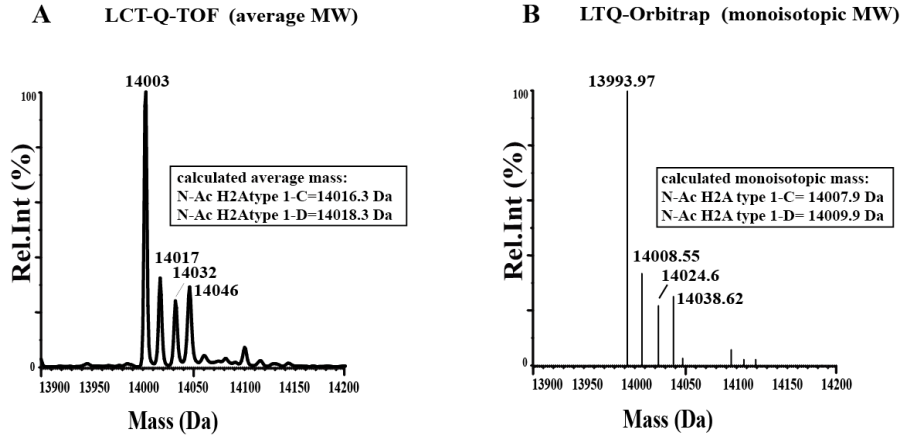

Figure 3.14 Comparison of mass accuracy for histone H2A variants from HEK293T cells between LCT-TOF MS (A) and LTQ-Orbitrap MS (B).

3.5.7.2 Oxidation of histones in sample preparation and LC-MS

There has not been direct evidence reported for the oxidations of histone residues and their biological functions, although some studies report the possibility of methionine oxidation on histone *in vivo* with potential links to the DNA repair pathway.[235,236] Artifactural oxidation of histones during sample preparation and the process of LC-MS could potentially complicate the analysis of MS profiles. Oxidation of histones can occur on methionines, resulting in a mass increase of 16 Da or 32 Da by partial or complete oxidation, respectively, resulting in overlapping peaks with PTMs such as one methylation (+14 Da) or two methylations (+ 28 Da).

Partial oxidation of histones has been noted to change the MS pattern of intact histones and the extent of change is dependent on the level of oxidation.[237] Oxidized forms of histones have been observed in samples prepared by acid-extraction, or HAP-purified methods, but in relatively low abundance. [215] Previous studies showed RPLC can separate some oxidized and non-oxidized forms of histones.[215] The oxidation of methionine to methionine sulfoxide or methionine sulfone oxidation status decreases the hydrophobicity of proteins and thus normally decreases their retention time in RPLC.[238] Oxidized peaks have been observed for all core histones except for some of the H2A variants that do not possess methionine residues e.g. H2A type1 and type1-B.[237] Although oxidation of histone samples is not uncommon, the oxidation of samples can be minimized by use of reducing agents, e.g. ß-mercaptoethanol or dithiothreitol (DTT) and careful sample handling, e.g. by maintaining a cold temperature during histone extraction. Previous studies have also reported evidence for oxidation of histones, particularly H3 and H4, in samples stored at -80 ºC for several months prior to analysis. However, samples processed and analysed immediately presented minimal oxidation.[237]

Another source for sample oxidation could be the LC-MS procedure. The use of

capillary or nanoscale columns with low flow rates has been reported to increase oxidation of proteins.[239] Electrospray ionization (ESI) with a voltage higher than 4,000 volts had been reported to cause oxidation of proteins, e.g. of methionine, tryptophan, or tyrosine residues.[240] It is reported that the oxidation of protein during nano LC-ESI-MS can be minimized by lowering the ESI flow rate and needle voltage.[239]

In my work, the use of a microscale column with flow rate of 300 μL/min and ESI needle voltage of 3,000 volts was used to minimise the oxidation of samples. In addition, the acid-extracted and acetone-purified samples were immediately analysed by the optimised LC-MS method. Given that oxidized forms of histones would be expected to elute in a separated fraction and no other fractions were observed in this study, oxidation is unlikely to be a significant factor in my analysis. Further, the observed masses for unmodified histones were consistent with no substantial amounts of oxidation occurring.

3.6 Validation of the LC-MS method for detection of histone PTMs

3.6.1 Sources of variability

To validate the LC-MS profiles collected in this work, factors that might cause variability in the relative abundance of species in mass spectra were then examined. Previous studies have shown no significant difference in spectra for core histones when using different mass spectrometers.[241,242] TOF mass spectrometry was reported to possess higher sensitivity and better resolution than ion trap mass spectrometry. A sample of histones from HEK293T cells was analysed in triplicate and the relative deviation (RSD) for each peak was found to be less than of 5% (data not shown). It suggests that the results produced by the current LC-MS method are reproducible.

3.6.2 Independent sample analysis

Next, the variability between different samples was investigated. Cells were subcultured from the same origin of HEK293T cells and histone extraction and LC-MS procedures were carried out identically for each sample (employing acid extraction). The results show low biological variability based on the relative abundance for all core histones variants and their PTMs (Figure 3.15).

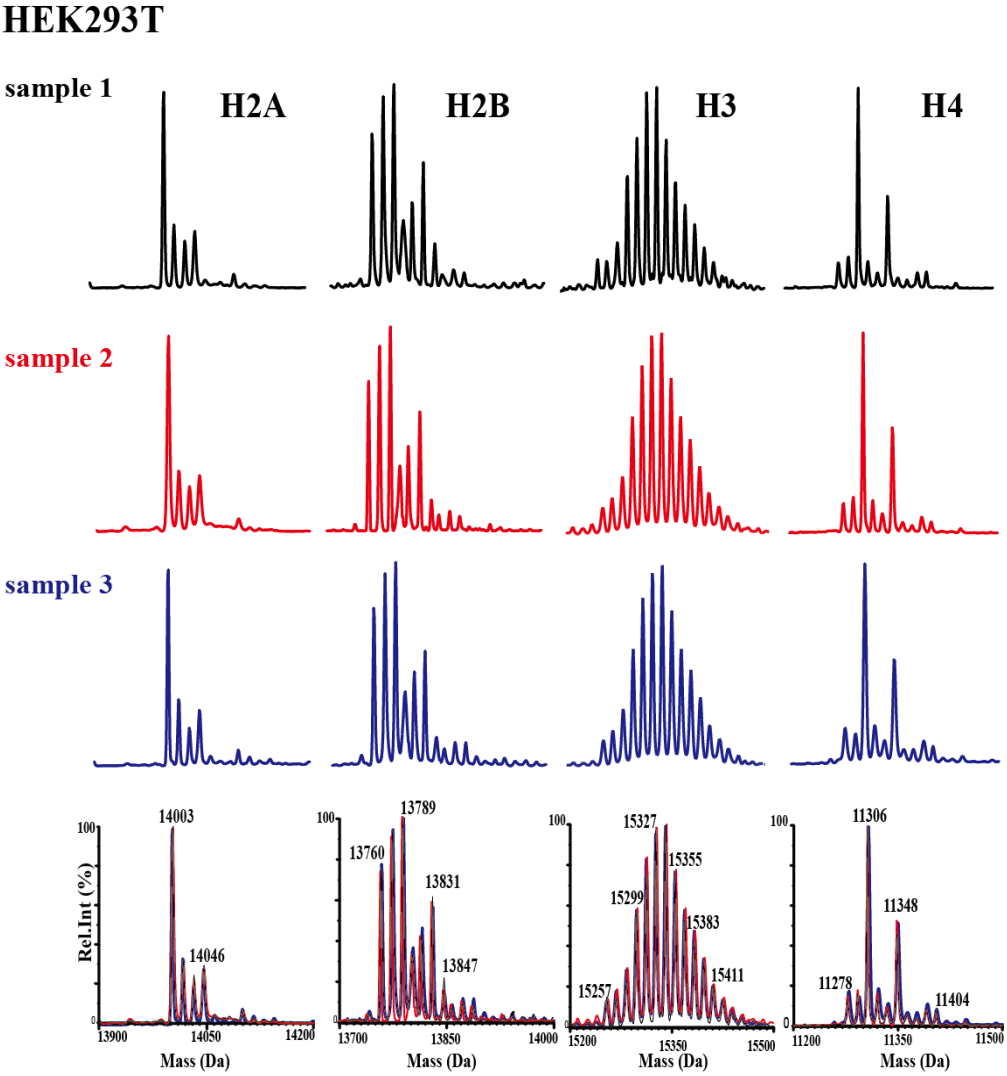

Figure 3.15 Evaluation of reproducibility of the LC-MS-based method using different samples of HEK293T cells. The bottom panel shows overlaid mass spectra for comparison. Note they are very similar.

3.6.3 Variability due to the extraction method

Sample preparation can often be a factor in inducing variability in LC-MS profiles. The acid-extraction method is widely used for histone experiments. Earlier work has indicated that there is little difference between the acid-extraction method and the HAP-separation method for the analysis of histones modifications, including with respect to the analysis of methylation, acetylation and even phosphorylation PTMs.[215]

As described in Section 3.3, an acid extraction coupled to acetone precipitation was found to give the greatest yield for isolating histones from mammalian cells. To determine whether the extraction method could influence the PTM profile, histones isolated using each of the previously described methods (dialysis, acetone or TCA precipitation) were analysed by LC-MS. The overlaid images show a very similar MS pattern for each histone analysis (Figure 3.16).

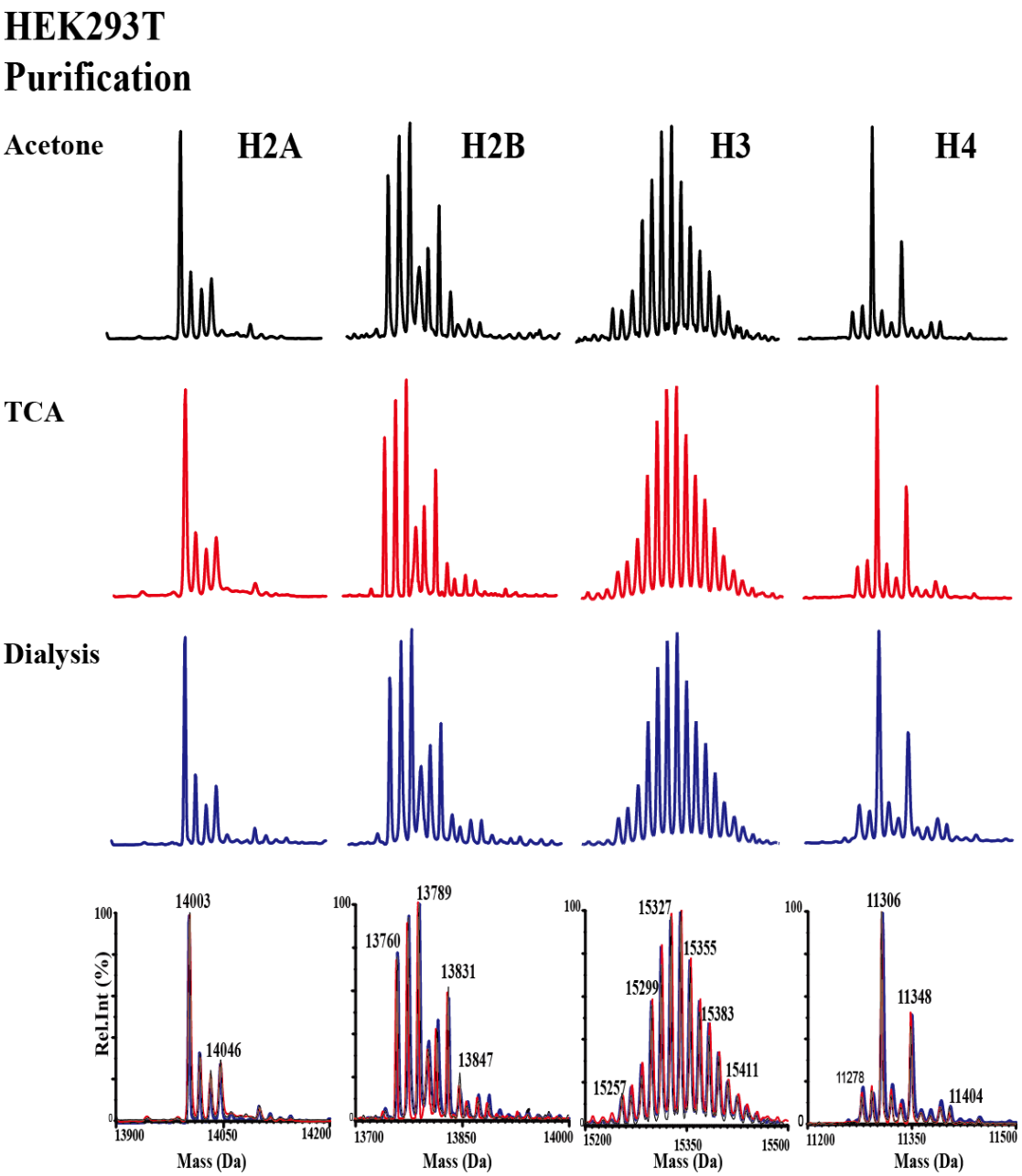

Figure 3.16 Evaluation of reproducibility of the LC-MS-based method by different samples preparation methods, including acetone, TCA and dialysis for purification from the same passage generation of HEK293T cell line. The bottom panel shows overlaid mass spectra for comparison.

3.6.4 Impact of delays in sample processing

Potential variations caused by sample processing delay were evaluated by running the same samples at different times. Three samples were processed for LC-MS profiling either immediately, after a 12- hour delay or after a 1-day delay. The results show no significant change of relative abundance distribution for core histones (data not shown). However, to minimise the effect of processing time, all subsequent samples were analysed at the same time as far as possible.

3.6.5 Summary

In summary, the above mentioned factors were all shown to have minimal effects on variability within the LC-MS method used in this study, suggesting the current method is sufficiently robust and suitable for analysing PTM patterns on intact histones.

3.7 LC-MS for analysis of histones from human normal and cancer cells

3.7.1 LC-MS for separation of core histones

The overall results demonstrate the optimised LC-MS-based method under TFA-free mobile phase conditions to be robust for identifying and characterising human HEK293T histone variants and their PTMs prepared by the acid-extraction method followed by acetone precipitation. To test the application of this approach for profiling histones from various human cancer cells, histone samples from HeLa (cervical carcinoma), RKO [d] (poorly differentiated colon carcinoma) and MCF-7 (breast adenocarcinoma) cells were analysed.

LC-MS chromatogram of histones extracted from normal HEK293T cells and three

[d] RKO samples in this work were provided by Monica Olcina from Dr. Ester Hammond Group, CRUK MRC Oxford Institute for Radiation Oncology, Department of Oncology, University of Oxford.

different cancer cells (HeLa, RKO and MCF-7) show the same elution order of histones (first peak for H1, second peak for H4 and H2B, third peak for H2A followed by the peaks for H3.2 and then H3.1, Figure 3.17 left panel). In addition, the chromatograms show that the retention time for individual histone types is similar for the one from human initially tested cell line and three human cancer cell lines. This result implies that the optimised LC-MS condition was applicable to a wide-range of cell types, including human normal and cancer cells.

3.7.2 LC-MS profiles of histone H4

Next, the LC-MS profiles for these histones of different cellular origins were investigated. The mass spectra of histone H4 from all four samples displayed a distribution of several differently modified histone forms (Figure 3.17 right panel). As previously described, H4 is different from other core histones in that it has no apparent sequence variants. Thus, the interpretation of different peaks in the mass spectra for H4 could be considered as relating only to its PTMs. For example, the most abundant species was observed at 11306 Da in all four cell lines and was consistent with N-Ac + 2Me. The species at 11348 Da, a 42 Da greater than the species at 11306 Da indicates an additional acetylation on H4.

Noticeably, the H4 peak of 11348 Da was the second most abundant in HEK293T cells, but is less abundant in the other three human cancer cells. The masses at 11278 Da and 11292 correspond to N-Ac H4 and N-Ac H4 with mono-methylation, respectively. A slight change in these two species was noted among the four cell lines. This assignment is consistent with reported data showing that 11306 Da corresponded to modification of N-Ac H4+ K20me2 and 11348 Da due to N-Ac H4+ K16Ac+ K20me2.[232] Global changes in histone PTMs have been reported to be relevant to tumour progression and

histone marks can be seen as a hallmark of human cancer. [243,244] The observation of decreased level of the 11348 Da species in the cancer cell lines is supported by previous studies reporting loss of H4K16Ac relating to tumour development in breast and colon cancer.[243,245]

3.7.3 LC-MS profiles of histone H2A and H2B

The mass spectra of H2A and H2B are shown on Figure 3.18. The majority of the species for H2A observed in the analysis on HEK293T cells were also observed in HeLa, RKO and MCF-7 cancer cells. The three most abundant species at 14003 Da, 14017 Da and 14046 Da were assigned as N-Ac H2A1, N-Ac H2A1C/1D and N-Ac H2A1B/1E (or N-Ac H2A1+ 1K-Ac, minority of signal).[242] The distribution of H2A variants in HEK293T cells is quite similar to that observed in HeLa and MCF-7 cells, except that the species at 14031 Da was decreased in abundance in HeLa and MCF-7 cells. Notably, relative to HEK293T cells the RKO cells had a higher relative abundance of the species at 14046 and 14060 Da. This observation suggests an increase in the abundance of N-Ac H2A1C/1D (14046 Da), and more acetylation on N-Ac H2B1B/1E (14017+42=14059 Da) in RKO cells, compared to the other three cells in this study. Minor changes are apparent for the species at 13817 Da (N-Ac H2A1H) and 13900 Da (N-Ac H2A2C) with increased and decreased abundances, respectively.

The relatively abundant distributions of LC-MS profiles for H2B were similar between HeLa, RKO and MCF-7 cells, but different from those in HEK293T cells. It is possible that changes in H2B variants observed between normal and cancer cells are relevant to tumour development. [246,247] The species at 13775 and 13819 Da were the two most abundant, followed by the species at 13760 and 13831 Da in HeLa, RKO and MCF-7 cells. The results indicate that H2B1C (13775 Da) and H2B1B (13819 Da) are the major

H2B variants existing in cancer cells followed by H2B1H/1K (13760 Da).

3.7.4 LC-MS profiles of histone H3

LC-MS profiles for H3.1 and H3.2 are presented in Figure 3.19. Approximately 16 or 17 peaks were recorded for H3.1 from HEK293T, HeLa and RKO cells, whereas 15 or 16 peaks were observed for H3.2. Only around 13-14 peaks were observed for H3.1 and H3.2 from MCF-7 cells. The most abundant peak was observed at 15343 Da for H3.1 and one at 15327 Da for H3.2 for all four cell lines. The second and third most abundant peaks at 15357 and 15371 Da were observed for H3.1 in HEK293T cells, whereas the peaks at 15329 Da and 15357 Da were the second and third most predominant species of H3.1 in HeLa, RKO and MCF-7 cells. On the other hand, the almost equally abundant species at 15313 Da and 15341 Da, the second and third highest peaks for H3.2 were observed in HEK293T, RKO and MCF-7 cells. HeLa cells presented the second and third highest peaks at 15341 and 15355 Da. In general, the LC-MS profiles for both H3.1 and H3.2 displayed a unimodal distribution with the most abundance at sixth peak for human normal and cancer cells. Noticeably, these relative abundance distributions for histone H3.1 and H3.2 were not identical and some of species were obviously different among different cell lines. The interpretation of peaks for histone H3 is relatively complex due to the many possible combinations of PTMs (Appendix 6).

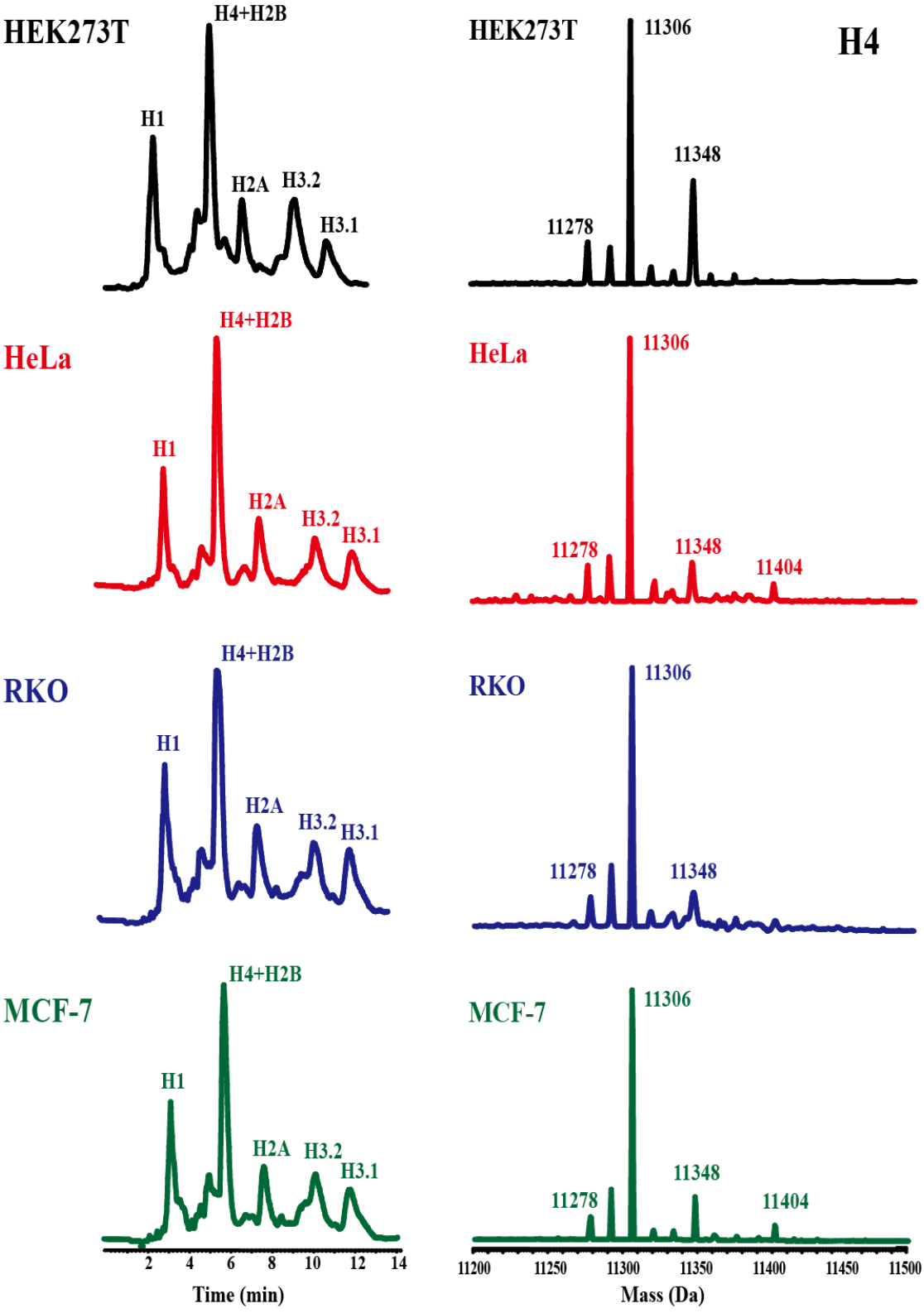

Figure 3.17 Left panel shows microbore LC-MS chromatograms of human histones extracted from one normal cell line and three cancer cell lines. Optimised LC-MS condition: 0.5% (v/v) formic acid, C4 column, 2.1 mm x 150 mm, 1.7 µm, 300 Å, flow of 300 µL/min. Data were collected using a LCT ESI-TOF MS machine. Right panel shows deconvoluted mass spectra of histone H4 from H4 fraction of LC-MS chromatogram.

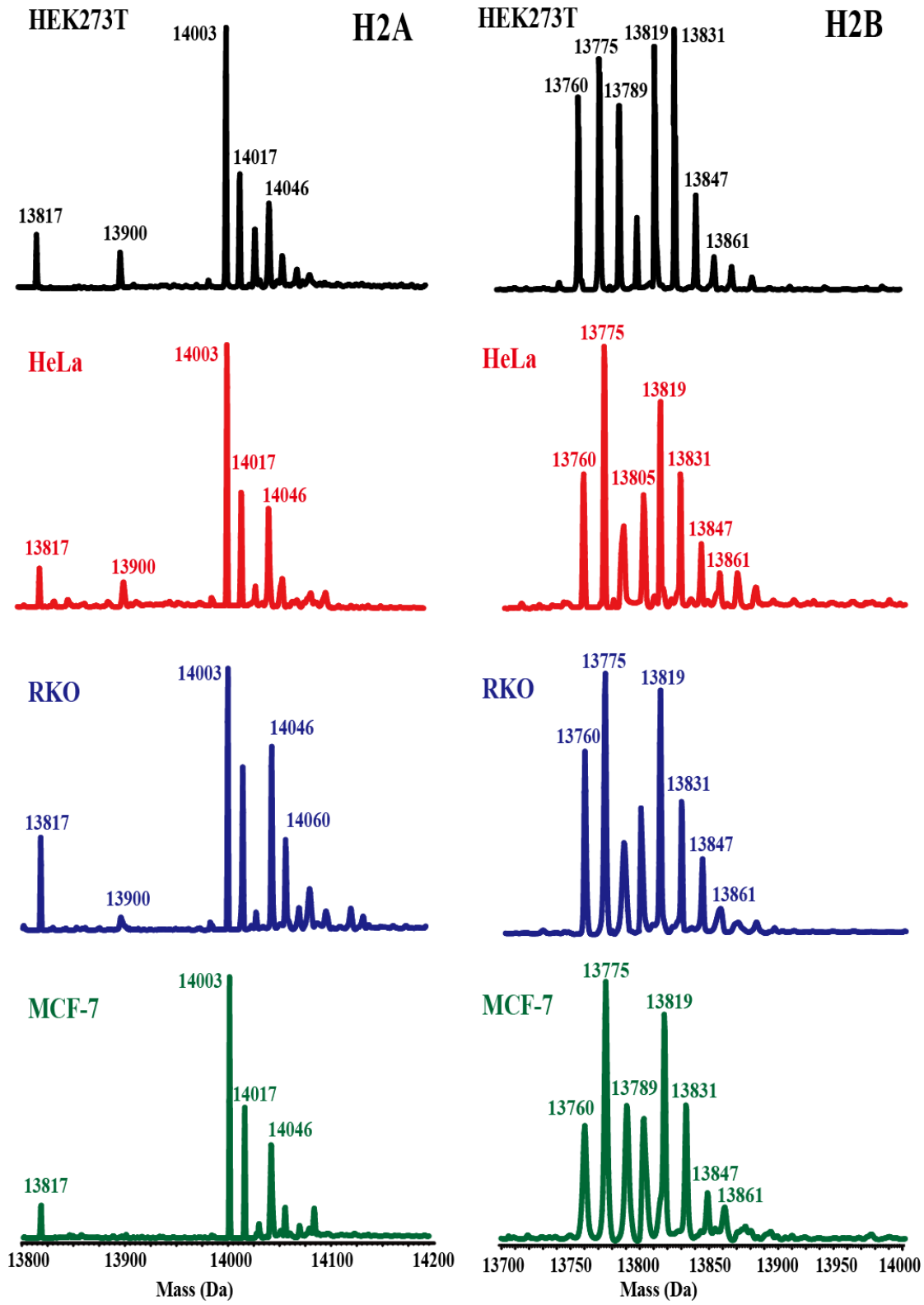

Figure 3.18 Deconvoluted mass spectra of histone H2A and H2B from their fractions of LC-MS chromatogram (Figure 3.17 left panel) for corresponding human cell lines. Data were collected using a LCT ESI-TOF MS machine.

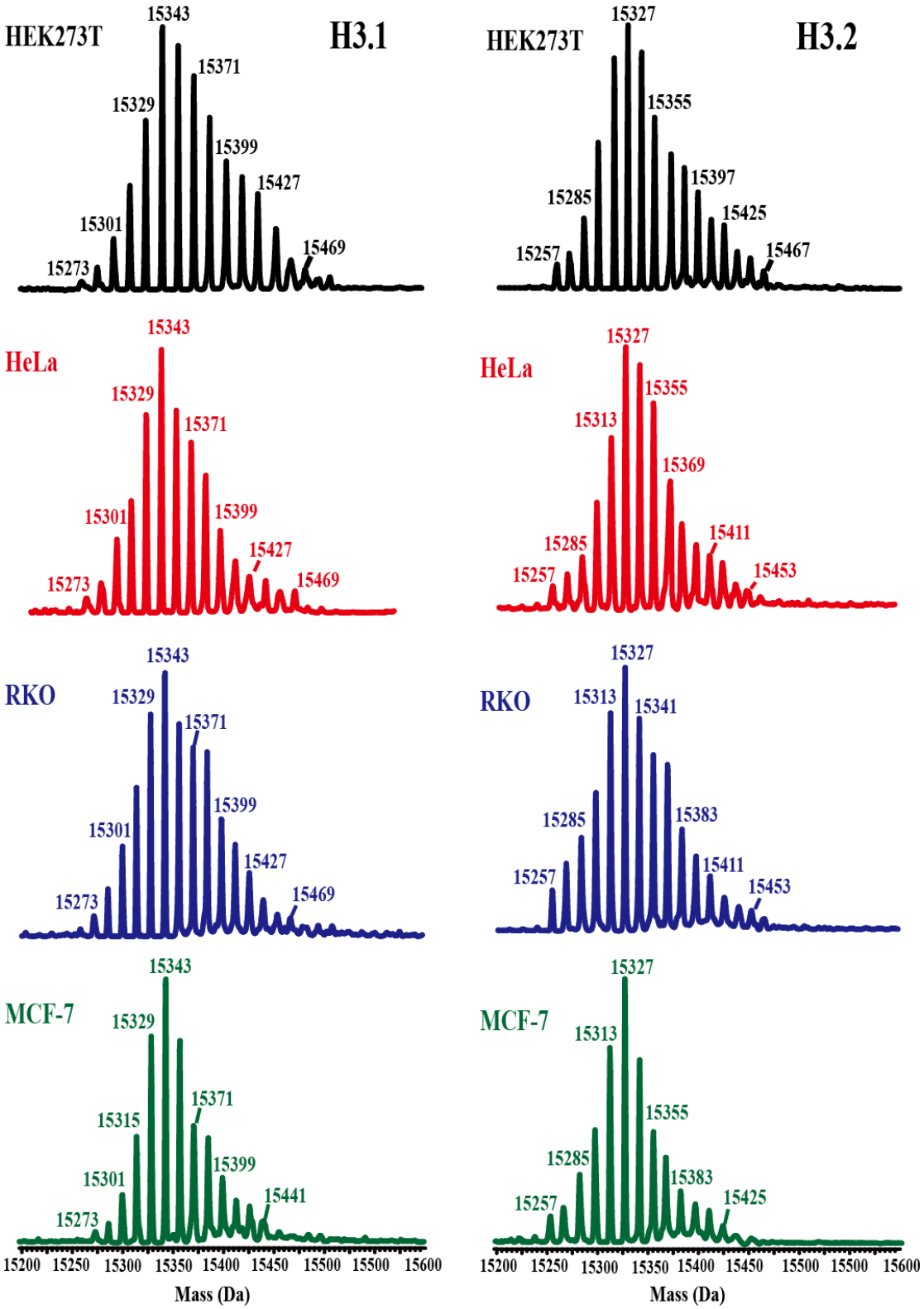

Figure 3.19 Deconvoluted mass spectra of histone H3.1 and H3.2 from their fractions of LC-MS chromatogram (Figure 3.17 left panel) for corresponding human cell lines. Data were collected using a LCT ESI-TOF MS machine.

3.8 LC-MS for analysis of histones from clinical patients with glioma

The experiments described above validate the optimised LC-MS method as a robust tool for studying histones from immortalized human normal and cancer cells. It was therefore of interest to test the feasibility of this method for analysis of clinical samples from patients with cancer. Clinical samples[e] from patients diagnosed with glioma were evaluated. As for the previous samples, histones were prepared from glioma samples using the acid-extraction method followed by acetone precipitation; the separated histones were analysed by LC-MS under the optimised conditions (C4 column, 2.1mm x 150mm, 1.7μm, 300 Å, flow of 300 μL/min, 0.5% (v/v) formic acid in acetonitrile as mobile phase solvent B, 0.5% (v/v) formic acid in water as solvent A, gradient programme as Figure 3.5). The deconvoluted mass profiles were generated using MassLynx 4.1 software (Waters).

For the samples from three patients, the LC-MS chromatograms (Figure 3.20) shows the same order of elution for the linker and core histones and the same retention time, as predicted from the analyses of human cell lines (Figure 3.17). The mass spectra in Figure 3.20 for histone H2A, H2B, H3.1, H3.2 and H4 are as high resolution as these for human cell lines described in Section 3.7. The results show the current optimised LC-MS method is robust not only for human cell lines but also for clinical samples from patients with cancer.

The relative abundance distribution for H2A, H2B, H3.2 and H4 were found to be highly similar among the three patients. However, for H3.1, some changes for patterns of mass spectra were noted among three patients. A slightly bimodal distribution for H3.1 was observed in patient 1. The highest peak at 15357 Da was noted in patient 3,

[e] samples gifted from Dr. Nick de Pennington, Department of Neurosurgery, John Radcliffe Hospital.

whereas the highest one was at 15343 Da in patient 1 and patient 2, as observed on H3.1 from HEK293T cells. Interestingly, a decreased abundance of the species at 11348 Da in H4 mass spectra is seen in analyses on the human cancer cell lines, including HeLa, RKO and MCF-7 cells, compared to HEK293T cells (Figure 3.17), which was not observed in cells from glioma patients (Figure 3.20). In addition, the peak at 14046 Da corresponding to N-Ac H2A type 1-B/E, was the second abundant species in the cells from all three glioma patients. The species at 14032 Da corresponding to N-Ac H2A3 was noted at very low abundance in all three glioma patients and this was also seen in HeLa, RKO and MCF-7 cells. The distribution pattern of H2B mass spectra for glioma patients is similar to HeLa and MCF-7 cells with the most abundant species at 13775 Da followed by species at 13819 and 13831 Da.

The LC-MS approach was successfully applied to profile intact histones in a small sample group of glioma patient cells. The method could be extended to various types of tumours from patients and could be further developed as a clinical tool for histone analysis. Furthermore, the comparison of mass spectra patterns of intact histones between brain tumours and normal brain cells would be interesting to get more information on how histone marks correlate with the tumour development. The link between MS profiles of histones from brain tumors and their histopathological behaviour may provide information important in prediction of prognosis and survival.

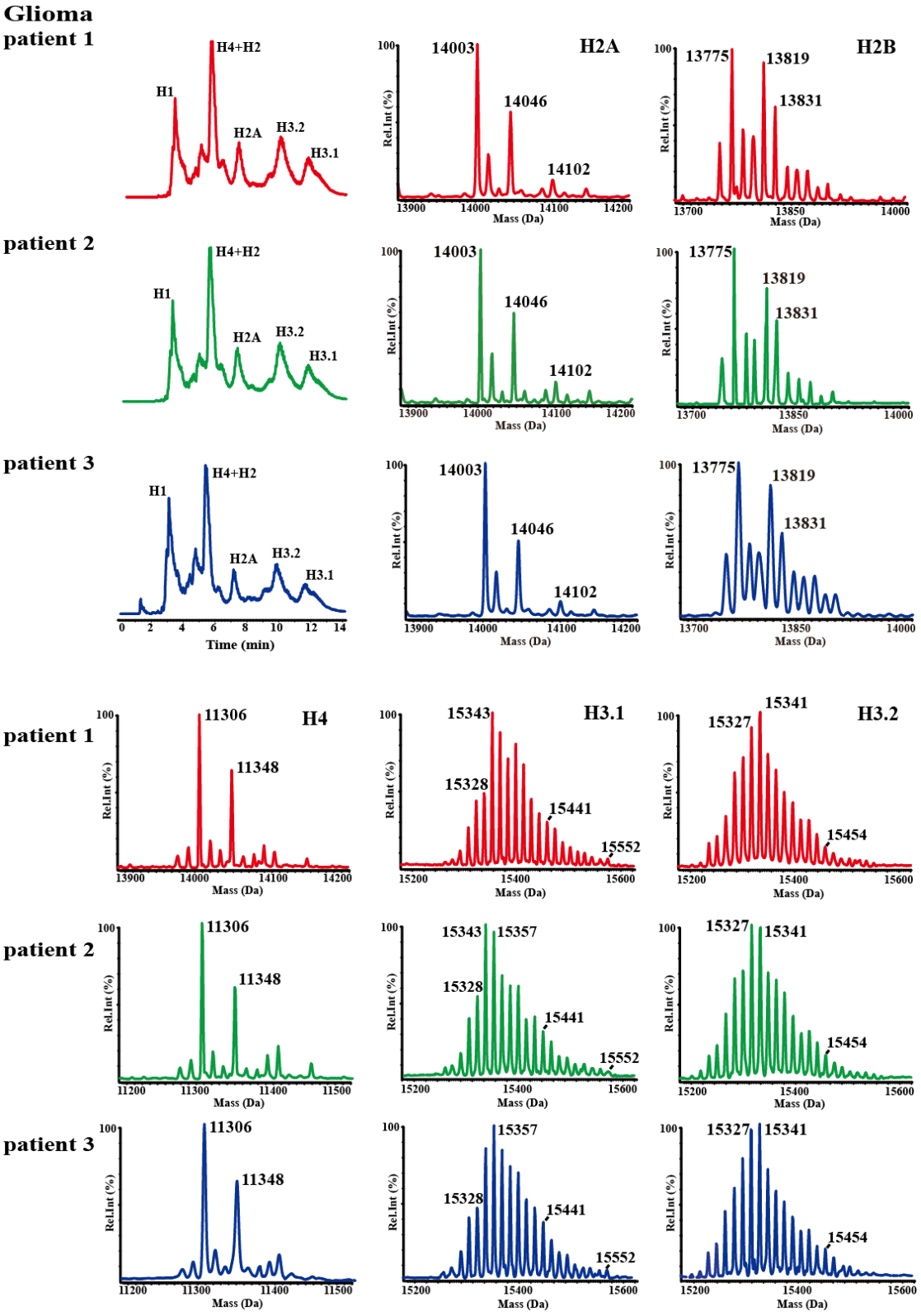

Figure 3.20 Application of the LC-MS-based method for histone analysis of clinical samples from three patients with glioma.

3.9 Summary and conclusion

An optimised LC-MS-based method for histone analysis has been developed. Use of formic acid as a TFA-free ion pairing agent for histone separation avoided the interference of TFA adducts and made the MS distribution more accurate. Acid-extraction followed by acetone purification gave a simple, rapid process of sample preparation and provided the greatest abundance of histones, though not in high purity. With the high resolution of LC and MS instruments, the characteristics of this current method require very small amounts of sample, providing information on the global modifications states of all core histones in their intact state in a single robust and reproducible LC-MS procedure. Only a small minority of histone variants were found to be below the limit of detection.

Furthermore, the validation of the current method showed it to be robust for analysing the relative abundance and distribution of histone PTMs. This method was used in histone profiles from normal and cancer cells. The application of this method was successfully extended to the clinical samples from the patients with glioma. The different mass profiles of intact H3.1 were observed between three samples from patients and the abundance distribution of intact H4 mass spectra was different from the human cancer cells. These results indicate that the mass profiles are specific for patients with glioma and there are differences in intact histone MS between glioma and other types of cancer. This information may be helpful in the diagnosis of disease or prediction of prognosis.

Chapter 4
Application of the LC-MS method for analysis of histone modifications under different conditions

4.1 Introduction

4.1.1 Hypoxia

The term hypoxia refers to a lack of oxygen in tissue, and is often defined as ≤ 2% atmospheric O_2.[248] Normoxia is considered to be atmospheric oxygen pressure (around 150 mmHg or 21% O_2 for cell cultures).[248] In response to hypoxia in animals, adaptive events take place in cells that work to maintain oxygen supply and/or economise oxygen consumption; such events included erythropoiesis, angiogenesis, and partial shutdown of high energy consuming processes.[249,250] Many of these responses involve major changes in gene expression, which are mediated by the hypoxia-inducible transcription factors (HIFs).[251] HIF is a heterodimer composed of an oxygen-sensitive subunit (HIF-α) and a constitutive subunit (HIF-ß).[250] α,ß-Dimeric HIF binds to specific DNA regions, known as hypoxia response elements (HREs); such binding triggers expression of HRE-associated target genes. HIF-α is regulated by two types of 2OG/Fe(II)-dependent oxygenases, the prolyl- hydroxylases (PHD1, PHD2 and PHD3 in humans) and the asparaginyl hydroxylase, factor inhibiting HIF (FIH).[252]

The PHDs catalyse hydroxylation of two proline residues within the oxygen dependent degradation domain of HIF-α.[253] The prolyl hydroxylated HIF-α is then targeted by the von Hippel-Lindau tumour suppressor protein (pVHL), a substrate recognition component of the E3-ubiquitin ligase complex; HIF-α isoforms are subsequently ubiquitinated, so causing their proteasomal degradation.[254] PHD2 is an indispensable PHD. Human PHD is reported to have an unusually K_M for oxygen and is considered

to be the most important HIF hydroxylase for hypoxia sensing.[255,256] FIH catalyses the hydroxylation of an asparagine residue, Asn-803 within the C-terminal transactivation domain (CAD) of HIF-α isoforms.[257] This hydroxylation prevents HIF-α interacting with the p300 transcriptional co-activator protein.[258] In hypoxia, the limited availability of oxygen inhibits the HIF hydroxylases and subsequently stablises HIF's interaction with p300, so promoting hypoxia-associated gene transcription.[249] Different patterns of histone modifications are reported to regulate the expression of different sets of HIF target genes expressed in different context.[249]

4.1.2 Epigenetics and hypoxia

Like the HIF hydroxylases, the JmjC KDMs are 2OG/Fe(II)-dependent oxygenases that also require oxygen as an essential cosubstrate during histone demethylation; their enzymatic activity has the potential to be compromised under hypoxia.[94,259] Consistent with this, decreased enzymatic activity of KDM4 family demethylases in cells under hypoxia has been reported.[123,249] Therefore, the alteration of JmjC KDM- modulated histone PTMs has the potential to link to the hypoxic response.[123] KDM3A, KDM4B, KDM4C, KDM5B and KDM6B have been reported to be transcriptionally activated under hypoxia.[123,260-262] The roles of these JmjC KDMs under hypoxia have also been investigated. For example, KDM3A has been reported to be necessary for hypoxic induction of adrenomedullin (*ADM*) and growth differentiation factor 15 (*GDF15*) by demethylating H3K9me2 in histones associated with hypoxia responsive promoters.[263]

Overall, increasing evidence suggests that hypoxia has the potential to induce global changes in histone methylation by compromising the enzymatic activity of JmjC KDMs, whereas upregulation of specific JmjC KDMs due to HIF-mediated transcriptional expression has been shown to act on specific hypoxia-responsive promoters.[249]

4.2 Aim of the work

The LC-MS method described in Chapter 3 was applied to study potential changes in the PTM patterns of intact histones in cells subjected to different treatments, with the main focus being hypoxia. The workflow for histone profiling under different conditions in this work is shown in Figure 4.1. Compounds used in the work are shown in Figure 4.2.

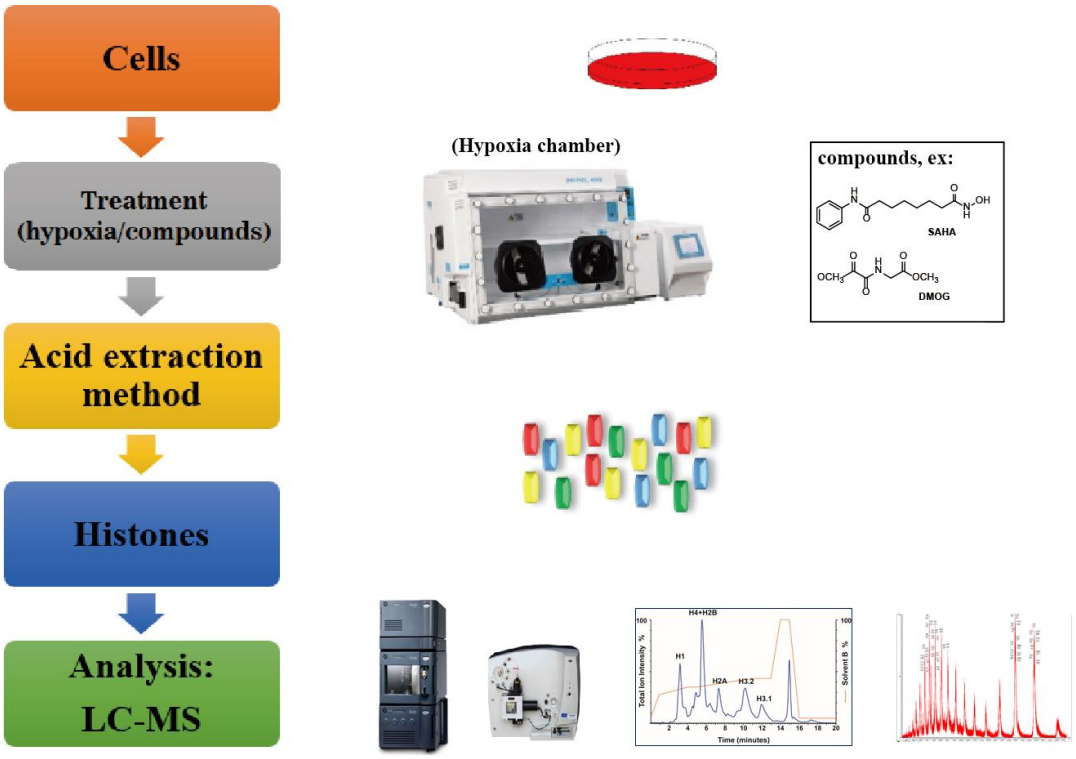

Figure 4.1 Workflow of histone profiling for cells under various conditions or compound treatments by using the optimised LC-MS-based method.

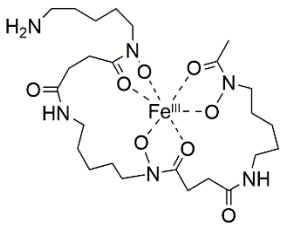

Chelation of iron with Deferoxamine (DFO)

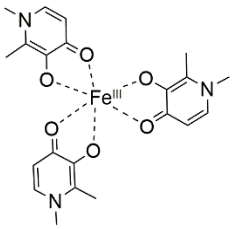

Chelation of iron with Deferiprone (CP20)

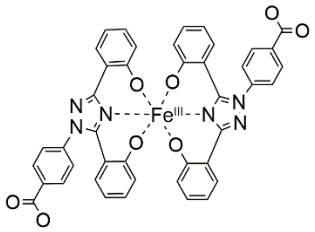

Chelation of iron with Deferasirox (Exjade)

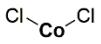

Cobalt Chloride($CoCl_2$)

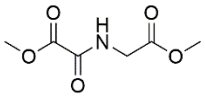

Dimethyloxalylglycine (DMOG)

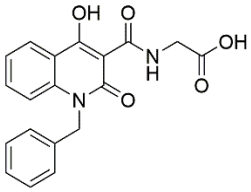

IOX2

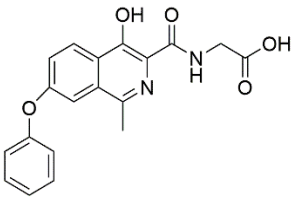

FG-4592

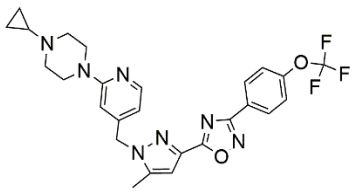

BAY-87 2243

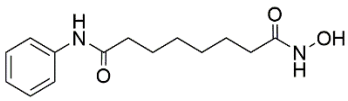

SAHA (Vorinostat)

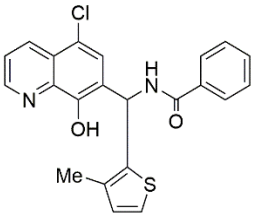

CCT1

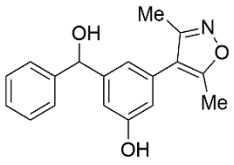

DSH122

Figure 4.2 Chemical structures of compounds used in this work. The modes of chelation of iron by DFO, CP20 and Exjade are shown.

4.3 Detection of change of histone PTMs by optimised LC-MS

4.3.1 Detection of hypoxia-induced PTMs change on core intact histones

To simplify analysis, mass spectra of core histones are presented as deconvoluted molecular mass profiles. Superimposed images of mass spectra from cells treated with normoxia or severe hypoxia (0.1% O_2) for 24 hours are shown for comparison (Figure 4.3). For both HEK293T and RKO cell lines, the most significant changes in the mass profiles of intact histones in hypoxia were observed for histones H3.1 and H4. The observed species (Figure 4.3) correspond to histone variants and their PTMs (see Appendix 6 for further interpretation).

No significant changes in PTMs were observed on H2A (except for H2A.X) and H2B in both HEK293T and RKO cells under severe hypoxia relative to the levels in normoxia. The major peak observed for H4, in both normoxia and hypoxia is at 11306 Da, which corresponds to N-Ac, dimethylated H4. Some changes in the intensity of other H4 peaks relative to the 11306 Da peak were also observed in hypoxia relative to normoxia. A peak corresponding to N-Ac H4 at 11278 Da together with a peak at 11292 Da (+14 Da, mono-methylation) were observed; these two species were observed at decreased levels (relate to the 11306 Da peak) in both HEK293T and RKO cells with severe hypoxia compared to normoxia (Figure 4.3, the superimposed image of H4). The changes of the relative intensities of peaks at 11278 and 11292 Da in response to hypoxia were more obvious in RKO cells than in HEK293T cells. Additionally, a relative increase in the intensity of the peak at 11348 Da was observed in HEK293 cells under hypoxia compared to normoxia (Figure 4.3A, the superimposed image of H4).

As mentioned in Chapter 3, histone H3 molecules do not have N-terminal acetylation.[187] Histone H3.1 and H3.2 are replication-dependent proteins and more

abundant than replication-independent H3.3 in rapidly growing cells.[264] In HEK293T cells, unmodified H3.1 molecules (15273 Da) were detected at a low relative abundance in both normoxia and severe hypoxia (Figure 4.3A, H3.1). However, the unmodified H3.1 and monomethylated H3.1 forms were not observed in RKO cells with severe hypoxia treatment (Figure 4.3B, H3.1). The MS profiles of intact H3.1 revealed a highly modified distribution with incremental shifts of 14 Da and 42 Da, corresponding in mass to combinations of methylation, acetylation and/or trimethylation (Figure 4.3B, H3.1). Notably, hypoxic treatment caused HEK293T cells to present more highly modified states of H3.1 where the most abundant peak appeared at 15357 Da. A higher proportion of H3.1 molecules at higher modified states was observed in RKO cells with severe hypoxia, where the unmodified, monomethylated, dimethylated forms of H3.1 were not detected or at very low abundance (Figure 4.3B, H3.1).

Interestingly, an increased level of phosphorylation was observed for the H2A variant, H2A.X in RKO cells in severe hypoxia, whereas no increased level of phosphorylated H2A.X was noted in HEK293T cells under the same hypoxic condition (Figure 4.4). The peak at 15056 Da in Figure 4.4 corresponds to N-Ac H2A.X. Another peak at 15098 Da (+42, mono-acetylation) is also observed in both HEK293T and RKO cells. The peak at 15136 Da (+80 Da, phosphorylation) was not detected in HEK293T cells under normoxia and was very low in RKO cells under normoxia (Figure 4.4). The mass profiles of H2A.X from HEK293T cells were identical in normoxia and hypoxia (Figure 4.4 superimposed image). The relative ratio of phosphorylated H2A.X to H2A.X was observed as nearly 1:2 in RKO cells under severe hypoxia. The modification of phosphorylation at S139 of H2A.X is known as γ-H2AX, and is a marker of DNA damage. [59]

Overall, the treatments of HEK293T and RKO cells with hypoxia showed detectable

differences in global PTMs of intact histones H3 and H4. Notably, γ-H2AX was observed in RKO cells under hypoxia, but not in HEK293T cells, suggesting different cell types have varied H2A.X mediated responses to hypoxic stress. No significant changes in PTMs were observed on H2A (except for H2A.X) and H2B in both HEK293T and RKO cells under severe hypoxia.

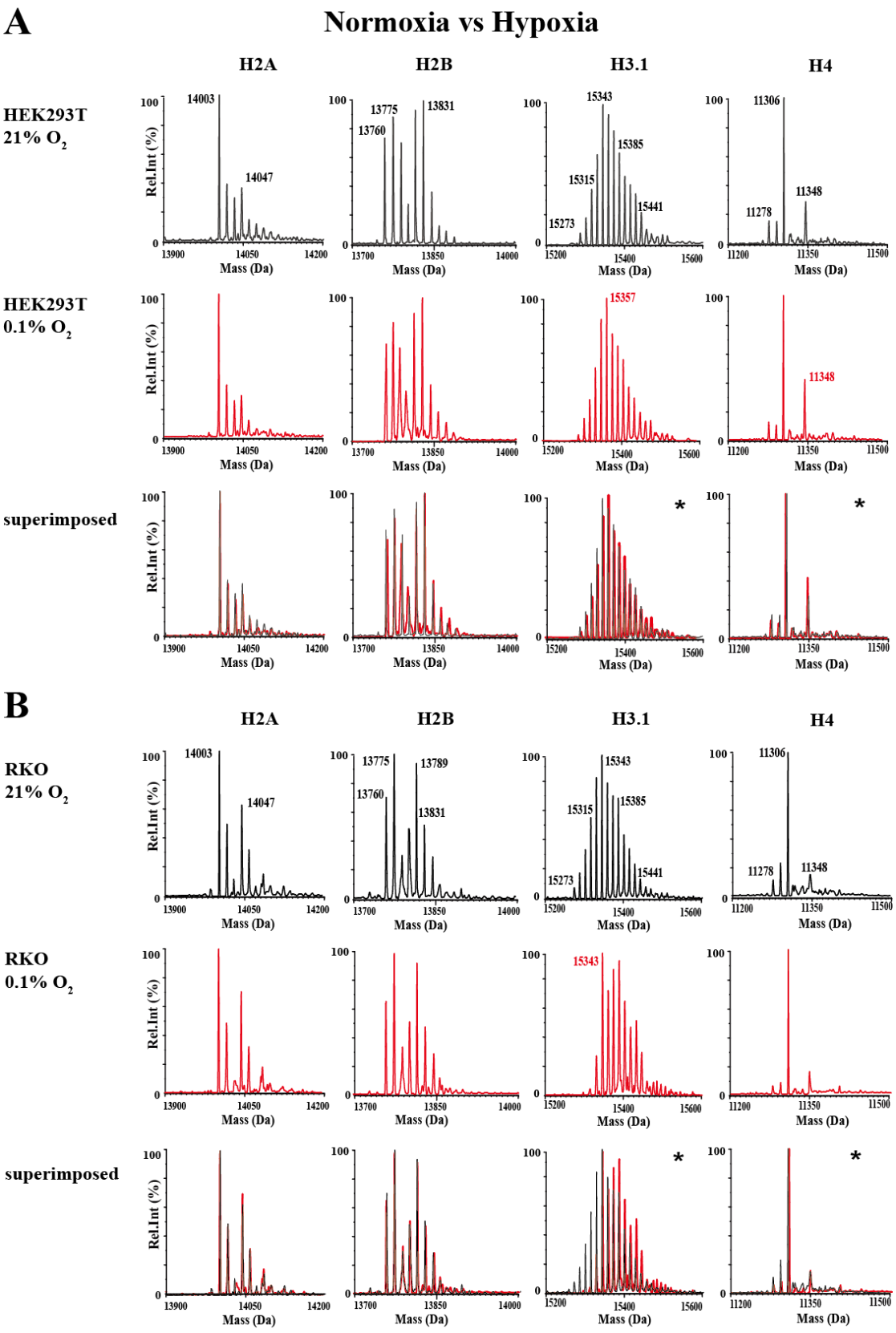

Figure 4.3 LC-MS analysis of intact core histones under hypoxia. (A) Intact histone profiles from HEK293T cells treated with severe hypoxia (0.1% O_2). (B) Intact histone profiles from RKO293T cells treated with severe hypoxia (0.1% O_2). Coloured traces indicate the sample from control cells (black) or cells treated under severe hypoxia for 24 h (red). An asterisk indicates an observed change between normoxia and severe hypoxia.

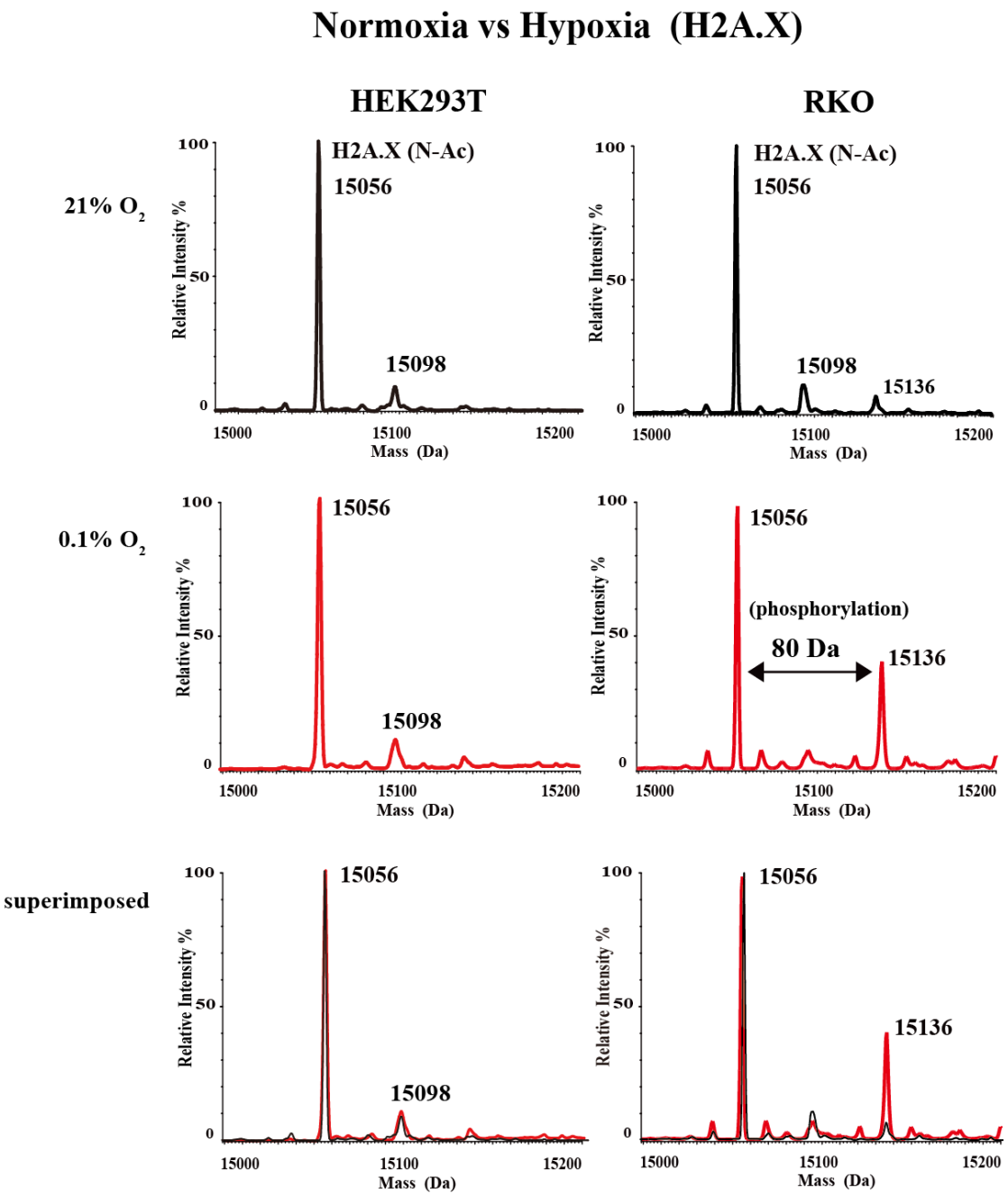

Figure 4.4 LC-MS analysis of H2A.X under normoxia and severe hypoxia. (A) Intact histone profiles for H2A.X from HEK293T cells treated with 0.1% O_2. (B) Intact histone profiles for H2A.X from RKO293T cells treated with 0.1% O_2. Coloured traces indicate the samples from normoxia (black) or severe hypoxia for 24 h (red).

4.3.2 Detection of SAHA-induced PTMs change on core intact histones

Histone deacetylase inhibitors (HDACi), such as Trichostatin A (TSA), vorinostat (SAHA) and belinostat (PXD101) have effects on cell growth arrest and apoptosis and are reported to alter the PTMs on the core histones, particularly H3 and H4.[196,265-268] Modifications to histone H3 and H4 are reported to take place during S-phase, nucleosome assembly and histone exchange.[269,270] Newly synthesized H3 and H4 molecules are abundant in growing cells and carry large amounts of PTMs. Alterations in histone PTMs were analysed under the conditions where the stress (compounds) did not cause significant effects on cell growth or induce cell death. The cells were treated with SAHA and the developed LC-MS method was used to detect changes in histone PTMs. It has previously been reported that treatment of K562 (human chronic myelogenous leukemia) cells with SAHA at a concentration of 1 μM for 24 hours does not trigger cell cycle arrest or cause any obvious decrease in cell viability.[271]

The mass profiles of intact histones from RKO cells with 1μM SAHA treatment for 24 hours are shown in Figure 4.5. The superimposed images for core histones H2A, H2B, H3.1 and H4 show substantial changes in their global PTM patterns. This result is consistent with a previous study where K562, WI38 (human lung fibroblasts) and IMR 90 (human embryo fibroblasts) cell lines were treated with SAHA.[271] Notably, the observed changes in H2A and H2B were more obvious than those observed in the previous study.[271] For H2A, the peak at 14003 Da is assigned as N-Ac H2A1C. The relative abundance of the peaks at 14047 (+42 Da, mono-acetylation), 14089 Da (+84, di-acetylation) increases significantly in RKO cells upon SAHA treatment, consistent with HDAC inhibitor occurring. The same trend of apparent increases in acetylated forms was observed, e.g. a peak at 13819 Da became the most abundant species and higher acetylated forms of H2B (ex: the peak at 13861 Da) were observed. For H4, the peak at 11306 Da (corresponding to N-Ac, dimethylated H4), along with four peaks

with a spacing of +42 Da (11348 Da, 11390 Da and 11432 Da) are predominant in RKO cells on SAHA treatment. The peak at 11390 Da corresponding to N-Ac, dimethylated and di-acetylated H4 is the most abundant; the peaks at 11278 and 11292 Da are at extremely low abundance in cells with SAHA treatment. This indicates that all the observed molecules of H4 have undergone at least two acetylations, except for the species at 11306 Da (corresponding to dimethylated N-Ac H4) on SAHA treatment. As observed for other core histones, the acetylated forms of H3 were inferred by the observed of species with incremental mass shifts of +14 and +42 Da. Peaks at 15273 Da, 15287 Da, 15301 Da were at very low abundance, whereas the highest modified peaks appeared at 15553 Da (+280 Da from unmodified form) in intact H3 under SAHA treatment. Overall, SAHA treatment appears to trigger extensive global acetylation of the major core histones, particularly on H3 and H4, consistent with its assigned role as an HDAC inhibitor.

The minor H2A variants, i.e. H2A.X and H2A.Z were observed to be acetylated in RKO cells with SAHA treatment (Figure 4.6). The intact mass profile for H2A-1 shows a predominant proportion of minor H2A variants, including H2A.Z (13422 Da), N-Ac H2A2C (13900 Da) and N-Ac H2A2A (14007 Da), which were further modified with one to three acetylations upon SAHA treatment. For H2A.Z, the mono-acetylated, di-acetylated and tri-acetylated forms were significantly increased upon SAHA treatment (Figure 4.6, left middle panel). The increased abundance of a peak at 14049 Da (+42 Da from 14007 Da) was also observed upon SAHA treatment. H2A.X from LC-MS was analysed and showed acetylated forms of H2A.X in RKO cells upon SAHA treatment (Figure 4.6, right middle panel). The peaks at 15098 D (+42 Da, mono-acetylation from N-Ac H2A), 15140 Da (+84 Da, di-acetylation) were increased substantially upon SAHA treatment. Again these results are consistent with the role of SAHA as an HDAC inhibitor.

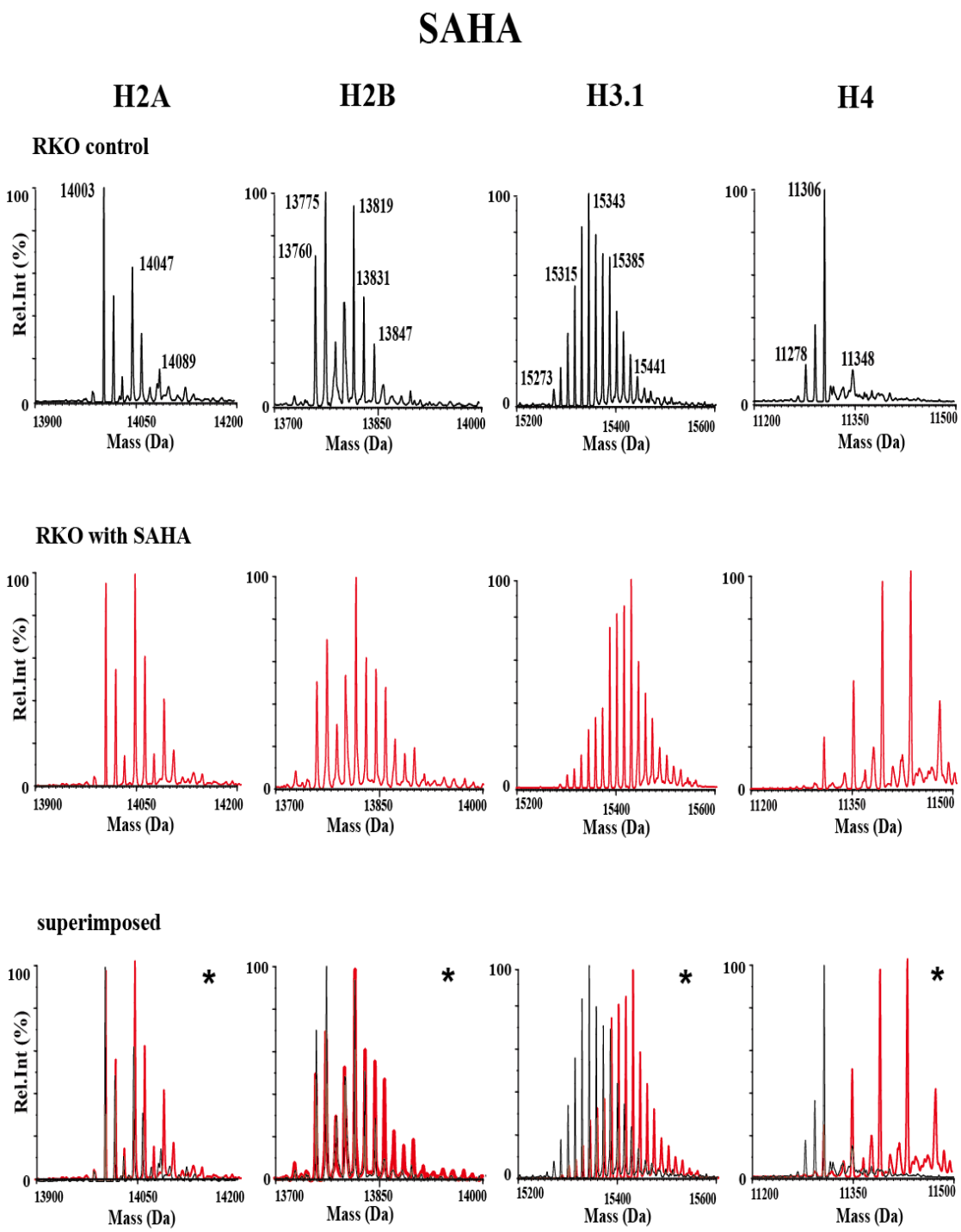

Figure 4.5 LC-MS analysis of intact histones following SAHA treatment. (A) Intact histone profiles from HEK293T cells treated with 1 μM SAHA (in DMSO). (B) Intact histone profiles from RKO293T cells treated with s with 1 μM SAHA. Coloured traces indicate samples from control cells (black) or cells treated with SAHA for 24 h (red). An asterisk indicates an observed change between control (DMSO only) and treated samples (1 μM SAHA).

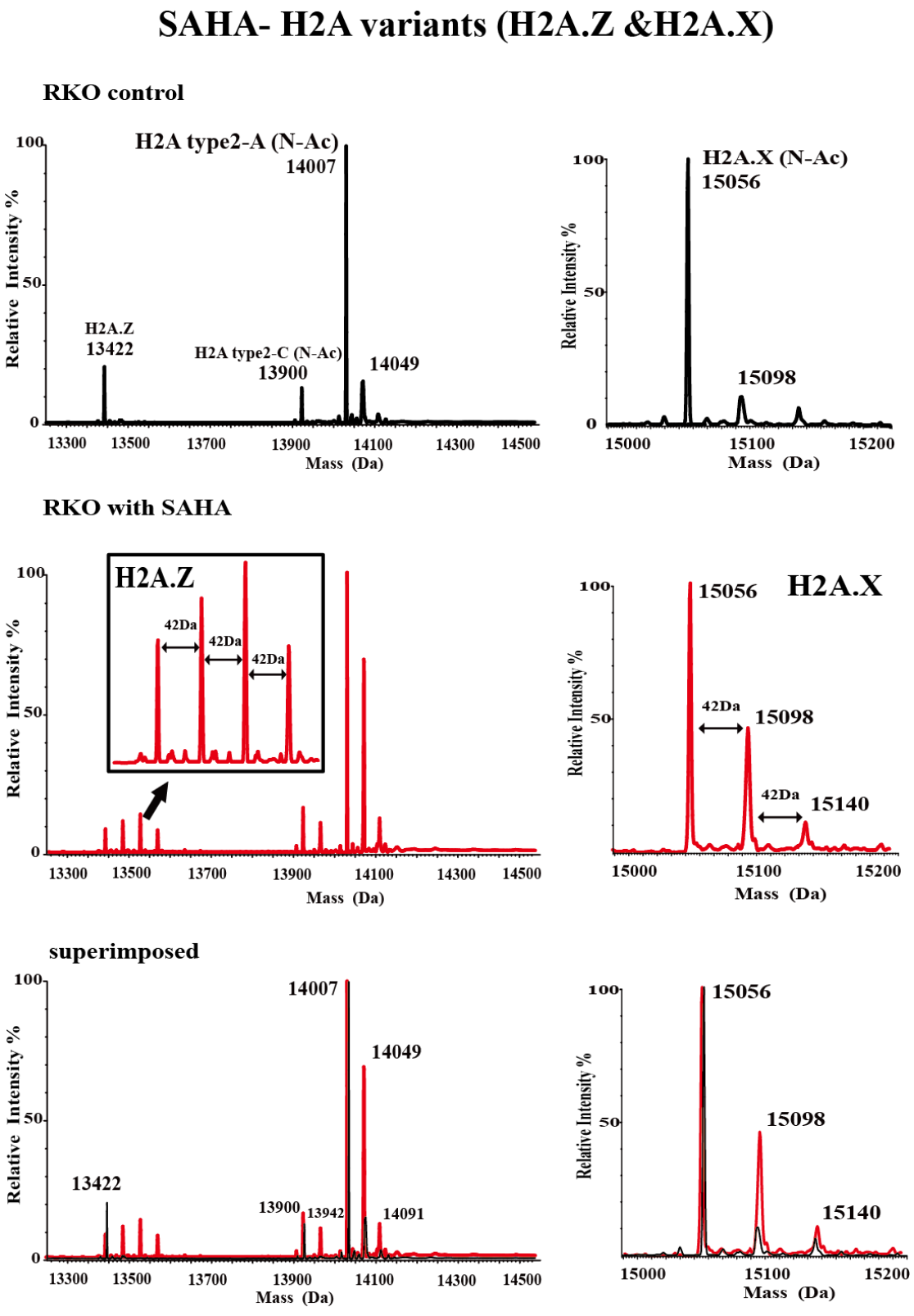

Figure 4.6 LC-MS analysis of H2A variants, following SAHA treatment. (A) Intact histone profiles for H2A variants from HEK293T cells treated with 1 µM SAHA (in DMSO). (B) Intact histone profiles for H2A variants from RKO293T cells treated with s with 1 µM SAHA. Coloured traces indicate the sample from control cells (black) or cells treated with SAHA for 24 h (red).

4.4 Quantification of intact histone PTMs by MS ion count

Mass profiles reflect the relative abundances of species as determined by their relative ion intensities. The protein/peptide ion relative ratio (PIRRs) is used in MS analysis for the relative quantification of the proteins/peptides; the fragment ion relative ratio (FIRRs) is used in tandem mass spectrometry.[272] The accurate quantification of species observed in MS depends on the efficiency of ionization and biases in selective ion accumulation. Previous reported work has shown that PIRRs are not constant across all observed charge states for small peptide mixtures due to the differences in ionization efficiency; thus PIRRs may not present the correct ratio of the species in the mixture.[201] However, the observed relative ratios of MS ion intensities can be consistent for many charge states of proteins and so correspond to the ratios of proteins in solution. The low tendency of ionization efficiency biases often makes MS ion intensity analysis for the quantification of proteins accurate and reliable.[201]

Ion intensity analysis was applied to MS profiling of histones and their PTMs.[273] In my work, the MS profiles of intact histones were analysed using the LC-MS method. Based on the validation of the current method along with the reported lack of ionization efficiency for intact proteins, use of MS ion intensity analysis for the relative quantification of variants was considered feasible. In Section 4.3, MS profiles are presented as the intensity of each species normalised relative to the intensity of the most abundant species. For further comparison of each species from different samples, the pattern of MS profile was transformed to each species expressed as a percentage of the total ion count. The procedure was applied for comparison of PTMs in cells with different treatments as detailed in this Chapter. The quantification of observed species of histones and their PTMs was calculated as follows: The species (%) = the ion count of the species/ total ion count x 100.

The isobaric issue between tri-methylation (+42 Da) and acetylation (+42 Da) in intact mass profiles of histones was described in Chapter 3. For convenience, "methylation equivalent (m.e)" is used to represent the mass difference by a shift of 14 Da between the peaks observed in intact mass profiles, though isobaric issue can arise. For example, tri-methylation and acetylation are considered as three methylation equivalents.

4.5 Effects of hypoxia and hypoxia-mimetics on intact histone profiles

Following the work Section 4.3, global PTM changes in intact histones under hypoxia were mainly observed in histone H3 and H4 from HEK293T and RKO cells. The HEK293T cell line was selected as a model to test responses to various conditions, including different O_2 concentrations and compounds mimicking hypoxia. The histone H3.1, H3.2 and H4 are focused and discussed.

4.5.1 Hypoxia

Different concentrations of oxygen were chosen to test the cell viability of HEK293T cells. Cells under normoxia (21% O_2) were used as control groups. The trypan blue assay[274] showed no major decrease in viability of cells treated with hypoxia (1% O_2) or severe hypoxia (0.1% O_2) for 24 hours μ μ (Figure 4.7). Around 90% cell viability under 0.1% O_2 was observed. HEK293T cells treated with normoxia and hypoxia were prepared as described in the optimised the workflow (Figure 4.1). For convenience, the MS profiles were deconvoluted and represented as percentages of the total ion count (Section 4.4). Intact histone H3.1 and H3.2 profiles for HEK293T cells treated with normoxia, 1% O_2 and 0.1% O_2 are shown in Figure 4.8. For H3.1, the most abundant peak appeared at 15343 Da (5 methyl equivalents, m.e) with 14 % of the total ion count in cells with normoxia shifted to 15357 Da (6 m.e) with 13% and 16% of the total ion count in cells treated with 1% O_2 and 0.1% O_2, respectively. The abundance of the peaks

at 15273 Da (unmodified form), 15287 Da (1 m.e), 15301 Da (2 m.e), 15315 Da (3 m.e), 15329 Da (4 m.e), and 15343 D (5 m.e) decreases in cells treated with severe hypoxia (0.1 % O_2), particularly at 15315 and 15329 Da with *p values* < 0.01 (Table 4.1), compared to normoxia. Of note, the unmodified form (15273 Da) was not detected and the species at 15511 Da (17 m.e) and 15525 Da (18 m.e) were observed under severe hypoxia, whereas no species containing more than 17 m.e was observed under normoxia. Overall, treatment of HEK293T cells with hypoxia causes the intact mass profile pattern to undergo a shift to more modified forms, particularly in severe hypoxia (0.1% O_2). The change trend in the intact mass profiles of H3.2 is similar to that of H3.1 (Tables 4.1 and 4.2).

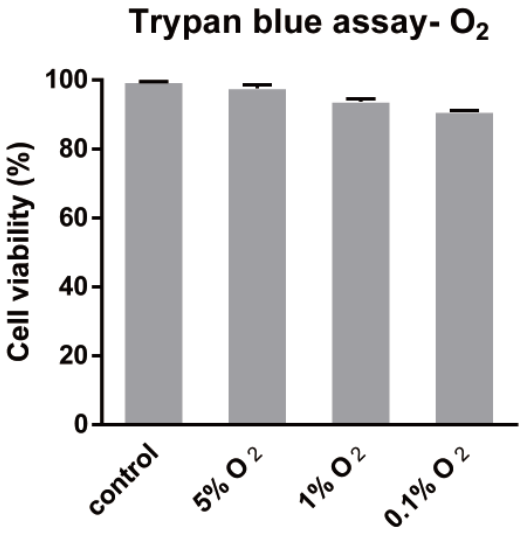

Figure 4.7 Trypan blue cell viability assays for HEK293T cells exposed to different O_2 concentrations for 24 hours. The percentage of cell viability is presented as a mean ± S.D (n=3).

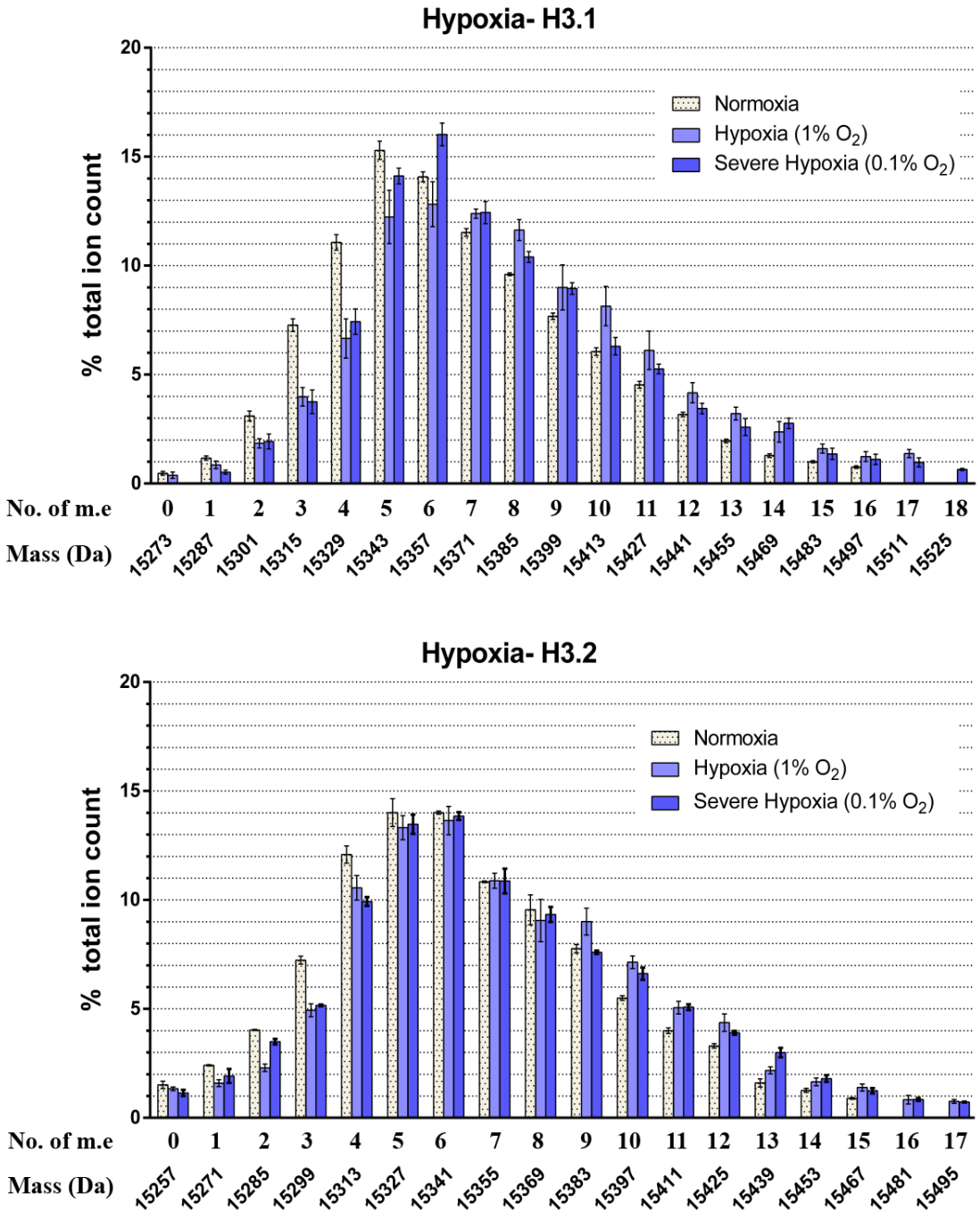

Figure 4.8 Quantitative analysis of the abundance of histone H3.1 (upper) and H3.2 (lower) following treatment of cells with normoxia (21% O_2), or hypoxia (1% O_2) and severe hypoxia (0.1% O_2) for 24 hours. The ion count for each peak is expressed as a percentage of the total ion count. Data are means ± SEM (n=3)**.** No. of m.e: number of methylation equivalents.

Table 4.1 Abundance change compared to controls for histone H3.1 from HEK293T cells after different treatments.

Mass (Da)	Methylation equivalents	0.1% O_2 (Δ%)	DFO150μM (Δ%)	CP20 125 μM (Δ%)	Exjade 75 μM (Δ%)	DMOG 1.25 mM (Δ%)	$CoCl_2$ 200 μM (Δ%)
15273	0	-0.473 ± 0.051	-0.294 ± 0.010	-0.294 ± 0.010	-0.321 ± 0.034	-0.139 ± 0.018	0.197 ± 0.022
15287	1	-0.645 ± 0.001	-1.309 ± 0.100	-0.748 ± 0.057	-1.066 ± 0.067	-0.362 ± 0.003	-0.231 ± 0.035
15301	2	-1.171 ± 0.066	-3.189 ± 0.126**	-1.580 ± 0.055	-2.538 ± 0.255**	-0.334 ± 0.058	-0.482 ± 0.001
15315	3	**-3.514 ± 0.144****	**-5.526 ± 0.269****	**-3.420 ± 0114****	**-5.813 ± 0.115****	**-3.698 ± 0.033****	-0.975 ± 0.110
15329	4	**-3.634 ± 0.133****	**-4.410 ± 0.135****	**-2.472 ± 0.037****	**-5.410 ± 0.338****	**-3.594 ± 0.103****	-0.103 ± 0.087
15343	5	-1.178 ± 0.034	1.684 ± 0.429	0.849 ± 0.162	0.330 ± 0.051	0.052 ± 0.524	**1.409 ± 0.044***
15357	6	**1.943 ± 0.175****	**6.726 ± 0.516****	**2.510 ± 0.091****	**8.162 ± 0.422****	**1.877 ± 0.233***	0.254 ± 0.336
15371	7	0.916 ± 0.191	**3.003 ± 0.369****	-0.298 ± 0.253	**3.266 ± 0.085****	1.524 ± 0.165	0.479 ± 0.293
15385	8	0.796 ± 0.106	0.750 ± 0.412	0.365 ±0.247	-0.062 ± 0.120	0.774 ± 0.203	0.224 ± 0.294
15399	9	**1.273 ± 0.067***	1.267 ± 0.630	1.229 ±0.375	0.582 ± 0.430	0.305 ± 0.319	-0.293 ± 0.265
15413	10	0.242 ± 0.129	1.331 ± 0.328	1.233 ± 0.222	-0.545 ± 0.128	0.586 ± 0.006	0.005 ± 0.097
15427	11	0.726 ± 0.035	0.152 ± 0.099	1.566 ± 0.093	-0.569 ± 0.131	0.354 ± 0.289	-0.122 ± 0.065
15441	12	0.274 ± 0.078	-0.336 ± 0.026	0.519 ± 0.042	0.796 ± 0.137	1.101 ± 0.048	-0.182 ± 0.051
15455	13	0.638 ± 0.175	0.077 ± 0.016	0.481 ± 0.059	0.433 ± 0.072	0.602 ± 0.245	-0.107 ± 0.026
15469	14	**1.479 ± 0.090****	-0.417 ± 0.052	-0.026 ± 0.037	-0.024 ± 0.083	0.316 ± 0.014	-0.035 ± 0.019
15483	15	0.357 ± 0.1244	0.120 ± 0.111	-0.156 ± 0.007	0.659 ± 0.043	0.077 ± 0.116	-0.084 ± 0.036
15497	16	0.354 ± 0.102	0.371 ± 0.009	0.242 ± 0.018	0.441 ± 0.009	-0.166 ± 0.055	0.044 ± 0.008
15511	17	0.969 ± 0.119	n/a	n/a	0.780 ± 0.037	0.727 ± 0.148	n/a
15525	18	0.648 ± 0.027	n/a	n/a	0.537 ± 0.041	n/a	n/a
15539	19	n/a	n/a	n/a	0.361 ± 0.041	n/a	n/a

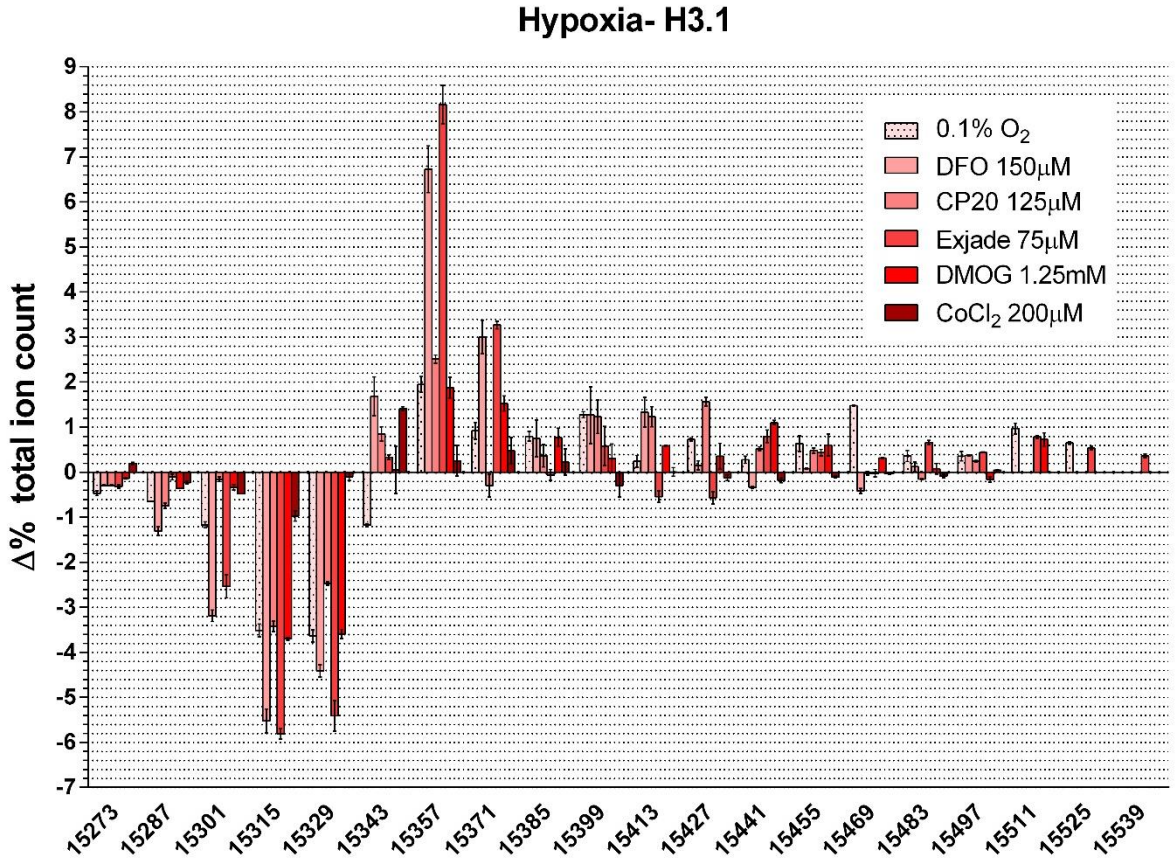

Figure corresponding to table 4.1.

Table 4.2 Abundance change compared to controls for histone H3.2 from HEK293T cells after different treatments.

Mass (Da)	Methylation equivalents	0.1% O_2 (Δ%)	DFO150μM (Δ%)	CP20 125 μM (Δ%)	Exjade 75 μM (Δ%)	DMOG 1.25 mM (Δ%)	$CoCl_2$ 200 μM (Δ%)
15257	0	-0.370 ± 0.014	-0.752 ± 0.002	-0.462 ± 0.040	-1.081 ± 0.082	-1.024 ± 0.062	0.381 ± 0.037
15271	1	-0.490 ± 0.171	-0.274 ± 0.129	0.030 ± 0.060	-1.080 ± 0.038	-0.860 ± 0.085	0.041 ± 0.013
15285	2	-0.537 ± 0.060	-0.806 ± 0.075	-0.443 ± 0.011	**-1.530 ± 0.055****	-0.920 ± 0.020	0.147 ±0.058
15299	3	**-2.071 ± 0.083****	**-3.862 ± 0.100****	**-1.855 ± 0.015****	**-5.277 ± 0.001****	**-1.791 ± 0.162****	-0.637 ± 0.008
15313	4	**-2.156 ± 0.108****	**-4.980 ± 0.295****	**-2.704 ± 0.108****	**-6.123 ± 0.039****	**-2.205 ± 0.262****	-0.197 ±0.037
15327	5	-0.535 ± 0.114	0.244 ± 0.010	0.473 ± 0.067	-0.418 ± 0.047	-1.090 ± 0.148	0.679 ±0.528
15341	6	-0.161 ± 0.061	**4.698 ± 0.051****	**2.370 ± 0.148****	**7.142 ± 0.039****	**1.776 ± 0.178****	0.974 ±0.001
15355	7	0.035 ± 0.302	**1.990 ± 0.016****	0.262 ± 0.303	**3.285 ± 0.189****	0.017 ± 0.158	-0.325 ±0.126
15369	8	-0.213 ± 0.195	-0.159 ± 0.012	-0.095 ± 0.095	1.251 ± 0.425	0.560 ± 0.352	-0.463 ±0.033
15383	9	-0.165 ± 0.066	0.874 ± 0.060	0.841 ± 0.046	0.608 ± 0.328	1.242 ± 0.210	-1.032 ±0.209
15397	10	**1.125 ± 0.100***	0.711 ± 0.005	0.822 ± 0.040	0.282 ± 0.118	0.893 ± 0.278	0.057 ±0.020
15411	11	1.081 ± 0.004	-0.863 ± 0.038	-0.453 ± 0.079	-0.720 ± 0.111	0.574 ± 0.108	0.167 ±0.079
15425	12	0.601 ± 0.009	0.112 ± 0.032	0.420 ± 0.138	0.577 ± 0.074	0.896 ± 0.157	0.244 ±0.010
15439	13	**1.391 ± 0.017****	0.250 ± 0.133	0.477 ± 0.082	0.542 ± 0.074	0.708 ± 0.057	-0.011 ±0.095
15453	14	0.544 ± 0.034	0.799 ± 0.080	0.187 ± 0.020	0.425 ± 0.043	0.284 ± 0.063	-0.048 ±0.062
15467	15	0.355 ± 0.048	0.079 ± 0.103	0.130 ± 0.025	-0.121 ± 0.004	0.075 ± 0.067	0.024 ±0.019
15481	16	0.842 ± 0.040	0.962 ±0.099	n/a	1.000 ± 0.106	0.865 ± 0.098	n/a
15495	17	0.726 ± 0.013	0.978 ± 0.152	n/a	0.712 ± 0.009	n/a	n/a
15509	18	n/a	n/a	n/a	0.524 ± 0.073	n/a	n/a

The value (Δ%) is expressed as the abundance changes in percentage of the total ion count. Data are means ± SEM (n=3). The values highlighted in bold indicate significant changes in abundance. ** Indicates p value <0.01; * Indicates p value<0.05. n/a: not available.

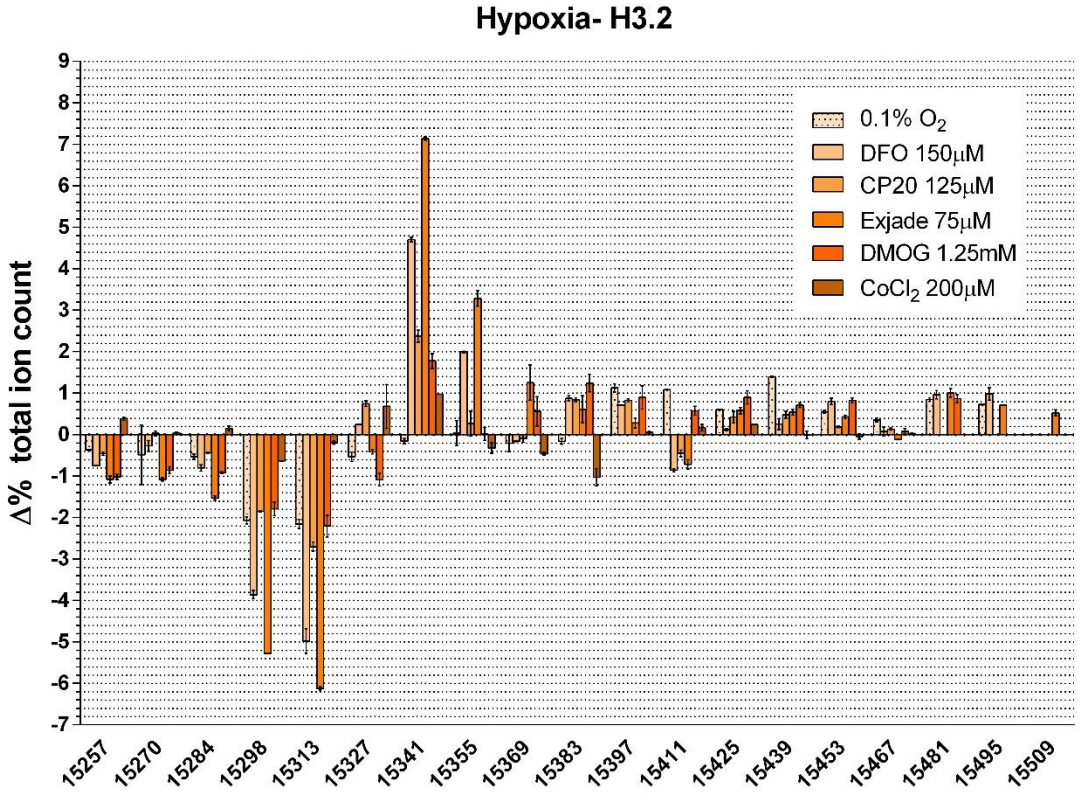

Figure corresponding to table 4.2.

4.5.2 Hypoxia-mimetics: Iron chelators

Prolyl-4-hydroxylases (PHDs) and the asparaginyl hydroxylase, factor inhibiting HIF (FIH) are involved in the regulation of HIF-α and belong to the family of 2OG/Fe(II)-dependent oxygenases.[254,257] Iron, therefore, plays a critical role in the activity of PHD and FIH and in turn correlates to HIF signaling pathway.[96] Iron chelators are commonly used to create hypoxia-mimetic conditions by inhibiting PHD and FIH and so blocking the degradation pathway of HIF-α.[251,275] Iron chelators such as desferrioxamine (DFO), deferiprone (CP20) and deferasirox (Exjade) are widely used clinically to treat human iron overload diseases. Herein, the effects of these three iron chelators on the alteration of intact histone PTMs were investigated.

4.5.2.1 Deferoxamine (DFO)

The varying concentrations of DFO (25, 50, 75, 100, 125 and 150 μM) were examined for HEK293T cell viability - no significant changes were observed (Figure 4.9). The intact histone mass profiles were obtained from HEK293T cells treated with 0, 50, 75, 100, 125 and 150 μM DFO for 24 hours (Figure 4.10). In the histone H3.1 intact mass profile, the most abundant peak was observed at 15357 (6 m.e); the unmodified form (15273 Da) at H3.1 was not detected in cells treated with 50-150 μM DFO. A large difference in abundance between the control group and 150 μM DFO treatment was observed at 15357 Da (6 m.e) (7% difference, Table 4.1). The lowest mass forms were observed at 15287 Da (2 m.e) with 50-75 μM DFO, 15301 Da (3 m.e) with 100-125 μM DFO and 15315 Da (4 m.e) with 150 μM DFO, suggesting a dose-dependent effect. The most apparent change in the PTMs was observed with 125-150 μM DFO. In general, the treatment of DFO induced apparent abundance changes in the mass range of 15273 Da (unmodified) to 15399 Da (9 m.e); however, no obvious changes were observed in

the species containing more than 10 methylation equivalents. Similar effects on intact histone H3.2 were observed on DFO treatment, including with respect to dose-dependent effects (Figure 4.10 lower panel).

4.5.2.2 Deferiprone (CP20)

Application of CP20 at 25-125 μM did not cause significant decreases in HEK293T cell viability (Figure 4.9). Analysis of HEK293T cells treated with 0, 25, 50, 75, 100 and 125 μM CP20 for 24 hours were then carried out in Figure 4.11. For H3.1, a dose-dependent effect was observed; the biggest effect of CP20 appeared at concentrations of 100-125 μM CP20. The lowest mass species was observed at 15287 Da (1 m.e) with 75-125 μM CP20. The most abundant species was at 15357 Da (6 m.e) with 125 μM CP20, whereas 15343 Da (5 m.e) was the most abundant with 0-100 μM CP20. Overall, the concentration of CP20 at 100-125 μM caused the intact H3.1 mass pattern to shift to more highly modified forms.

In H3.2, the most discernible change in the mass profile was at 100-125 μM CP20, where the species at 15298 (3 m.e), 15313 Da (4 m.e) and 15341 Da (6 m.e) show significant changes in abundance (Figure 4.11 lower panel, Table 4.2). Overall, the apparent effects of CP20 on H3.2 PTMs were similar to that on H3.1.

4.5.2.3 Deferasirox (Exjade)

Application of Exjade at 0-75 μM did not cause a distinct decrease in HEK293T cell viability, while use of 100 μM and 125 μM Exjade led to 34% and 55% decrease in cell viability (Figure 4.9). Thus, treatment of HEK293T cells with Exjade was carried out using concentrations of 0, 25, 50, 75 μM. The intact mass profiles of histone H3.1 and H3.2 show a dramatic shift to more highly modified states in cells treated with 25-75 μM Exjade (Figure 4.12). No obvious dose-dependent effect was observed between 25

and 75 μM Exjade. In H3.1 intact mass profile from cells treated with 75 μM Exjade, the first peak appeared at 15301 Da (2 m.e) and the highest mass peak was observed at 15539 Da (19 m.e). For H3.2, highly modified forms at 15481 Da (16 m.e), 15495 Da (17 m.e), and 15509 Da (18 m.e) were detected with Exjade treatment (25-75 μM). The most distinct change occurred with the species containing 3, 4, 6 and 7 methylation equivalents for both H3.1 and H3.2 in cells treated with 75 μM Exjade (Tables 4.1 and 4.2).

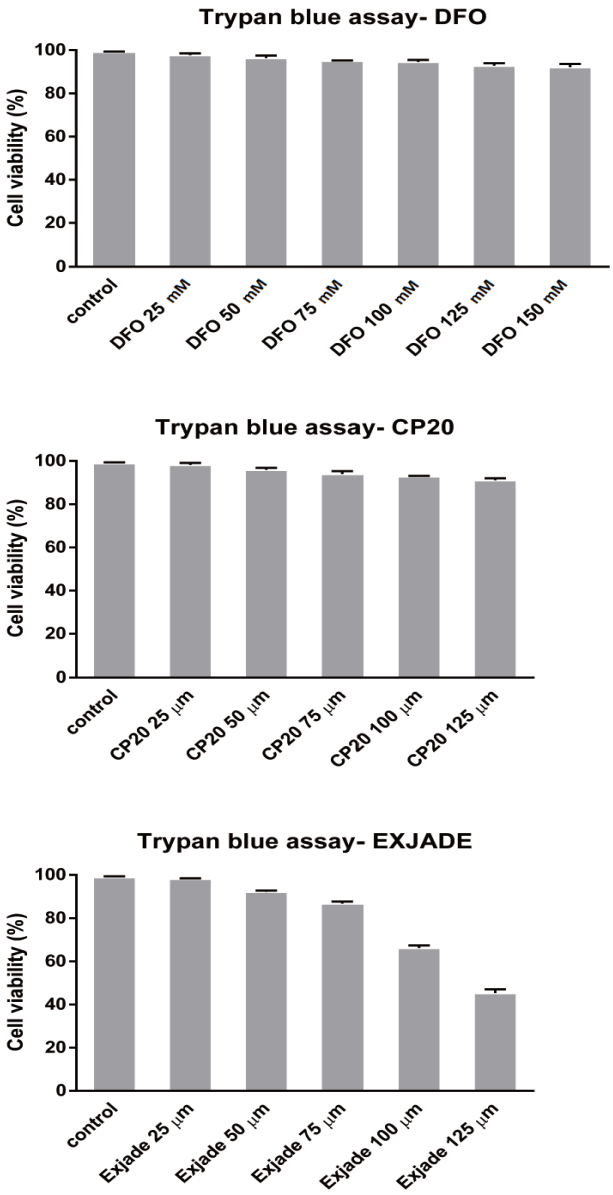

Figure 4.9 Trypan blue cell viability assays for HEK293T cells exposed to different iron chelators for 24 hours. Different concentrations of DFO (upper), CP20 (middle) and Exjade (lower) were examined. The percentage of cell viability is presented as a mean ± S.D (n=3).

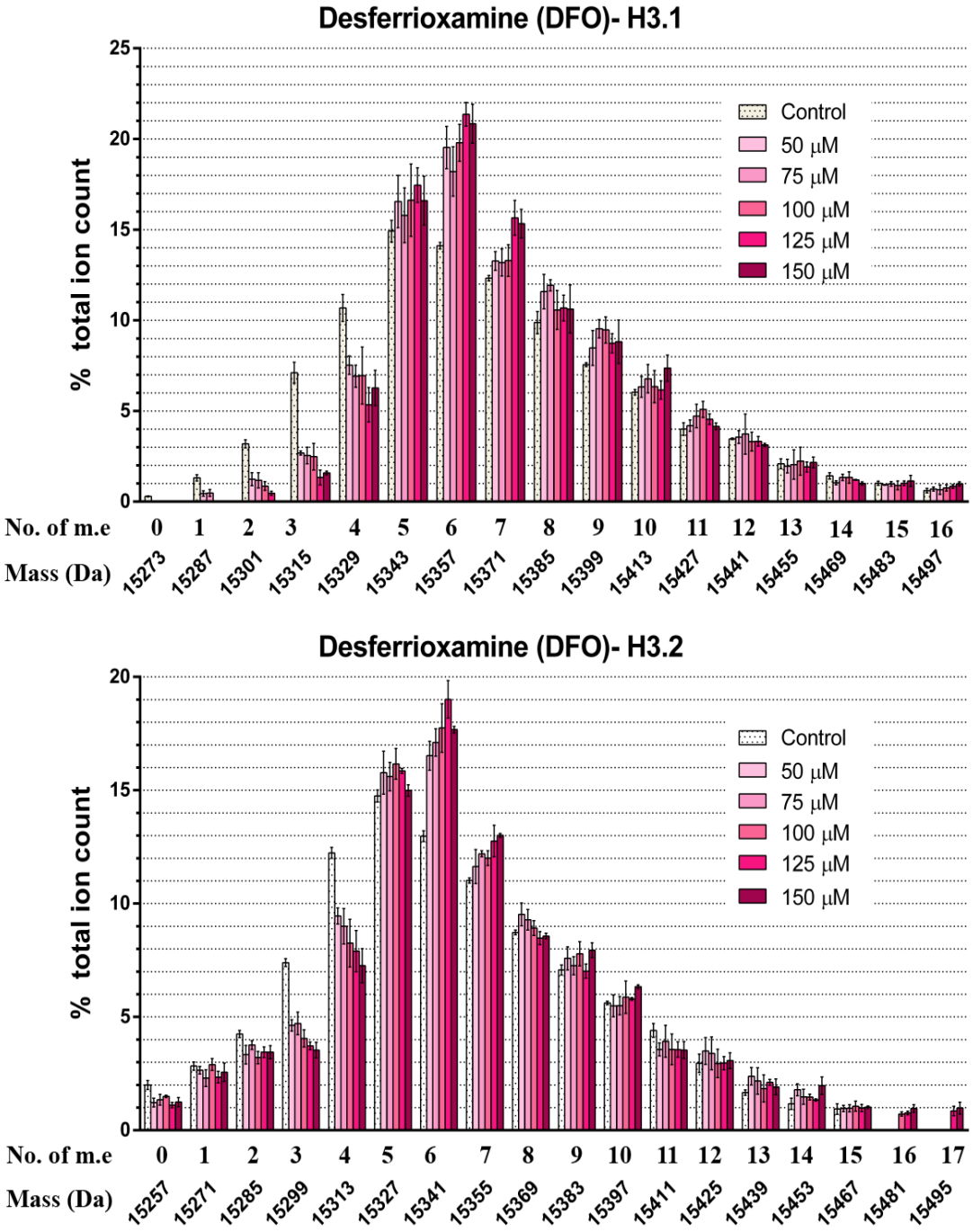

Figure 4.10 Quantitative analysis of the abundance of differently modified species of histone H3.1 (upper) and H3.2 (lower) following treatment of cells with 0, 50, 75, 100, 125 and 150 μM DFO for 24 hours. The ion count for each peak is expressed as a percentage of the total ion count. Data are means ± SEM (n=3)**.** No. of m.e: number of methylation equivalents.

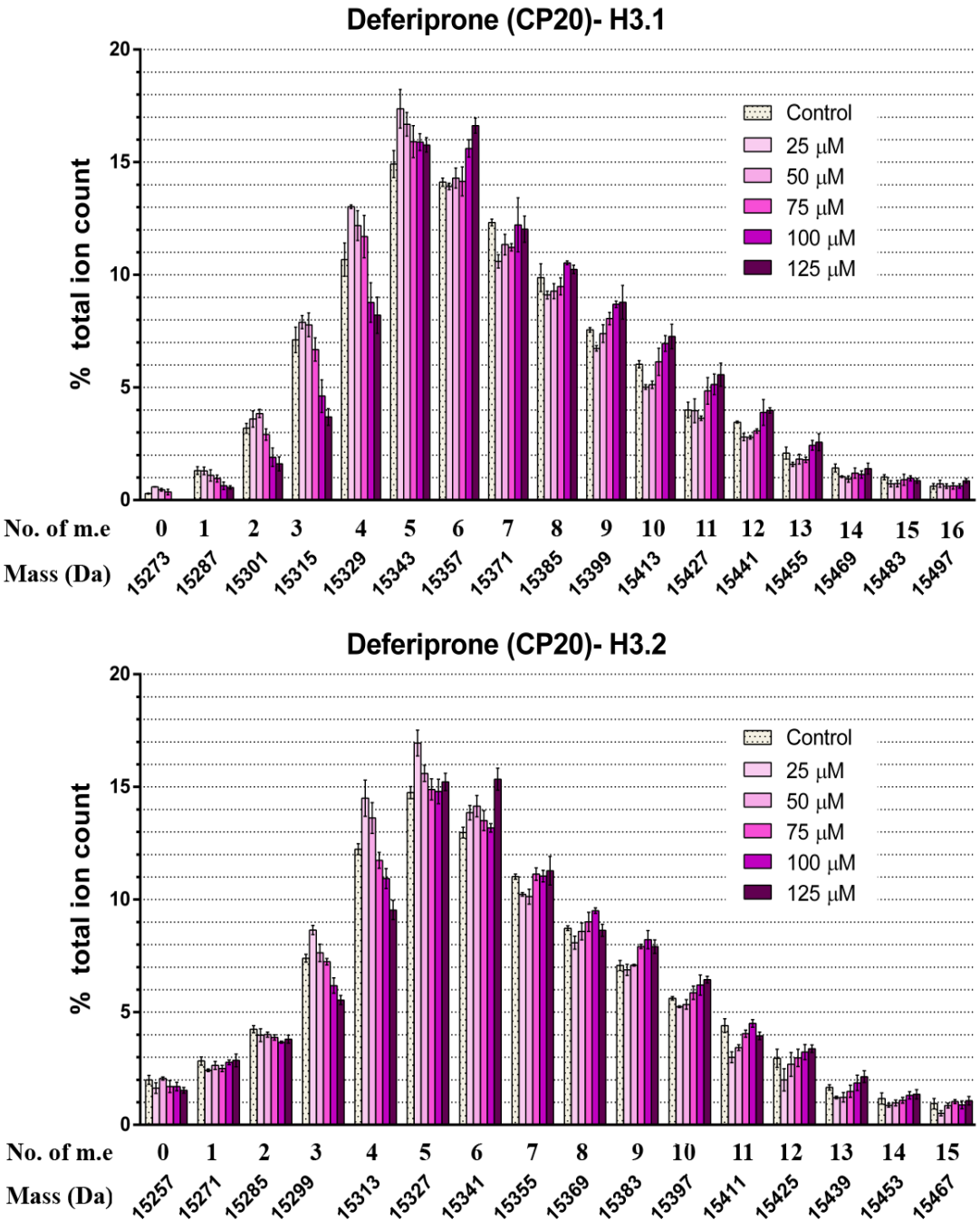

Figure 4.11 Quantitative analysis of the abundance of differently modified species of histone H3.1 (upper) and H3.2 (lower) following treatment of cells with 0, 25, 50, 75, 100 and 125 μM CP20 for 24 hours. The ion count for each peak is expressed as a percentage of the total ion count. Data are means ± SEM (n=3)**.** No. of m.e: number of methylation equivalents.

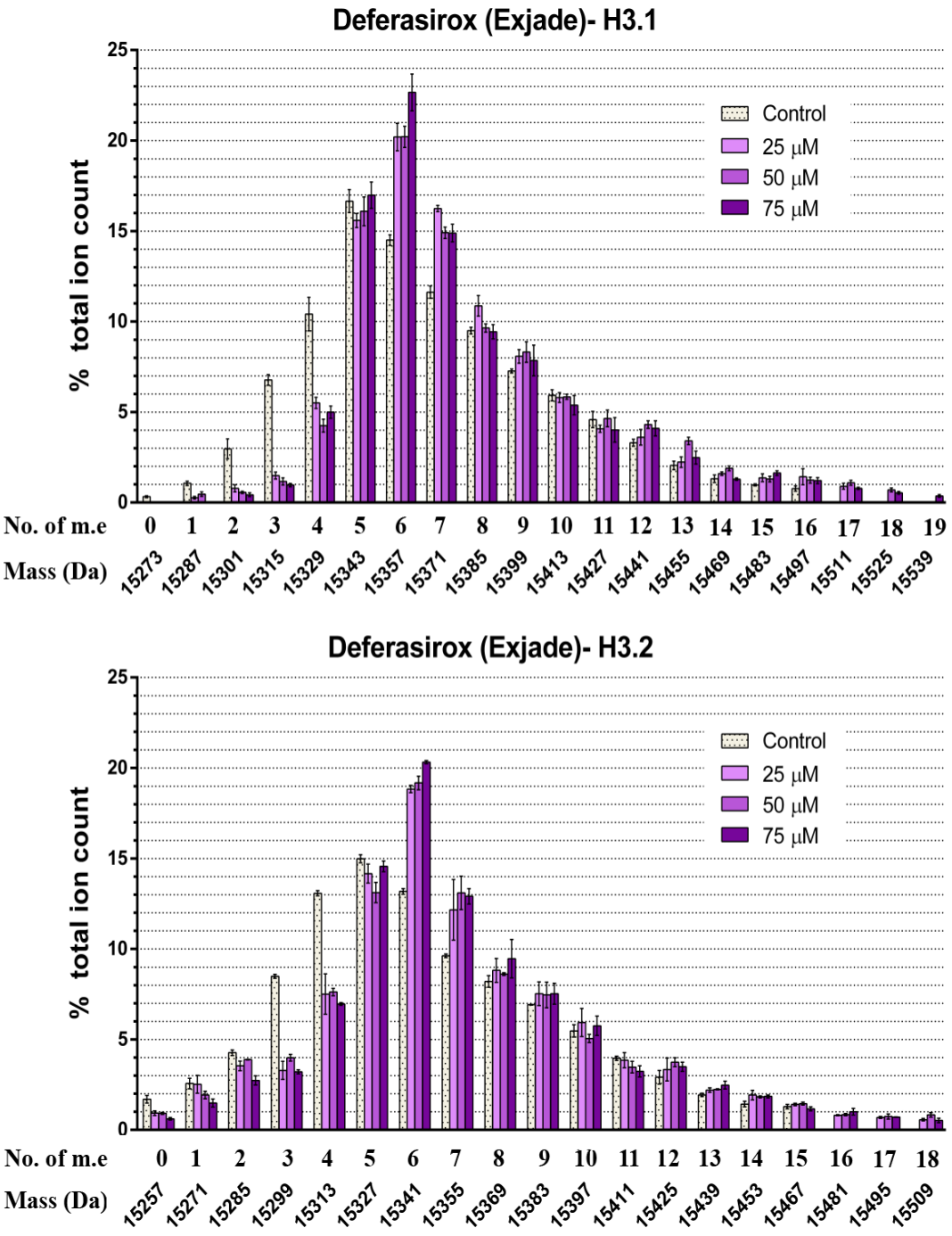

Figure 4.12 Quantitative analysis of the abundance of differently modified species of histone H3.1 (upper) and H3.2 (lower) following treatment of cells with 0, 25, 50 and 75 μM Exjade for 24 hours. The ion count for each peak is expressed as a percentage of the total ion count. Data are means ± SEM (n=3)**.** No. of m.e: number of methylation equivalents.

4.5.3 A hypoxia mimetic - dimethyloxaloglycine (DMOG)

DMOG is a cell-permeable 2OG analogue which acts as a broad spectrum inhibitor of 2OG/Fe(II)-dependent oxygenases.[105] DMOG stabilises HIF-α in normoxia, likely predominantly via inhibition of the HIF-α prolyl hydroxylases (PHDs), and used as a hypoxia-mimetic. DMOG was used to treat HEK293 cells and mass profiles of intact histones were analysed to monitor the change of global histone PTMs. First, the varying concentrations of DMOG (0, 250, 500, 750, 1000 and 1250 μM) were tested for effects on HEK293T cell viability; no obvious decreased viability was observed (Figure 4.13). Using these concentrations of DMOG to treat HEK293T cells, intact mass profiles for H3 were obtained (Figure 4.14). Discernible changes in abundance were observed at the species containing 3, 4, and 6 methylation equivalents for both H3.1 and H3.2 between control group and exposure to DMOG at 1.25 mM (Tables 4.1 and 4.2). The dose-dependent effects were also observed for H3.1 and H3.2. The highest mass of species at 15511 Da (17 m.e) and 15481 Da (16 m.e) were observed in H3.1 and H3.2, respectively, from cells treated with DMOG (0.5-1.25 mM). Overall, treatment with DMOG causes the H3 intact mass profiles to have an overall shift to more highly modified states in a dose-dependent manner as was observed for the iron chelators.

4.5.4 A hypoxia mimetic- cobalt chloride ($CoCl_2$)

Cobalt is an essential element for animal life.[276] Cobalt is reported to have carcinogenic effects at high levels through the alteration of gene expression and dysregulation of reactive oxygen species (ROS).[277,278] Cobalt chloride ($CoCl_2$) is commonly used to create hypoxia-mimetic stress by inducing the accumulation of HIF-α via inhibition of the HIF prolyl hydroxylases.[253] The effect of $CoCl_2$ on alteration of global PTMs on intact histones, including at concentrations known induce HIF-α, was thus investigated.

The tested concentrations of $CoCl_2$ (50, 100, 150 and 200 μM) did not induce significant decreases in HEK293T cell viability (Figure 4.13). Treatment of HEK293T cells with 50, 100, 150 and 200 μM $CoCl_2$ was carried out and intact histone H3 mass profiles are presented in Figure 4.15. A small apparent change in global PTM patterns on intact histone H3.1 is only observed in cells treated with 200 μM $CoCl_2$, in which the significant change is detected at 15343 Da (5 m.e), with 1.4% of the total ion count (p value <0.05, Table 4.1). No significant changes were observed in the intact H3.2 mass profiles for cells treated with $CoCl_2$ (50-200 μM). These results imply the changes in histone PTMs induced by Co (II) ions are less (at least under the tested condition) than for DMOG or the iron chelators (especially Exjade) since all 3 of the treatment hypoxia-induced HIF-α, including of the tested concentrations, the results imply that changes in histone PTMs are substantially not (directly) mediated by HIF-α upregulation.

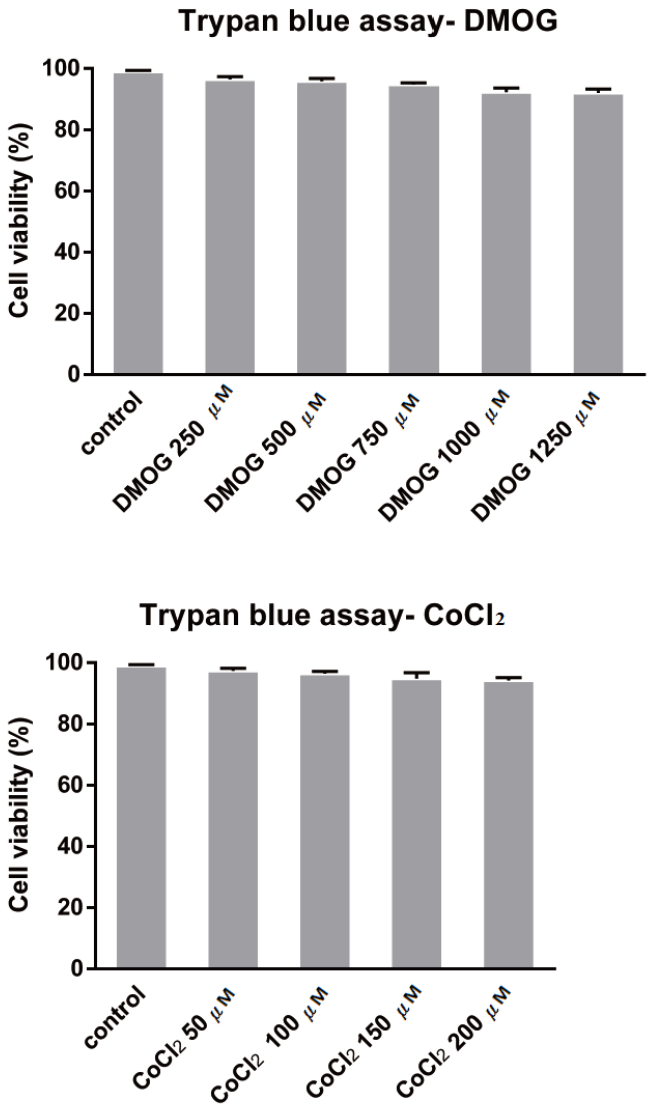

Figure 4.13 Trypan blue cell viability assays for HEK293T cells exposed to different concentration of DMOG (upper) and $CoCl_2$ (lower) for 24 hours. The percentage of cell viability is presented as a mean ± S.D (n=3).

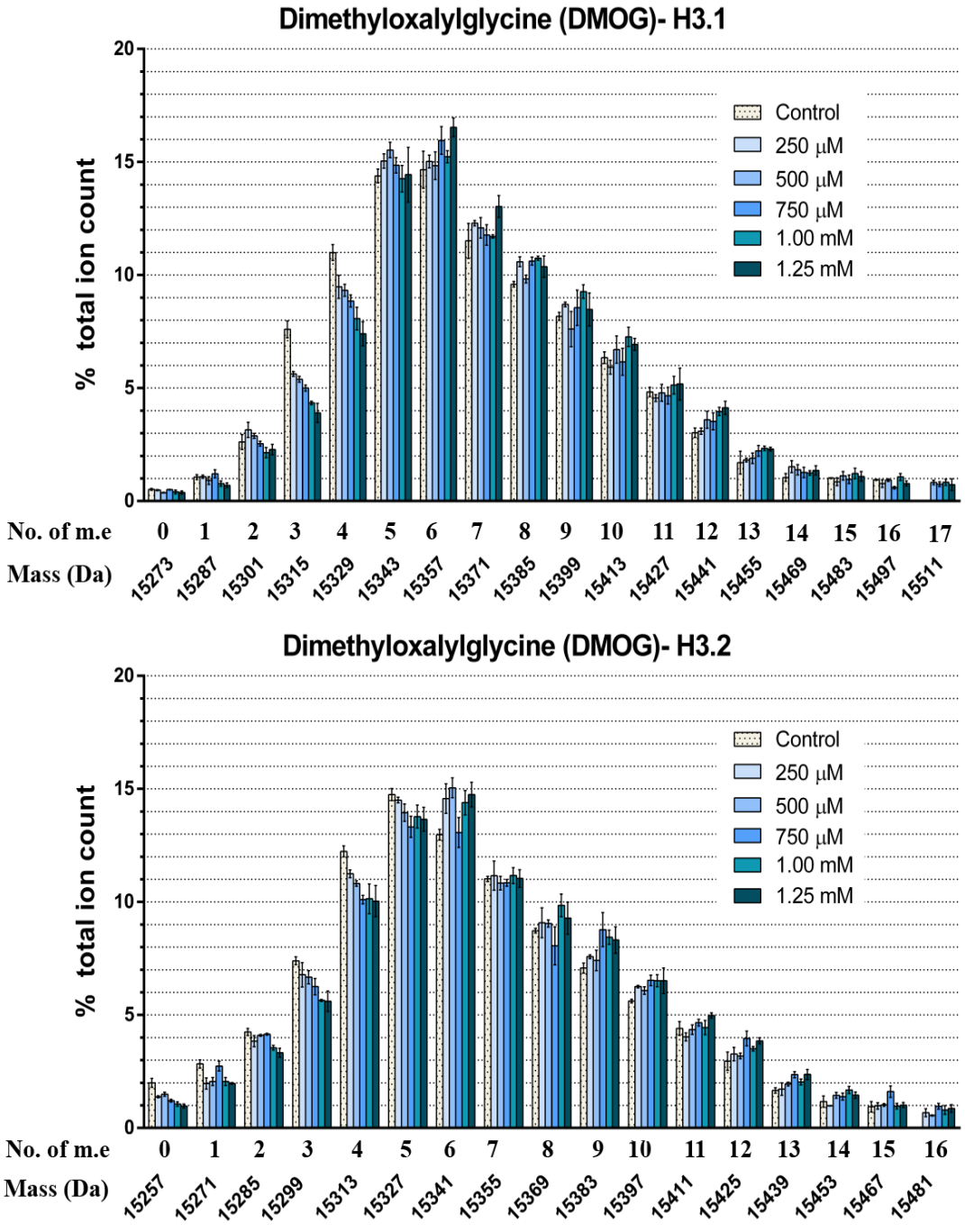

Figure 4.14 Quantitative analysis of the abundance of differently modified species of histone H3.1 (upper) and H3.2 (lower) following treatment of cells with 0, 250, 500, 750, 1000 and 1250 µM DMOG for 24 hours. The ion count for each peak is expressed as a percentage of the total ion count. Data are means ± SEM (n=3)**.** No. of m.e: number of methylation equivalents.

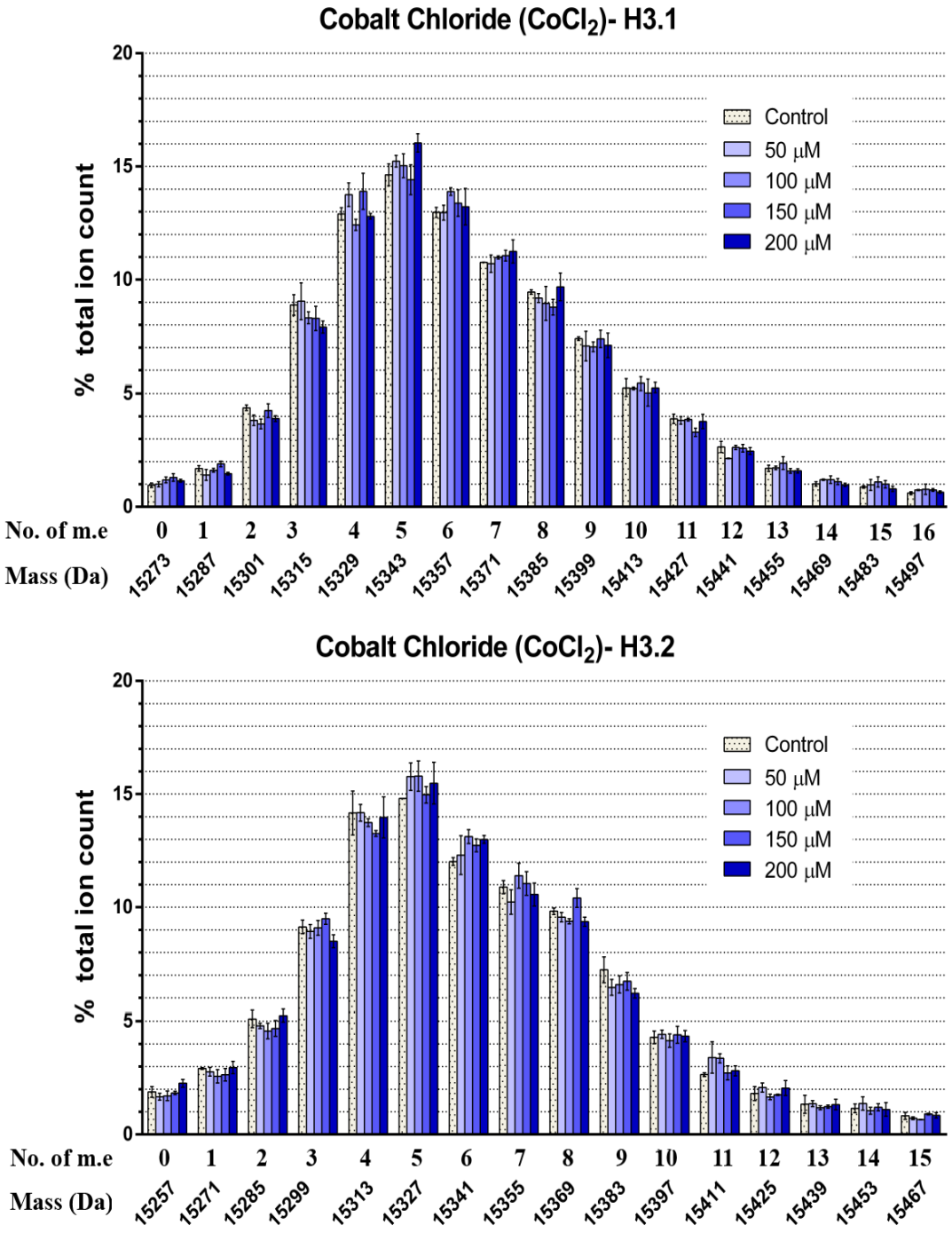

Figure 4.15 Quantitative analysis of the abundance of differently modified species of histone H3.1 (upper) and H3.2 (lower) following treatment of cells with 0, 50, 100, 150 and 200 µM $CoCl_2$ for 24 hours. The ion count for each peak is expressed as a percentage of the total ion count. Data are means ± SEM (n=3)**.** No. of m.e: number of methylation equivalents.

4.5.5 The effects of hypoxia and DMOG in HeLa cells

Following the observed effects of hypoxia and hypoxia-mimetic treatments on HEK293T cells, treatments with hypoxia and DMOG-induced hypoxia were examined in another human cancer cell line. The intact H3.1 mass profile from HeLa cells with different concentrations of oxygen at 21%, 5%, 1%, 0.5% and 0.1% is shown in Figure 4.16 (upper panel). A small change in the intact mass pattern was detected between normoxia and 5% O_2; however, distinct changes were observed with 1%, 0.5% and 0.1% O_2. These results are consistent with evidence that most human tissues exist within the context of concentrations of 3-5% O_2, known as "tissue normoxia".[279] A different H3.1 mass profile was noted between HeLa and HEK293T cells under the same conditions, consistent with the results (Figure 3.19) in Chapter 3, suggesting cell type-specific patterns of intact histone mass profiles. The highest observed H3.1 mass species appears at 15525 Da (18 m.e) in HeLa cells treated with 0.1-1% O_2 (Figure 4.16). In hypoxia, decreased abundance was detected in species corresponding to 0-5 methylation equivalents, whereas increase abundance was observed in species corresponding to 7-12 and 17-18 methylation equivalents. Overall, hypoxia (0.1-1% O_2) causes a shift to more highly modified states of intact H3.1 mass profiles for HeLa cells, as observed for HEK293T cells.

Treatment of HeLa cells treated with DMOG (0, 250, 500 and 1000 μM) was then carried out and the intact H3.1 mass profile was analysed (Figure 4.16, lower panel). The trend of global PTM changes and dose-dependent effects of DMOG on HeLa cells is highly similar to that observed for HEK293T cells (Figure 4.14), but not identical. In general, the treatment of DMOG leads to an overall shift to more highly modified states.

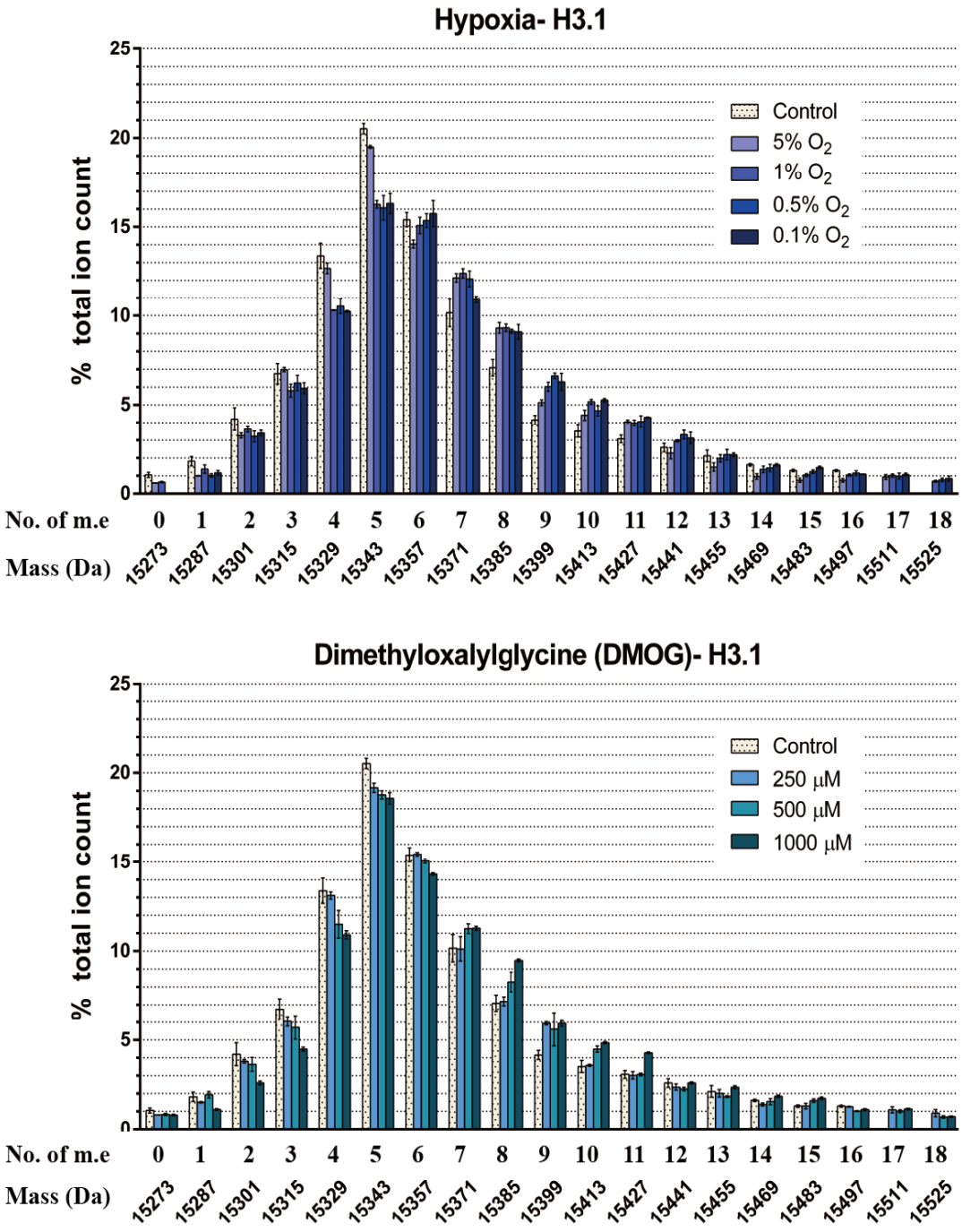

Figure 4.16 Quantitative analysis of the abundance of differently modified species of histone H3.1 following treatment of cells with normoxia (21% O_2), 5% O_2, 1%O_2, and 0.1% O_2 for 24 hours (upper); with 250, 500 and 1,000 µM DMOG for 24 hours (lower). The ion count for each peak is expressed as a percentage of the total ion count. Data are means ± SEM (n=3)**.** No. of m.e: number of methylation equivalents.

4.5.6 Time-dependent experiments of hypoxia and hypoxia-mimetics

Time-dependent effects of hypoxia and hypoxia-mimetic agents on the intact histone profiles were of interest. HEK293T cells were typically treated with hypoxia or hypoxia mimetic for between 1 and 24 hours prior to analysis. 0.1% O_2 (severe hypoxia), 150 μM DFO, 1.25 mM DMOG and 200 μM $CoCl_2$ were used to investigate the extent to which the histone profile changes with length of treatment. The resultant histone H3.1 intact mass profiles are shown in Figures 4.17 and 4.18.

In severe hypoxia, changes of PTMs profiles became obvious after a 6-hour exposure; the maximum effects were observed between 12 and 24 hours, suggesting cells might tolerate hypoxic stress for a short time and change over a longer stress exposure period (Figure 4.17 upper panel). The treatment of 150 μM DFO causes alteration of intact H3.1 PTMs profile after a 6-hour exposure; a dramatic change was observed after a 24-hour exposure (Figure 4.17 lower panel).

For DMOG, changes in the intact H3.1 PTMs mass profile were detected after a 2-hour exposure; the maximum effect was observed after a 24-hour exposure (Figure 4.18 upper panel). Following $CoCl_2$ treatment (200 μM), obvious changes were observed between 15315 Da (3 m.e) and 15385 Da (8 m.e), while the other species changed only slightly in abundance over time (Figure 4.18 lower panel).

These results indicate the response to the duration of hypoxia is not identical to the duration of compound-induced hypoxia-mimetic stresses. Together, time-dependent effects on the global histone modification profiles were observed following hypoxia and hypoxia-mimetic agents (DFO, DMOG and $CoCl_2$), but the extents of changes depend on the individual types of stress.

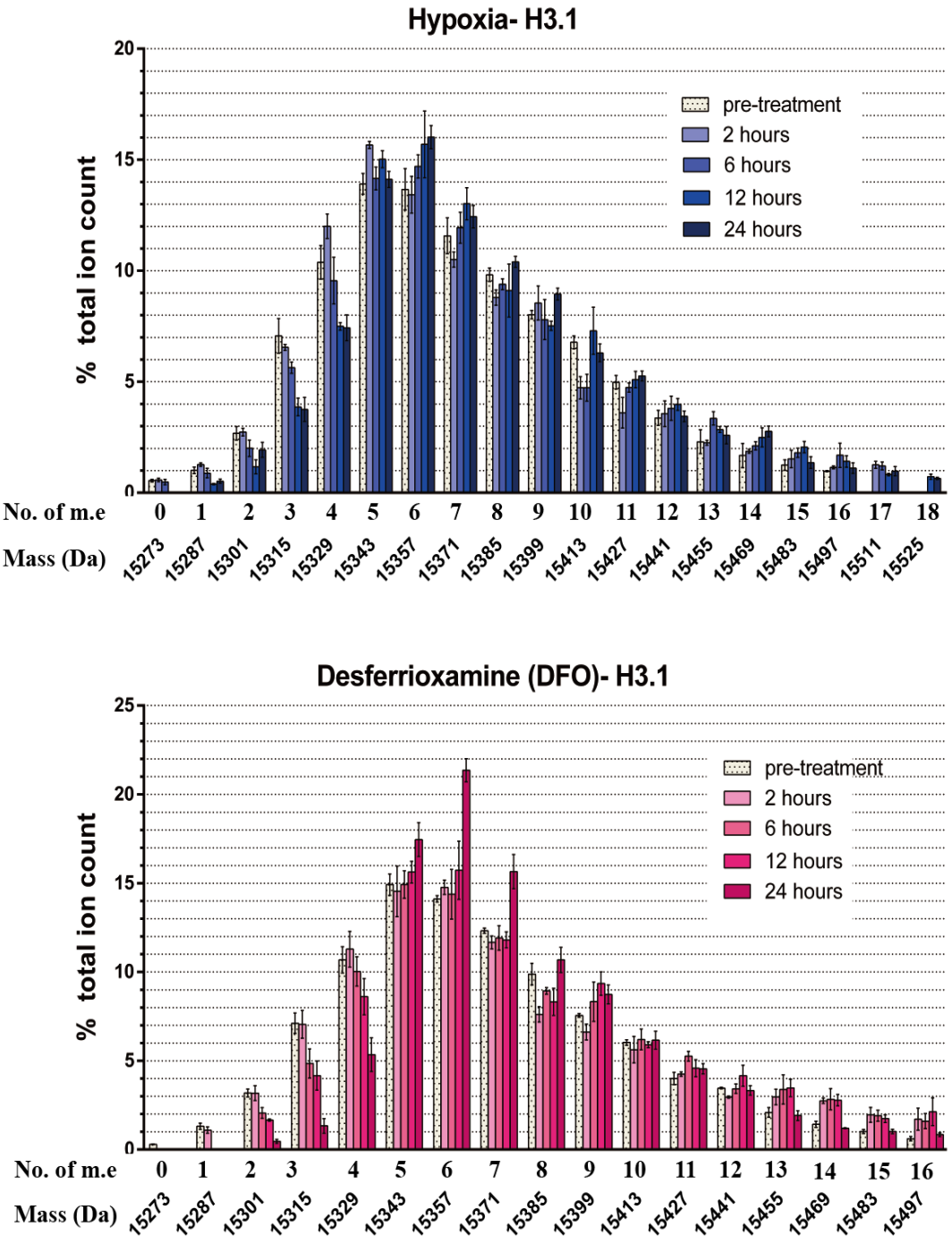

Figure 4.17 Quantitative analysis of the abundance of differently modified species of histone H3.1 following treatment of cells with hypoxia (0.1% O_2) (upper) or 150 µM DFO (lower) for 0-24 hours. The ion count for each peak is expressed as a percentage of the total ion count. Data are means ± SEM (n=3). No. of m.e: number of methylation equivalents.

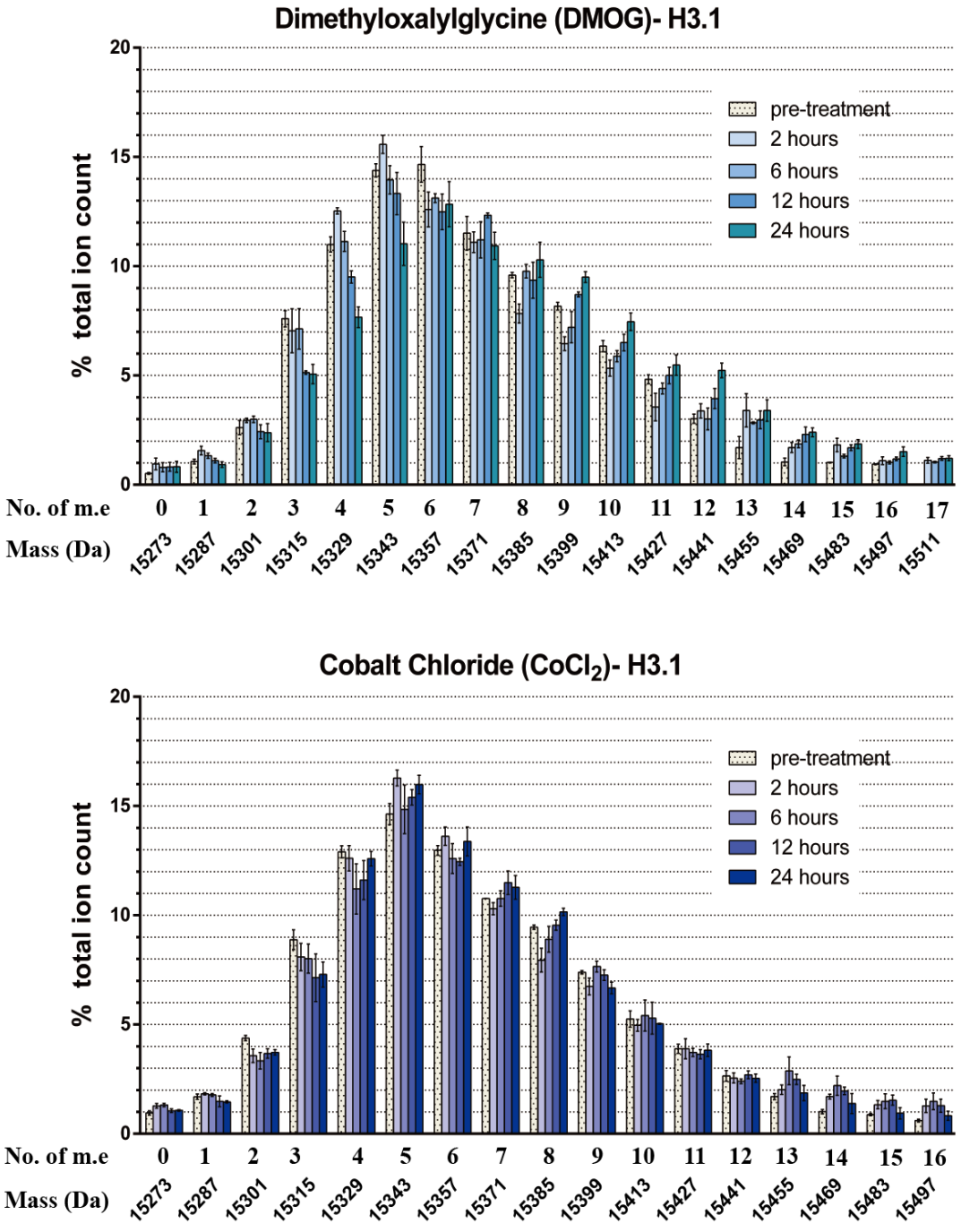

Figure 4.18 Quantitative analysis of the abundance of differently modified species of histone H3.1 following treatment of cells with 1.25 mM DMOG (upper) or 200 μM $CoCl_2$ (lower) for 0-24 hours. The ion count for each peak is expressed as a percentage of the total ion count. Data are means ± SEM (n=3). No. of m.e: number of methylation equivalents.

4.5.7 Effect of hypoxia and hypoxia-mimetics on histone H4

Analysis of the intact H4 mass profile was performed following treatment of HEK293T cells with hypoxia and hypoxia-mimetics (Figure 4.19).

In hypoxia, the most abundance change was observed for the species at 11348 Da (5 m.e), followed by the species at 11278 Da (0 m.e) (Figure 4.19, left upper panel). Of note, the change patterns in the intact H4 mass profile were different between treatments with hypoxia and DFO. With DFO treatment, the abundance of the species at 11306 Da (2 m.e) increases significantly while the levels of species at 11278 Da (0 m.e) and 11292 Da (1 m.e) decrease (Figure 4.19, right upper panel). The changed patterns of intact H4 mass profiles were similar for application of the three iron chelators (DFO, CP20 and Exjade) and $CoCl_2$ (Figure 4.19), although the extent of changes differed. Notably, a change in pattern of the H4 mass profile was observed with DMOG treatment, as observed in hypoxia (Figure 4.19).

The species at 11306 Da (2 m.e) correlate to N-Ac H4+ 2me, consistent with the reported dimethylation of K20 while the species at 11348 (5 m.e) correlate to N-Ac H4+ 2me +1K-Ac (likely including K20me2 and K16Ac).[201] The results indicate the hypoxia and DMOG treatments cause similarly a higher population of the species of N-Ac H4+ 2me +1K-Ac (11348 Da), possibly due to inhibition of histone modifying enzymes (e.g. histone deacetylases, demethylases, acetyltransferases). Iron chelators and $CoCl_2$ have comparable effects, causing a higher population of the species corresponding to N-Ac H4+ 2me (11306 Da), again possibly due to enzyme inhibition.

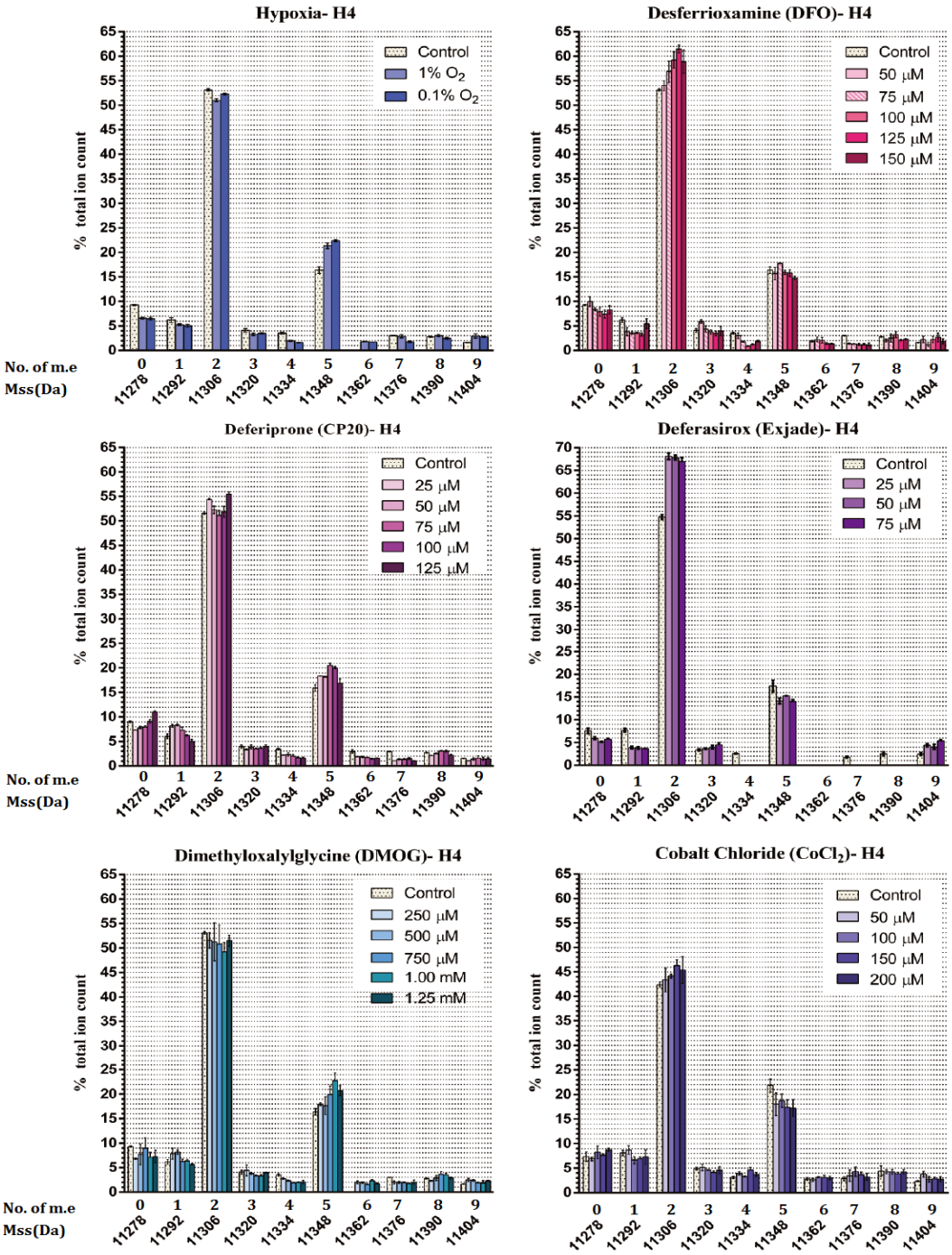

Figure 4.19 Quantitative analysis of the abundance of differently modified species of histone H4 following treatment of cells with hypoxia and hypoxia-mimetics (iron chelators, DMOG and $CoCl_2$) for 24 hours. The ion count for each peak is expressed as a percentage of the total ion count. Data are means ± SEM (n=3). No. of m.e: number of methylation equivalents.

4.5.8 Immunoblotting analysis of histone PTMs

Immunoblotting is a method for analysing the extent of global histone modifications.[280] The methylation level of histone H3 is of interest from the perspective of hypoxia, as well as analysing the activity of hypoxia-mimetics and acetylation levels. Common and important histone methylated modification sites (i.e. H3K4, H3K9, H3K27, H3K36, and H3K79) and pan-acetylation of H3 were examined (Figure 4.20). The antibodies used are listed in Section 6.8.

Levels of acetylated histone H3

The extent of pan-acetylation of H3 did not appear to significantly change in HEK293T cells treated with hypoxia or hypoxia-mimetics (iron chelators, DMOG and $CoCl_2$), compared to untreated cells. For comparison of the effects of hypoxia and hypoxia mimetic agents, no significant difference was observed either between hypoxia and iron chelators or between hypoxia and DMOG/$CoCl_2$ (Figure 4.20 B). Decreased levels of H3K9ac and increased levels of H3K14ac have been reported in hypoxia.[281,282] Yun *et al.* have reported decreased levels of acetylated H3 at the *myo*D promoter, but no obvious global changes of the acetylated H3 levels in mouse myoblast cells treated with 0.5% O_2, compared to that in normoxia.[283] The collective results suggest that different levels of acetylation could be found on individual H3 lysine residues, which may have an impact on the expression of individual sets of genes but it is possible that global changes of acetylated H3 levels are small.

Levels of trimethylated histone H3K4

A significant increase in H3K4me3 levels was observed in HEK293T cells treated with hypoxia and the different hypoxia-mimetics (Figure 4.20C). A 1.9-fold increase in H3K4me3 levels was observed under severe hypoxia (0.1% O_2). The increased levels

of H3K4me3 observed following treatment with 150 μM DFO, 125 μM CP20 and 75 μM Exjade was 1.6-, 1.4- and 1.5-fold, respectively. Significant differences were observed between hypoxia and the three iron chelators, whereas no significant differences were observed for the three iron chelators. Approximately a 1.3-fold increase in H3K4me3 was observed following treatment with DMOG and $CoCl_2$, although a smaller change was noted, compared to hypoxia (Figure 4.20C). These results are consistent with literature reports; at histone H3K4me3 is associated with activation of transcription.[281,284] Hypoxia-induced increased H4K3me3 levels at both global and gene-specific levels have been proposed to lead to tumor progression.[284]

Levels of trimethylated histone H3K9

In general, hypoxia, iron chelators, DMOG and $CoCl_2$ caused a small increase in H3K9me3, compared to normoxia (Figure 4.20D); only one iron chelator, Exjade causes a significant increase in H3K9me3 (Figure 4.20D). Among hypoxia and hypoxia-mimetic agents, there was no significant difference in the level of H3K9me3 (Figure 4.20D).

Pogribny *et al.* have reported no increase in H3K9me3 levels in the 24-hour DFO-treated MCF-7 cells, but significant increases in H3K9me3 levels in MDA-MB-231 cells treated with DFO for 6-48 hours.[285] Overall, the results suggest that hypoxia-mediated changes in the H3K9me3 level are likely dependent on the cell types. The extent of changes in H3K9me3 levels may be different in the different hypoxic stress related conditions.

Levels of trimethylated histone H3K27

A significant change of H3K27me3 levels was observed in hypoxia and hypoxia-mimetic conditions (Figure 4.20E). Approximately a 1.5- to 1.7-fold increase in

H3K27me3 levels was observed in hypoxia/ the three iron chelators; no significant difference was noted with the different treatments. A 1.3-fold increase in H3K27me3 was induced by DMOG and $CoCl_2$; however, a greater increase in H3K27me3 was observed in severe hypoxia (Figure 4.20E). Increased H3K27me3 has been reported in Hepa 1-6 cells under severe hypoxia.[281]

Levels of trimethylated histone H3K36

Effects of hypoxia, iron chelators, DMOG and $CoCl_2$ were observed on the levels of H3K36me3 (Figure 4.20F). There was evidence for small increases in H3K36me3 levels on treatment of CP20, DMOG and $CoCl_2$, whereas hypoxia, DFO and Exjade caused significant increases in H3K36me3, compared to normoxia. No significant difference was noted among the treatment of three iron chelators, and no obvious difference of H3K36me3 level was revealed between DMOG and $CoCl_2$ (Figure 4.20F). Tausendschon *et al.* have reported hypoxia and DMOG increase the levels of H3K9me2/3 and H3K36me3 in macrophages and further decrease the chemokine expression.[115]

Levels of trimethylated histone H3K79

The levels of H3K79me3 in HEK293T cells treated with hypoxia or hypoxia-mimetics did not differ from the respective untreated cells (Figure 4.20G). The result is consistent with the literature, since H3K79me2, but not H3K79me3, has been reported to be increased by approximately 1.4-fold level in response to hypoxia.[281]

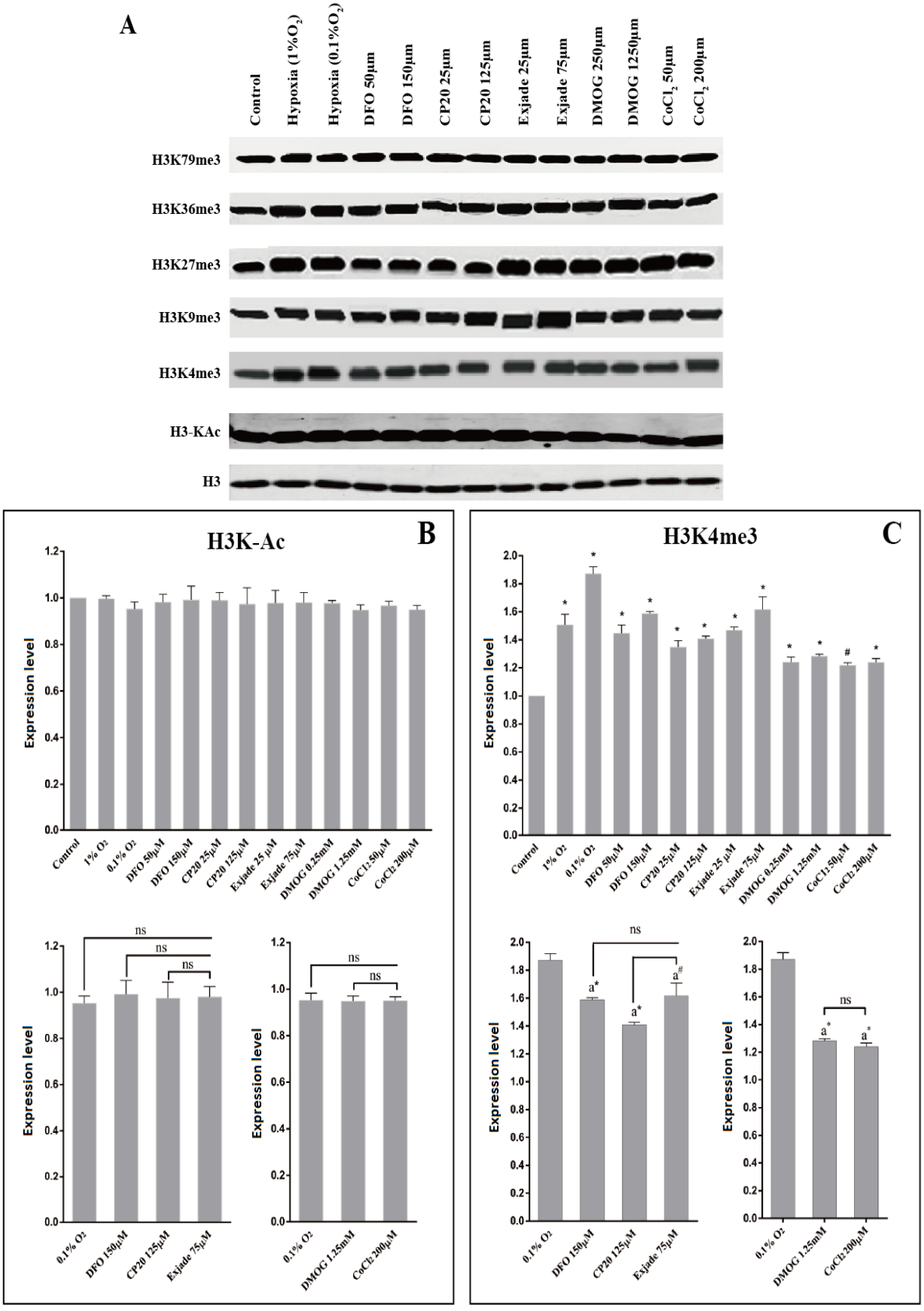
A
Control
Hypoxia (1%O2)
Hypoxia (0.1%O2)
DFO 50μm
DFO 150μm
CP20 25μm
CP20 125μm
Exjade 25μm
Exjade 75μm
DMOG 250μm
DMOG 1250μm
CoCl2 50μm
CoCl2 200μm
H3K79me3
H3K36me3
H3K27me3
H3K9me3
H3K4me3
H3-KAc
H3
B
H3K-Ac
Expression level
C
H3K4me3
ns

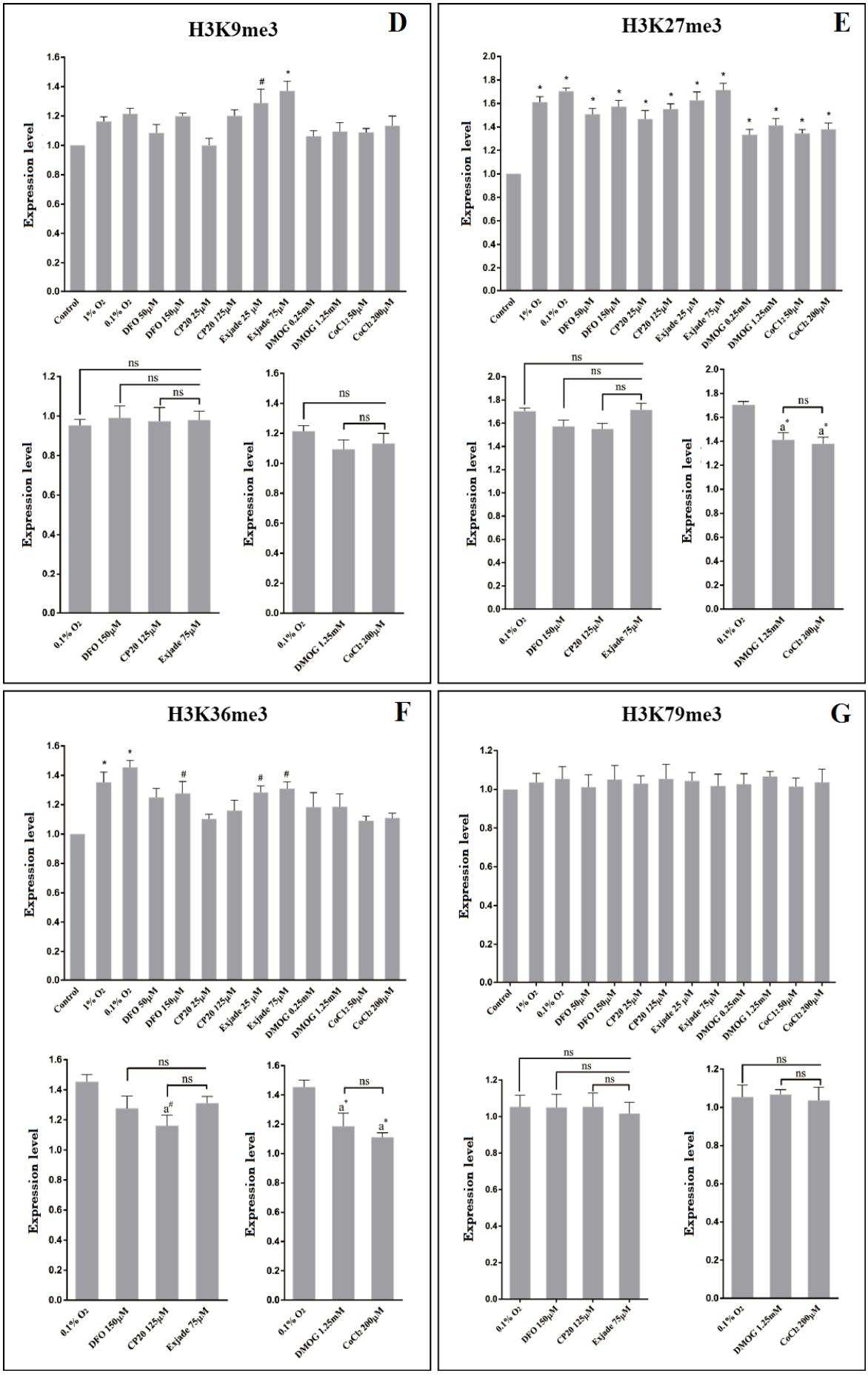
H3K9me3
D
H3K27me3
E
H3K36me3
F
H3K79me3
G
Expression level
Control
1% O2
0.1% O2
DFO 50μM
DFO 150μM
CP20 25μM
CP20 125μM
Exjade 25 μM
Exjade 75μM
DMOG 0.25mM
DMOG 1.25mM
CoCl2 50μM
CoCl2 200μM
ns

Figure 4.20 Western blot analysis of histone marks in HEK293T cells treated with hypoxia and hypoxia-mimetic agents for 24 hours**.** (A) The levels of H3K-Ac, H3K4me3, H3K9me3, H3K27me3, H3K36me3 and H3K79 me3 were assessed. Anti-H3 antibody was used as a loading control. Representative western blot images are shown. Blot quantitation and statistical analysis for H3K-Ac (B), H3K4me3 (C), H3K9me3 (D), H3K27me3 (E), H3K36me3 (F) and H3K79me3 (G). Data are presented as protein detection levels, normalised to the corresponding control group (21% O_2). # and * denote significant difference with $p<0.05$ and $p<0.01$, respectively from the corresponding control group (21% O_2). $a^{\#}$ and a* indicate $p<0.05$ and $p<0.01$, respectively from the group treated with 0.1 % O_2. Results were obtained from 3 independent experiments.

4.5.9 Discussion

Hypoxia causes changes in histone PTMs, not only on local chromatin environments, but also, in some cases, globally.[259,260,281,286] Hypoxia-induced epigenetic alterations have been linked to transcriptional activation and repression.[249] Overall, hypoxia induces general reduction of gene transcription.[281] However, hypoxia mediated histone modification changes appear more complex and are likely incorporated in a gene-specific manner to associate with gene regulation in response to hypoxia.[281] The global level of histone lysine methylation is mainly mediated by cooperation of histone methyltransferases and demethylases. Therefore, the enzymatic activities of these two functionally opposite enzyme families in hypoxia likely determine global levels of histone methyl marks. The increased activity of the methyltransferase G9a and the decreased activity of JmjC KDMs in 0.2% O_2 have been reported.[281,282]

Increased levels of H3K4me3, linked to gene transcriptional activation, have been shown to correlate with inhibition of KDM5A activity in hypoxia.[284] JmjC KDMs are members of 2OG/Fe(II)-dependent oxygenases require oxygen as a cofactor to perform their demethylase activity, consistent with the observation of compromised activity of JmjC KDMs in hypoxia.[287] Notably, a number of JmjC KDMs have been identified to be transcriptionally induced in hypoxia.[123,261,288] Thus, the induction of JmjC KDMs in hypoxic conditions may (in part, at least) compensate for their reduced activity due to

limiting oxygen.[260] Thus, the relationship between hypoxia and JmjC KDMs may be sophisticated.

In this work, hypoxia and hypoxia-mimetics were found to induce the alteration of some global histone PTMs as revealed by LC-MS-based analysis of intact histones. The changes in patterns of PTMs histone mass profiles induced by hypoxia and hypoxia-mimetics, reveals the changes in highly modified histone states. Overall, the results are consisted with alterations in chromatin structure, consistent with the proposal that there is in general "a hypoxia-induced reduction in gene transcription". The results of intact histone MS profiles for hypoxic and hypoxia-mimetic stresses are supported by immunoblotting analyses, which indicate increases in methylation of H3, particularly at K4, K9, K27 and K36.

The magnitude of the observed changes from intact mass profiles differs considerably among hypoxia and compounds. Many factors may contribute to the results. Firstly, the influence of the oxygen concentration, Fe(II) and 2OG for JmjC KDMs activity may differ and induce the various extent of decreased activity, leading to different populations of histone PTMs. Secondly, the different strength for chelating iron may have an impact for DFO, CP20 and Exjade to affect the JmjC KDMs enzymatic behaviour.[289] (Note, recent unpublished work from the Schofield group has indicated Exjade, but not DFO, may bind directly to the PHDs). In addition, hypoxia and hypoxia-mimetic compounds may also have various influences on other histone modifying enzymes such as histone methyltransferase, acetyltransferases, and deacetylases.[282] Furthermore, the different level of HIF induction by hypoxia and hypoxia-mimetic agents may have differing effects on the JmjC-KDM expression, which in turn may contribute to alterations in histone PTMs.

Together these factors complicate the interpretation of the results of modulation of

histone marks to response to hypoxia and hypoxia-mimetics. However, collectively, the results reveal that, at least in tissue culture work, hypoxia, iron chelators, DMOG and $CoCl_2$ clearly have distinct effects on global histone PTMs, all of them causing overall shifts toward more highly modified states.

4.6 Effect of HIF prolyl-hydroxylase inhibitors on intact histone profiles

The HIF prolyl-hydroxylases, PHDs are one of the two types of HIF-α hydroxylases. The PHDs play an important role in the degradation of HIF-α, which regulates the cellular response to hypoxia.[254] Inhibitors of PHD reduce HIF-α prolyl-hydroxylation, so elevating HIF-α levels and leading to the activation of HIF target genes. The effects of selective PHD inhibitors on global PTMs on intact histone were of interest. Two potent and selective PHD inhibitors, IOX2 and FG-4592 were tested, as compounds are in clinical trials for the treatment of anemia.[290-292]

4.6.1 IOX2

Two concentrations of IOX2, 50 and 250 μM, were examined for HEK293T cell viability; the results show no obvious decreased viability (Figure 4.21). The global PTM patterns on intact H3.1 mass profiles (Figure 4.22) show generally mild changes following 50 or 250 μM IOX2 treatment. A significant decrease in the level (1.6%, $p<0.05$) was detected in the species at 15343 Da (5 m.e), whereas an increased level (1.3%, $p<0.05$) was observed in the species at 15385 Da (8 m.e) for HEK293T cells treated with 250 μM IOX2 (Table 4.3). More obvious PTM changes were observed on the intact mass profile of H3.2 than that of H3.1 following treatment with 250 μM IOX2 (Table 4.4). However, 50 μM IOX2 had slight effects on intact H3.2 mass profiles (Figure 4.22).

No significant changes were observed in H2A; however, some changes were observed in H4 and H2B on IOX2 treatment (see Appendix 7). In respect of changes on intact histone H2B mass profiles, further investigations are needed to determine whether the observed changes are due to different proportion of H2B variants or due to changes in PTMs.

4.6.2 FG-4592

Like IOX2, FG-4592, is a potent small molecule inhibitor of HIF prolyl hydroxylases; FG-4592 is in phase III clinical trials for treatment of human renal anaemia.[291] Different concentrations of FG-4592 (25, 50, 75 and 100 μM) were used to treat HEK293T cells; no significant decreased cell viability was observed. The intact H3 mass profiles show no distinct changes in histone modified forms for cells treated with FG-4592 (25-100 μM), compared to the untreated cells (Figure 4.23). Even the largest difference in abundance was for the species at 15343 Da (5 m.e) from H3.1, that had a 1.0 % of total ion count between untreated cells and cells treated with 100 μM FG-4592 but it was not statistically significant (p= 0.079), shown in Table 4.3). The results indicate that FG-4592 has little or (at least no discernible effects) on global PTMs on intact H3. It is interesting to compare the results for H3, with those for $CoCl_2$, little change in histone profiles, and for DMOG/ iron chelators where substantial changes for histone profiles were observed.

The effects of FG-4592 on other core histones (H2A, H2B and H4) were small and apparently similar to those of IOX2 (Appendix 7). The substantial changes were observed on mass profiles of the intact H2A and H4; however, some apparent changes in the pattern of the intact H2B mass profile were observed. As with IOX2, further investigations are needed to determine the effects of FG-4592 on H2B.

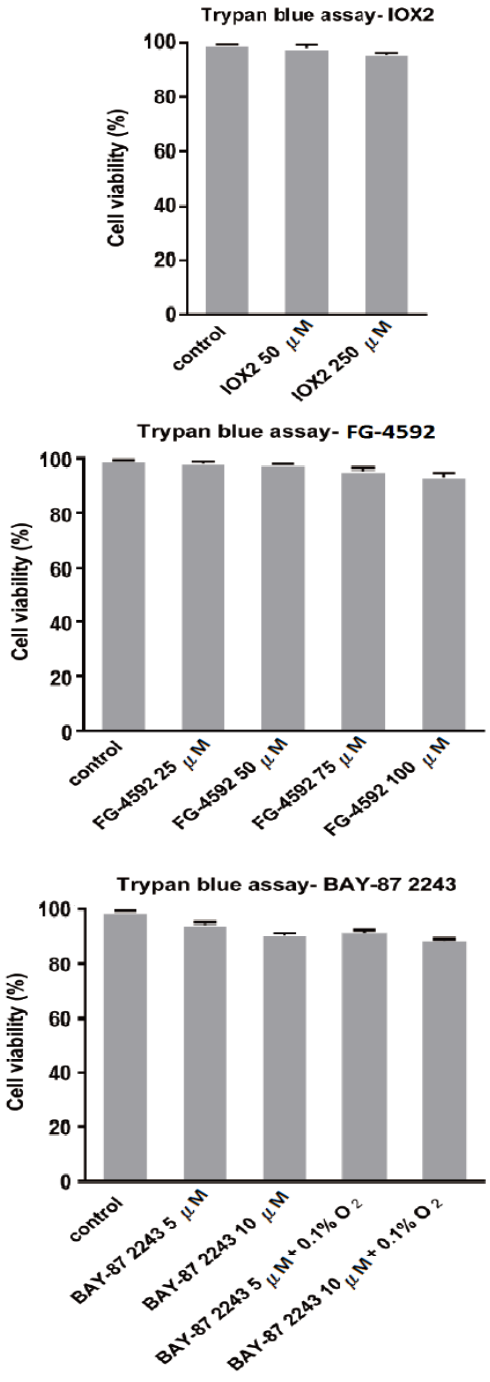

Figure 4.21 Trypan blue cell viability assays for HEK293T cells exposed to HIF prolyl hydroxylase (PHD) inhibitors, IOX2 (left), FG-4592 (middle) and HIF inhibitor, BAY-87 2243 (right) for 24 hours. The percentage of cell viability is presented as a mean ± S.D (n=3).

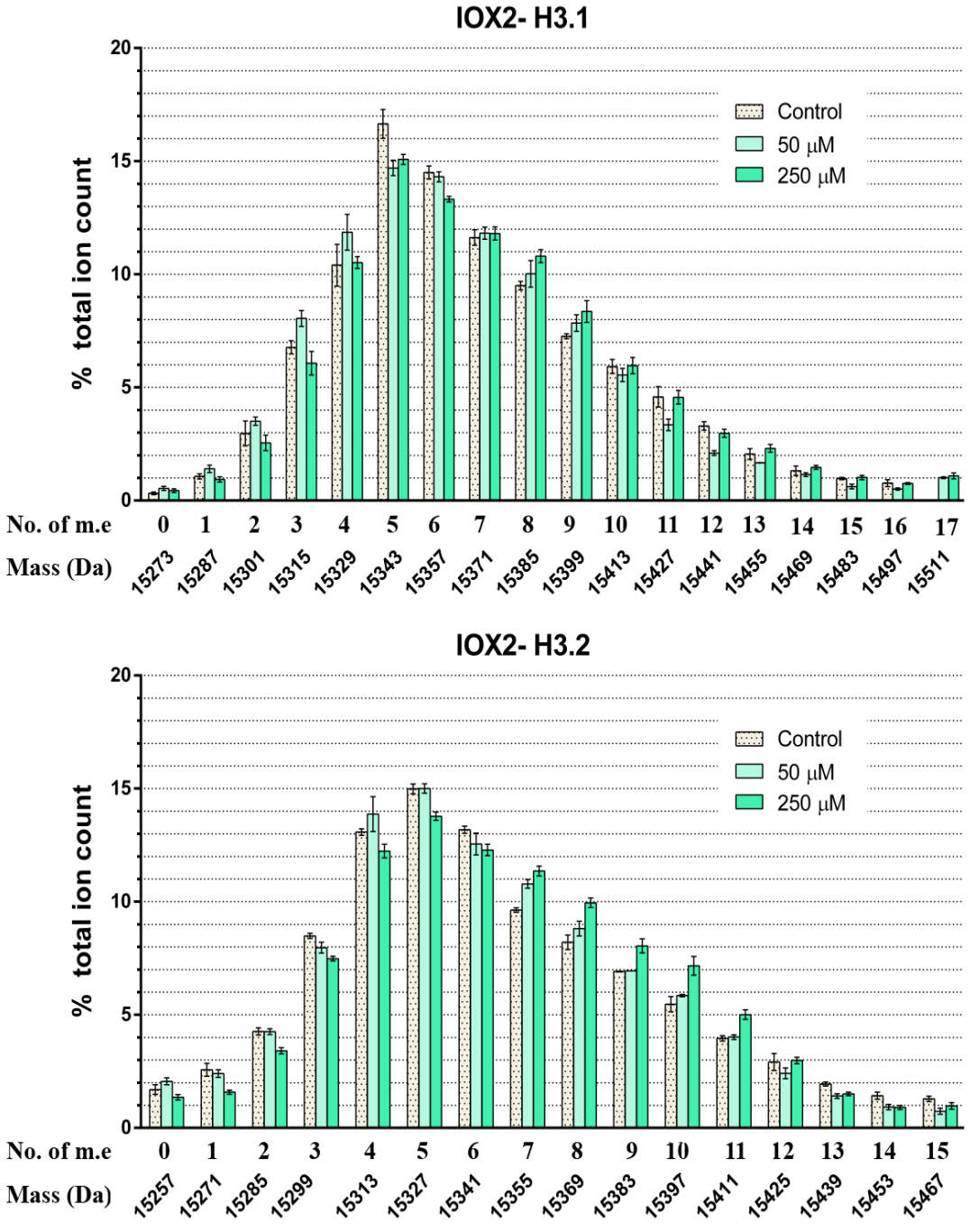

Figure 4.22 Quantitative analysis of the abundance of differently modified species of histone H3.1 (upper) and H3.2 (lower) following treatment of cells with 0, 50 and 250 μM IOX2 for 24 hours. The ion count for each peak is expressed as a percentage of the total ion count. Data are means ± SEM (n=3). No. of m.e: number of methylation equivalents.

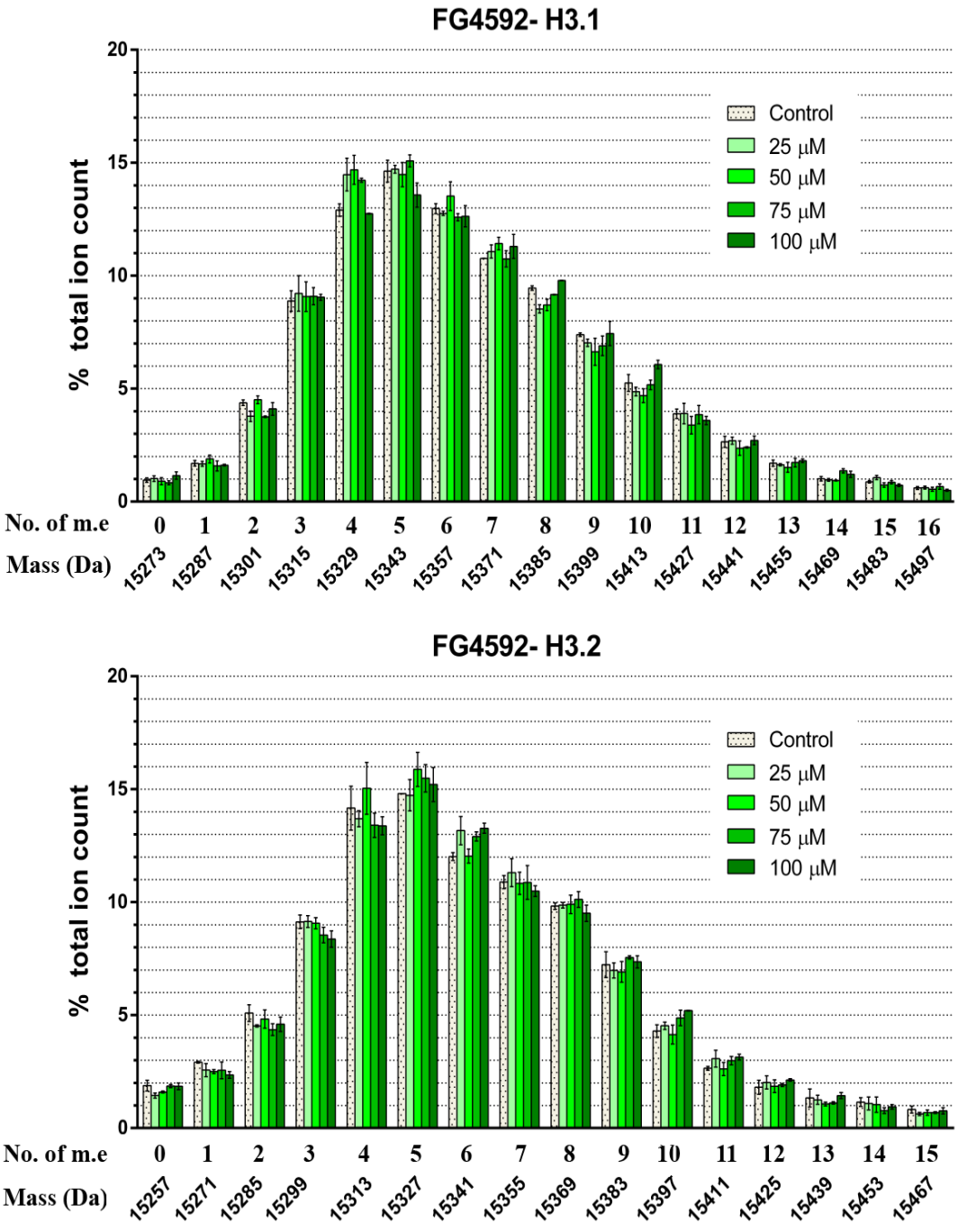

Figure 4.23 Quantitative analysis of the abundance of differently modified species of histone H3.1 (upper) and H3.2 (lower) following treatment of cells with FG-4592 (0, 25, 50, 75, 100 μM) for 24 hours. The ion count for each peak is expressed as a percentage of the total ion count. Data are means ± SEM (n=3). No. of m.e: number of methylation equivalents.

4.6.3 HIF down regulator - BAY 87-2243

BAY 87-2243 has been identified as down regulating HIF-α levels and to have potential antitumor activity by inhibiting mitochondrial complex I.[293,294] Under hypoxic conditions, BAY 87-2243 inhibits the accumulation of HIF-α; however, BAY 87-2243 is reported not to have an effect on the relatively high levels of HIF-α induced by hypoxia-mimetic agents such as DFO.[293] BAY 87-2243 also has been found to inhibit cell proliferation under glucose depletion but not under normal glucose availability conditions.[293] The effects of BAY 87-2243 on global PTMs of intact histones are of interest.

BAY 87-2243 was used at concentrations of 5 and 10 μM with HEK293T cells for 24 hours under normoxia or severe hypoxia (0.1% O_2); cell viability post-treatment was > 85% (Figure 4.21). The global PTM patterns of intact H3 mass profiles from cells treated with 5 or 10 μM BAY 87-2243 under normoxia (Figure 4.24) show no significant change in abundance of species (modified forms), compared to untreated cells (Tables 4.3 and 4.4). However, the effects of hypoxia on global PTM changes on H3.1 and H3.2 appeared to be partially reversed by use of 5 or 10 μM BAY 87-2243 (Figure 4.25). The more highly modified H3 forms containing 17 and 18 methylation equivalents were observed under severe hypoxia but not detected under severe hypoxia combined with BAY 87-2243. In addition, the distinct decreases in levels of the species of 15315 Da, 15329 Da and 15357 Da observed under severe hypoxia were apparently alleviated (at least in part) by BAY 87-2243. Overall, BAY 87-2243 has obvious effects on global PTMs of intact H3 under hypoxic conditions, whereas it does not have significant effects under normoxia, suggesting the effects of BAY 87-2243 may not be limited to reducing HIF-α levels.

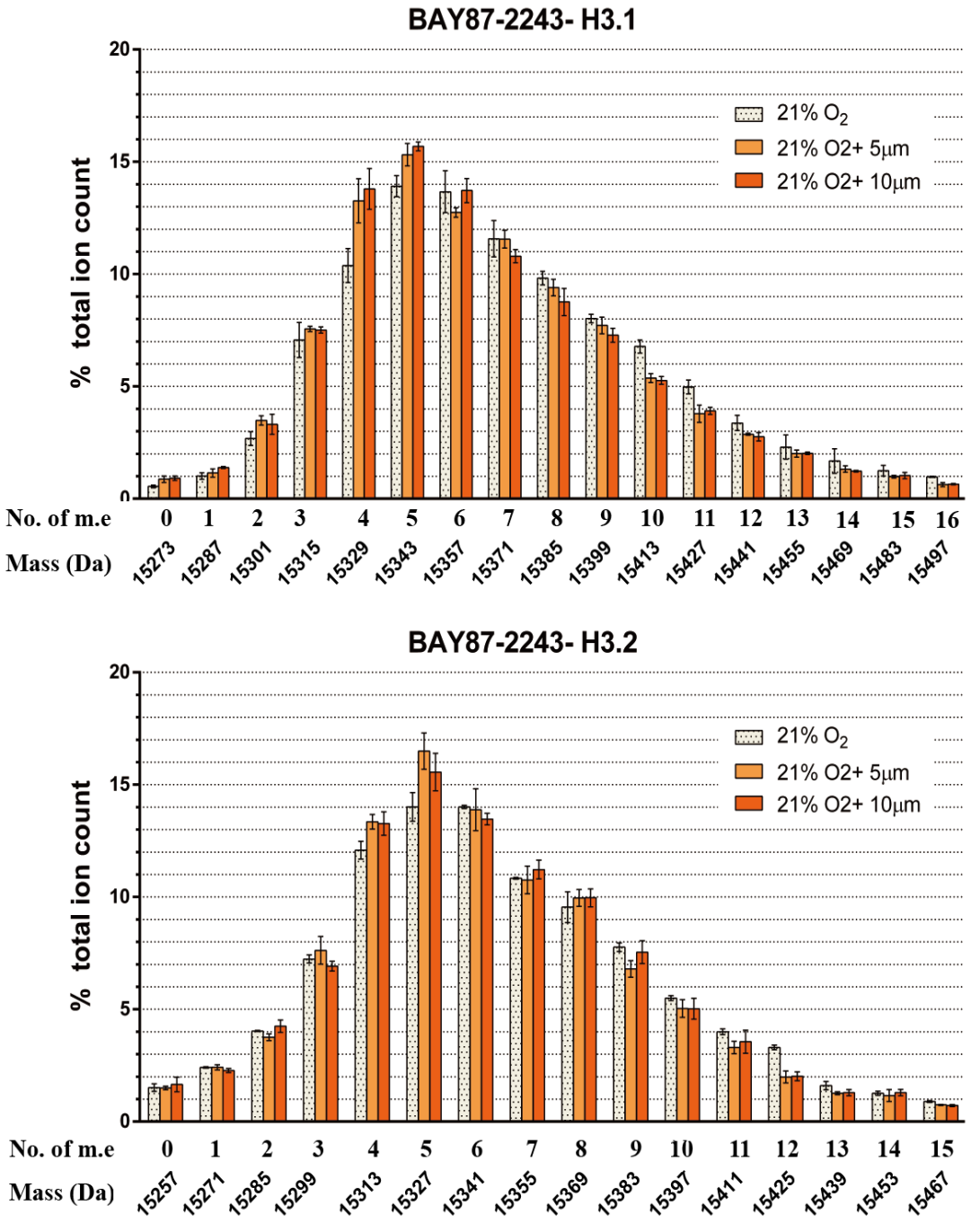

Figure 4.24 Quantitative analysis of the abundance of differently modified species of histone H3.1 (upper) and H3.2 (lower) following treatment of cells with BAY 87-2243 (0, 5 and 10 µM) for 24 hours. The ion count for each peak is expressed as a percentage of the total ion count. Data are means ± SEM (n=3). No. of m.e: number of methylation equivalents.

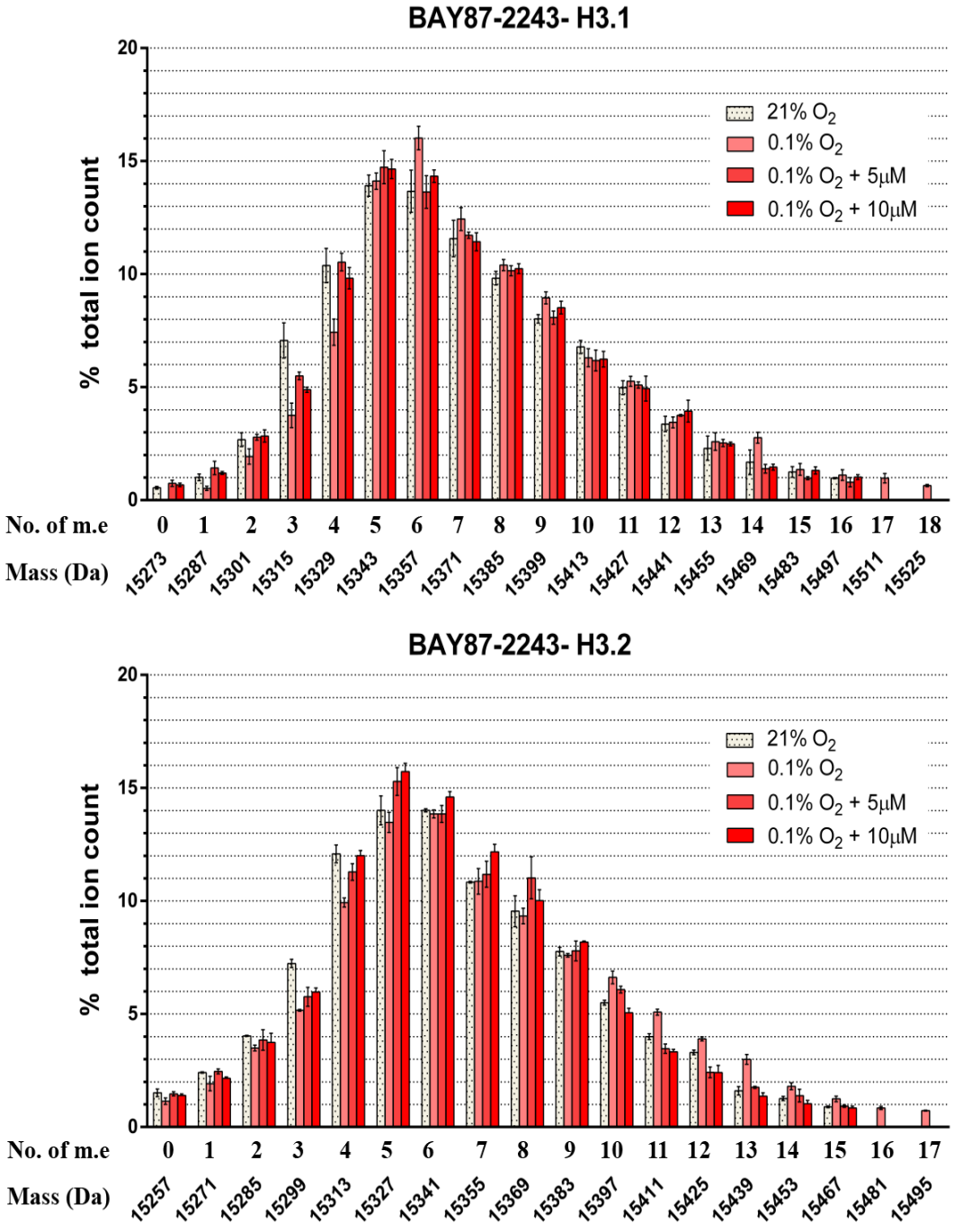

Figure 4.25 Quantitative analysis of the abundance of differently modified species of histone H3.1 (upper) and H3.2 (lower) following treatment of cells with normoxia, severe hypoxia (0.1%) combined BAY 87-2243 (0, 5 and 10 µM) for 24 hours. The ion count for each peak is expressed as a percentage of the total ion count. Data are means ± SEM (n=3). No. of m.e: number of methylation equivalents.

Table 4.3 List of abundance change of each species of histone H3.1 from HEK293T cells with different treatments compared to control group

Mass (Da)	Methylation equivalents	0.1% O_2 (Δ%)	IOX2 250μM (Δ%)	FG-4592 100μM (Δ%)	BAY87-2243 10 μM (Δ%)	0.1 % O_2 & BAY87-2243 10 μM (Δ%)
15273	0	-0.473 ± 0.051	0.113 ± 0.015	0.199 ± 0.038	0.115 ± 0.033	0.130 ± 0.014
15287	1	-0.645 ± 0.001	-0.131 ± 0.001	-0.080 ± 0.054	0.168 ± 0.035	0.193 ± 0.047
15301	2	-1.171 ± 0.066	-0.421 ± 0.117	-0.273 ± 0.090	0.119 ± 0.042	0.161 ± 0.020
15315	3	**-3.514 ± 0.144****	-0.705 ± 0.134	0.168 ± 0.186	**-2.263 ± 0.384****	**-2.185 ± 0.385****
15329	4	**-3.634 ± 0.133****	0.112 ± 0.381	-0.157 ± 0.147	-0.481 ± 0.058	-0.560 ± 0.166
15343	5	-1.178 ± 0.034	**-1.570 ± 0.241***	-1.059 ± 0.033	0.354 ± 0.120	0.733 ± 0.028
15357	6	**1.943 ± 0.175****	-1.177 ± 0.093	-0.339 ± 0.140	0.861 ± 0.376	0.668 ± 0.378
15371	7	0.916 ± 0.191	0.180 ± 0.027	0.527 ± 0.301	-0.007 ± 0.160	-0.142 ± 0.237
15385	8	0.796 ± 0.106	**1.302 ± 0.056***	0.331 ± 0.051	0.519 ± 0.013	0.420 ± 0.046
15399	9	**1.273 ± 0.067***	1.087 ± 0.215	0.053 ± 0.263	0.273 ± 0.022	0.501 ± 0.053
15413	10	0.242 ± 0.129	0.039 ± 0.027	0.818 ±0.108	-0.527 ± 0.111	-0.541 ± 0.029
15427	11	0.726 ± 0.035	-0.020 ± 0.089	-0.301 ± 0.016	0.022 ± 0.270	-0.042 ± 0.141
15441	12	0.274 ± 0.078	-0.330 ± 0.003	0.062 ± 0.031	0.580 ± 0.200	0.570 ± 0.084
15455	13	0.638 ± 0.175	0.254 ± 0.035	0.107 ± 0.034	0.132 ± 0.264	0.192 ± 0.263
15469	14	**1.479 ± 0.090****	0.151 ± 0.069	0.197 ± 0.022	-0.091 ± 0.312	-0.219 ± 0.241
15483	15	0.357 ± 0.1244	0.047 ± 0.023	-0.151 ± 0.003	0.088 ± 0.009	0.071 ± 0.046
15497	16	0.354 ± 0.102	-0.020 ± 0.061	-0.101 ± 0.012	0.139 ± 0.038	0.050 ± 0.048
15511	17	0.969 ± 0.119	1.087 ± 0.075	n/a	n/a	n/a
15525	18	0.648 ± 0.027	n/a	n/a	n/a	n/a

Table 4.4 List of abundance change of each species of histone H3.2 from HEK293T cells with different treatments compared to control group

Mass (Da)	Methylation equivalents	0.1% O_2 (Δ%)	IOX2 250μM (Δ%)	FG-4592 100μM (Δ%)	BAY87-2243 10 μM (Δ%)	0.1 % O_2 & BAY87-2243 10 μM (Δ%)
15257	0	-0.370 ± 0.014	-0.338 ± 0.053	-0.033 ± 0.050	-0.048 ± 0.078	-0.117 ± 0.055
15270	1	-0.490 ± 0.171	**-0.987 ± 0.112***	-0.561 ± 0.062	-0.319 ± 0.003	-0.262 ± 0.020
15284	2	-0.537 ± 0.060	-0.857 ± 0.011	-0.491 ± 0.028	-0.701 ± 0.024	-0.294 ± 0.220
15298	3	**-2.071 ± 0.083****	**-1.006 ± 0.004***	-0.761 ± 0.038	-1.091 ± 0.105	**-1.265 ± 0.005***
15313	4	**-2.156 ± 0.108****	-0.842 ± 0.092	-0.786 ± 0.331	0.143 ± 0.192	-0.083 ± 0.094
15327	5	-0.535 ± 0.114	**-1.207 ± 0.022****	0.405 ± 0.431	**2.083 ± 0.348****	**1.716 ± 0.157****
15341	6	-0.161 ± 0.061	-0.893 ± 0.055	1.252 ± 0.028	0.398 ± 0.087	0.585 ± 0.100
15355	7	0.035 ± 0.302	**1.729 ± 0.067****	-0.404 ± 0.029	1.589 ± 0.156	**1.343 ± 0.167****
15369	8	-0.213 ± 0.195	**1.742 ± 0.066****	-0.315 ± 0.124	-0.011 ± 0.377	0.467 ± 0.119
15383	9	-0.165 ± 0.066	**1.130 ± 0.171****	0.125 ± 0.171	0.448 ± 0.085	0.421 ± 0.088
15397	10	**1.125 ± 0.100***	**1.694 ± 0.045****	0.907 ± 0.155	-0.615 ± 0.021	-0.442 ± 0.054
15411	11	1.081 ± 0.004	**1.047 ± 0.057***	0.497 ± 0.026	-0.568 ± 0.040	-0.667 ± 0.011
15425	12	0.601 ± 0.009	0.066 ± 0.137	0.323 ± 0.151	-0.593 ± 0.018	-0.888 ± 0.121
15439	13	**1.391 ± 0.017****	-0.433 ±0.008	0.104 ± 0.151	-0.380 ± 0.079	-0.238 ± 0.023
15453	14	0.544 ± 0.034	-0.525 ±0.040	-0.208 ± 0.053	-0.372 ± 0.041	-0.226 ± 0.031
15467	15	0.355 ± 0.048	-0.320 ±0.016	-0.056 ± 0.007	0.035 ± 0.016	-0.049 ± 0.026
15481	16	0.842 ± 0.040	n/a	n/a	n/a	n/a
15495	17	0.726 ± 0.013	n/a	n/a	n/a	n/a

The value (Δ%) is expressed as the abundance changes in percentage of the total ion count. Data are means ± SEM (n=3). The values highlighted in bold indicate significant changes in abundance. ** Indicates p value <0.01; * Indicates p value<0.05. n/a: not available.

4.6.4 Immunoblotting analysis of histone PTMs

The effects of the HIF hydroxylase inhibitors, IOX2 and FG-4592, and the HIF down-regulating compound, BAY87-2243, on individual histone PTMs were assessed by immunoblotting (Figure 4.26). No significant changes in the acetylation of H3 were observed following treatment of cells with these three compounds (Figure 4.26B), consistent with them not being HDAC inhibitors, in contrast with the results for SAHA (Section 4.3.2). Likewise, there were no significant changes in the levels of all H3 methylation marks investigated (H3K4me3, H3K9me3, H3K27me3, H3K36me3 and H3K79me3, Figure 4.26C-G) for cells treated with compounds (IOX2, FG-4592 and BAY 87-2243). Notably, the levels of multiple marks, including H3K4me3, H3K9me3, H3K27me3 and K3K36me3 are significantly increased in samples treated with severe hypoxia compared to the normoxia control (see Section 4.5.8). This was most apparent for the H3K4me3 and H3K27me3 marks, for which a ~2-fold increase was observed in severe hypoxia. Interestingly, these effects (i.e. increases in methylation states) were not observed when cells were treated with severe hypoxia in combination with BAY87-2243 (where levels were comparable to the normoxia control, Figure 4.26), suggesting that BAY87-2243 might counteract the effects of atmospheric hypoxia on these methylation states.

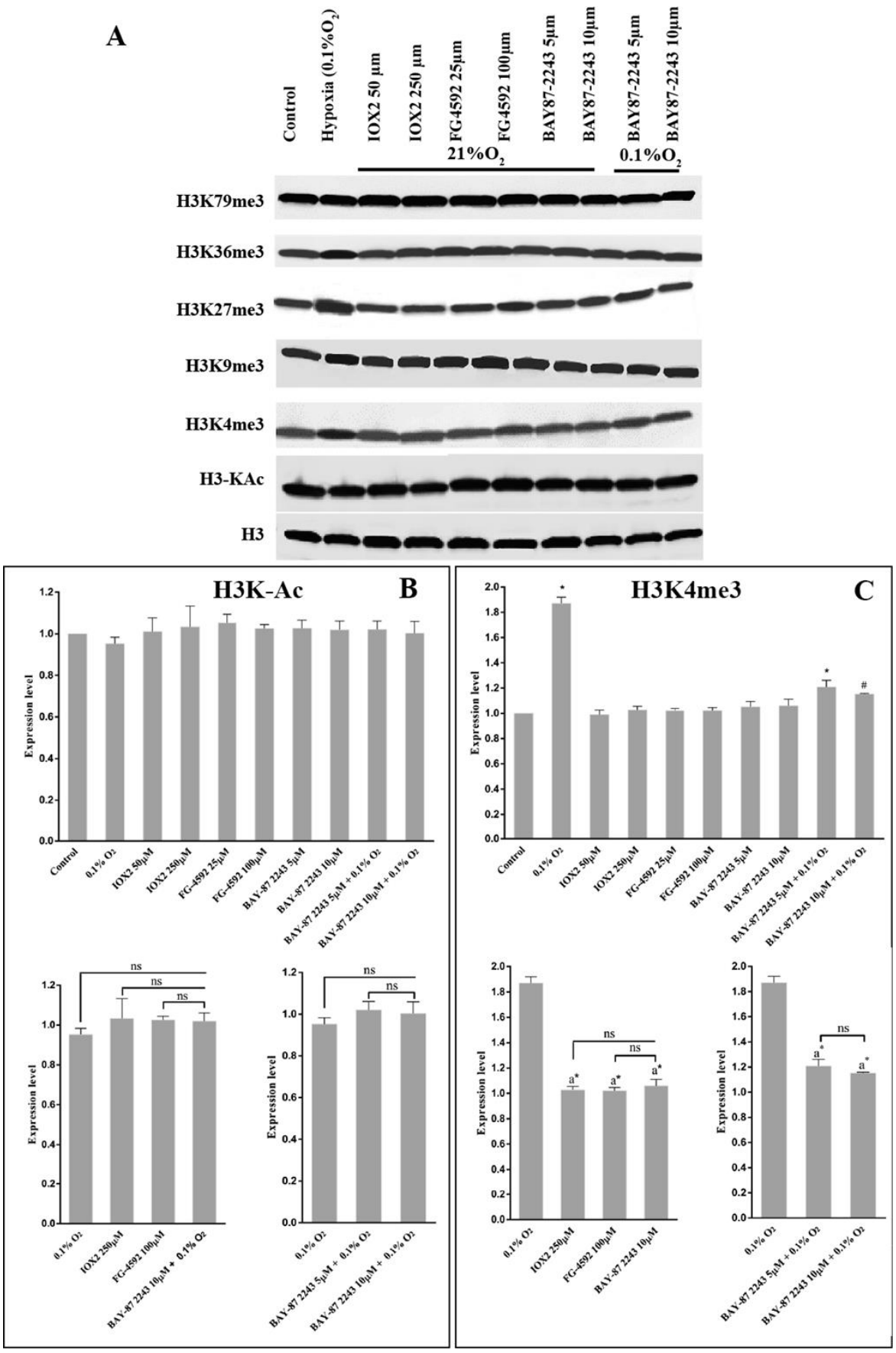
A
Control
Hypoxia (0.1%O2)
IOX2 50 μm
IOX2 250 μm
FG4592 25μm
FG4592 100μm
BAY87-2243 5μm
BAY87-2243 10μm
BAY87-2243 5μm
BAY87-2243 10μm
21%O2
0.1%O2
H3K79me3
H3K36me3
H3K27me3
H3K9me3
H3K4me3
H3-KAc
H3
H3K-Ac
B
H3K4me3
C
Expression level
ns
a*
*
#

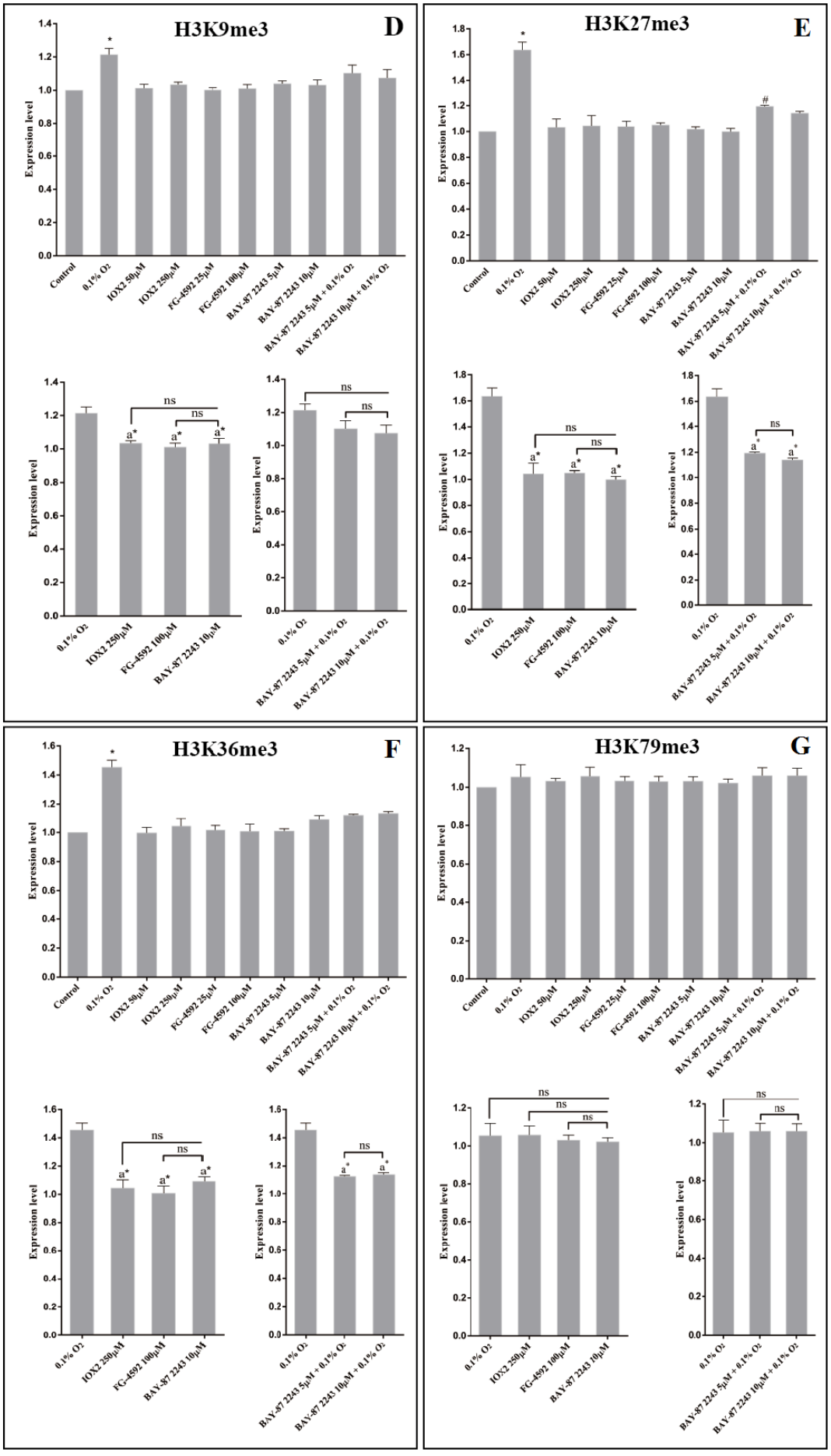
H3K9me3
D
H3K27me3
E
H3K36me3
F
H3K79me3
G
Expression level
Control
0.1% O2
IOX2 50μM
IOX2 250μM
FG-4592 25μM
FG-4592 100μM
BAY-87 2243 5μM
BAY-87 2243 10μM
BAY-87 2243 5μM + 0.1% O2
BAY-87 2243 10μM + 0.1% O2
ns
a*
#

Figure 4.26 Western blot analysis of histone marks in HEK293T cells treated with of HIF hydroxylases inhibitors or HIF down-regulating compound for 24 hours. (A) The levels of H3K-Ac, H3K4me3, H3K9me3, H3K27me3, H3K36me3 and H3K79 me3 were assessed. Anti-H3 antibody was used as a loading control. Representative western blot images are shown. Blot quantitation and statistical analysis for H3K-Ac (B) and H3K4me3 (C), H3K9me3 (D), H3K27me3 (E), H3K36me3 (F) and H3K79me3 (G). Data are presented as the protein detection levels, normalised to the corresponding control group (21% O_2). # and * denote significant difference with $p<0.05$ and $p<0.01$, respectively from the corresponding control group. **a**$^{\#}$ and **a*** indicate $p<0.05$ and $p<0.01$, respectively from the group treated with 0.1 % O_2. Results were obtained from 3 independent experiments.

4.6.5 Discussion

IOX2 is reported as a selective small molecule inhibitor of PHD2 with an IC_{50} of 22 nM.[290] Its effect on JmjC KDM inhibition is much weaker with IC_{50} values of more than 100 μM for KDM3A, KDM4E, KDM5C and KDM6B, and an IC_{50} of 52 μM for KDM2A being reported.[290] The intact mass profiles of H3 for HEK293T cells treated with IOX2 indicated relatively subtle changes of PTMs, compared to that for untreated cells (Figure 4.22). In contrast, DMOG causes significant global PTM changes on intact H3 (Figure 4.14). These results support the proposal that IOX2 has minimal inhibition of the JmjC KDMs, whilst DMOG causes extensive inhibition of the JmjC KDMs.[105] The immunoblotting studies show no obvious changes of trimethylated H3K4, H3K9, H3K27, H3K36 and H3K79 in cells treated with 250 μM IOX2 (Figure 4.26), supporting IOX2 as a highly selective inhibitor of the HIF prolyl hydroxylases. Similar results were obtained with FG-4592 (Figure 4.26).

The inhibitors of HIF prolyl hydroxylases induce the accumulation of HIF-α protein and thereby mimic hypoxia-driven gene expression.[295] Some of JmjC KDMs, such as KDM3A and KDM4B, are also transcriptional targets of HIF and their expression can be promoted by HIF associated transcription.[261,262] HIF-1α is proposed to be more responsible for hypoxia-inducible histone KDMs than HIF-2*α*.[296] The expression of the specific JmjC KDMs may have change the global levels of their corresponding histone

marks. However, the change of global PTMs was not observed in HEK293T cells treated with FG-4592, consistent with the proposal, that it is a selective PHD inhibitor.[292]

BAY 87-2243 has been shown to inhibit mitochondrial complex I activity and then decrease mitochondrial oxygen consumption.[294] This effect may have impacts on cells suffering from hypoxia and the oxygen may be redistributed in the cell. Interestingly, the results of intact H3 mass profiles and immunoblotting suggests BAY 87-2243 can potentially reverse, or at least partially offset, the effects of limiting oxygen on histone marks. These results indirectly support inhibition of mitochondrial complex by BAY 87-2243, in a manner that may release oxygen for use by 2OG/Fe(II)-dependent oxygenases, including the PHDs.

4.7 Testing the effects of new enzyme inhibitors on histone PTMs

The optimised LC-MS-based method was also applied to investigate the effects of two new enzyme inhibitors on intact histone profiles. DSH122[f] is a bromodomain inhibitor, specific for BRD4. CCT1[g] is a KDM4 inhibitor.[297,298] The mass profiles of the intact histone H3.1 imply little change with the bromodomain inhibitor, but a shift to a higher mass with the KDM inhibitor, consistent with increased methylation (Figure 4.27), in support of its recently reported profile as inhibiting multiple 2OG oxygenases in cells.[298]

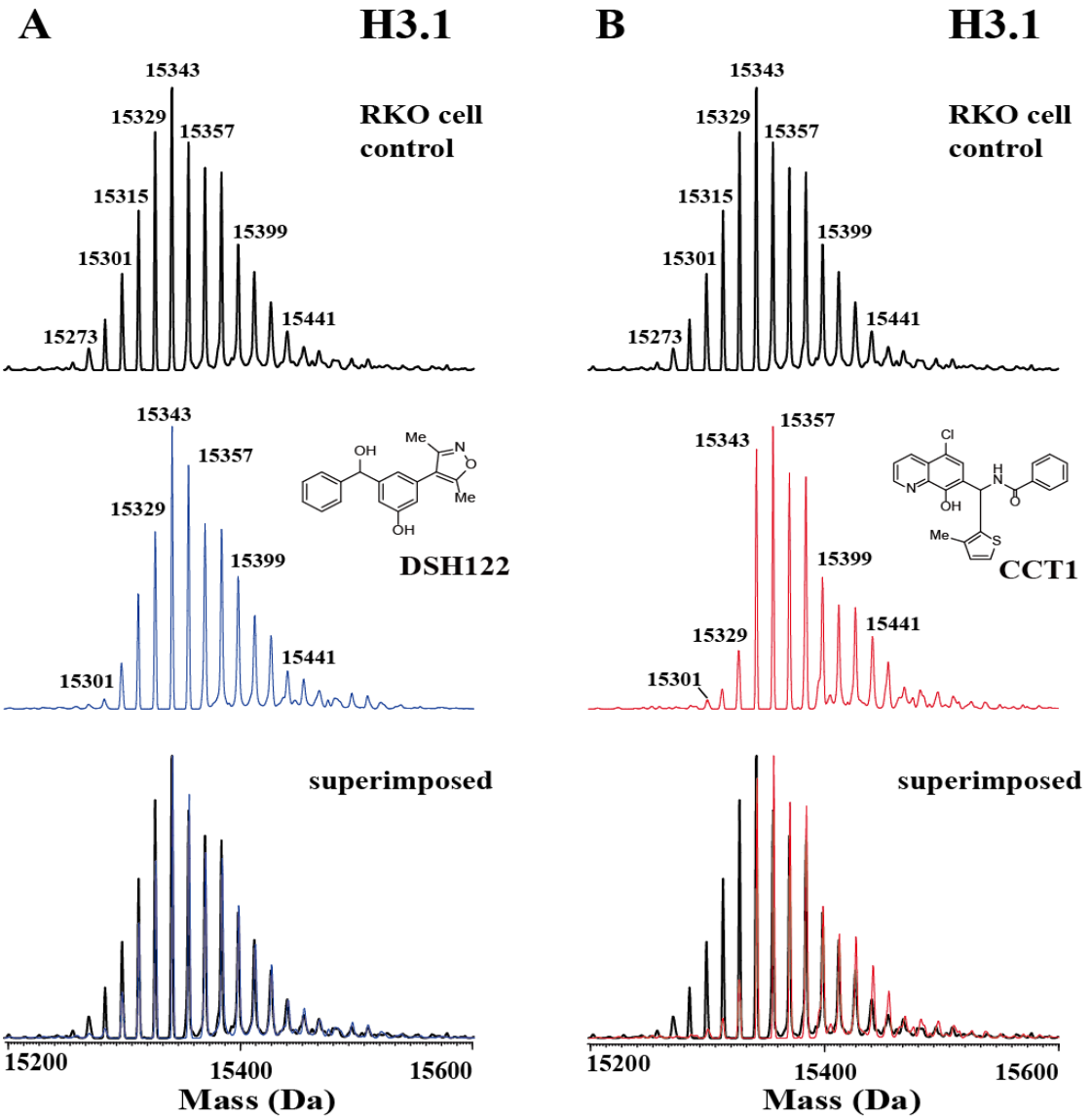

Figure 4.27 LC-MS analysis of intact H3.1 from RKO cells treated with compound treatment. (A) RKO cells treated with BRD4 inhibitor, DSH122 (1 μM) for 24 hours. (B) RKO cells treated with KDM4 inhibitor, CCT1 (30 μM) for 24 hours. Coloured traces indicate the sample from control cells (black) or cells treated with DSH122 (blue); CCT1(red).

[f] DSH122 was synthesised by David Hewings from the Conway group.
[g] CCT1 was synthesised by Cyrille Thinnes from the Schofield group.

4.8 Summary

Following the developed LC-MS-based method for profiling histone, this approach was successfully used to detect global PTMs change on intact histone under hypoxia and drug treatment. This was further applied to analyse PTMs in response to hypoxia and hypoxia-mimetics. The intact mass profiles provide an overview of histone PTMs. Immunoblotting for specific sites of histone PTMs complements the intact mass profiles providing information on site specific PTMs.

The impacts of HIF prolyl hydroxylase inhibitors and HIF down regulator on histone PTMs were analysed by the LC-MS method and immunoblotting methods. The effects of IOX2 and FG-4592 on histone PTMs were far less than the effects observed under hypoxia, consistent with them inhibiting the HIF prolyl hydroxylase, but not (or to a much lesser extent) the JmjC KDMs. Interestingly, BAY 87-2243, inhibiting the mitochondrial complex I[293], appears to compensate for the effect of limiting oxygen and reverse partially the global PTMs detected on intact mass profiles.

The effects of a KDM4 inhibitor and a bromodomain inhibitor on histone PTMs were examined; PTM changes were detected on the intact H3 mass profile for the KDM inhibitor. In conclusion, application of the LC-MS method coupled with immunoblotting for analysis of histone PTMs is helpful in understanding the effects of hypoxia and different compounds-induced hypoxia-mimetics on epigenetic marks.

The method maybe useful in selectivity studies on oxygenase and other enzyme inhibitors, in which histone modification are undesirable, i.e. one would look for compounds do not cause changes in histone profiles. It is important to note that if the goal is only to analyse histone profile, assigning the changes in PTMs that give rise to the changes, may be desirable, but is not necessary if the aim is to screen for compounds that do not cause changes in histone PTMs.

Chapter 5
Summary

Epigenetic mechanisms have an important impact on many biological and pathological processes, in the latter case including many developmental defects and cancer. The mechanisms of epigenetic regulation are sophisticated and complex. In particular, histone proteins and their modifications play critical roles in transcriptional regulation. A comprehensive undestanding of histone post-translational modifications (PTMs), as well as the enzymes that catalyse their additional/removal from histone tails, is central to a molecular understanding epigenetic regulation in animals. The work described in this thesis focused on three fields relating to epigenetic regulation (i) the impact of human JmjC histone demethylases in fission yeast, (ii) the development of a method for detection of global PTMs on intact histones, and (iii) the analysis of alterations to histone PTMs in response to different stresses, relating to hypoxia response.

Fission yeast was used as a model to investigate the roles of JmjC-demethylases. The results show that JMJD2A can catalyse demethylation of yeast H3K36me3/me2 and that the core JmjC domain is needed for enzymatic activity. Mutation of one of the key iron-binding residues in JMJD2A (H188A) leads to loss of demethylase function. The decreased levels of H3K36me3 mediated by overexpression of JMJD2A, combined with a temperature-sensitive mutation in *wee1 (wee1-50),* causes synthetic lethality in fission yeast. Similar effects were observed with overexpression of FBXL11, but to a lesser extent compared to the results for JMJD2A. The mechanism behind the observed synthetic lethality was investigated using *spd1*Δ*wee1-50 S. pombe* overexpressing hsJMJD2A or hsFBXL11, and a model for synthetic lethality between H3K36 and *wee1-50* mutant was established. Together, the work presented in Chapter 2 provides a

potential yeast model for investigation of human JmjC demethylases and an *in vivo* system to screen for potential inhibitors of human KDMs

Mass spectrometry is emerging as a powerful tool to study histone PTMs. The experiments detailed in Chapter 3 describe the development of a rapid, practical method for profiling global histone PTM patterns on intact proteins. Hyphenated MS techniques enable extensive analysis of histones and an optimised LC-MS-based method was developed in this work. Trifluroacetic acid (TFA) is widely used in reversed phase LC because it aids in separation. However, the presence of TFA adducts in mass spectra make accurate analysis of histones more complicated. Therefore, a TFA-free LC-MS method was developed and the LC conditions were optimised for use with a micro-scale column. Coupled with advancements in LC and MS resolution, the optimised LC-MS method is a powerful tool for monitoring histones and analysing their global PTM states. This robustness of the method was validated by independent sample preparations, variations in culture conditions and the use of different human cell lines. The optimised LC-MS method was also applied to the study of clinical samples from patients with glioma. Using the method, high quality LC-MS profiles of all core histones can be attained in a single run of the optimised LC-MS-based method wthin 15 minutes.

Following the optimization of the LC-MS method, subsequent work, as described in Chapter 4, focused on changes in the global pattern of PTMs on intact histones responding to various conditions. Hypoxia and hypoxia-mimetics were of particular interest given that oxygen is a co-substrate for JmjC oxygenase-catalysed histone demethylation. Three clinically used iron-chelators (deferoxamine, deferiprone and deferasirox), cobalt chloride and dimethyloxalglycine (a 2OG analogue) along with several different concentrations of oxygen were found to cause different alterations of PTMs on intact histones. The dose- and time-dependencies of these effects were

investigated to gain further insights into the effects of hypoxic/hypoxia-mimetic stresses. The results reveal important differences in the cellular effects of 'true' hypoxia and hypoxia-mimetics, and will help understanding the different impacts of oxygen and ferrous iron (two important cofactors for the 2OG/Fe(II)-dependent oxygenase family) in cells.

Related compounds targeting the HIF transcription factor hydroxylases were also of interest. Recently, 'selective' inhibitors for specific 2-oxoglutarate-dependent oxygenases have been developed, in particular, for the prolyl hydroxylases invloved in regulating the hypoxia inducible factor (HIF) pathway.[290] Considering that HIF mediates the upregulation of genes encoding several JmjC histone demethylases, these compounds may also have effects on histone PTMs, especially methylation.[112] The results presented in Chapter 4 reveal different PTM patterns are manifested on intact histones from cells treated with HIF hydroxylase inhibitors (IOX2 and FG-4592) compare to hypoxia or the non-selective 2OG oxygenase inhibitor DMOG. The differences may be due to HIF regulated expression of JmjC demethylases, or the possibility of 'off-target' effects due to similarities in enzyme structures or substrates. Notably, a HIF down-regulating compound (BAY-87 2243) was found to counteract some of the effects of hypoxia.

The optimised LC-MS method for profiling intact histones can be considered as a screening tool to determine whether a compound of interest has downstream or 'off-target' effects on histone PTMs. Currently, due to limitations in sensitivity and the complexity of histone PTM patterns, top-down mass spectrometry is not yet of practical use for the sequecing and quantification of histone PTMs.[46] Combining different approaches is a feasible way to gain a comprehensive picture of histone modification states. The rapid, efficient LC-MS method developed and applied in this thesis will

complement other biological techniques (e.g. immunoblotting) to provide an overview of alterations in histone PTMs relating to external stimuli.

Chapter 6
Materials and methods

6.1 General experimental procedures and reagents

pH measurement

pH measurements were determined using a Hanna Instruments HI 9321 microprocessor pH meter fitted with a 5 mm diameter pH electrode. Calibration was carried out by putting the probe in either the range pH 4.0-7.0 or pH 7.0-10.0 standard calibration solutions (Fisher Scientific) before use. The pH electrode was stored in 4 M KCl solution between uses. The pH of solutions was adjusted with stock solutions of HCl or NaOH as appropriate.

Water bath

A Grant Y14 waterbath was used for incubation at 37 ^{o}C, and a Grant W14 waterbath was used for bacterial transformation at 42 ^{o}C.

Centrifuge

During the course of this work the following centrifuges were used: Fisher AccuSpin microcentrifuge, Beckman Coulter microfuge 22R, Beckman Coulter Allergra X-30R or Beckman Coulter Avanti J-26 XP machines. The practices were carried out following the standard instrument guidelines and experimental procedures.

Reagents

All general chemicals were of analytic grade obtained from Sigma-Aldrich, Fisher Scientific and Invitrogen and Roche unless otherwise stated. Bacto-agar, Bacto-Tryptone and yeast extract for use in culture media were purchased from Oxoid. DNA ladders, restriction endonucleases, ligases and DNA polymerase were obtained from

Invitrogen and New England Biolabs. Purified water for experiments was obtained from a Millipore Elix® Reverse Osmosis system and then passed through a 0.22 μm membrane filter by a Millipore Milli-Q® Synthesis system

Throughout, all standard sterile practices were followed. Media and equipment were autoclaved for suggested time at 121 ºC as sterilisation. Heat-sensitive solutions were sterilised using 0.22 μm membrane filter.

6.2 Mammalian cell culture

General

All mammalian cell culture procedures were carried out in a Class II Biological Safety Cabiner (Nuaire Nu 437-400E). Human Embryonic Kidney 293T (HEK293T), HeLa, MCF-7 and RKO cells were cultivated in Dulbecco's modified Eagle's medium (DMEM, Lonza) supplemented with 10% fetal bovine serum (FBS, Invitrogen) and L-glutamine (Invitrogen) with/without penicillin and streptomycin. Cells were maintained in a Binder BD 53 incubator with a 95% air and 5% CO_2 incubator at 37 ºC unless otherwise described. Cells were normally kept between 15% and 90% confluence.

Cell passaging

All needed reagents were pre-warmed to 37 °C in water bath. After reagents are warmed, the hood was prepared using ethanol for sterilisation. Spent culture media was aspirated from the cell culture vessels.

Strongly adherent HeLa cells and MCF-7 cells were washed with PBS, and then trypsinised from the plate using 0.2 mg/mL trypsin (Lonza) 1-2 mL per 25 cm^2 of cell vessel surface at 37 ºC for 5 minutes or until cells were released from the surface of the vessel. The trypsin reaction was quenched by addition of fresh serum-containing media 2-3 times amount of trypsin solution. Cells were fully resuspended by pipetting and

collected into an appropriate tube. Cells were centrifuged at 200 g for 5 minutes. The media above the cell pellet was aspirated and the cells were resuspended in a logical volume (5-10 mL). An appropriate volume was added to new culture vessels containing pre-warmed media.

Semi-adherent HEK293T were washed with PBS and then removed from the plate surface by pipetting in PBS to form a suspension. Cells were collected and centrifuged. Fresh media was added to resuspend cells. An appropriate volume of cells was added to new cell vessels containing pre-warmed media.

Hypoxia and hypoxia-mimetics experiments

Cells were incubated in optimal condition (95% air and 5% CO_2 incubator at 37^0C) and grown to approximate 80% confluence. Then cells were treated with different conditions described as below.

Hypoxia:

Oxygen concentration experiments: cells were exposed to different oxygen concentration (21%, 5%, 1% and 0.1% O_2) at 37^0C (Ruskinn Invivo2 400 hypoxic chamber) for 24 hours.

Time-dependent experiment: 0.1% O_2 was selected to treat cell for 1 to 24 hours. The cells were harvested at 2, 6, 12, and 24-hour severe hypoxia exposure.

Hypoxia-mimetics (compounds)

Dose-effect experiments: The varying concentration of DFO (25-150 μM), CP20 (25-125μM), Exjade (25-125 μM), DMOG (250-1250 μM) and CoCl2 (50-200 μM) for 24 hours were used in the dose-effect experiments.

Time-dependent experiments: DFO (25-150 μM), DMOG (250-1250 μM) and CoCl2 (50-200 μM) were used to treat cells for 1-24 hours. The cells were harvested at 2, 6,

12, and 24-hour compound treatments.

Treatments of HIF prolyl-hydroxylase inhibitors

IOX2 (50 and 250 μM) and FG-4592 (25-100 μM) were used to treat HEK293T cells for 24 hours.

Treatment of HIF down regulator

BAY 87-2243 (5 and 10 μM) were used to treat HEK293T cells under normoxia or severe hypoxia (0.1% O_2) for 24 hours.

Treatment of other compounds

SAHA (1 μM), DSH122 (1μM) and CCT1 (30 μM) were used to treat RKO cells for 24 hours.

Trypan blue assay of cell via**bility**

The proper aliquot of cells (e.g., $5x10^5$ cells/mL) were prepared in PBS for viability test. The same volume (10-20μL) of the cell suspension and 0.4% trypan blue was mixed and incubated 3 minutes at room temperature. A drop of the mixture of cells and trypan blue was placed onto a hemocytometer and then put on the stage of the binocular microscope. The stained (dead cells) and unstained (viable cells) were counted separately. The cells over the four corner squares were calculated and the number were averaged. Each square of hemocytometer, with cover glass in place, has a total volume of 0.1 mm^3(10^{-4} cm^3) which was equivalent to nearly 1 mL. The total number of cells per mL was calculated as: average cell count per square x 2 (dilution factor for trypan blue) x 10^4. The percentage of viable cells was calculated as follow: viable cells (%) = total number of viable cells (unstained cells) / total number of cells (unstained + stained cells) x 100.[274]

Cell Storage

Cells were frozen in DMEM containing 20% FBS and 10% DMSO and stored in a -80 ºC freezer for short-term storage (less than 1 year). Cells were stored in a liquid nitrogen Dewar for longer-term storage.

Transfection

Cells were transiently transfected with plasmid DNA using linear polyethylenimine (PEI) (1 mg/mL, pH 7.2). Transfection was carried out with cells at approximately 50% confluency as determined using a Motic AE20 (Ted Pella) microscope.

Media was exchanged for fresh media 2 hours before transfection. For each 10 cm dish, 7-8 μg plasmid DNA and 20ul PEI diluted in OptiMEM® (Invitrogen) were incubated for 5 minute at room temperature. PEI was added to the diluted DNA and then mixed immediately by pipetting or vortexing. The mixture was incubated for 20 min at room temperature before adding to the cells. The cells were harvested at 24- hour post-transfection.

6.3 Mammalian histones extraction

Acid extraction method

Prepared cell (HEK293T, HeLa, MCF-7, or RKO cells) pellets were resuspended in iced hypotonic lysis buffer (10mM Tris-Cl pH8.0, 1mM KCl, 1.5 mM $MgCl_2$, 1mM Dithiothreitol (DDT) and 1mM phenylmethanesulfonylfluoride (PMSF), supplemented with 1x protease and phosphatase inhibitor (Thermo Fisher Scientific) and then incubated on rotator at 4 ºC for 30 minutes. The nuclei were pelleted by centrifugation at 10,000 g for 10 min at 4 ºC, and then the supernatant was removed. Pellets were resuspended in 400 μL 0.4N ice-cold HCl. The sample was then centrifuged at 16,000 g for 10 min and at 4 ºC and the supernatant containing histones was transferred into a

fresh tube. Subsequently, three different methods were used to purify the histones as below.

Method 1 - Acetone precipitation: Following application of the above described acid extraction method, approximately 400 µL supernatant was added to the 15mL falcon tube with 4mL acetone and then was placed at -20 ºC overnight for precipitation. The sample was centrifuged at 2,500 g for 10 min at 4 ºC. The supernatant was carefully discarded and the pellet was transferred into the fresh 1.5 mL Eppendorf tube. Three washes with ice-cold acetone were carried out by centrifugation at 16,000 g for 5 min and at 4 ºC. The pellet was then dried at room temperature. The appropriate volume of 0.1% (v/v) formic acid or Milli-Q water (typically 100µL) was add to dissolve the final pellet and the solution was stored at -20 ºC.

Method 2 - Trichloroacetic acid (TCA) precipitation: Following application of the above described acid extraction method, 132µL TCA was added dropwise to the supernatant containing histones and mixed well. The sample was then incubated on ice for 30 min. Following three washes with ice-cold acetone, the pellet was dried at room temperature. The appropriate volume of 0.1% (v/v) formic acid or Milli-Q water (typically 100µL) was add to dissolve the final pellet and the solution was stored at -20 ºC.

Method 3 - Dialysis and lyophilization: Following application of the above described acid extraction method, the supernatant containing histones was put in the dialysis tubing with approximately 3,000 molecular weight cut-off membrane and dialysed against 2.5% acetic acid for 2 hours. The dialyzed solution was transferred to 1.5 mL Eppendorf tube and frozen at -80 ºC. The frozen histone solution was loaded into a SpeedVac with a vacuum until complete solvent removal. The approximate volume of

0.1% (v/v) formic acid or Milli-Q water (approximately 100μL) was add to dissolve the final pellet and the solution was stored at -20 ^{o}C.

Determination of histone proteins concentration- Bradford method

A series of bovine serum albumin (BSA) concentration of 0, 0.2, 0.4, 0.6, 0.8, 1.0 mg/mL were prepared and mixed with Bradford reagent in a spectrophotometer cuvette according the manufacturer's instruction (Bio-Rad). The standard curve was generated by measuring the absorbance of BSA at the wavelength 595 nm. A 20 μL histone sample (10 times dilution) was prepared and then mixed with 980μL Bradford reagent. The absorbance of the sample was measured at the wavelength 595 nm. The concentration of the histone sample was calculated according to the standard curve.

6.4 SDS-PAGE gel electrophoresis

SDS-PAGE was used as the initial method for analysing the interest proteins. The sample was mixed with an equal amount of 2X SDS-PAGE loading buffer and then boiled for 5 minutes at 100 ^{o}C in a hot block for denaturing the proteins. The sample was centrifuged shortly and loaded appropriate amount into the well of the gel. The gel was run at 200 volts in 1x running buffer (25 mM Tris pH 8.3, 192 mM glycine, 0.1% SDS) using Bio-Rad Mini-PROTEAN II system until the smallest molecular weight band of the ladder was visibly approaching the bottom. The gel was washed with water and then stained in stain buffer (0.25% w/v Coomasssie Brillant Blue R, 10% acetic acid, 40% methanol in Milli-Q water) for 10 min with mild shaking. The gel was destained by 10% acetic acid, 40% methanol in Milli-Q water overnight.

SDS-PAGE recipe (2 gels)

Reagent	Resolving gel (10% / 12.5% / 15%)	Stack gel
Milli-Q water	4mL/ 3.14mL/ 2.3mL	3.14mL
30% (w/v) Acrylamide mix	3.32mL/ 4.1mL/ 5mL	0.5mL
1M Tris-HCl (pH 7.5)	2.5mL/ 2.5mL/ 2.5mL	-
0.5 M Tris-HCl (pH 6.8)	-	1.26mL
10% (w/v) SDS	100µL	50µL
10% (w/v) APS	100µL	50µL
TEMED	8µL	5µL

TEMED and APS were added just prior to gel casting. Resolving gel % was determined based on the size of interest proteins to be separated.

10X SDS-PAGE running buffer (1L)

Reagent	Amount (g)
Tris-Base	30
Glycine	144
SDS	10

2X SDS-PAGE sample loading buffer (10 mL)

Reagent	Amount
1M Tris-HCl (pH 6.8)	1.08mL
10% (w/v) SDS	3.6mL
Glycerol	1.8mL
Bromophenol Blue	0.02g
β-mercaptoethanol	1mL
Milli-Q water	2.52mL

6.5 Microbiologic procedures

6.5.1 General methods and reagents

Optical density measurements

For OD measurement, a wavelength of 600 nm was used (OD_{600}) is for estimating the concentrations of bacterial and other cells. OD_{600} values were measured in a 1.6 mL cuvette, against a reference sample of initial growth media in a Novaspec® III spectrophotometer (**Amersham** Biosciences).

Glycerol stocks

Samples of bacterial cells were preserved by gently mixing 250 µL sterile glycerol and 750 µL cell culture and were stored at -80 ºC.

Starter cultures

100 mL 2TY media containing the appropriate antibiotic or no antibiotic was inoculated with a single colony from an LB-agar plate or a scraping from a glycerol stock and then incubated overnight in a New Brunswick Scientific G25 environmental shaker at 220 rpm shaking and 37 ºC.

Bacterial cultures

Petri dishes with LB media containing 2% (w/v) agar and the appropriate antibiotic were used for bacterial plate cultures. Standard procedure included incubation of plate overnight in 37 ºC and plates were stored at 4 ºC if desired. 100 mL 2TY medium in each 500 mL conical flask or 10 mL 2TY medium in each 50 Ml Falcon tube was prepared for liquid culture. A single colony was picked up from LB-agar plate or cells from glycerol stocks to inoculate prepared liquid media. Liquid culture was incubated overnight at 37 ºC with shaking at 220 rpm. Large scale growths were performed in 2 L conical flasks containing 600 mL 2TY media containing appropriate antibiotic, with shaking at 180 rpm. Growth was initiated by addition of 6 mL of starter culture prepared night before. The observation of growth was determined by optical density readings at 600 nm referenced to the fresh growth media.

Reagents

All culture media were autoclaved at 121 ºC for 20 minutes before use.

Lysogeny broth (LB) media (1L)

Reagent	Amount (g)
Bacto-tryptone	10
Yeast extract	5
NaCl	10

2X Tryptone-Yeast (2TY) media (1L)

Reagent	Amount (g)
Bacto-tryptone	16
Yeast extract	10
NaCl	5

Super optimal broth with catabolite repression (SOC) media (1L)

Reagent	Amount
Bacto-tryptone	20g
Yeast extract	5g
1M NaCl	10mL
1M KCl	2.5mL
1M $MgCl_2$	10mL
1M $MgSO_4$	10mL
1M glucose	20mL

Antibiotics: Final working concentrations of antibiotics for experiments were as follows unless indicated otherwise.

Antibiotics	Working concentration
Ampicillin	100 μg/mL
Chloramphenicol	33 μg/mL
Kanamycin	30 μg/mL
Tetracycline	15 μg/mL

6.5.2 Preparation of competent cells

Competent cells were either purchased from Stratagene or prepared in the laboratory. The following protocol was used for preparation of chemically competent cells:

Selected *E. coli* cells were streaked onto an LB-agar plate without any antibiotics and incubated at 37 ºC overnight. One colony was picked from the cultured plate to inoculate in 100mL antibiotic-free 2TY growth media and was grown with shaking in the incubator (220 rpm, 37 ºC) overnight. 0.2 mL of overnight starter culture was added

into 100 mL of 2TY growth media and grown with shaking (220 rpm, 37 ºC) to OD600 0.6-0.8. Cells were centrifuged at 750 g, 4 ºC for 5 minutes using pre-chilled sterile 50 mL Falcon tubes, gently resuspended in 25 mL sterile 100 mM $CaCl_2$, 20% (v/v) glycerol solution for each Falcon tube and incubated on ice for 20 minutes prior to another centrifugation at 750 g, 4 ºC for 5 minutes. Cell pellets were resuspended in 1 mL of 100 mM CaCl2, 20% (v/v) glycerol solution and then were aliquoted into sterile Eppendorf tubes and stored immediately at -80 ºC.

E. coli strains used were:

BL21(DE3)*: E. coli B F- dcm ompT hsdS (r_B^- m_B^-) gal λ(DE3)*

BL21(DE3) pLysS*: E. coli B F- dcm ompT hsdS (r_B^- m_B^-) gal λ(DE3)[pLysS Cam^r]*

Rosetta(DE3)*: F- ompT hsdS$_B$(r_B^- m_B^-) gal dcm (DE3) pRARE (Cam^r)*

ArcticExpress (DE3)*: E. coli B F– ompT hsdS(r_B^- m_B^-) dcm+ Tet^r gal λ(DE3) endA Hte [cpn10 cpn60 Gent^r]*

XL1-Blue*: recA1 endA1 gyrA96 thi-1 hsdR17 supE44 relA1 lac [F'proAB lacI^q ZΔM15 Tn10(Tet^r)]*

XL10-Gold*: Tet^r Δ(mcrA)183 Δ(mcrCB-hsdSMR-mrr)173 endA1 supE44 thi-1 recA1 gyrA96 relA1 lac Hte [F' proAB lacI^{q}ZΔM15 Tn10 (Tet^r) Amy Cam^r].*

6.5.3 Bacterial transformation

Heat shock method

Chemical competent cells (30µL) were thawed on ice for 5-10 minutes and then transferred to a pre-chilled 15 mL Falcon tube. 1-2 µL of a solution of plasmid DNA (100 ng/µL) was added to the competent cells. The mixture was then incubated on ice for 30 minutes and was heat shocked in the 42 ºC water bath for 30 sec or 45 sec. Cells were incubated on ice for further 2 min and then pre-warmed to 37 ºC SOC medium (0.4 mL) was added. The mixture was incubated in 37 ºC with shaking at 220 rpm. 200µL of the mixture was taken out and spread onto LB-agar plates containing appropriate antibiotic. For LIC cloning, plates also contained 5 % sucrose. The plates were incubated upside down at 37 ºC overnight (<24 hours).

Electroporation method

Electrocompetent cells (40μL) were thawed on ice for 5-10 minutes and then transferred to a pre-chilled electroporation cuvette (2 mm gap). 1-4 μL of plasmid DNA (10 pg/μL) was added into competent cells and the cuvette was tapped until the cell-DNA mixture settles evenly to the bottom. The cuvette was slid into the electroporation chamber where electroporation was carried out once using Electroporator 2510 (Eppendorf) at a voltage of 1700 V (17 kV/cm field strength), a resistance of 200 Ω and a capacitance of 25 μF until the cuvette sits flush against the electrical contacts. After that, 400 μL of prewarmed 37 ºC SOC medium was immediately added to resuspend the cells. The cells were transferred to a sterile 14-mL BD Falcon and incubated at 37 ºC for 1 hour with shaking at 220 rpm.200 μL of the transformation mixture was spread on LB agar plates containing the appropriate antibiotic (and containing IPTG and X-gal if colour screening is desired). The plates were incubated upside down at 37 ºC overnight (<24 hours). For blue-white colour screening, incubation at 37 ºC was for at least 17 hours to allow colour development

6.6 Cloning

6.6.1 DNA purification and concentration determination

DNA purification for PCR products was performed using an appropriate DNA purification kit (Thermo Scientific Genomic) following the manufacturer's instructions. Plasmid DNA was purified from an adequate amount of cell culture using a GeneJET Plasmid Miniprep/Midiprep Kit (Thermo Scientific) following the manufacturer's protocol. DNA was eluted with an appropriate amount of sterile Milli-Q water.

DNA concentration analyses were carried out using a NanoDrop ND-1000 UV/Vis spectrophotometer to measure the absorbance at 260 nm (A_{260}) against the reference of

Milli-Q water. The purity of the DNA was assessed by the A_{260}/A_{280} ratio.

6.6.2 Agarose gel electrophoresis

DNA samples were analysed using horizontal agarose gel electrophoresis. Gels were prepared by boiling 1% (w/v) agarose in 50 mL TAE buffer (40 mM Tris-HCl, 20 mM acetic acid and 1 mM EDTA, pH adjusted to 8.3). The agarose gel solution was allowed to cool to around 60 ^{o}C. 5μL SYBR® Safe DNA gel stain (Invitrogen) was added prior to gel casting (1/10000 v/v) into gel tray to a depth of 0.7 cm. The comb was inserted at one end of the gel and the gel was allowed to solidify at room temperature. Samples were mixed with loading buffer (6X, New England Biolabs), loaded on gel and run in TAE buffer on a Bio-Rad microprocessor (Model 1000/500 or Model 200/2.0) system at 100 V for 35-50 minutes. 1 kb DNA ladder (Thermo Scientific GeneRuler) was used as a reference marker to allow molecular weight determination. The gel was visualized by UV irradiation in a Gel Logic 200 imaging system (Kodak) and a 535 nm emission filter. For purification of DNA from an agarose gel, bands were cut using sharp blade and purified using Gel extraction kit (GeneJET) following the manufacturer's protocol.

50X TAE (adjusted to pH 8.3)

Reagent	**Amount**
Tris-Base	24.2 g
Glacial acetic acid	5.71 mL
EDTA	1.86 g

6.6.3 Plasmids and DNA sequences

pREP3X, pREP41X and pREP81X plasmids for expression in *S. pombe* were from ATCC®. pGEM-T plasmid was from Promega.

Name	Base plasmid	Yeast/Antibiotic markers	Yeast origin of replication	Promoter	Reference and sources
pREP3X	pUC119	LEU2, AmpR	ars1	strong *nmt1*	Forsburg, ATCC®

pREP41X	pUC119	LEU2, AmpR	ars1	weaker *nmt1*	Forsburg, ATCC®
pREP81X	pUC119	LEU2, AmpR	ars1	much weaker *nmt1*	Forsburg, ATCC®

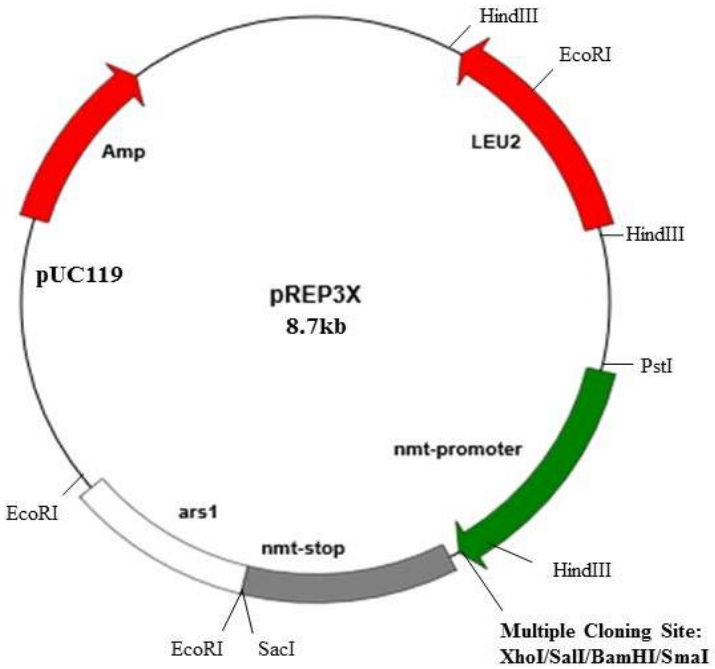

pREP 3X, this *LEU2* multi-copy plasmid contains strong nmt promoter (no message in thiamine), given from the Humphrey laboratory.
MCS sequence: **CTCGAGGTCGAC***TCTAGA***GGATCCCCGGG**
(XhoI/SalI/BamHI/SmaI)

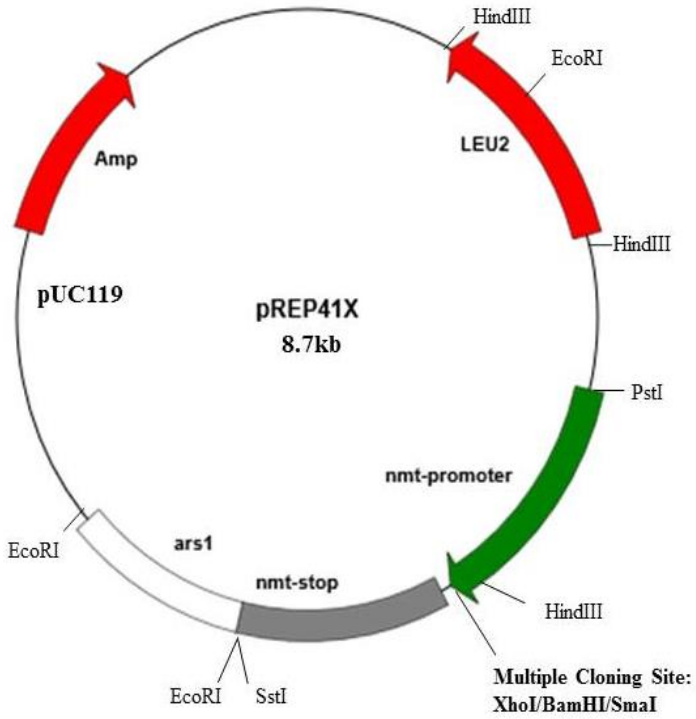

pREP41X, this *LEU2* multi-copy plasmid contains much weaker nmt promoter (no message in thiamine), given from the Humphrey lab (Department of Oncology, University of Oxford).
MCS sequence: **CTCGAGGGATCCCCGGG**
(**XhoI/BamHI/SmaI**)

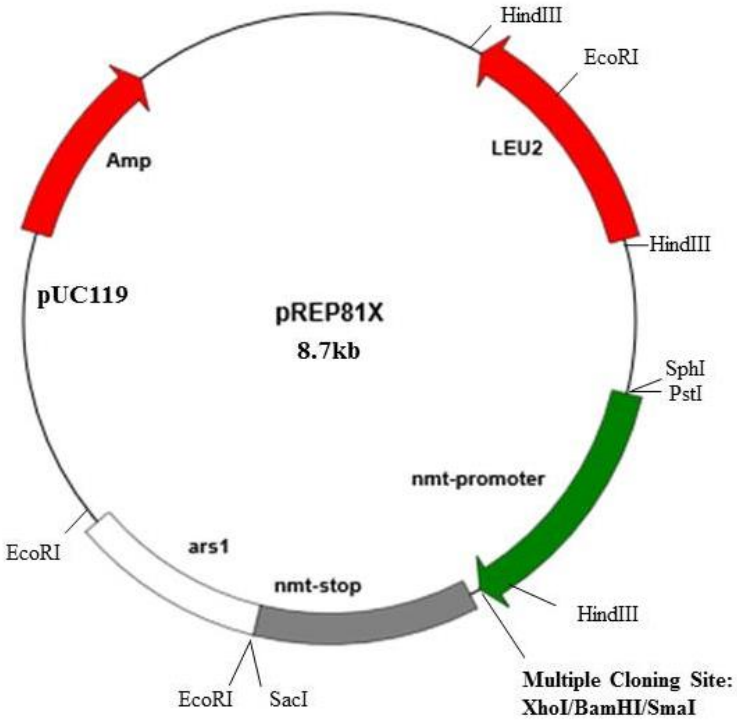

pREP81X, this *LEU2* multi-copy plasmid contains much weaker nmt promoter (no message in thiamine), given from the Humphrey lab (Department of Oncology, University of Oxford).
MCS sequence: **CTCGAGGGATCCCCGGG**
(**XhoI/BamHI/SmaI**)

All oligonucleotide primers were purchased from Sigma Aldrich and resuspended in specific amount of sterile Milli-Q water to achieve a concentration of 100 μM.

Gene	Vector	Direction	Sequences	RS
FLAG-FL JMJD2A	pREP3X pREP41X pREP81X	Fwd	AACTGTCGACATGGACTACAAAGACGATG	SalI
		Rev	ACTTGTCGACCTACTCCATGATGGCC	SalI
FLAG-FL JMJD2A -H188A	pREP3X pREP41X pREP81X	Fwd	GACATCCTTTGCTTGG**GC**CACTGAAGACATGGAC	-
		Rev	GTCCATGTCTTCAGTG**GC**CCAAGCAAAGGATGTC	-
FLAG-FL FBXL11	pREP3X pREP41X pREP81X	Fwd	AACTGTCGACATGGACTACAAAGACGATG	SalI
		Rev	ATATAGATCTTTAGCTGATCTTCTGTATCAG	BglII
FLAG-FL FBXL11 -H212A	pREP3X pREP41X pREP81X	Fwd	GGCTGCTATACTGACTTC**GC**TGTGGACTTTGGTGGTACC	-
		Rev	GGTACCACCAAAGTCCACA**G C**GAAGTCAGTATAGCAGCC	-
truncated JMJD2A wt/ H188A (1-324)	pREP3X pREP41X	Fwd	GGATGTGTTTGTGAGAAAGTTC**T**AGCCAGAAAGGTACAAACTTTG	-
		Rev	CAAAGTTTGTACCTTTCTGGCT**A**GAACTTTCTCACAAACACATCC	-
truncated FBXL11 wt/H212A (1-322)	pREP3X pREP41X	Fwd	GATCGGACACGGGTTCCAAAT**T**AGTTTCGCTATCCATTCTAC	-
		Rev	GTAGAATGGATAGCGAAACT**A**ATTTGGAACCCGTGTCCGATC	-
FL Jmj3	pNIC28-Bsa4 pNH-TrxT pNIC-ZB	Fwd	tacttccaatccatgCAGCAAAATGTTAAAGAGAAAC	-
		Rev	tatccacctttactgTTATTCTAAGGAAGGAAAGAGAG	-
truncated Jmj3 (1-445)	pNIC28-Bsa4 pNH-TrxT pNIC-ZB	Fwd	tacttccaatccatgCAGCAAAATGTTAAAGAGAAAC	-
		Rev	tatccacctttactgTTAAGGAAGCGATCGGTTTTTG	-

All DNA bases were shown in capitals except for LIC overhangs. Alterations from the original DNA bases were shown in bold and underlined. Direction- Fwd: forward, Rev: reverse; RS: restriction enzyme was used for cloning. FL: full length.

DNA sequencing was carried out by Source BioScience Lifesciences. Constructs under the T7 promoter were sequenced using standard T7 primers:
T7 forward: 5'- TAATACGACTCACTATAGGG -3'
T7 reverse: 5'- GCTAGTTATTGCTCAGCGG -3'

6.6.4 DNA amplification

DNA sequences for cloning were amplified by the PCR following the protocol as below:

Reagent	Volume (µL)	Final concentration
5X Q5® reaction buffer	5	1X
dNTP mix (10 mM)	1	400 µM
Forward primer (10 µM)	1.25	0.5 µM
Reverse primer (10 µM)	1.25	0.5 µM
DNA template (50 ng/µL)	1	50 ng
Q5® High Fidelity DNA Polymerase (2 unit/µL)	0.25	0.02 unit/µL
5X Q5® High GC Enhancer (optional)	(5)	1X
Sterile Milli-Q water	to 25	

Step	Cycle	Temperature (ºC)	Time
Initial denature	1	95	30 seconds
Denaturation	25-35	95	10 seconds
Annealing		50-72 (based on lower Tm + 3 ºC)	30 seconds
Extension		72	30 seconds/kb
Final extension	1	72	10 minutes
Hold	1	4	∞

A Techne Genius thermal cycler was used for PCR.

6.6.5 Site-directed mutagenesis

Variants of DNA sequences were generated by site-directed mutagenesis using the QuikChange™ site-directed mutagenesis kit from Stratagene. Primers containing the desired mutation sites were used to amplify the new plasmid including vector and insert sequence.

Reagent	Stock concentration	Volume (µL)
5X Q5® reaction buffer	5X	5
dNTP mix	10 mM	2.5
Forward primer	10 µM	1.25
Reverse primer	10 µM	1.25
DNA template	20 ng/µL	1
Q5® High Fidelity DNA Polymerase	(2 unit/µL)	0.5
5X Q5® High GC Enhancer (optional)	5X	5
Sterile Milli-Q water	-	8.5
Total volume: 25 µL		

PCR protocol for site-directed mutagenesis

Step	Cycle	Temperature (ºC)	Time
Initial denature	1	95	2 minute
Denaturation	18-25	95	45 seconds
Annealing		55	1 minute
Extension		68	1 minute/kb
Final extension	1	68	20 minutes
Hold	1	4	∞

After the PCR procedure was completed, 1 µL DpnI restriction enzyme (10u/µL) was added to the reaction solution. The mixture was incubated at 37 ºC for 3 hours to digest the parental DNA before samples were transformed into competent *E. coli* for growth. Plasmids from cell culture were purified using GeneJET plasmid miniprep kit and then sequenced by Source BioScience for verification.

6.6.6 pGEM-T vector for cloning

pGEM-T vector cloning was used to store the DNA inserts of interest for subsequent cloning. DNA inserts were generated from constructed plasmid using pGEM-T vector using appropriate restriction enzymes and was ligated to the vector of interest to raise the success rate of cloning. A-tailing procedure was carried out for the blunt-end PCR products. DNA of interest was amplified by PCR. PCR fragments were purified using GeneJET PCR Purification kit. 5µL purified DNA of interest was added into the

solution containing 1µL 10X Taq DNA polymerase reaction buffer with $MgCl_2$, 1µL 2mM dATP, 1µL Taq DNA polymerase and 2 µL Milli-Q water. The mixture was incubated at 70 ºC for 30 minutes. 1-2 µL Taq DNA polymerase- treated DNA was used in a ligation reaction and the mixture was incubated at 4 ºC for overnight. The adequate amount of the mixture was transformed into competent *E. coli* and plated onto agar plates containing IPTG, X-Gal and ampicillin to select for clones. White colonies were picked for further DNA sequencing.

Ligation reaction components

Reagent	**Volume (µL)**
2X Rapid ligation buffer	5
pGEM-T vector (50 ng/µL)	1
A-tailing DNA of interest	1-2
T4 DNA Ligase (3 u/µL)	1
Milli-Q water	to 10

6.6.7 Colony PCR

Single colonies on transformation plates from cloning procedure were picked and added to a mixture containing Biomix Red reagent (Bioline) and forward and reverse primers. The PCR cycle used was the same as described for DNA amplification. PCR products were examined directly by agarose gel electrophoresis and colonies shown to contain a correct size of the insert were grown to allow plasmid extraction for DNA sequencing.

Colony PCR components

Reagent	**Concentration**	**Volume (µL)**
BioMix Red	2X	10
Forward primer	10 µM	1
Reverse primer	10 µM	1
Sterile Milli-Q water	-	8

6.7 *S. pombe* experiments

6.7.1 Media

Edinburgh Minimal Medium (EMM): 14.7 mM potassium hydrogen phthalate ($C_8H_5KO_4$), 15.5 mM disodium hydrogen orthophosphate (Na_2HPO_4), 93.5 mM ammonium chloride (NH_4Cl), 2% (w/v) glucose, 1X salt stock,1X vitamin stock, 1X mineral stock. Supplements of adenine (A), L-leucine (L), L- histidine (H), arginine (R) and uracil (U) were added to a final concentration of 150 mg/L. For repressing nmt promoter, thiamine was added to a final concentration of 15 μM (5 μg/mL, from filter sterilized 1000X stock at 5 mg/mL).

EMM Agar: 2% (w/v) Bacto-agar added into EMM solution for solid media.

Salts stock (50X): 260 mM magnesium chloride ($MgCl_2$), 5 mM calcium chloride ($CaCl_2$), 670 mM potassium chloride (KCl), 14.1 mM disodium phosphate (Na_2SO_4).

Vitamin stock (1000X): 4.2 mM pantothenic acid, 81.2 mM nicotinic acid, 55.5 mM inositol, 40.8 μM biotin.

Minerals stock (10000X): 80.9 mM boric acid (H_3BO_3), 23.7 mM manganese sulphate ($MnSO_4$), 13.9 mM zinc sulphate ($ZnSO_4$), 7.4 mM iron(II) chloride ($FeCl_2$), 2.47 mM molybdic acid, 6.02 mM potassium iodide (KI), 1.6 mM copper sulphate ($CuSO_4$), 47.6 mM citric acid.

SPAS mating media: 1% (w/v) glucose, 7.3 mM KH2PO4, 1X vitamins, 45 mg/l for each supplement of adenine, leucine, histidine, arginine and uracil.

SPAS Agar: 2% Bacto-agar added into SPAS solution for solid media.

Yeast Extract + 6 supplements (YE6S): 3% (w/v) glucose, 0.5% (w/v) yeast extract (Sigma), 225 mg/L for each adenine, L-leucine, L-histidine, arginine, uracil, and L-lysine.

YE6S Agar: 2% Bacto-agar added into YE6S solution for solid media.

Yeast freezing mix (YFM): 1:1 mix of YE6S and glycerol.

***S. pombe* strains used in this study**

Strain	Genotype	Source
TH350	*leu1-32 ade6-M216 ura4-D18 h*$^{+}$	Humphrey lab
TH357	*972 h*$^{-}$*/h*$^{-}$	Humphrey lab
TH358	*wee1-50 leu1-32 h*$^{-}$	Humphrey lab
TH2093	*leu1-32 arg3-D4 ade6-M210 ura4-D18 his3-D1 h*$^{-}$	Humphrey lab
TH2094	*leu1-32 arg3-D4 ade6-M210 ura4-D18 his3-D1 h*$^{+}$	Humphrey lab
TH3271	*set2::ura4 leu1-32 arg3-D4 ade6-M210 his3-D1 ura4-D18 h*$^{-}$	Humphrey lab
TH6241	*H3.2K36R H3.1/H4.1::his3 H3.3/H4.3::arg3 ura4-DS/E leu1-32 arg3-D4 ade6-M210 his3-D1 h*$^{-}$	Humphrey lab
TH8216	*set2-flag-kanR h?*	Humphrey lab
TH7972	*wee1-50 spd1::hygroR leu1-32 arg3-D4, his3-D1 ura4-D18 h?*	Humphrey lab
TH3273	*clr4::KAN leu1-32 ade6-210 ura4DS/E arg3? his3? h*$^{-}$	Humphrey lab

Denotation: genes in the wild-type locus are given the + suffix e, deletion/null mutants are denoted by ∆. A double colon (::) indicates an insertion into the genome disrupting the gene in question. Letters and numbers following the gene name identify mutant alleles.

6.7.2 Growth and storage of *S. pombe*

Cells were cultured in either non-selective, nutrient rich media YE6S or conditioned media, EMM with 15 mg/L required supplements. Strains from -80 ºC were grown at 25 or 32 ºC for 2-3 days and then stored at room temperature. Liquid cultures were prepared by inoculating a single colony or a 5 mm inoculating loop of cells, taken from a fresh agar plate, into liquid media. Cultures were grown overnight with shaking at the appropriate temperature. The measurement of cell density was determined using the absorbance at 595 nm (OD_{595}) in a Pharmacia Biotech Ultraspec 2000; an OD_{595} of 0.1 being about 2 x 10^6 cells/mL. Cultures were harvested in mid-exponential growth phase with cell number between 2 x 10^6 and 1 x 10^7 cells/mL (OD_{595}: 0.1 to 0.5) unless otherwise stated. Permanent stocks of yeast strains were stored in Nunc cryo-tubes in 0.5 mL YE6S and 0.5 mL YFM at -80 ºC.

6.7.3 Transformation by LiAc method

150 mL of cell culture was grown at 25 or 32 ºC until OD_{595} reached 0.2-0.5. Cells were centrifuged at 3000 rpm at room temperature for 5 minutes and then were washed once in Milli-Q water. Cells was resuspended in 1 mL 0.1 M LiAc and transferred to a 1.5 mL Eppendorf tube. Cells were dispensed into 100 µL aliquots of 1.5 mL Eppendorf tubes and incubated at 25 or 30 ºC for 1-2 hours. 1 µg of plasmid DNA in 15µL TE (10 mM Tris-HCl pH 8.0, 1 mM EDTA pH 8.0), 290 µL of 50% (w/v) PEG400 prewarmed at 25 or 30 ºC and 2 µL carrier ssDNA (10 mg/mL) were added to each tube with gentle vortexing and mixtures were incubated at 25 or 30 ºC for 1 hour. Cells was heated at 42 ºC for 15 minutes and cooled to room temperature for 10 minutes. Cells were centrifuged at 5000 rpm for 2 minutes and the supernatant was removed. Cells were resuspended in 1 mL EMM and incubated at 25 or 32 ºC for 1 hour with shaking. 200µL cell cultures were plated onto selective media plates and grown at 25 or 32 ºC for 4-5 days.

6.7.4 Genetic crosses, random spore analysis and tetrad analysis

Genetic crosses were carried out on SPAS6S agar and incubated at 25 ºC for 48-72 hours. Light microscopy was used to check for spores and the correct genotype was identified using random spore analysis or tetrad analysis.

For free spore analysis, 1 mL Milli-Q water was inoculated with a 1 µL loop of cells from the desired cross and 5 µL β-glucuronidase, and incubated at 25 ºC overnight. A 1:100 dilution was plated onto YES agar or selective medium and grown at an appropriate temperature for 4-5 days at 32 ºC. The desired progeny was selected by replica plating onto selective plates and the phenotype was determined.

Tetrad analysis was carried out by micromanipulation of the asci onto YE6S agar plates using a Singer MSM micro-manipulator. The ascus walls were allowed to break down at 37 ºC for 3-5 hours or 20 ºC overnight. After that, the four spores of each ascus were separated onto lines of virtual grid. The spores were incubated at the appropriate temperature until colonies formed. The colonies were selected by replica plating onto selective plates to identify desired progeny and determine the phenotype.

6.7.5 Serial dilution assay: spotting test

Cells were grown in required liquid culture at 25 or 32 ºC with shaking until the culture reached an OD_{595} of approximately 0.2-0.4. The concentration of cells was adjusted to OD595 0.2 in 200 µL, and 10-fold serial dilutions made using Milli-Q water. 8 µL of each dilution was spotted onto plates with or without thiamine. The plates were incubated at selected temperature for 3-4 days and then pho4ographed.

6.7.6 TCA protein extraction

50 mL cell culture was harvested at OD_{595} 0.2 (approximately 2 x 10^8 cells) by centrifugation at 3000 rpm for 2 minutes. The pellet was then resuspended in 1 mL 1.2 M sorbitol. The cells were centrifuged at 14000 rpm for 30 seconds, the pellet resuspended in 100 µL 20% TCA and vortexed. Glass beads (Sigma Aldrich) were added to 0.5 mL volume and the tubes vortexed for 5-10 minutes at 4 ºC using Bead Beater (BioSpec). 900 µL 5% TCA was added and the mixture was vortexed briefly. 800 µL was taken out and centrifuged at 5000 rpm for 10 minutes. The protein pellet was resuspended in 250 µL 1 x Laemmli buffer, vortexed and then boiled at 95 ºC for 3 minutes. The extract was centrifuged at 5000 rpm *g* for 10 minutes and the supernatant were ready to use or stored at -20 ºC.

1X Laemmli buffer: 125 mM Tris-Cl (pH 6.8), 100 mM dithiothreitol (DTT), 2% (w/v) sodium dodecyl sulphate (SDS), 10% (w/v) glycerol, 0.1% (w/v) bromophenol blue.

6.8 Western blotting

Protein samples were separated by SDS-PAGE electrophoresis including a lane marked with PageRuler™ prestained protein ladder. The gel was blotted onto a Hybond ECL membrane (0.2 µm pore size, GE Healthcare), sandwiched between two triple layers of 3M paper in transfer buffer (2.5 mM Tris, 192 mM glycine, 20% methanol) for 90 minutes at a constant current of 200 mA on ice, using a Mini Trans-Blot Electrophore (Bio-Rad). Ponceau S dye was used to visualise protein transfer condition after blotting. The membrane was destained using Milli-Q water for 5-10 minutes and then blocked in either 5% milk in PBS or sea block blocking buffer (ThermoFisher) at room temperature for 1 hour with shaking. Membranes were probed with primary antibody at appropriate dilutions in 5 mL blocking buffer at 4 ºC overnight with shaking. HRP-

conjugated secondary antibodies or DyLight 680/800 Conjugate secondary antibodies (ThermoFisher) at 1:15000 in 10 mL blocking buffer, each for 1 hour at room temperature. After each antibody incubation membranes were washed with PBS-T (137 mM NaCl, 12 mM Phosphate, 2.7 mM KCl, 0.1 % Tween 20, pH 7.4) for 10 min, 3 times with shaking. Bands were visualised using ECL™ reagents (GE Healthcare) for chemiluminescence detection, using 1 mL each of reagent 1 and 2 per gel blot. Blots were incubated with the combined detection reagent for 1 min and exposed to Amersham™ Hyperfilm ECL film (GE Healthcare) using a Compack X4 (Xograph) film developer or detected by ChemiDoc™ Touch Image System (Bio-Rad). Alternate fluorescence detection method was carried out using Odyssey® Imaging Systems.

Primary antibodies used in this study

Antibody	Species	Dilution	Producer
α-H3	Mouse	1:1000	Abcam,10799
α-H3	Rabbit	1:2000	Cell Signaling,9715
α-H3K4me3	Rabbit	1:1000	Abcam,8580
α-H3K9me3	Rabbit	1:2000	Abcam,8898
α-H3K9me2	Rabbit	1:1000	Cell Signaling,9753
α-H3K9me1	Rabbit	1:2000	Abcam,8896
α-H3K27me3	Rabbit	1:1000	Millipore,07-449
α-H3K36me3	Rabbit	1:1000	Abcam,9050
α-H3K36me2	Rabbit	1:2000	Active Motif, 39255
α-H3K36me1	Rabbit	1:1000	Abcam,9048
α-H3K79me3	Rabbit	1:2000	Abcam,2621
α-KAc	Rabbit	1:1000	Abcam,61257
α-Tubulin	Mouse	1:5000	Sigma, T5168
α-FLAG	Mouse	1:5000	Sigma, F3165

6.9 Liquid chromatography-mass spectrometry

Samples of histones, extracted as described above, were separated by reversed phase ultra-performance liquid chromatography (RP-UPLC) and analysed by electrospray ionization time-of-flight mass spectrometry (ESI-TOF MS). A Waters Acquity UPLC system connected directly to Waters LCT ESI-TOF MS machine was used for analysis. UPLC separation was carried out at a flow of 0.25 mL/min on a Waters BEH C4 reversed phase column (2.1 x 150 mm, 1.7 μm particle size, 300 Å pore size) at 40 ºC. The column was equilibrated with solvent A (0.5% (v/v) formic acid in Milli-Q water) and solvent B (0.5% (v/v) formic acid in acetonitrile). 5 μL of histone sample was injected into the column and histones were eluted by using a stepped gradient from solvent A to solvent B.

LCT-TOF MS (Water) parameters settings were as follows: polarity mode: ES+; capillary voltage: 3,000 V; sample cone voltage: 35 V; extraction cone voltage: 2.5V; desolvation temperature: 250 ºC; cone gas flow rate: 10 L/hour; desolvation gas flow (N_2): 500 L/hour. The mass range were covered from 100 to 2000 *m/z* using MassLynx 4.1 software (Waters) and histones molecular weight and distribution were acquired using Maxent 1 with mass accuracy 70 ppm and continum mode at the rate of 1spectrum/s. Masses were confirmed using manual component analysis. Leu-Enkephalin was used as lock spray reagent for calibration of the mass spectrometer at the monoisotopic mass of 556.277 $[M+H]^+$.

LTQ-Orbitrap MS (Thermo Scientific™) parameters setting were as follows: polarity mode: ES+; electrospray voltage: 3,000 V; capillary temperature: 200 ºC; sheath gas flow: 25 AU; auxillary gas flow: 8 AU. The mass range were covered from 200 to 2000 *m/z* using Xtract software (Thermo) and molecular weight and distribution of histone isoforms were acquired with 1 scan every 2 seconds (mass accuracy 5 ppm).

References

1 Crick, F. Central dogma of molecular biology. *Nature* **227**, 561-563 (1970).

2 Nanney, D. L. Epigenetic factors affecting mating type expression in certain ciliates. *Cold Spring Harb. Symp. Quant. Biol.* **23**, 327-335 (1958).

3 Noble, D. Conrad Waddington and the origin of epigenetics. *J. Exp. Biol.* **218**, 816-818 (2015).

4 Berger, S. L., Kouzarides, T., Shiekhattar, R. & Shilatifard, A. An operational definition of epigenetics. *Genes Dev.* **23**, 781-783 (2009).

5 Esteller, M. Epigenetics in cancer. *N. Engl. J. Med.* **358**, 1148-1159 (2008).

6 Brunet, A. & Berger, S. L. Epigenetics of aging and aging-related disease. *J. Gerontol. A Biol. Sci. Med. Sci.* **69 Suppl 1**, S17-20 (2014).

7 Maki, N. & Kimura, H. Epigenetics and regeneration. *Curr. Top. Microbiol. Immunol.* **367**, 237-252 (2013).

8 Boland, M. J., Nazor, K. L. & Loring, J. F. Epigenetic regulation of pluripotency and differentiation. *Circ. Res.* **115**, 311-324 (2014).

9 Nicholson, J. M. & Wood, C. M. *Chromatin structure and function, 2006*. (Transworld Research Network, 2006).

10 Kornberg, R. D. Chromatin structure: a repeating unit of histones and DNA. *Science* **184**, 868-871 (1974).

11 Luger, K., Mader, A. W., Richmond, R. K., Sargent, D. F. & Richmond, T. J. Crystal structure of the nucleosome core particle at 2.8 A resolution. *Nature* **389**, 251-260 (1997).

12 Thoma, F. & Koller, T. Influence of histone H1 on chromatin structure. *Cell* **12**, 101-107 (1977).

13 Girton, J. R. & Johansen, K. M. Chromatin structure and the regulation of gene expression: the lessons of PEV in Drosophila. *Adv. Genet.* **61**, 1-43 (2008).

14 Woodcock, C. L. & Ghosh, R. P. Chromatin higher-order structure and dynamics. *Cold Spring Harb. Perspect. Biol.* **2**, a000596 (2010).

15 Davey, C. A., Sargent, D. F., Luger, K., Maeder, A. W. & Richmond, T. J. Solvent mediated interactions in the structure of the nucleosome core particle at 1.9 a resolution. *J. Mol. Biol.* **319**, 1097-1113 (2002).

16 Iwasaki, W. *et al.* Contribution of histone N-terminal tails to the structure and stability of nucleosomes. *FEBS Open Bio.* **3**, 363-369 (2013).

17 Gao, M. *et al.* Histone H3 and H4 N-terminal tails in nucleosome arrays at cellular concentrations probed by magic angle spinning NMR spectroscopy. *J. Am. Chem. Soc.* **135**, 15278-15281 (2013).

18 Saikusa, K. *et al.* Gas-phase structure of the histone multimers characterized by ion mobility mass spectrometry and molecular dynamics simulation. *Anal. Chem.* **85**, 4165-4171 (2013).

19 du Preez, L. L. & Patterton, H. G. Secondary structures of the core histone N-terminal tails: their role in regulating chromatin structure. *Subcell. Biochem.* **61**, 37-55 (2013).

20 Talbert, P. B. & Henikoff, S. Histone variants--ancient wrap artists of the epigenome. *Nat. Rev. Mol. Cell Biol.* **11**, 264-275 (2010).

21 Maze, I., Noh, K. M., Soshnev, A. A. & Allis, C. D. Every amino acid matters: essential contributions of histone variants to mammalian development and disease. *Nat. Rev. Genet.* **15**, 259-271 (2014).

22 Weber, C. M. & Henikoff, S. Histone variants: dynamic punctuation in transcription. *Genes Dev.* **28**, 672-682 (2014).

23 Skene, P. J. & Henikoff, S. Histone variants in pluripotency and disease. *Development* **140**, 2513-2524 (2013).

24 Rangasamy, D. Histone variant H2A.Z can serve as a new target for breast cancer therapy. *Curr. Med. Chem.* **17**, 3155-3161 (2010).

25 Dunican, D. S., McWilliam, P., Tighe, O., Parle-McDermott, A. & Croke, D. T. Gene expression differences between the microsatellite instability (MIN) and chromosomal instability (CIN) phenotypes in colorectal cancer revealed by high-density cDNA array hybridization. *Oncogene* **21**, 3253-3257 (2002).

26 Sporn, J. C. *et al.* Histone macroH2A isoforms predict the risk of lung cancer recurrence. *Oncogene* **28**, 3423-3428 (2009).

27 Daxinger, L. & Whitelaw, E. Transgenerational epigenetic inheritance: more questions than answers. *Genome Res.* **20**, 1623-1628 (2010).

28 Robertson, K. D. & Jones, P. A. DNA methylation: past, present and future directions. *Carcinogenesis* **21**, 461-467 (2000).

29 Illingworth, R. S. & Bird, A. P. CpG islands--'a rough guide'. *FEBS Lett.* **583**, 1713-1720 (2009).

30 Straussman, R. *et al.* Developmental programming of CpG island methylation profiles in the human genome. *Nat. Struct. Mol. Biol.* **16**, 564-571 (2009).

31 Reik, W. & Lewis, A. Co-evolution of X-chromosome inactivation and imprinting in mammals. *Nat. Rev. Genet.* **6**, 403-410 (2005).

32 Esteller, M. Epigenetic gene silencing in cancer: the DNA hypermethylome. *Hum. Mol. Genet.* **16 Spec No 1**, R50-59 (2007).

33 Hellman, A. & Chess, A. Gene body-specific methylation on the active X chromosome. *Science* **315**, 1141-1143 (2007).

34 Zilberman, D., Gehring, M., Tran, R. K., Ballinger, T. & Henikoff, S. Genome-wide analysis of Arabidopsis thaliana DNA methylation uncovers an interdependence between methylation and transcription. *Nat. Genet.* **39**, 61-69 (2007).

35 Rose, N. R. & Klose, R. J. Understanding the relationship between DNA methylation and histone lysine methylation. *Biochim. Biophys. Acta* **1839**, 1362-1372 (2014).

36 Robertson, K. D. DNA methylation and human disease. *Nat. Rev. Genet.* **6**, 597-610 (2005).

37 Bostick, M. *et al.* UHRF1 plays a role in maintaining DNA methylation in mammalian cells. *Science* **317**, 1760-1764 (2007).

38 Bestor, T. H. The DNA methyltransferases of mammals. *Hum. Mol. Genet.* **9**, 2395-2402 (2000).

39 Hackett, J. A. *et al.* Germline DNA demethylation dynamics and imprint erasure through 5-hydroxymethylcytosine. *Science* **339**, 448-452 (2013).

40 Wu, H. & Zhang, Y. Mechanisms and functions of Tet protein-mediated 5-methylcytosine oxidation. *Genes Dev.* **25**, 2436-2452 (2011).

41 He, Y. F. *et al.* Tet-mediated formation of 5-carboxylcytosine and its excision by TDG

in mammalian DNA. *Science* **333**, 1303-1307 (2011).

42 Walsh, C. *Posttranslational modification of proteins : expanding nature's inventory*. (Roberts and Co. Publishers, 2006).

43 Kouzarides, T. Chromatin modifications and their function. *Cell* **128**, 693-705 (2007).

44 Berger, S. L. The complex language of chromatin regulation during transcription. *Nature* **447**, 407-412 (2007).

45 Tan, M. *et al.* Identification of 67 histone marks and histone lysine crotonylation as a new type of histone modification. *Cell* **146**, 1016-1028 (2011).

46 Huang, H., Lin, S., Garcia, B. A. & Zhao, Y. Quantitative proteomic analysis of histone modifications. *Chem. Rev.* **115**, 2376-2418 (2015).

47 Huang, H., Sabari, B. R., Garcia, B. A., Allis, C. D. & Zhao, Y. SnapShot: histone modifications. *Cell* **159**, 458-458 e451 (2014).

48 Wisniewski, J. R., Zougman, A. & Mann, M. Nepsilon-formylation of lysine is a widespread post-translational modification of nuclear proteins occurring at residues involved in regulation of chromatin function. *Nucleic Acids Res.* **36**, 570-577 (2008).

49 Lorch, Y., LaPointe, J. W. & Kornberg, R. D. Nucleosomes inhibit the initiation of transcription but allow chain elongation with the displacement of histones. *Cell* **49**, 203-210 (1987).

50 Csordas, A. On the biological role of histone acetylation. *The Biochemical journal* **265**, 23-38 (1990).

51 Linggi, B. E., Brandt, S. J., Sun, Z. W. & Hiebert, S. W. Translating the histone code into leukemia. *J. Cell. Biochem.* **96**, 938-950 (2005).

52 Nightingale, K. P., O'Neill, L. P. & Turner, B. M. Histone modifications: signalling receptors and potential elements of a heritable epigenetic code. *Curr. Opin. Genet. Dev.* **16**, 125-136 (2006).

53 Taverna, S. D., Li, H., Ruthenburg, A. J., Allis, C. D. & Patel, D. J. How chromatin-binding modules interpret histone modifications: lessons from professional pocket pickers. *Nat. Struct. Mol. Biol.* **14**, 1025-1040 (2007).

54 Lee, J. S., Smith, E. & Shilatifard, A. The language of histone crosstalk. *Cell* **142**, 682-685 (2010).

55 Lo, W. S. *et al.* Phosphorylation of serine 10 in histone H3 is functionally linked in vitro and in vivo to Gcn5-mediated acetylation at lysine 14. *Mol. Cell* **5**, 917-926 (2000).

56 Shilatifard, A. Chromatin modifications by methylation and ubiquitination: implications in the regulation of gene expression. *Annu. Rev. Biochem.* **75**, 243-269 (2006).

57 Tessarz, P. & Kouzarides, T. Histone core modifications regulating nucleosome structure and dynamics. *Nat. Rev. Mol. Cell Biol.* **15**, 703-708 (2014).

58 Redon, C. *et al.* Histone H2A variants H2AX and H2AZ. *Curr. Opin. Genet. Dev.* **12**, 162-169 (2002).

59 Sharma, A., Singh, K. & Almasan, A. Histone H2AX phosphorylation: a marker for DNA damage. *Methods Mol. Biol.* **920**, 613-626 (2012).

60 Rossetto, D., Avvakumov, N. & Cote, J. Histone phosphorylation: a chromatin modification involved in diverse nuclear events. *Epigenetics* **7**, 1098-1108 (2012).

61 Wei, Y., Yu, L., Bowen, J., Gorovsky, M. A. & Allis, C. D. Phosphorylation of histone

H3 is required for proper chromosome condensation and segregation. *Cell* **97**, 99-109 (1999).

62 Lau, P. N. & Cheung, P. Histone code pathway involving H3 S28 phosphorylation and K27 acetylation activates transcription and antagonizes polycomb silencing. *Proc. Natl. Acad. Sci. U S A.* **108**, 2801-2806 (2011).

63 Verdone, L., Caserta, M. & Di Mauro, E. Role of histone acetylation in the control of gene expression. *Biochem. Cell Biol.* **83**, 344-353 (2005).

64 Struhl, K. Histone acetylation and transcriptional regulatory mechanisms. *Genes Dev.* **12**, 599-606 (1998).

65 Battu, A., Ray, A. & Wani, A. A. ASF1A and ATM regulate H3K56-mediated cell-cycle checkpoint recovery in response to UV irradiation. *Nucleic Acids Res.* **39**, 7931-7945 (2011).

66 Wang, H. *et al.* Histone H3 and H4 ubiquitylation by the CUL4-DDB-ROC1 ubiquitin ligase facilitates cellular response to DNA damage. *Mol. Cell* **22**, 383-394 (2006).

67 Zhu, B. *et al.* Monoubiquitination of human histone H2B: the factors involved and their roles in HOX gene regulation. *Mol. Cell* **20**, 601-611 (2005).

68 Pavri, R. *et al.* Histone H2B monoubiquitination functions cooperatively with FACT to regulate elongation by RNA polymerase II. *Cell* **125**, 703-717 (2006).

69 Klose, R. J. & Zhang, Y. Regulation of histone methylation by demethylimination and demethylation. *Nat. Rev. Mol. Cell Biol.* **8**, 307-318 (2007).

70 Gershey, E. L., Haslett, G. W., Vidali, G. & Allfrey, V. G. Chemical studies of histone methylation. Evidence for the occurrence of 3-methylhistidine in avian erythrocyte histone fractions. *J. Biol. Chem.* **244**, 4871-4877 (1969).

71 Di Lorenzo, A. & Bedford, M. T. Histone arginine methylation. *FEBS Lett.* **585**, 2024-2031 (2011).

72 Wei, H., Mundade, R., Lange, K. C. & Lu, T. Protein arginine methylation of non-histone proteins and its role in diseases. *Cell Cycle* **13**, 32-41 (2014).

73 Miranda, T. B., Miranda, M., Frankel, A. & Clarke, S. PRMT7 is a member of the protein arginine methyltransferase family with a distinct substrate specificity. *J. Biol. Chem.* **279**, 22902-22907 (2004).

74 Fuhrmann, J. & Thompson, P. R. Protein Arginine Methylation and Citrullination in Epigenetic Regulation. *ACS Chem. Biol.* **11**, 654-668 (2016).

75 Migliori, V. *et al.* Symmetric dimethylation of H3R2 is a newly identified histone mark that supports euchromatin maintenance. *Nat. Struct. Mol. Biol.* **19**, 136-144 (2012).

76 Kirmizis, A. *et al.* Arginine methylation at histone H3R2 controls deposition of H3K4 trimethylation. *Nature* **449**, 928-932 (2007).

77 Chang, B., Chen, Y., Zhao, Y. & Bruick, R. K. JMJD6 is a histone arginine demethylase. *Science* **318**, 444-447 (2007).

78 Unoki, M. *et al.* Lysyl 5-hydroxylation, a novel histone modification, by Jumonji domain containing 6 (JMJD6). *J. Biol. Chem.* **288**, 6053-6062 (2013).

79 Greer, E. L. & Shi, Y. Histone methylation: a dynamic mark in health, disease and inheritance. *Nat. Rev. Genet.* **13**, 343-357 (2012).

80 Schneider, R. & Grosschedl, R. Dynamics and interplay of nuclear architecture, genome organization, and gene expression. *Genes Dev.* **21**, 3027-3043 (2007).

81 Barski, A. *et al.* High-resolution profiling of histone methylations in the human genome. *Cell* **129**, 823-837 (2007).

82 Bannister, A. J. *et al.* Spatial distribution of di- and tri-methyl lysine 36 of histone H3 at active genes. *J. Biol. Chem.* **280**, 17732-17736 (2005).

83 Bernstein, B. E. *et al.* A bivalent chromatin structure marks key developmental genes in embryonic stem cells. *Cell* **125**, 315-326 (2006).

84 Black, J. C., Van Rechem, C. & Whetstine, J. R. Histone lysine methylation dynamics: establishment, regulation, and biological impact. *Mol. Cell* **48**, 491-507 (2012).

85 Byvoet, P., Shepherd, G. R., Hardin, J. M. & Noland, B. J. The distribution and turnover of labeled methyl groups in histone fractions of cultured mammalian cells. *Arch. Biochem. Biophys.* **148**, 558-567 (1972).

86 Paik, W. K. & Kim, S. Enzymatic demethylation of calf thymus histones. *Biochem. Biophys. Res. Commun.* **51**, 781-788 (1973).

87 Shi, Y. *et al.* Histone demethylation mediated by the nuclear amine oxidase homolog LSD1. *Cell* **119**, 941-953 (2004).

88 Chen, Y. *et al.* Crystal structure of human histone lysine-specific demethylase 1 (LSD1). *Proc. Natl. Acad. Sci. U S A.* **103**, 13956-13961 (2006).

89 Anand, R. & Marmorstein, R. Structure and mechanism of lysine-specific demethylase enzymes. *J. Biol. Chem.* **282**, 35425-35429 (2007).

90 Gaweska, H. & Fitzpatrick, P. F. Structures and Mechanism of the Monoamine Oxidase Family. *Biomol Concepts* **2**, 365-377 (2011).

91 Shi, Y. & Whetstine, J. R. Dynamic regulation of histone lysine methylation by demethylases. *Mol. Cell* **25**, 1-14 (2007).

92 Metzger, E. *et al.* LSD1 demethylates repressive histone marks to promote androgen-receptor-dependent transcription. *Nature* **437**, 436-439 (2005).

93 Karytinos, A. *et al.* A novel mammalian flavin-dependent histone demethylase. *J. Biol. Chem.* **284**, 17775-17782 (2009).

94 Klose, R. J., Kallin, E. M. & Zhang, Y. JmjC-domain-containing proteins and histone demethylation. *Nat. Rev. Genet.* **7**, 715-727 (2006).

95 Whetstine, J. R. *et al.* Reversal of histone lysine trimethylation by the JMJD2 family of histone demethylases. *Cell* **125**, 467-481 (2006).

96 McDonough, M. A., Loenarz, C., Chowdhury, R., Clifton, I. J. & Schofield, C. J. Structural studies on human 2-oxoglutarate dependent oxygenases. *Curr. Opin. Struct. Biol.* **20**, 659-672 (2010).

97 Clifton, I. J. *et al.* Structural studies on 2-oxoglutarate oxygenases and related double-stranded beta-helix fold proteins. *J. Inorg. Biochem.* **100**, 644-669 (2006).

98 Ng, S. S. *et al.* Crystal structures of histone demethylase JMJD2A reveal basis for substrate specificity. *Nature* **448**, 87-91 (2007).

99 Flashman, E. & Schofield, C. J. The most versatile of all reactive intermediates? *Nat. Chem. Biol.* **3**, 86-87 (2007).

100 Schneider, J. & Shilatifard, A. Histone demethylation by hydroxylation: chemistry in action. *ACS Chem. Biol.* **1**, 75-81 (2006).

101 Hausinger, R. P. & Schofield, C. J. *2-oxoglutarate-dependent oxygenases*. (Royal Society of Chemistry, 2015).

102 Horton, J. R. *et al.* Enzymatic and structural insights for substrate specificity of a family of jumonji histone lysine demethylases. *Nat. Struct. Mol. Biol.* **17**, 38-43 (2010).

103 Valegard, K. *et al.* Structure of a cephalosporin synthase. *Nature* **394**, 805-809 (1998).

104 Chowdhury, R. *et al.* Structural basis for binding of hypoxia-inducible factor to the oxygen-sensing prolyl hydroxylases. *Structure* **17**, 981-989 (2009).

105 Rose, N. R., McDonough, M. A., King, O. N., Kawamura, A. & Schofield, C. J. Inhibition of 2-oxoglutarate dependent oxygenases. *Chem. Soc. Rev.* **40**, 4364-4397 (2011).

106 McNeill, L. A. *et al.* Hypoxia-inducible factor prolyl hydroxylase 2 has a high affinity for ferrous iron and 2-oxoglutarate. *Mol. Biosyst.* **1**, 321-324 (2005).

107 McCusker, K. P. & Klinman, J. P. Modular behavior of tauD provides insight into the origin of specificity in alpha-ketoglutarate-dependent nonheme iron oxygenases. *Proc. Natl. Acad. Sci. U S A.* **106**, 19791-19795 (2009).

108 Hausinger, R. P. FeII/alpha-ketoglutarate-dependent hydroxylases and related enzymes. *Crit. Rev. Biochem. Mol. Biol.* **39**, 21-68 (2004).

109 Zhou, J. *et al.* Spectroscopic studies of substrate interactions with clavaminate synthase 2, a multifunctional alpha-KG-dependent non-heme iron enzyme: correlation with mechanisms and reactivities. *J. Am. Chem. Soc.* **123**, 7388-7398 (2001).

110 Myllyla, R., Majamaa, K., Gunzler, V., Hanauske-Abel, H. M. & Kivirikko, K. I. Ascorbate is consumed stoichiometrically in the uncoupled reactions catalyzed by prolyl 4-hydroxylase and lysyl hydroxylase. *J. Biol. Chem.* **259**, 5403-5405 (1984).

111 Flashman, E. *et al.* Evidence for the slow reaction of hypoxia-inducible factor prolyl hydroxylase 2 with oxygen. *FEBS J* **277**, 4089-4099 (2010).

112 Lee, H. Y., Choi, K., Oh, H., Park, Y. K. & Park, H. HIF-1-dependent induction of Jumonji domain-containing protein (JMJD) 3 under hypoxic conditions. *Mol. Cells* **37**, 43-50 (2014).

113 Chowdhury, R., Hardy, A. & Schofield, C. J. The human oxygen sensing machinery and its manipulation. *Chem. Soc. Rev.* **37**, 1308-1319 (2008).

114 Sanchez-Fernandez, E. M. *et al.* Investigations on the oxygen dependence of a 2-oxoglutarate histone demethylase. *Biochem. J.* **449**, 491-496 (2013).

115 Tausendschon, M., Dehne, N. & Brune, B. Hypoxia causes epigenetic gene regulation in macrophages by attenuating Jumonji histone demethylase activity. *Cytokine* **53**, 256-262 (2011).

116 Kooistra, S. M. & Helin, K. Molecular mechanisms and potential functions of histone demethylases. *Nat. Rev. Mol. Cell Biol.* **13**, 297-311 (2012).

117 Stender, J. D. *et al.* Control of proinflammatory gene programs by regulated trimethylation and demethylation of histone H4K20. *Mol. Cell* **48**, 28-38 (2012).

118 Liu, W. *et al.* PHF8 mediates histone H4 lysine 20 demethylation events involved in cell cycle progression. *Nature* **466**, 508-512 (2010).

119 Horton, J. R., Upadhyay, A. K., Hashimoto, H., Zhang, X. & Cheng, X. Structural basis for human PHF2 Jumonji domain interaction with metal ions. *J. Mol. Biol.* **406**, 1-8 (2011).

120 Lu, T. *et al.* Regulation of NF-kappaB by NSD1/FBXL11-dependent reversible lysine

methylation of p65. *Proc. Natl. Acad. Sci. U S A.* **107**, 46-51 (2010).

121 Watanabe, S. *et al.* JMJD1C demethylates MDC1 to regulate the RNF8 and BRCA1-mediated chromatin response to DNA breaks. *Nat. Struct. Mol. Biol.* **20**, 1425-1433 (2013).

122 Ponnaluri, V. K., Vavilala, D. T., Putty, S., Gutheil, W. G. & Mukherji, M. Identification of non-histone substrates for JMJD2A-C histone demethylases. *Biochem. Biophys. Res. Commun.* **390**, 280-284 (2009).

123 Hancock, R. L., Dunne, K., Walport, L. J., Flashman, E. & Kawamura, A. Epigenetic regulation by histone demethylases in hypoxia. *Epigenomics* **7**, 791-811 (2015).

124 Blackledge, N. P. *et al.* CpG islands recruit a histone H3 lysine 36 demethylase. *Mol. Cell* **38**, 179-190 (2010).

125 Wang, H. *et al.* Structure of the JmjC-domain-containing protein JMJD5. *Acta Crystallogr. D Biol. Crystallogr.* **69**, 1911-1920 (2013).

126 Iyer, V. R. Nucleosome positioning: bringing order to the eukaryotic genome. *Trends Cell Biol.* **22**, 250-256 (2012).

127 Schones, D. E. *et al.* Dynamic regulation of nucleosome positioning in the human genome. *Cell* **132**, 887-898 (2008).

128 Tillo, D. & Hughes, T. R. G+C content dominates intrinsic nucleosome occupancy. *BMC Bioinformatics* **10**, 442 (2009).

129 Cairns, B. R. The logic of chromatin architecture and remodelling at promoters. *Nature* **461**, 193-198 (2009).

130 Dawson, M. A. & Kouzarides, T. Cancer epigenetics: from mechanism to therapy. *Cell* **150**, 12-27 (2012).

131 Chi, P., Allis, C. D. & Wang, G. G. Covalent histone modifications--miswritten, misinterpreted and mis-erased in human cancers. *Nat. Rev. Cancer* **10**, 457-469 (2010).

132 Marks, P. A. The clinical development of histone deacetylase inhibitors as targeted anticancer drugs. *Expert Opin Investig Drugs* **19**, 1049-1066 (2010).

133 Sidoli, S., Cheng, L. & Jensen, O. N. Proteomics in chromatin biology and epigenetics: Elucidation of post-translational modifications of histone proteins by mass spectrometry. *J. Proteomics* **75**, 3419-3433 (2012).

134 Aebersold, R. & Goodlett, D. R. Mass spectrometry in proteomics. *Chem. Rev.* **101**, 269-295 (2001).

135 Smith, R. D., Loo, J. A., Edmonds, C. G., Barinaga, C. J. & Udseth, H. R. New developments in biochemical mass spectrometry: electrospray ionization. *Anal. Chem.* **62**, 882-899 (1990).

136 Egestad, B. & Sjoberg, P. Analysis by fast atom bombardment mass spectrometry of conjugated metabolites of bis(2-ethylhexyl) phthalate. *Biomed. Environ. Mass Spectrom.* **16**, 151-154 (1988).

137 Glish, G. L. & Vachet, R. W. The basics of mass spectrometry in the twenty-first century. *Nat Rev Drug Discov* **2**, 140-150 (2003).

138 Wichitnithad, W., McManus, T. J. & Callery, P. S. Identification of isobaric product ions in electrospray ionization mass spectra of fentanyl using multistage mass spectrometry and deuterium labeling. *Rapid Commun. Mass Spectrom.* **24**, 2547-2553 (2010).

139 Olsen, J. V. *et al.* Parts per million mass accuracy on an Orbitrap mass spectrometer

via lock mass injection into a C-trap. *Mol. Cell. Proteomics* **4**, 2010-2021 (2005).

140 Xiong, L., Ping, L., Yuan, B. & Wang, Y. Methyl group migration during the fragmentation of singly charged ions of trimethyllysine-containing peptides: precaution of using MS/MS of singly charged ions for interrogating peptide methylation. *J. Am. Soc. Mass Spectrom.* **20**, 1172-1181 (2009).

141 Waterborg, J. H. & Harrington, R. E. Western blotting of histones from acid-urea-Triton- and sodium dodecyl sulfate-polyacrylamide gels. *Analytical biochemistry* **162**, 430-434 (1987).

142 Collas, P. The current state of chromatin immunoprecipitation. *Mol. Biotechnol.* **45**, 87-100 (2010).

143 Aebersold, R. & Mann, M. Mass spectrometry-based proteomics. *Nature* **422**, 198-207 (2003).

144 Zee, B. M., Young, N. L. & Garcia, B. A. Quantitative proteomic approaches to studying histone modifications. *Curr. Chem. Genomics* **5**, 106-114 (2011).

145 Botstein, D. & Fink, G. R. Yeast: an experimental organism for modern biology. *Science* **240**, 1439-1443 (1988).

146 Yanagida, M. The model unicellular eukaryote, Schizosaccharomyces pombe. *Genome Biol.* **3**, COMMENT2003 (2002).

147 Matuo, R. *et al.* Saccharomyces cerevisiae as a model system to study the response to anticancer agents. *Cancer Chemother. Pharmacol.* **70**, 491-502 (2012).

148 Forsburg, S. L. The yeasts Saccharomyces cerevisiae and Schizosaccharomyces pombe: models for cell biology research. *Gravit. Space Biol. Bull.* **18**, 3-9 (2005).

149 Allshire, R. C. & Ekwall, K. Epigenetic Regulation of Chromatin States in Schizosaccharomyces pombe. *Cold Spring Harb. Perspect. Biol.* **7**, a018770 (2015).

150 Huarte, M. *et al.* The fission yeast Jmj2 reverses histone H3 Lysine 4 trimethylation. *J. Biol. Chem.* **282**, 21662-21670 (2007).

151 Ayoub, N. *et al.* A novel jmjC domain protein modulates heterochromatization in fission yeast. *Mol. Cell. Biol.* **23**, 4356-4370 (2003).

152 Yamada, T., Fischle, W., Sugiyama, T., Allis, C. D. & Grewal, S. I. The nucleation and maintenance of heterochromatin by a histone deacetylase in fission yeast. *Mol. Cell* **20**, 173-185 (2005).

153 Becker, M. *et al.* Pmt1, a Dnmt2 homolog in Schizosaccharomyces pombe, mediates tRNA methylation in response to nutrient signaling. *Nucleic Acids Res.* **40**, 11648-11658 (2012).

154 Bannister, A. J. *et al.* Selective recognition of methylated lysine 9 on histone H3 by the HP1 chromo domain. *Nature* **410**, 120-124 (2001).

155 Lachner, M., O'Carroll, D., Rea, S., Mechtler, K. & Jenuwein, T. Methylation of histone H3 lysine 9 creates a binding site for HP1 proteins. *Nature* **410**, 116-120 (2001).

156 Lanouette, S., Mongeon, V., Figeys, D. & Couture, J. F. The functional diversity of protein lysine methylation. *Mol. Syst. Biol.* **10**, 724 (2014).

157 Noma, K. & Grewal, S. I. Histone H3 lysine 4 methylation is mediated by Set1 and promotes maintenance of active chromatin states in fission yeast. *Proc. Natl. Acad. Sci. U S A.* **99 Suppl 4**, 16438-16445 (2002).

158 Nakayama, J., Rice, J. C., Strahl, B. D., Allis, C. D. & Grewal, S. I. Role of histone H3 lysine 9 methylation in epigenetic control of heterochromatin assembly. *Science*

292, 110-113 (2001).

159 Sanders, S. L. *et al.* Methylation of histone H4 lysine 20 controls recruitment of Crb2 to sites of DNA damage. *Cell* **119**, 603-614 (2004).

160 Berdasco, M. *et al.* Epigenetic inactivation of the Sotos overgrowth syndrome gene histone methyltransferase NSD1 in human neuroblastoma and glioma. *Proc. Natl. Acad. Sci. U S A.* **106**, 21830-21835 (2009).

161 Huang, N. *et al.* Two distinct nuclear receptor interaction domains in NSD1, a novel SET protein that exhibits characteristics of both corepressors and coactivators. *EMBO J.* **17**, 3398-3412 (1998).

162 Luco, R. F. *et al.* Regulation of alternative splicing by histone modifications. *Science* **327**, 996-1000 (2010).

163 Fnu, S. *et al.* Methylation of histone H3 lysine 36 enhances DNA repair by nonhomologous end-joining. *Proc. Natl. Acad. Sci. U S A.* **108**, 540-545 (2011).

164 Wagner, E. J. & Carpenter, P. B. Understanding the language of Lys36 methylation at histone H3. *Nat. Rev. Mol. Cell Biol.* **13**, 115-126 (2012).

165 Kim, W., Choi, M. & Kim, J. E. The histone methyltransferase Dot1/DOT1L as a critical regulator of the cell cycle. *Cell Cycle* **13**, 726-738 (2014).

166 Lachner, M., Sengupta, R., Schotta, G. & Jenuwein, T. Trilogies of histone lysine methylation as epigenetic landmarks of the eukaryotic genome. *Cold Spring Harb. Symp. Quant. Biol.* **69**, 209-218 (2004).

167 Saksouk, N., Simboeck, E. & Dejardin, J. Constitutive heterochromatin formation and transcription in mammals. *Epigenetics Chromatin* **8**, 3 (2015).

168 Fernandez Sarabia, M. J., McInerny, C., Harris, P., Gordon, C. & Fantes, P. The cell cycle genes cdc22+ and suc22+ of the fission yeast Schizosaccharomyces pombe encode the large and small subunits of ribonucleotide reductase. *Mol. Gen. Genet.* **238**, 241-251 (1993).

169 Beck, H. *et al.* Cyclin-dependent kinase suppression by WEE1 kinase protects the genome through control of replication initiation and nucleotide consumption. *Mol. Cell. Biol.* **32**, 4226-4236 (2012).

170 Kellogg, D. R. Wee1-dependent mechanisms required for coordination of cell growth and cell division. *J. Cell Sci.* **116**, 4883-4890 (2003).

171 Pfister, S. X. *et al.* Inhibiting WEE1 Selectively Kills Histone H3K36me3-Deficient Cancers by dNTP Starvation. *Cancer Cell* **28**, 557-568 (2015).

172 Tsukada, Y. *et al.* Histone demethylation by a family of JmjC domain-containing proteins. *Nature* **439**, 811-816 (2006).

173 Hillringhaus, L. *et al.* Structural and evolutionary basis for the dual substrate selectivity of human KDM4 histone demethylase family. *J. Biol. Chem.* **286**, 41616-41625 (2011).

174 Wood, V. *et al.* PomBase: a comprehensive online resource for fission yeast. *Nucleic Acids Res.* **40**, D695-699 (2012).

175 Cloos, P. A. *et al.* The putative oncogene GASC1 demethylates tri- and dimethylated lysine 9 on histone H3. *Nature* **442**, 307-311 (2006).

176 Kim, T. D., Shin, S., Berry, W. L., Oh, S. & Janknecht, R. The JMJD2A demethylase regulates apoptosis and proliferation in colon cancer cells. *J. Cell. Biochem.* **113**, 1368-1376 (2012).

177 Wagner, K. W. *et al.* KDM2A promotes lung tumorigenesis by epigenetically

enhancing ERK1/2 signaling. *J. Clin. Invest.* **123**, 5231-5246 (2013).

178 Thuriaux, P., Nurse, P. & Carter, B. Mutants altered in the control co-ordinating cell division with cell growth in the fission yeast Schizosaccharomyces pombe. *Mol. Gen. Genet.* **161**, 215-220 (1978).

179 Maundrell, K. nmt1 of fission yeast. A highly transcribed gene completely repressed by thiamine. *J. Biol. Chem.* **265**, 10857-10864 (1990).

180 Moreno, M. B., Duran, A. & Ribas, J. C. A family of multifunctional thiamine-repressible expression vectors for fission yeast. *Yeast* **16**, 861-872 (2000).

181 Couture, J. F., Collazo, E., Ortiz-Tello, P. A., Brunzelle, J. S. & Trievel, R. C. Specificity and mechanism of JMJD2A, a trimethyllysine-specific histone demethylase. *Nat. Struct. Mol. Biol.* **14**, 689-695 (2007).

182 Morris, S. A. *et al.* Histone H3 K36 methylation is associated with transcription elongation in Schizosaccharomyces pombe. *Eukaryot Cell* **4**, 1446-1454 (2005).

183 Chen, Z. *et al.* Structural insights into histone demethylation by JMJD2 family members. *Cell* **125**, 691-702 (2006).

184 Hakansson, P., Dahl, L., Chilkova, O., Domkin, V. & Thelander, L. The Schizosaccharomyces pombe replication inhibitor Spd1 regulates ribonucleotide reductase activity and dNTPs by binding to the large Cdc22 subunit. *J. Biol. Chem.* **281**, 1778-1783 (2006).

185 Klose, R. J. *et al.* Demethylation of histone H3K36 and H3K9 by Rph1: a vestige of an H3K9 methylation system in Saccharomyces cerevisiae? *Mol. Cell. Biol.* **27**, 3951-3961 (2007).

186 Bannister, A. J. & Kouzarides, T. Regulation of chromatin by histone modifications. *Cell Res.* **21**, 381-395 (2011).

187 Khare, S. P. *et al.* HIstome--a relational knowledgebase of human histone proteins and histone modifying enzymes. *Nucleic Acids Res.* **40**, D337-342 (2012).

188 Turner, B. M. Cellular memory and the histone code. *Cell* **111**, 285-291 (2002).

189 Houben, A. *et al.* Methylation of histone H3 in euchromatin of plant chromosomes depends on basic nuclear DNA content. *Plant J.* **33**, 967-973 (2003).

190 Esteller, M. Cancer epigenomics: DNA methylomes and histone-modification maps. *Nat. Rev. Genet.* **8**, 286-298 (2007).

191 Xu, D., Bai, J., Duan, Q., Costa, M. & Dai, W. Covalent modifications of histones during mitosis and meiosis. *Cell Cycle* **8**, 3688-3694 (2009).

192 Dyson, M. H. *et al.* MAP kinase-mediated phosphorylation of distinct pools of histone H3 at S10 or S28 via mitogen- and stress-activated kinase 1/2. *J. Cell Sci.* **118**, 2247-2259 (2005).

193 Burlingame, A. L., Zhang, X. & Chalkley, R. J. Mass spectrometric analysis of histone posttranslational modifications. *Methods* **36**, 383-394 (2005).

194 Pesavento, J. J., Kim, Y. B., Taylor, G. K. & Kelleher, N. L. Shotgun annotation of histone modifications: a new approach for streamlined characterization of proteins by top down mass spectrometry. *J. Am. Chem. Soc.* **126**, 3386-3387 (2004).

195 Galasinski, S. C., Louie, D. F., Gloor, K. K., Resing, K. A. & Ahn, N. G. Global regulation of post-translational modifications on core histones. *J. Biol. Chem.* **277**, 2579-2588 (2002).

196 Zhang, L. *et al.* Differential expression of histone post-translational modifications in acute myeloid and chronic lymphocytic leukemia determined by high-pressure liquid

chromatography and mass spectrometry. *J. Am. Soc. Mass Spectrom.* **15**, 77-86 (2004).

197 Bonenfant, D., Coulot, M., Towbin, H., Schindler, P. & van Oostrum, J. Characterization of histone H2A and H2B variants and their post-translational modifications by mass spectrometry. *Mol. Cell. Proteomics* **5**, 541-552 (2006).

198 Thomas, C. E., Kelleher, N. L. & Mizzen, C. A. Mass spectrometric characterization of human histone H3: a bird's eye view. *J. Proteome Res.* **5**, 240-247 (2006).

199 Boyne, M. T., 2nd, Pesavento, J. J., Mizzen, C. A. & Kelleher, N. L. Precise characterization of human histones in the H2A gene family by top down mass spectrometry. *J. Proteome Res.* **5**, 248-253 (2006).

200 Siuti, N., Roth, M. J., Mizzen, C. A., Kelleher, N. L. & Pesavento, J. J. Gene-specific characterization of human histone H2B by electron capture dissociation. *J. Proteome Res.* **5**, 233-239 (2006).

201 Pesavento, J. J., Mizzen, C. A. & Kelleher, N. L. Quantitative analysis of modified proteins and their positional isomers by tandem mass spectrometry: human histone H4. *Anal. Chem.* **78**, 4271-4280 (2006).

202 Shechter, D., Dormann, H. L., Allis, C. D. & Hake, S. B. Extraction, purification and analysis of histones. *Nat. Protoc.* **2**, 1445-1457 (2007).

203 Shi, Y., Xiang, R., Horvath, C. & Wilkins, J. A. The role of liquid chromatography in proteomics. *J. Chromatogr. A* **1053**, 27-36 (2004).

204 You, J. *et al.* High-sensitivity TFA-free LC-MS for profiling histones. *Proteomics* **11**, 3326-3334 (2011).

205 Garcia, M. C., Hogenboom, A. C., Zappey, H. & Irth, H. Effect of the mobile phase composition on the separation and detection of intact proteins by reversed-phase liquid chromatography-electrospray mass spectrometry. *J. Chromatogr. A* **957**, 187-199 (2002).

206 Chen, Y., Mehok, A. R., Mant, C. T. & Hodges, R. S. Optimum concentration of trifluoroacetic acid for reversed-phase liquid chromatography of peptides revisited. *J. Chromatogr. A* **1043**, 9-18 (2004).

207 Eshraghi, J. & Chowdhury, S. K. Factors affecting electrospray ionization of effluents containing trifluoroacetic acid for high-performance liquid chromatography/mass spectrometry. *Anal. Chem.* **65**, 3528-3533 (1993).

208 Mirza, U. A. & Chait, B. T. Effects of anions on the positive ion electrospray ionization mass spectra of peptides and proteins. *Anal. Chem.* **66**, 2898-2904 (1994).

209 Fic, E., Kedracka-Krok, S., Jankowska, U., Pirog, A. & Dziedzicka-Wasylewska, M. Comparison of protein precipitation methods for various rat brain structures prior to proteomic analysis. *Electrophoresis* **31**, 3573-3579 (2010).

210 Linder, C. & Thoma, F. Histone H1 expressed in Saccharomyces cerevisiae binds to chromatin and affects survival, growth, transcription, and plasmid stability but does not change nucleosomal spacing. *Mol. Cell. Biol.* **14**, 2822-2835 (1994).

211 Dou, Y., Mizzen, C. A., Abrams, M., Allis, C. D. & Gorovsky, M. A. Phosphorylation of linker histone H1 regulates gene expression in vivo by mimicking H1 removal. *Mol. Cell* **4**, 641-647 (1999).

212 Gurley, L. R., Valdez, J. G. & Buchanan, J. S. Characterization of the mitotic specific phosphorylation site of histone H1. Absence of a consensus sequence for the p34cdc2/cyclin B kinase. *J. Biol. Chem.* **270**, 27653-27660 (1995).

213 Garcia, B. A. *et al.* Characterization of phosphorylation sites on histone H1 isoforms by tandem mass spectrometry. *J. Proteome Res.* **3**, 1219-1227 (2004).

214 Ficarro, S. B. *et al.* Phosphoproteome analysis by mass spectrometry and its application to Saccharomyces cerevisiae. *Nat. Biotechnol.* **20**, 301-305 (2002).

215 Su, X. *et al.* Liquid chromatography mass spectrometry profiling of histones. *J. Chromatogr. B Analyt. Technol. Biomed. Life Sci.* **850**, 440-454 (2007).

216 Bloom, K. S. & Anderson, J. N. Fractionation and characterization of chromosomal proteins by the hydroxyapatite dissociation method. *J. Biol. Chem.* **253**, 4446-4450 (1978).

217 Costanzi, C. & Pehrson, J. R. Histone macroH2A1 is concentrated in the inactive X chromosome of female mammals. *Nature* **393**, 599-601 (1998).

218 Chadwick, B. P. & Willard, H. F. A novel chromatin protein, distantly related to histone H2A, is largely excluded from the inactive X chromosome. *J. Cell Biol.* **152**, 375-384 (2001).

219 Cook, P. J. *et al.* Tyrosine dephosphorylation of H2AX modulates apoptosis and survival decisions. *Nature* **458**, 591-596 (2009).

220 Xu, Y. *et al.* Histone H2A.Z controls a critical chromatin remodeling step required for DNA double-strand break repair. *Mol. Cell* **48**, 723-733 (2012).

221 Zhang, L., Eugeni, E. E., Parthun, M. R. & Freitas, M. A. Identification of novel histone post-translational modifications by peptide mass fingerprinting. *Chromosoma* **112**, 77-86 (2003).

222 Bonenfant, D. *et al.* Analysis of dynamic changes in post-translational modifications of human histones during cell cycle by mass spectrometry. *Mol. Cell. Proteomics* **6**, 1917-1932 (2007).

223 Portela, A. & Esteller, M. Epigenetic modifications and human disease. *Nat. Biotechnol.* **28**, 1057-1068 (2010).

224 Ito, T., Ikehara, T., Nakagawa, T., Kraus, W. L. & Muramatsu, M. p300-mediated acetylation facilitates the transfer of histone H2A-H2B dimers from nucleosomes to a histone chaperone. *Genes Dev.* **14**, 1899-1907 (2000).

225 Osley, M. A., Fleming, A. B. & Kao, C. F. Histone ubiquitylation and the regulation of transcription. *Results Probl. Cell Differ.* **41**, 47-75 (2006).

226 Black, B. E. & Bassett, E. A. The histone variant CENP-A and centromere specification. *Curr. Opin. Cell Biol.* **20**, 91-100 (2008).

227 Tagami, H., Ray-Gallet, D., Almouzni, G. & Nakatani, Y. Histone H3.1 and H3.3 complexes mediate nucleosome assembly pathways dependent or independent of DNA synthesis. *Cell* **116**, 51-61 (2004).

228 Ahmad, K. & Henikoff, S. Histone H3 variants specify modes of chromatin assembly. *Proc. Natl. Acad. Sci. U S A.* **99 Suppl 4**, 16477-16484 (2002).

229 Kadyrova, L. Y., Rodriges Blanko, E. & Kadyrov, F. A. Human CAF-1-dependent nucleosome assembly in a defined system. *Cell Cycle* **12**, 3286-3297 (2013).

230 Nakatani, Y., Ray-Gallet, D., Quivy, J. P., Tagami, H. & Almouzni, G. Two distinct nucleosome assembly pathways: dependent or independent of DNA synthesis promoted by histone H3.1 and H3.3 complexes. *Cold Spring Harb. Symp. Quant. Biol.* **69**, 273-280 (2004).

231 Lindner, H., Helliger, W. & Puschendorf, B. Separation of Friend erythroleukaemic cell histones and high-mobility-group proteins by reversed-phase high-performance

liquid chromatography. *J. Chromatogr.* **450**, 309-316 (1988).

232 Zhang, K. *et al.* Histone acetylation and deacetylation: identification of acetylation and methylation sites of HeLa histone H4 by mass spectrometry. *Mol. Cell. Proteomics* **1**, 500-508 (2002).

233 Zhang, K. Histone acetylation and deacetylation- identification of acetylation and methylation sites of HeLa histone H4 by mass spectrometry. *Mol. Cell. Proteomics* **1**, 500-508 (2002).

234 Perry, R. H., Cooks, R. G. & Noll, R. J. Orbitrap mass spectrometry: instrumentation, ion motion and applications. *Mass Spectrom. Rev.* **27**, 661-699 (2008).

235 Cabreiro, F., Picot, C. R., Friguet, B. & Petropoulos, I. Methionine sulfoxide reductases: relevance to aging and protection against oxidative stress. *Ann. N. Y. Acad. Sci.* **1067**, 37-44 (2006).

236 Milligan, J. R. *et al.* Repair of oxidative DNA damage by amino acids. *Nucleic Acids Res.* **31**, 6258-6263 (2003).

237 Pesavento, J. J., Garcia, B. A., Streeky, J. A., Kelleher, N. L. & Mizzen, C. A. Mild performic acid oxidation enhances chromatographic and top down mass spectrometric analyses of histones. *Mol. Cell. Proteomics* **6**, 1510-1526 (2007).

238 Anantharamaiah, G. M. *et al.* Effect of oxidation on the properties of apolipoproteins A-I and A-II. *J. Lipid Res.* **29**, 309-318 (1988).

239 Kim, K. *et al.* Reducing protein oxidation in low-flow electrospray enables deeper investigation of proteoforms by top down proteomics. *EuPA Open Proteom.* **8**, 40-47 (2015).

240 Morand, K., Talbo, G. & Mann, M. Oxidation of peptides during electrospray ionization. *Rapid Commun. Mass Spectrom.* **7**, 738-743 (1993).

241 Naldi, M. *et al.* Histone proteins determined in a human colon cancer by high-performance liquid chromatography and mass spectrometry. *J. Chromatogr. A* **1129**, 73-81 (2006).

242 Su, X. *et al.* Validation of an LC-MS based approach for profiling histones in chronic lymphocytic leukemia. *Proteomics* **9**, 1197-1206 (2009).

243 Fraga, M. F. *et al.* Loss of acetylation at Lys16 and trimethylation at Lys20 of histone H4 is a common hallmark of human cancer. *Nat. Genet.* **37**, 391-400 (2005).

244 Chervona, Y. & Costa, M. Histone modifications and cancer: biomarkers of prognosis? *Am. J. Cancer Res.* **2**, 589-597 (2012).

245 Elsheikh, S. E. *et al.* Global histone modifications in breast cancer correlate with tumor phenotypes, prognostic factors, and patient outcome. *Cancer Res.* **69**, 3802-3809 (2009).

246 Kamakaka, R. T. & Biggins, S. Histone variants: deviants? *Genes Dev.* **19**, 295-310 (2005).

247 Nayak, S. R. *et al.* A Role for Histone H2B Variants in Endocrine-Resistant Breast Cancer. *Horm. Cancer* **6**, 214-224 (2015).

248 Bertout, J. A., Patel, S. A. & Simon, M. C. The impact of O2 availability on human cancer. *Nat. Rev. Cancer* **8**, 967-975 (2008).

249 Perez-Perri, J. I., Acevedo, J. M. & Wappner, P. Epigenetics: new questions on the response to hypoxia. *Int. J. Mol. Sci.* **12**, 4705-4721 (2011).

250 Majmundar, A. J., Wong, W. J. & Simon, M. C. Hypoxia-inducible factors and the

response to hypoxic stress. *Mol. Cell* **40**, 294-309 (2010).

251 Semenza, G. L. Hypoxia-inducible factor 1: master regulator of O2 homeostasis. *Curr. Opin. Genet. Dev.* **8**, 588-594 (1998).

252 Kaelin, W. G., Jr. & Ratcliffe, P. J. Oxygen sensing by metazoans: the central role of the HIF hydroxylase pathway. *Mol. Cell* **30**, 393-402 (2008).

253 Schofield, C. J. & Ratcliffe, P. J. Oxygen sensing by HIF hydroxylases. *Nat. Rev. Mol. Cell Biol.* **5**, 343-354 (2004).

254 Semenza, G. L. HIF-1, O(2), and the 3 PHDs: how animal cells signal hypoxia to the nucleus. *Cell* **107**, 1-3 (2001).

255 Dao, J. H. *et al.* Kinetic characterization and identification of a novel inhibitor of hypoxia-inducible factor prolyl hydroxylase 2 using a time-resolved fluorescence resonance energy transfer-based assay technology. *Anal. Biochem.* **384**, 213-223 (2009).

256 Berra, E. *et al.* HIF prolyl-hydroxylase 2 is the key oxygen sensor setting low steady-state levels of HIF-1alpha in normoxia. *EMBO J.* **22**, 4082-4090 (2003).

257 Hewitson, K. S. *et al.* Hypoxia-inducible factor (HIF) asparagine hydroxylase is identical to factor inhibiting HIF (FIH) and is related to the cupin structural family. *J. Biol. Chem.* **277**, 26351-26355 (2002).

258 Lando, D. *et al.* FIH-1 is an asparaginyl hydroxylase enzyme that regulates the transcriptional activity of hypoxia-inducible factor. *Genes Dev.* **16**, 1466-1471 (2002).

259 Shmakova, A., Batie, M., Druker, J. & Rocha, S. Chromatin and oxygen sensing in the context of JmjC histone demethylases. *Biochem. J.* **462**, 385-395 (2014).

260 Xia, X. *et al.* Integrative analysis of HIF binding and transactivation reveals its role in maintaining histone methylation homeostasis. *Proc. Natl. Acad. Sci. U S A.* **106**, 4260-4265 (2009).

261 Pollard, P. J. *et al.* Regulation of Jumonji-domain-containing histone demethylases by hypoxia-inducible factor (HIF)-1alpha. *Biochem. J.* **416**, 387-394 (2008).

262 Beyer, S., Kristensen, M. M., Jensen, K. S., Johansen, J. V. & Staller, P. The histone demethylases JMJD1A and JMJD2B are transcriptional targets of hypoxia-inducible factor HIF. *J. Biol. Chem.* **283**, 36542-36552 (2008).

263 Krieg, A. J. *et al.* Regulation of the histone demethylase JMJD1A by hypoxia-inducible factor 1 alpha enhances hypoxic gene expression and tumor growth. *Mol. Cell. Biol.* **30**, 344-353 (2010).

264 Orsi, G. A., Couble, P. & Loppin, B. Epigenetic and replacement roles of histone variant H3.3 in reproduction and development. *Int. J. Dev. Biol.* **53**, 231-243 (2009).

265 Dokmanovic, M., Clarke, C. & Marks, P. A. Histone deacetylase inhibitors: overview and perspectives. *Mol. Cancer Res.* **5**, 981-989 (2007).

266 Ninios, Y. P., Sekeri-Pataryas, K. E. & Sourlingas, T. G. Differential sensitivity of human leukemic cell lines to the histone deacetylase inhibitor, trichostatin A. *Leuk. Res.* **34**, 786-792 (2010).

267 Johnstone, R. W. Histone-deacetylase inhibitors: novel drugs for the treatment of cancer. *Nat Rev Drug Discov* **1**, 287-299 (2002).

268 Beck, H. C. *et al.* Quantitative proteomic analysis of post-translational modifications of human histones. *Mol. Cell. Proteomics* **5**, 1314-1325 (2006).

269 Benson, L. J. *et al.* Modifications of H3 and H4 during chromatin replication, nucleosome assembly, and histone exchange. *J. Biol. Chem.* **281**, 9287-9296 (2006).

270 Loyola, A., Bonaldi, T., Roche, D., Imhof, A. & Almouzni, G. PTMs on H3 variants before chromatin assembly potentiate their final epigenetic state. *Mol. Cell* **24**, 309-316 (2006).

271 Drogaris, P. *et al.* Histone deacetylase inhibitors globally enhance h3/h4 tail acetylation without affecting h3 lysine 56 acetylation. *Sci. Rep.* **2**, 220 (2012).

272 Price, P. Standard definitions of terms relating to mass spectrometry : A report from the committee on measurements and standards of the American society for mass spectrometry. *J. Am. Soc. Mass Spectrom.* **2**, 336-348 (1991).

273 Drogaris, P., Wurtele, H., Masumoto, H., Verreault, A. & Thibault, P. Comprehensive profiling of histone modifications using a label-free approach and its applications in determining structure-function relationships. *Anal. Chem.* **80**, 6698-6707 (2008).

274 Strober, W. Trypan blue exclusion test of cell viability. *Curr. Protoc. Immunol.* **Appendix 3**, Appendix 3B (2001).

275 An, W. G. *et al.* Stabilization of wild-type p53 by hypoxia-inducible factor 1alpha. *Nature* **392**, 405-408 (1998).

276 Bleackley, M. R. & Macgillivray, R. T. Transition metal homeostasis: from yeast to human disease. *Biometals* **24**, 785-809 (2011).

277 Leonard, S. *et al.* Cobalt-mediated generation of reactive oxygen species and its possible mechanism. *J. Inorg. Biochem.* **70**, 239-244 (1998).

278 Kang, G. S., Li, Q., Chen, H. & Costa, M. Effect of metal ions on HIF-1alpha and Fe homeostasis in human A549 cells. *Mutat. Res.* **610**, 48-55 (2006).

279 Carreau, A., El Hafny-Rahbi, B., Matejuk, A., Grillon, C. & Kieda, C. Why is the partial oxygen pressure of human tissues a crucial parameter? Small molecules and hypoxia. *J. Cell. Mol. Med.* **15**, 1239-1253 (2011).

280 Jayani, R. S., Ramanujam, P. L. & Galande, S. Studying histone modifications and their genomic functions by employing chromatin immunoprecipitation and immunoblotting. *Methods Cell Biol.* **98**, 35-56 (2010).

281 Johnson, A. B., Denko, N. & Barton, M. C. Hypoxia induces a novel signature of chromatin modifications and global repression of transcription. *Mutat. Res.* **640**, 174-179 (2008).

282 Chen, H., Yan, Y., Davidson, T. L., Shinkai, Y. & Costa, M. Hypoxic stress induces dimethylated histone H3 lysine 9 through histone methyltransferase G9a in mammalian cells. *Cancer Res.* **66**, 9009-9016 (2006).

283 Yun, Z., Lin, Q. & Giaccia, A. J. Adaptive myogenesis under hypoxia. *Mol. Cell. Biol.* **25**, 3040-3055 (2005).

284 Zhou, X. *et al.* Hypoxia induces trimethylated H3 lysine 4 by inhibition of JARID1A demethylase. *Cancer Res.* **70**, 4214-4221 (2010).

285 Pogribny, I. P. *et al.* Modulation of intracellular iron metabolism by iron chelation affects chromatin remodeling proteins and corresponding epigenetic modifications in breast cancer cells and increases their sensitivity to chemotherapeutic agents. *Int. J. Oncol.* **42**, 1822-1832 (2013).

286 Costa, M. *et al.* Nickel carcinogenesis: epigenetics and hypoxia signaling. *Mutat. Res.* **592**, 79-88 (2005).

287 Yang, J. *et al.* Role of hypoxia-inducible factors in epigenetic regulation via histone demethylases. *Ann. N. Y. Acad. Sci.* **1177**, 185-197 (2009).

288 Wellmann, S. *et al.* Hypoxia upregulates the histone demethylase JMJD1A via HIF-1.

Biochem. Biophys. Res. Commun. **372**, 892-897 (2008).

289 Gaboriau, F. *et al.* Effects of deferasirox and deferiprone on cellular iron load in the human hepatoma cell line HepaRG. *Biometals* **23**, 231-245 (2010).

290 Chowdhury, R. *et al.* Selective small molecule probes for the hypoxia inducible factor (HIF) prolyl hydroxylases. *ACS Chem. Biol.* **8**, 1488-1496 (2013).

291 Rabinowitz, M. H. Inhibition of hypoxia-inducible factor prolyl hydroxylase domain oxygen sensors: tricking the body into mounting orchestrated survival and repair responses. *J. Med. Chem.* **56**, 9369-9402 (2013).

292 Besarab, A. *et al.* Randomized placebo-controlled dose-ranging and pharmacodynamics study of roxadustat (FG-4592) to treat anemia in nondialysis-dependent chronic kidney disease (NDD-CKD) patients. *Nephrol. Dial. Transplant.* **30**, 1665-1673 (2015).

293 Ellinghaus, P. *et al.* BAY 87-2243, a highly potent and selective inhibitor of hypoxia-induced gene activation has antitumor activities by inhibition of mitochondrial complex I. *Cancer Med.* **2**, 611-624 (2013).

294 Schockel, L. *et al.* Targeting mitochondrial complex I using BAY 87-2243 reduces melanoma tumor growth. *Cancer Metab.* **3**, 11 (2015).

295 Muchnik, E. & Kaplan, J. HIF prolyl hydroxylase inhibitors for anemia. *Expert. Opin. Investig. Drugs* **20**, 645-656 (2011).

296 Hu, C. J., Sataur, A., Wang, L., Chen, H. & Simon, M. C. The N-terminal transactivation domain confers target gene specificity of hypoxia-inducible factors HIF-1alpha and HIF-2alpha. *Mol. Biol. Cell* **18**, 4528-4542 (2007).

297 Hewings, D. S. *et al.* Optimization of 3,5-dimethylisoxazole derivatives as potent bromodomain ligands. *J. Med. Chem.* **56**, 3217-3227 (2013).

298 Thinnes, C. C. *et al.* Betti reaction enables efficient synthesis of 8-hydroxyquinoline inhibitors of 2-oxoglutarate oxygenases. *Chem. Commun. (Camb.)* **51**, 15458-15461 (2015).

Appendix 1

Sequences of proteins involved in this work.

Human JMJD2A (1064 amino acids)

MASESETLNPSARIMTFYPTMEEFRNFSRYIAYIESQGAHRAGLAKVVPPKEWKPRASYD
DIDDLVIPAPIQQLVTGQSGLFTQYNIQKKAMTVREFRKIANSDKYCTPRYSEFEELERK
YWKNLTFNPPIYGADVNGTLYEKHVDEWNIGRLRTILDLVEKESGITIEGVNTPYLYFGM
WKTSFAWHTEDMDLYSINYLHFGEPKSWYSVPPEHGKRLERLAKGFFPGSAQSCEAFLRH
KMTLISPLMLKKYGIPFDKVTQEAGEFMITFPYGYHAGFNHGFNCAESTNFATRRWIEYG
KQAVLCSCRKDMVKISMDVFVRKFQPERYKLWKAGKDNTVIDHTLPTPEAAEFLKESELP
PRAGNEEECPEEDMEGVEDGEEGDLKTSLAKHRIGTKRHRVCLEIPQEVSQSELFPKEDL
SSEQYEMTECPAALAPVRPTHSSVRQVEDGLTFPDYSDSTEVKFEELKNVKLEEEDEEEE
QAAAALDLSVNPASVGGRLVFSGSKKKSSSSLGSGSSRDSISSDSETSEPLSCRAQGQTG
VLTVHSYAKGDGRVTVGEPCTRKKGSAARSFSERELAEVADEYMFSLEENKKSKGRRQPL
SKLPRHHPLVLQECVSDDETSEQLTPEEEAEETEAWAKPLSQLWQNRPPNFEAEKEFNET
MAQQAPHCAVCMIFQTYHQVEFGGFNQNCGNASDLAPQKQRTKPLIPEMCFTSTGCSTDI
NLSTPYLEEDGTSILVSCKKCSVRVHASCYGVPPAKASEDWMCSRCSANALEEDCCLCSL
RGGALQRANDDRWVHVSCAVAILEARFVNIAERSPVDVSKIPLPRFKLKCIFCKKRRKRT
AGCCVQCSHGRCPTAFHVSCAQAAGVMMQPDDWPFVVFITCFRHKIPNLERAKGALQSIT
AGQKVISKHKNGRFYQCEVVRLTTETFYEVNFDDGSFSDNLYPEDIVSQDCLQFGPPAEG
EVVQVRWTDGQVYGAKFVASHPIQMYQVEFEDGSQLVVKRDDVYTLDEELPKRVKSRLSV
ASDMRFNEIFTEKEVKQEKKRQRVINSRYREDYIEPALYRAIME

Human JMJD2A-H188A (1064 amino acids)

MASESETLNPSARIMTFYPTMEEFRNFSRYIAYIESQGAHRAGLAKVVPPKEWKPRASYD
DIDDLVIPAPIQQLVTGQSGLFTQYNIQKKAMTVREFRKIANSDKYCTPRYSEFEELERK
YWKNLTFNPPIYGADVNGTLYEKHVDEWNIGRLRTILDLVEKESGITIEGVNTPYLYFGM
WKTSFAWATEDMDLYSINYLHFGEPKSWYSVPPEHGKRLERLAKGFFPGSAQSCEAFLRH
KMTLISPLMLKKYGIPFDKVTQEAGEFMITFPYGYHAGFNHGFNCAESTNFATRRWIEYG
KQAVLCSCRKDMVKISMDVFVRKFQPERYKLWKAGKDNTVIDHTLPTPEAAEFLKESELP
PRAGNEEECPEEDMEGVEDGEEGDLKTSLAKHRIGTKRHRVCLEIPQEVSQSELFPKEDL
SSEQYEMTECPAALAPVRPTHSSVRQVEDGLTFPDYSDSTEVKFEELKNVKLEEEDEEEE
QAAAALDLSVNPASVGGRLVFSGSKKKSSSSLGSGSSRDSISSDSETSEPLSCRAQGQTG
VLTVHSYAKGDGRVTVGEPCTRKKGSAARSFSERELAEVADEYMFSLEENKKSKGRRQPL
SKLPRHHPLVLQECVSDDETSEQLTPEEEAEETEAWAKPLSQLWQNRPPNFEAEKEFNET
MAQQAPHCAVCMIFQTYHQVEFGGFNQNCGNASDLAPQKQRTKPLIPEMCFTSTGCSTDI
NLSTPYLEEDGTSILVSCKKCSVRVHASCYGVPPAKASEDWMCSRCSANALEEDCCLCSL
RGGALQRANDDRWVHVSCAVAILEARFVNIAERSPVDVSKIPLPRFKLKCIFCKKRRKRT
AGCCVQCSHGRCPTAFHVSCAQAAGVMMQPDDWPFVVFITCFRHKIPNLERAKGALQSIT
AGQKVISKHKNGRFYQCEVVRLTTETFYEVNFDDGSFSDNLYPEDIVSQDCLQFGPPAEG
EVVQVRWTDGQVYGAKFVASHPIQMYQVEFEDGSQLVVKRDDVYTLDEELPKRVKSRLSV
ASDMRFNEIFTEKEVKQEKKRQRVINSRYREDYIEPALYRAIME

Human FBXL11 (1162 amino acids)

MEPEEERIRYSQRLRGTMRRRYEDDGISDDEIEGKRTFDLEEKLHTNKYNANFVTFMEGK
DFNVEYIQRGGLRDPLIFKNSDGLGIKMPDPDFTVNDVKMCVGSRRMVDVMDVNTQKGIE
MTMAQWTRYYETPEEEREKLYNVISLEFSHTRLENMVQRPSTVDFIDWVDNMWPRHLKES
QTESTNAILEMQYPKVQKYCLMSVRGCYTDFHVDFGGTSVWYHIHQGGKVFWLIPPTAHN
LELYENWLLSGKQGDIFLGDRVSDCQRIELKQGYTFVIPSGWIHAVYTPTDTLVFGGNFL
HSFNIPMQLKIYNIEDRTRVPNKFRYPFYYEMCWYVLERYVYCITNRSHLTKEFQKESLS
MDLELNGLESGNGDEEAVDREPRRLSSRRSVLTSPVANGVNLDYDGLGKTCRSLPSLKKT
LAGDSSSDCSRGSHNGQVWDPQCAPRKDRQVHLTHFELEGLRCLVDKLESLPLHKKCVPT
GIEDEDALIADVKILLEELANSDPKLALTGVPIVQWPKRDKLKFPTRPKVRVPTIPITKP
HTMKPAPRLTPVRPAAASPIVSGARRRRVRCRKCKACVQGECGVCHYCRDMKKFGGPGRM
KQSCVLRQCLAPRLPHSVTCSLCGEVDQNEETQDFEKKLMECCICNEIVHPGCLQMDGEG
LLNEELPNCWECPKCYQEDSSEKAQKRKMEESDEEAVQAKVLRPLRSCDEPLTPPPHSPT
SMLQLIHDPVSPRGMVTRSSPGAGPSDHHSASRDERFKRRQLLRLQATERTMVREKENNP
SGKKELSEVEKAKIRGSYLTVTLQRPTKELHGTSIVPKLQAITASSANLRHSPRVLVQHC
PARTPQRGDEEGLGGEEEEEEEEEEEDDSAEEGGAARLNGRGSWAQDGDESWMQREVWMS
VFRYLSRRELCECMRVCKTWYKWCCDKRLWTKIDLSRCKAIVPQALSGIIKRQPVSLDLS
WTNISKKQLTWLVNRLPGLKDLLLAGCSWSAVSALSTSSCPLLRTLDLRWAVGIKDPQIR
DLLTPPADKPGQDNRSKLRNMTDFRLAGLDITDATLRLIIRHMPLLSRLDLSHCSHLTDQ
SSNLLTAVGSSTRYSLTELNMAGCNKLTDQTLIYLRRIANVTLIDLRGCKQITRKACEHF
ISDLSINSLYCLSDEKLIQKIS

Human FBXL11-H212A (1162 amino acids)

MEPEEERIRYSQRLRGTMRRRYEDDGISDDEIEGKRTFDLEEKLHTNKYNANFVTFMEGK
DFNVEYIQRGGLRDPLIFKNSDGLGIKMPDPDFTVNDVKMCVGSRRMVDVMDVNTQKGIE
MTMAQWTRYYETPEEEREKLYNVISLEFSHTRLENMVQRPSTVDFIDWVDNMWPRHLKES
QTESTNAILEMQYPKVQKYCLMSVRGCYTDF**A**VDFGGTSVWYHIHQGGKVFWLIPPTAHN
LELYENWLLSGKQGDIFLGDRVSDCQRIELKQGYTFVIPSGWIHAVYTPTDTLVFGGNFL
HSFNIPMQLKIYNIEDRTRVPNKFRYPFYYEMCWYVLERYVYCITNRSHLTKEFQKESLS
MDLELNGLESGNGDEEAVDREPRRLSSRRSVLTSPVANGVNLDYDGLGKTCRSLPSLKKT
LAGDSSSDCSRGSHNGQVWDPQCAPRKDRQVHLTHFELEGLRCLVDKLESLPLHKKCVPT
GIEDEDALIADVKILLEELANSDPKLALTGVPIVQWPKRDKLKFPTRPKVRVPTIPITKP
HTMKPAPRLTPVRPAAASPIVSGARRRRVRCRKCKACVQGECGVCHYCRDMKKFGGPGRM
KQSCVLRQCLAPRLPHSVTCSLCGEVDQNEETQDFEKKLMECCICNEIVHPGCLQMDGEG
LLNEELPNCWECPKCYQEDSSEKAQKRKMEESDEEAVQAKVLRPLRSCDEPLTPPPHSPT
SMLQLIHDPVSPRGMVTRSSPGAGPSDHHSASRDERFKRRQLLRLQATERTMVREKENNP
SGKKELSEVEKAKIRGSYLTVTLQRPTKELHGTSIVPKLQAITASSANLRHSPRVLVQHC
PARTPQRGDEEGLGGEEEEEEEEEEEDDSAEEGGAARLNGRGSWAQDGDESWMQREVWMS
VFRYLSRRELCECMRVCKTWYKWCCDKRLWTKIDLSRCKAIVPQALSGIIKRQPVSLDLS
WTNISKKQLTWLVNRLPGLKDLLLAGCSWSAVSALSTSSCPLLRTLDLRWAVGIKDPQIR
DLLTPPADKPGQDNRSKLRNMTDFRLAGLDITDATLRLIIRHMPLLSRLDLSHCSHLTDQ
SSNLLTAVGSSTRYSLTELNMAGCNKLTDQTLIYLRRIANVTLIDLRGCKQITRKACEHF
ISDLSINSLYCLSDEKLIQKIS

Human JMJD2A$_{1-324}$ (324 amino acids)

MASESETLNPSARIMTFYPTMEEFRNFSRYIAYIESQGAHRAGLAKVVPPKEWKPRASYD
DIDDLVIPAPIQQLVTGQSGLFTQYNIQKKAMTVREFRKIANSDKYCTPRYSEFEELERK
YWKNLTFNPPIYGADVNGTLYEKHVDEWNIGRLRTILDLVEKESGITIEGVNTPYLYFGM
WKTSFAWHTEDMDLYSINYLHFGEPKSWYSVPPEHGKRLERLAKGFFPGSAQSCEAFLRH
KMTLISPLMLKKYGIPFDKVTQEAGEFMITFPYGYHAGFNHGFNCAESTNFATRRWIEYG
KQAVLCSCRKDMVKISMDVFVRKF

Human JMJD2A$_{1-324}$-H188A (324 amino acids)

MASESETLNPSARIMTFYPTMEEFRNFSRYIAYIESQGAHRAGLAKVVPPKEWKPRASYD
DIDDLVIPAPIQQLVTGQSGLFTQYNIQKKAMTVREFRKIANSDKYCTPRYSEFEELERK
YWKNLTFNPPIYGADVNGTLYEKHVDEWNIGRLRTILDLVEKESGITIEGVNTPYLYFGM
WKTSFAW**A**TEDMDLYSINYLHFGEPKSWYSVPPEHGKRLERLAKGFFPGSAQSCEAFLRH
KMTLISPLMLKKYGIPFDKVTQEAGEFMITFPYGYHAGFNHGFNCAESTNFATRRWIEYG
KQAVLCSCRKDMVKISMDVFVRKF

Human FBXL11$_{1-322}$ (322 amino acids)

MEPEEERIRYSQRLRGTMRRRYEDDGISDDEIEGKRTFDLEEKLHTNKYNANFVTFMEGK
DFNVEYIQRGGLRDPLIFKNSDGLGIKMPDPDFTVNDVKMCVGSRRMVDVMDVNTQKGIE
MTMAQWTRYYETPEEEREKLYNVISLEFSHTRLENMVQRPSTVDFIDWVDNMWPRHLKES
QTESTNAILEMQYPKVQKYCLMSVRGCYTDFHVDFGGTSVWYHIHQGGKVFWLIPPTAHN
LELYENWLLSGKQGDIFLGDRVSDCQRIELKQGYTFVIPSGWIHAVYTPTDTLVFGGNFL
HSFNIPMQLKIYNIEDRTRVPN

Human FBXL11$_{1-322}$-H212A (322 amino acids)

MEPEEERIRYSQRLRGTMRRRYEDDGISDDEIEGKRTFDLEEKLHTNKYNANFVTFMEGK
DFNVEYIQRGGLRDPLIFKNSDGLGIKMPDPDFTVNDVKMCVGSRRMVDVMDVNTQKGIE
MTMAQWTRYYETPEEEREKLYNVISLEFSHTRLENMVQRPSTVDFIDWVDNMWPRHLKES
QTESTNAILEMQYPKVQKYCLMSVRGCYTDF**A**VDFGGTSVWYHIHQGGKVFWLIPPTAHN
LELYENWLLSGKQGDIFLGDRVSDCQRIELKQGYTFVIPSGWIHAVYTPTDTLVFGGNFL
HSFNIPMQLKIYNIEDRTRVPN

***S. pombe* Jmj3 (752 amino acids)**

MQQNVKEKHAGKSDTSVSSLECEIDYHIEGSDGIPVVEPKISEFVDMESFIRRVERLGKK
YGAIKVVRPSSVLNPWNEDTMKPSDVKMDLWLERMVRRKGEYFEIQSDIDHGSAGPKKPT
DMNVDDRFPSNAGSSNDFENNVAKAIAYYWRSLTHDSLWYGYTNRPSIPFYFIPSISAAQ
KDRVHLRSNTLINTWPNVGHLFAGKWKTTLPWRVESPELHAVQVHLGGSSLQWYVIPSAH
SESFKKLAGKLAQDEHWRCSDFLLHQNILFPPSTLVQNGIVTYSTVLKQDELLITFPGTH
HSAFCLGDAVLRRFVFRSPRSASNYEFSNLRRLMVSESLYSSKSLWPHSHKPQRACSQKF
LDEFYLHDLPESNIHDSGNFHPIHSSVDNNSFSQRDFDSPNSINPPSPLMSNHESASTEH
FNSTTTTEKELSSLHVGEERKNRSLPLSLIWNSKAREEYIKKQKEENGDNIEFSHFDPLY
TRPSSHPLHPPPILGLPVPAQFARGELFLGRILEDRVSEHMLLLECEKSDVVEVPYECIL
TSSSAAGRRESSYYNPALKAPNIVYDDGVPINWNEYSELPSLDRFVLPKLLPGKPIEFTP
PISVEPTSIKTIAAEESSEPTSSVDVAPTPVEDVNVNLESISNTNESVVDLSDPLVSKNG
FEDVERSSVADLEEDVLETRSSIFETSDIDDRLTVIDRSQSVVPSESEFSIAGANLTRRN
AVDFSVSLDTYELYVSDEVENVDDFSLFPSLE

***S. pombe* Jmj3$_{1\text{-}445}$ (445 amino acids)**

MQQNVKEKHAGKSDTSVSSLECEIDYHIEGSDGIPVVEPKISEFVDMESFIRRVERLGKK
YGAIKVVRPSSVLNPWNEDTMKPSDVKMDLWLERMVRRKGEYFEIQSDIDHGSAGPKKPT
DMNVDDRFPSNAGSSNDFENNVAKAIAYYWRSLTHDSLWYGYTNRPSIPFYFIPSISAAQ
KDRVHLRSNTLINTWPNVGHLFAGKWKTTLPWRVESPELHAVQVHLGGSSLQWYVIPSAH
SESFKKLAGKLAQDEHWRCSDFLLHQNILFPPSTLVQNGIVTYSTVLKQDELLITFPGTH
HSAFCLGDAVLRRFVFRSPRSASNYEFSNLRRLMVSESLYSSKSLWPHSHKPQRACSQKF
LDEFYLHDLPESNIHDSGNFHPIHSSVDNNSFSQRDFDSPNSINPPSPLMSNHESASTEH
FNSTTTTEKELSSLHVGEERKNRSL

Appendix 2

Sequences and calculated masses* of human histone H1 variants analysed in this study.

Histone H1.2 (212 amino acids)
SETAPAAPAAAPPAEKAPVKKKAAKKAGGTPRKASGPPVSELITKAVAAS
KERSGVSLAALKKALAAAGYDVEKNNSRIKLGLKSLVSKGTLVQTKGTGA
SGSFKLNKKAASGEAKPKVKKAGGTKPKKPVGAAKKPKKAAGGATPKKSA
KKTPKKAKKPAAATVTKKVAKSPKKAKVAKPKKAAKSAAKAVKPKAAKPK
VVKPKKAAPKKK
Calculated mass: 21233.56 (average mass), 21220.71 (monoisotopic mass)

Histone H1.3 (220 amino acids)
SETAPLAPTIPAPAEKTPVKKKAKKAGATAGKRKASGPPVSELITKAVAA
SKERSGVSLAALKKALAAAGYDVEKNNSRIKLGLKSLVSKGTLVQTKGTG
ASGSFKLNKKAASGEGKPKAKKAGAAKPRKPAGAAKKPKKVAGAATPKKS
IKKTPKKVKKPATAAGTKKVAKSAKKVKTPQPKKAAKSPAKAKAPKPKAA
KPKSGKPKVTKAKKAAPKKK
Calculated mass: 22218.71 (average mass), 22205.28 (monoisotopic mass)

Histone H1.4 (218 amino acids)
SETAPAAPAAPAPAEKTPVKKKARKSAGAAKRKASGPPVSELITKAVAAS
KERSGVSLAALKKALAAAGYDVEKNNSRIKLGLKSLVSKGTLVQTKGTGA
SGSFKLNKKAASGEAKPKAKKAGAAKAKKPAGAAKKPKKATGAATPKKSA
KKTPKKAKKPAAAAGAKKAKSPKKAKAAKPKKAPKSPAKAKAVKPKAAKP
KTAKPKAAKPKKAAAKKK
Calculated mass: 21734.08 (average mass), 21720.96 (monoisotopic mass)

* Histone masses were calculated using the ExPASy ProtParam tool (http://web.expasy.org/protparam/)

Appendix 3

Sequences and calculated masses of human histone H2A variants analysed in this study.

Histone H2A type1 (129 amino acids)
SETAPAAPAAAPPAEKAPVKKKAAKKAGGTPRKASGPPVSELITKAVAAS
KERSGVSLAALKKALAAAGYDVEKNNSRIKLGLKSLVSKGTLVQTKGTGA
SGSFKLNKKAASGEAKPKVKKAGGTKPKKPVGAAKKPKKAAGGATPKKSA
KKTPKKAKKPAAATVTKKVAKSPKKAKVAKPKKAAKSAAKAVKPKAAKPK
VVKPKKAAPKKK
Calculated mass: 21233.56 (average mass), 21220.71 (monoisotopic mass)

H2A type 1-B/E (129 amino acids)
SGRGKQGGKARAKAKTRSSRAGLQFPVGRVHRLLRKGNYSERVGAGAPVY
LAAVLEYLTAEILELAGNAARDNKKTRIIPRHLQLAIRNDEELNKLLGRV
TIAQGGVLPNIQAVLLPKKTESHHKAKGK
Calculated mass: 14004.30 (average mass), 13995.91 (monoisotopic mass)

H2A type 1-C (129 amino acids)
SGRGKQGGKARAKAKSRSSRAGLQFPVGRVHRLLRKGNYAERVGAGAPVY
LAAVLEYLTAEILELAGNAARDNKKTRIIPRHLQLAIRNDEELNKLLGRV
TIAQGGVLPNIQAVLLPKKTESHHKAKGK
Calculated mass: 13974.28 (average mass), 13965.90 (monoisotopic mass)

H2A type 1-D (129 amino acids)
SGRGKQGGKARAKAKTRSSRAGLQFPVGRVHRLLRKGNYSERVGAGAPVY
LAAVLEYLTAEILELAGNAARDNKKTRIIPRHLQLAIRNDEELNKLLGKV
TIAQGGVLPNIQAVLLPKKTESHHKAKGK
Calculated mass: 13976.29 (average mass), 13967.90 (monoisotopic mass)

H2A type 1-H (127 amino acids)
SGRGKQGGKARAKAKTRSSRAGLQFPVGRVHRLLRKGNYAERVGAGAPVY
LAAVLEYLTAEILELAGNAARDNKKTRIIPRHLQLAIRNDEELNKLLGKV
TIAQGGVLPNIQAVLLPKKTESHHKAK
Calculated mass: 13775.06 (average mass), 13766.79 (monoisotopic mass)

H2A type 2-A (129 amino acids)
SGRGKQGGKARAKAKSRSSRAGLQFPVGRVHRLLRKGNYAERVGAGAPVY
MAAVLEYLTAEILELAGNAARDNKKTRIIPRHLQLAIRNDEELNKLLGKV
TIAQGGVLPNIQAVLLPKKTESHHKAKGK
Calculated mass:13964.30 (average mass), 13955.85 (monoisotopic mass)

H2A type 2-C (128 amino acids)
SGRGKQGGKARAKAKSRSSRAGLQFPVGRVHRLLRKGNYAERVGAGAPVYMAAVLEYLTAEILELAGNAARDNKK
TRIIPRHLQLAIRNDEELNKLLGKVTIAQGGVLPNIQAVLLPKKTESHKAKSK
Calculated mass: 13857.18 (average mass), 13848.80 (monoisotopic mass)

H2A type 3 (129 amino acids)
SGRGKQGGKARAKAKSRSSRAGLQFPVGRVHRLLRKGNYSERVGAGAPVY
LAAVLEYLTAEILELAGNAARDNKKTRIIPRHLQLAIRNDEELNKLLGRV
TIAQGGVLPNIQAVLLPKKTESHHKAKGK
Calculated mass:13990.28 (average mass), 13981.89 (monoisotopic mass)

H2A.X (142 amino acids)
SGRGKTGGKARAKAKSRSSRAGLQFPVGRVHRLLRKGHYAERVGAGAPVY
LAAVLEYLTAEILELAGNAARDNKKTRIIPRHLQLAIRNDEELNKLLGGV
TIAQGGVLPNIQAVLLPKKTSATVGPKAPSGGKKATQASQEY
Calculated mass: 15013.38 (average mass), 15004.37 (monoisotopic mass)

H2A.Z (127 amino acids)
AGGKAGKDSGKAKTKAVSRSQRAGLQFPVGRIHRHLKSRTTSHGRVGATA
AVYSAAILEYLTAEVLELAGNASKDLKVKRITPRHLQLAIRGDEELDSLI
KATIAGGGVIPHIHKSLIGKKGQQKTV
Calculated mass:13421.55 (average mass), 13413.51 (monoisotopic mass)

```
H2A.1    SG--RGKQGG KARAKAKTRS SRAGLQFPVG RVHRLLR-KG NYAERVGAGA
H2A.X    SG--RGKTGG KARAKAKSRS SRAGLQFPVG RVHRLLR-KG HYAERVGAGA
H2A.Z    AGGKAGKDSG KAKTKAVSRS QRAGLQFPVG RIHRHLKSRT TSHGRVGATA

H2A.1    PVYLAAVLEY LTAEILELAG NAARDNKKTR IIPRHLQLAI RNDEELNKLL
H2A.X    PVYLAAVLEY LTAEILELAG NAARDNKKTR IIPRHLQLAI RNDEELNKLL
H2A.Z    AVYSAAILEY LTAEVLELAG NASKDLKVKR ITPRHLQLAI RGDEELDSLI

H2A.1    GKVTIAQGGV LPNIQAVLLP KKTESHHKAK GK-------- -----
H2A.X    GGVTIAQGGV LPNIQAVLLP KKTSATVGPK APSGGKKATQ ASQEY
H2A.Z    -KATIAGGGV IPHIHKSLIG KKGQQKTV-- ---------- -----
```

Sequence alignment of human H2A variants, H2A.1, H2A.X and H2A.Z. Residues of H2A.X and H2A.Z different from H2A.1 are shown in red.

Appendix 4

Sequences and calculated masses of human histone H2B variants analysed in this study.

H2B type 1-B (125 amino acids)
PEPSKSAPAPKKGSKKAITKAQKKDGKKRKRSRKESYSIYVYKVLKQVHP
DTGISSKAMGIMNSFVNDIFERIAGEASRLAHYNKRSTITSREIQTAVRL
LLPGELAKHAVSEGTKAVTKYTSSK
Calculated mass: 13819.00 (average mass), 13810.54 (monoisotopic mass)

H2B type 1-C/E/F/G/I (125 amino acids)
PEPAKSAPAPKKGSKKAVTKAQKKDGKKRKRSRKESYSVYVYKVLKQVHP
DTGISSKAMGIMNSFVNDIFERIAGEASRLAHYNKRSTITSREIQTAVRL
LLPGELAKHAVSEGTKAVTKYTSSK
Calculated mass: 13774.95 (average mass), 13766.52 (monoisotopic mass)

H2B type 1-D (125 amino acids)
PEPTKSAPAPKKGSKKAVTKAQKKDGKKRKRSRKESYSVYVYKVLKQVHP
DTGISSKAMGIMNSFVNDIFERIAGEASRLAHYNKRSTITSREIQTAVRL
LLPGELAKHAVSEGTKAVTKYTSSK
Calculated mass: 13804.97 (average mass), 13796.53 (monoisotopic mass)

H2B type 1-H (125 amino acids)
PDPAKSAPAPKKGSKKAVTKAQKKDGKKRKRSRKESYSVYVYKVLKQVHP
DTGISSKAMGIMNSFVNDIFERIAGEASRLAHYNKRSTITSREIQTAVRL
LLPGELAKHAVSEGTKAVTKYTSSK
Calculated mass: 13760.92 (average mass), 13752.50 (monoisotopic mass)

H2B type 1-J (125 amino acids)
PEPAKSAPAPKKGSKKAVTKAQKKDGKKRKRSRKESYSIYVYKVLKQVHP
DTGISSKAMGIMNSFVNDIFERIAGEASRLAHYNKRSTITSREIQTAVRL
LLPGELAKHAVSEGTKAVTKYTSAK
Calculated mass: 13772.97 (average mass), 13764.54 (monoisotopic mass)

H2B type 1-K (125 amino acids)
PEPAKSAPAPKKGSKKAVTKAQKKDGKKRKRSRKESYSVYVYKVLKQVHP
DTGISSKAMGIMNSFVNDIFERIAGEASRLAHYNKRSTITSREIQTAVRL
LLPGELAKHAVSEGTKAVTKYTSAK
Calculated mass: 13758.95 (average mass), 13750.52 (monoisotopic mass)

H2B type 1-N (125 amino acids)
PEPSKSAPAPKKGSKKAVTKAQKKDGKKRKRSRKESYSVYVYKVLKQVHP
DTGISSKAMGIMNSFVNDIFERIAGEASRLAHYNKRSTITSREIQTAVRL
LLPGELAKHAVSEGTKAVTKYTSSK
Calculated mass: 13790.95 (average mass), 13782.51 (monoisotopic mass)

H2B type 1-O (125 amino acids)
PDPAKSAPAPKKGSKKAVTKAQKKDGKKRKRSRKESYSIYVYKVLKQVHP
DTGISSKAMGIMNSFVNDIFERIAGEASRLAHYNKRSTITSREIQTAVRL
LLPGELAKHAVSEGTKAVTKYTSSK
Calculated mass:13774.95 (average mass), 13766.52 (monoisotopic mass)

H2B type 2-E (125 amino acids)
PEPAKSAPAPKKGSKKAVTKAQKKDGKKRKRSRKESYSIYVYKVLKQVHP
DTGISSKAMGIMNSFVNDIFERIAGEASRLAHYNKRSTITSREIQTAVRL
LLPGELAKHAVSEGTKAVTKYTSSK
Calculated mass: 13788.97 (average mass), 13780.53 (monoisotopic mass)

H2B type 2-F (125 amino acids)
PDPAKSAPAPKKGSKKAVTKVQKKDGKKRKRSRKESYSVYVYKVLKQVHP
DTGISSKAMGIMNSFVNDIFERIAGEASRLAHYNKRSTITSREIQTAVRL
LLPGELAKHAVSEGTKAVTKYTSSK
Calculated mass: 13788.97 (average mass), 13780.53 (monoisotopic mass)

isobaric variants (13760 Da)

H2B1H	P**D**PAKSAPAP	KKGSKKAVTK	AQKKDGKKRK	RSRKESYSVY	VYKVLKQVHP
H2B1K	P**E**PAKSAPAP	KKGSKKAVTK	AQKKDGKKRK	RSRKESYSVY	VYKVLKQVHP
H2B1H	DTGISSKAMG	IMNSFVNDIF	ERIAGEASRL	AHYNKRSTIT	SREIQTAVRL
H2B1K	DTGISSKAMG	IMNSFVNDIF	ERIAGEASRL	AHYNKRSTIT	SREIQTAVRL
H2B1H	LLPGELAKHA	VSEGTKAVTK	YTS**S**K		
H2B1K	LLPGELAKHA	VSEGTKAVTK	YTS**A**K		

isobaric variants (13775 Da)

H2B1C	P**E**PAKSAPAP	KKGSKKAVTK	AQKKDGKKRK	RSRKESYS**V**Y	VYKVLKQVHP
H2B1J	P**E**PAKSAPAP	KKGSKKAVTK	AQKKDGKKRK	RSRKESYS**I**Y	VYKVLKQVHP
H2B1O	P**D**PAKSAPAP	KKGSKKAVTK	AQKKDGKKRK	RSRKESYS**I**Y	VYKVLKQVHP
H2B1C	DTGISSKAMG	IMNSFVNDIF	ERIAGEASRL	AHYNKRSTIT	SREIQTAVRL
H2B1J	DTGISSKAMG	IMNSFVNDIF	ERIAGEASRL	AHYNKRSTIT	SREIQTAVRL
H2B1O	DTGISSKAMG	IMNSFVNDIF	ERIAGEASRL	AHYNKRSTIT	SREIQTAVRL
H2B1C	LLPGELAKHA	VSEGTKAVTK	YTS**S**K		
H2B1J	LLPGELAKHA	VSEGTKAVTK	YTS**A**K		
H2B1O	LLPGELAKHA	VSEGTKAVTK	YTS**S**K		

isobaric variants (13789 Da)

H2B1N	P**E**P**S**KSAPAP	KKGSKKAVTK	**A**QKKDGKKRK	RSRKESYS**V**Y	VYKVLKQVHP
H2B2E	P**E**P**A**KSAPAP	KKGSKKAVTK	**A**QKKDGKKRK	RSRKESYS**I**Y	VYKVLKQVHP
H2B2F	P**D**P**A**KSAPAP	KKGSKKAVTK	**V**QKKDGKKRK	RSRKESYS**V**Y	VYKVLKQVHP
H2B1N	DTGISSKAMG	IMNSFVNDIF	ERIAGEASRL	AHYNKRSTIT	SREIQTAVRL
H2B2E	DTGISSKAMG	IMNSFVNDIF	ERIAGEASRL	AHYNKRSTIT	SREIQTAVRL
H2B2F	DTGISSKAMG	IMNSFVNDIF	ERIAGEASRL	AHYNKRSTIT	SREIQTAVRL
H2B1N	LLPGELAKHA	VSEGTKAVTK	YTSSK		
H2B2E	LLPGELAKHA	VSEGTKAVTK	YTSSK		
H2B2F	LLPGELAKHA	VSEGTKAVTK	YTSSK		

Sequence alignment of human H2B variants, grouped in the 3 sets of isobaric species. Amino acid residues differing between the variants are in bold.

Appendix 5

Sequences and calculated masses of human histone H3 variants analysed in this study.

H3.1 (135 amino acids)
ARTKQTARKSTGGKAPRKQLATKAARKSAPATGGVKKPHRYRPGTVALRE
IRRYQKSTELLIRKLPFQRLVREIAQDFKTDLRFQSSAVMALQEACEAYL
VGLFEDTNLCAIHAKRVTIMPKDIQLARRIRGERA
Calculated mass: 15272.89 (average mass), 15263.44 (monoisotopic mass)

H3.2 (135 amino acids)
ARTKQTARKSTGGKAPRKQLATKAARKSAPATGGVKKPHRYRPGTVALRE
IRRYQKSTELLIRKLPFQRLVREIAQDFKTDLRFQSSAVMALQEASEAYL
VGLFEDTNLCAIHAKRVTIMPKDIQLARRIRGERA
Calculated mass: 15256.83 (average mass), 15247.47 (monoisotopic mass)

H3.3 (135 amino acids)
ARTKQTARKSTGGKAPRKQLATKAARKSAPSTGGVKKPHRYRPGTVALRE
IRRYQKSTELLIRKLPFQRLVREIAQDFKTDLRFQSAAIGALQEASEAYL
VGLFEDTNLCAIHAKRVTIMPKDIQLARRIRGERA
Calculated mass: 15196.72 (average mass), 15187.46 (monoisotopic mass)

```
                                                  24        29  31
H3.1    ARTKQTARKS TGGKAPRKQL ATKAARKSAP ATGGVKKPHR YRPGTVALRE
H3.2    ARTKQTARKS TGGKAPRKQL ATKAARKSAP ATGGVKKPHR YRPGTVALRE
H3.3    ARTKQTARKS TGGKAPRKQL ATKAARKSAP STGGVKKPHR YRPGTVALRE
H3.1t   ARTKQTARKS TGGKAPRKQL ATKVARKSAP ATGGVKKPHR YRPGTVALRE
H3.3C   ARTKQTARKS TGGKAPRKQL ATKAARKSTP STCGVK-PHR YRPGTVALRE
                                                  71        79              87 89 90          96 98
H3.1    IRRYQKSTEL LIRKLPFQRL VREIAQDFKT DLRFQSSAVM ALQEACEAYL
H3.2    IRRYQKSTEL LIRKLPFQRL VREIAQDFKT DLRFQSSAVM ALQEASEAYL
H3.3    IRRYQKSTEL LIRKLPFQRL VREIAQDFKT DLRFQSAAIG ALQEASEAYL
H3.1t   IRRYQKSTEL LIRKLPFQRL MREIAQDFKT DLRFQSSAVM ALQEACESYL
H3.3C   IRRYQKSTEL LIRKLPFQRL VREIAQDFNT DLRFQSAAVG ALQEASEAYL
                104             111
H3.1    VGLFEDTNLC AIHAKRVTIM PKDIQLARRI RGERA
H3.2    VGLFEDTNLC AIHAKRVTIM PKDIQLARRI RGERA
H3.3    VGLFEDTNLC AIHAKRVTIM PKDIQLARRI RGERA
H3.1t   VGLFEDTNLC VIHAKRVTIM PKDIQLARRI RGERA
H3.3C   VGLLEDTNLC AIHAKRVTIM PKDIQLARRI RGERA
```

Sequence alignment of human H3 variants: H3.1, H3.2, H3.3, H3.1t and H3.3C. Different amino acid residues in the H3 variants are in red.

Sequences and calculated masses of human histone H4 analysed in this study

H4 (102 amino acids)
SGRGKGGKGLGKGGAKRHRKVLRDNIQGITKPAIRRLARRGGVKRISGLI
YEETRGVLKVFLENVIRDAVTYTEHAKRKTVTAMDVVYALKRQGRTLYGF
GG
Calculated mass:11236.15 (average mass), 11229.34 (monoisotopic mass)

Appendix 6

Potential assignments for the observed masses from the optimised LC-MS based results.

Fraction	Mass (Da) exp.	Histone variants	Histone variants Mass (Da) theor.	Interpretation
H1	21,276	**H1.2**	**21,275.6**	H1.2+ **N-Ac**
	21,356			H1.2+ **N-Ac**+ 1P
	21,436			H1.2+ **N-Ac**+ 2P
	22,261	**H1.3**	**22,260.7**	H1.3+ **N-Ac**
	21,776	**H1.4**	**21,776.1**	H1.4+ **N-Ac**
	21,856			H1.4+ **N-Ac**+ 1P
H2A-1	14,007	**H2A type 2-A**	**14006.3**	H2A type 2-A+ **N-Ac**
	14,049			H2A type 2-A+ **N-Ac**+ 1K-Ac
	13,900	**H2A type 2-C**	**13,899.2**	H2A type 2-C+ **N-Ac**
	13,422	**H2A.Z**	**13,421.6**	H2A.Z
H2A-2	14,003	**H2A type 1**	**14,002.3**	H2A type 1+ **N-Ac**
	14,017	**H2A type 1-C/ type 1-D**	**14,016.3/ 14018.3**	H2A type 1-C/ 1-D+ **N-Ac*** *or* H2A type 1+ **N-Ac**+ 1Me
	14,032	**H2A type 3**	**14032.3**	H2A type 1+ **N-Ac**
	14,046	**H2A type 1-B/E**	**14046.3**	H2A type 1-B/E+ **N-Ac** * *or* H2A type 1-C/ 1-D+ **N-Ac** + 1K-Ac H2A type 1+ **N-Ac** + 1Me
	14,060			H2A type 1-C/ 1-D+ **N-Ac** + 1K-Ac
	13,900	**H2A type 2-C**	**13,899.2**	H2A type 2-C+ **N-Ac**
	13,817	**H2A type 1-H**	**13,817.1**	H2A type 1-H+ **N-Ac**
	15,056	**H2A.X**	**15,055.5**	H2A.X+ **N-Ac** c
H2B	13,760	**H2B type1-H/ type 1-K**	**13,760.9/ 13759.0**	H2B type1-H/ type 1-K
	13,775	**H2B type1-C/E/F/G/I**	**13774.9**	H2B type1-C/E/F/G/I
	13,789	**H2B type1-N/ type2-E/ type 2-F**	**13,790.9/ 13,788.9/ 1,3788.9**	H2B type1-N/ type2-E/ type 2-F* *or* H2B type1-C/E/F/G/I+ 1 1Me
	13,805	**H2B type1-D**	**13,804.9**	H2B type1-D
	13,819	**H2B type1-B**	**13,819.0**	H2B type1-B* *or* H2B type1-D+ 1Me
	13,831			H2B type1-N/ type2-E/ type 2-F+ 1K-Ac* *or* H2B type1-B+ 1Me *or* H2B type1-D+ 2Me
	13,847			H2B type1-D+ 1K-Ac
	13,861			H2B type1-B+ 1K-Ac* *or* H2B type1-D+1K-Ac+ 1Me
	13,873			H2B type1-N/ type2-E/ type 2-F+ 2K-Ac* *or* H2B type1-B+1K-Ac+ 1Me *or* H2B type1-D+1K-Ac+ 2Me
	13,889			H2B type1-D+ 2K-Ac

H4	11,278	**H4**	**11,278.2**	H4+ **N**-**Ac**
	11,292			H4+ **N**-**Ac**+ 1Me
	11,306			H4+ **N**-**Ac**+ 2Me
	11,320			H4+ **N**-**Ac**+ 1K-Ac *or* H4+ **N**-**Ac**+ 3Me*
	11,334			H4+ **N**-**Ac**+ 1K-Ac+ 1Me* *or* H4+ **N**-**Ac**+ 4Me
	11,348			H4+ **N**-**Ac**+ 1K-Ac+ 2Me* or H4+ **N**-**Ac**+ 5Me
	11,362			H4+ **N**-**Ac**+ 2K-Ac* *or* H4+ **N**-**Ac**+ 1K-Ac+ 3Me H4+ **N**-**Ac**+ 6Me
	11,376			H4+ **N**-**Ac**+ 2K-Ac+ 1Me* *or* H4+ **N**-**Ac**+ 1K-Ac+ 4Me H4+ **N**-**Ac**+ 7Me
	11,390			H4+ **N**-**Ac**+ 2K-Ac+ 2Me* *or* H4+ **N**-**Ac**+ 1K-Ac+ 5Me H4+ **N**-**Ac**+ 8Me
	11,404			H4+ **N**-**Ac**+ 3K-Ac* *or* H4+ **N**-**Ac**+ 2K-Ac+ 3Me *or* H4+ **N**-**Ac**+ 1K-Ac+ 6Me H4+ **N**-**Ac**+ 9Me
	11,432			H4+ **N**-**Ac**+ 3K-Ac+ 1Me* *or* H4+ **N**-**Ac**+ 2K-Ac+ 4Me *or* H4+ **N**-**Ac**+ 1K-Ac+ 7Me H4+ **N**-**Ac**+ 10Me
	11,476			H4+ **N**-**Ac**+ 3K-Ac+ 2Me* *or* H4+ **N**-**Ac**+ 2K-Ac+ 5Me *or* H4+ **N**-**Ac**+ 1K-Ac+ 8Me *or* H4+ **N**-**Ac**+ 11Me
H3	15,273/ 15,257	**H3.1/H3.2**	**15,272.9/ 15,256.8**	H3.1/H3.2
	15,287/ 15,271			H3.1/H3.2+ 1Me
	15,301/ 15,285			H3.1/H3.2+ 2Me
	15,315/ 15,299			H3.1/H3.2+ 3Me *or* 1K-Ac
	15,329/ 15,313			H3.1/H3.2+ 4Me *or* 1K-Ac+ 1Me
	15,343/ 15,327			H3.1/H3.2+ 5Me *or* 1K-Ac+ 2Me
	15,357/ 15,341			H3.1/H3.2+ 6Me *or* 1K-Ac+ 3Me *or* 2K-Ac
	15,371/ 15,355			H3.1/H3.2+ 7Me *or* 1K-Ac+ 4Me *or* 2K-Ac+ 1Me
	15,385/ 15,369			H3.1/H3.2+ 8Me *or* 1K-Ac+ 5Me *or* 2K-Ac+ 2Me
	15,399/ 15,383			H3.1/H3.2+ 9Me *or* 1K-Ac+ 6Me *or* 2K-Ac+ 3Me *or* 3K-Ac
	15,413/ 15,397			H3.1/H3.2+ 10Me *or* 1K-Ac+ 7Me *or* 2K-Ac+ 4Me *or* 3K-Ac+ 1Me
	15,427/ 15,411			H3.1/H3.2+ 11Me *or* 1K-Ac+ 8Me *or* 2K-Ac+ 5Me *or* 3K-Ac+ 2Me
	15,441/ 15,425			H3.1/H3.2+ 12Me *or* 1K-Ac+ 9Me *or* 2K-Ac+ 6Me or 3K-Ac+ 3Me *or* 4K-Ac

15,455/ 15,439	H3.1/H3.2+ 13Me *or* 1K-Ac+ 10Me *or* 2K-Ac+ 7Me or 3K-Ac+ 4Me or 4K-Ac+ 1Me
15,469/ 15,453	H3.1/H3.2+ 14Me *or* 1K-Ac+ 11Me *or* 2K-Ac+ 8Me or 3K-Ac+ 5Me *or* 4K-Ac+ 2Me
15,483/ 15,467	H3.1/H3.2+ 15Me *or* 1K-Ac+ 12Me *or* 2K-Ac+ 9Me or 3K-Ac+ 6Me *or* 4K-Ac+ 3Me *or* 5K-Ac
15,497/15,481	H3.1/H3.2+ 16Me *or* 1K-Ac+ 13Me *or* 2K-Ac+ 10Me or 3K-Ac+ 7Me *or* 4K-Ac+ 4Me *or* 5K-Ac+ 1Me
15,511/ 15,495	H3.1/H3.2+ 17Me *or* 1K-Ac+ 14Me *or* 2K-Ac+ 11Me or 3K-Ac+ 8Me *or* 4K-Ac+ 5Me *or* 5K-Ac+ 2Me
15,525/15,509	H3.1/H3.2+ 18Me *or* 1K-Ac+ 15Me *or* 2K-Ac+ 12Me *or* 3K-Ac+ 9Me *or* 4K-Ac+ 6Me *or* 5K-Ac+ 3Me *or* 6K-Ac

* Indicates the most likely species.
N-Ac: *N*-acetylation; Ac: acetylation; Me: methylation.

Appendix 7

IOX2-H2A

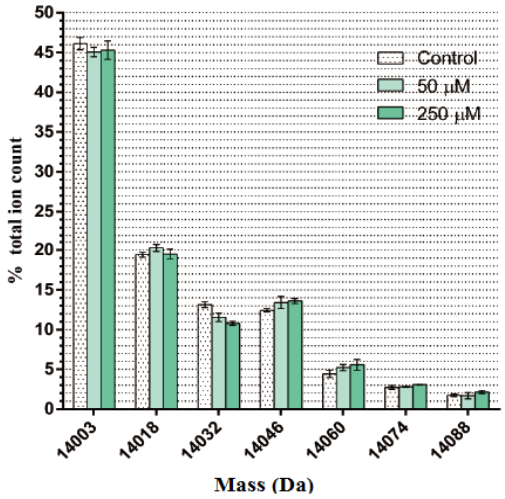

FG-4592-H2A

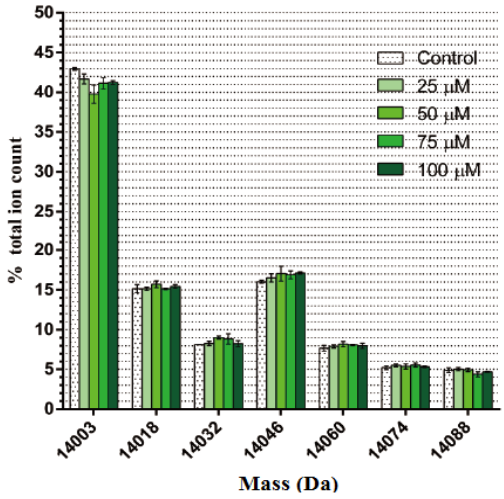

IOX2-H2B

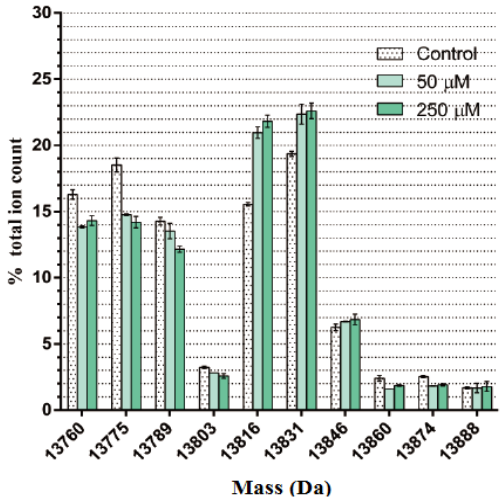

FG-4592-H2B

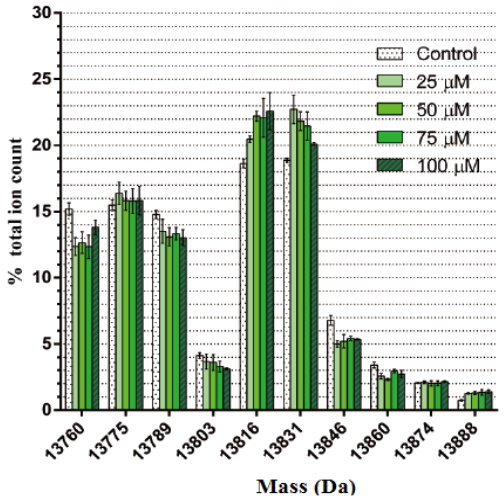

IOX2-H4

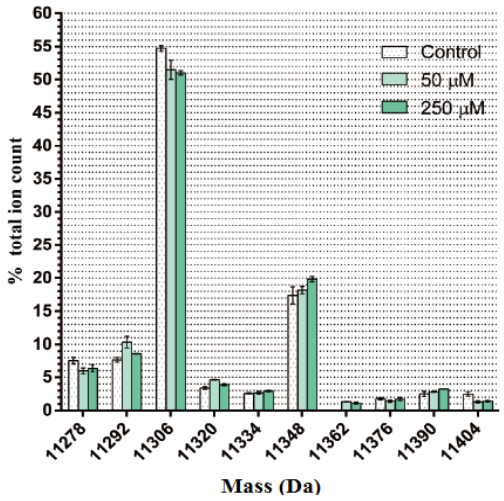

FG-4592-H4

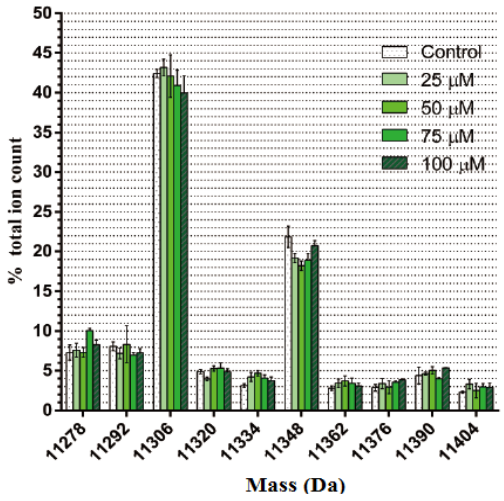

Appendix 7 Quantitative analysis of the abundance of differently modified species of histone H2A, H2B and H4 following treatment of cells with 0, 50 and 250 μM IOX2 (left panel) or 0, 25, 50, 75 and 100 μM FG-4592 (right panel) for 24 hours. The ion count for each peak is expressed as a percentage of the total ion count. Data are means ± SEM (n=3).